Dynamical synthesis and analysis of healthy and pathological human walking

Alexandra Pimenta dos Santos

▶ To cite this version:

HAL Id: tel-01912813

https://theses.hal.science/tel-01912813

Submitted on 5 Nov 2018

**THÈSE DE DOCTORAT
DE L'UNIVERSITÉ PIERRE ET MARIE CURIE**

École Doctorale Sciences Mécaniques, Acoustique, Électronique et Robotique de Paris

Spécialité
Robotique

Présenté par
Alexandra PIMENTA DOS SANTOS

Pour obtenir le grade de
Docteur de l'Université Pierre et Marie Curie

Dynamical synthesis and analysis of healthy and pathological human walking

Soutenance prévue le 27 Novembre 2017

Devant le jury composé de :

Mme Laurence CHÈZE	Professeur à l'Université de Lyon 1	Rapporteur
M Philippe FRAISSE	Professeur à l'Université de Montpellier	Rapporteur
M Franck MULTON	Professeur à l'Université de Rennes 2	Examinateur
M Philippe THOUMIE	Professeur à l'Université Pierre et Marie Curie, - PH	Examinateur
M Eric DESAILLY	Directeur Pôle Recherche & Innovation à la Fondation Ellen Poidatz	Co-Encadrant
M Faiz BEN AMAR	Professeur à l'Université Pierre et Marie Curie	Directeur

Invités :

M Philippe BIDAUD	Professeur à l'Université Pierre et Marie Curie	Co-encadrant
M Vincent PADOIS	Maître de Conférences à l'Université Pierre et Marie Curie	Co-encadrant

Acknowledgements

ABSTRACT

Children with cerebral palsy generally develop gait impairments. Orthopaedic surgery aims to improve the gait and the function of those children by specific procedures. The perspective of this work is to simulate their effects. This would allow surgeons not only to test different surgical plans, but also to improve the communication with patients and families, by clarifying the expected outcomes.

The patient's specificities, which take a great part in surgical treatment need to be represented. In this work, an anthropomorphic 3D human model with an articulated foot (divided in rear/midfoot and forefoot parts) and 40 degrees of freedom is developed. This manikin is scalable to the studied patient.

A task-oriented Linear Quadratic Programming (LQP) controller is used to dynamically simulate walking through constrained optimization. The optimization cost function is defined with a weighting sum of tasks that are related to feet motion, pelvis, torso and head orientation and to the Center of Mass (CoM) trajectory projected on the ground. A Linear Inverted Pendulum Model and the Zero-Moment Point (ZMP) are used to determine the CoM trajectory. The modelled system respects the equations of motion, used as constraints, together with joint angles and torques limits, and contacts constraints. The motion is simulated in the multibody dynamics XDE framework.

Three different patterns of foot contacts with the ground are implemented. Asymptomatic human walking is first generated with all the normal foot rockers. Experimental data from motion capture systems are used to build a model of the trajectory of the Center of Pressure (CoP) during stance phase and of the feet displacement during swing phase. Greater walking speeds and step lengths than usually obtained with flat feet humanoid robots are simulated. They are close to those of healthy human walking. Sagittal kinematics is quite similar to healthy human walking. Dynamical data stay within the magnitudes encountered in human walking. Toe walking and flat feet walking with heel off motion, currently observed in children with cerebral palsy, are the two other developed patterns. Different steps lengths and walking speeds are possible for these two types of motion.

The virtual effect of modifying joint limits constraints is tested on different asymptomatic or toe walking simulations. This assessment of the adaptability of the simulator

to constraints modifications is a first approach to simulate the effect on gait of some surgical procedures aimed to modify the limits of the kinematic model of the patient. The developed simulation system is able to deal with these changes and to produce walking motions. In some cases, the generated gait patterns reproduce features of cerebral palsy children's walking.

Limits and perspectives of this dynamic simulation approach are extensively discussed.

CONTENTS

INTRODUCTION

Walking is an essential activity for human beings in the everyday life. It is a locomotion mode in an upright standing posture "involving the use of the two legs, alternately, to provide both support and propulsion" and with "at least one foot being in contact with the ground at all times" [Levine et al., 2012]. A person's manner of walking is defined as gait, according to the Oxford Dictionaries.

For a specific population, a typical pattern of walking can be retrieved. When analysing the walking pattern of a specific individual in this population, if it deviates considerably from its normalcy, we are facing an abnormal/pathological gait. Multiple causes may explain this deviation: injuries, neurological conditions, muscular or structural disorders, pain, fatigue, etc.

The resulting impairment caused may be just temporary (in the case of a minor injury like an ankle sprain, for instance), aggravating with time or just stationary. Independently of the gravity of the disorder, it often carries on a lack of autonomy, and have an impact on everyday life. In the case of children, locomotion disorders can complicate normal growth but also have an impact on social life. As for the elders, locomotion disorders may implicate a dependence on others for everyday tasks, or, in severe cases, cause falls.

Independently of the severity of the impairment, treatments may be employed to improve, help or correct the disorders. Non invasive treatments include physical therapy, the use of walking aids, like canes, crutches or walkers, and orthotics devices. Yet, these can be insufficient to correctly deal with locomotion disorders, and orthopaedic surgery may be necessary.

In order to choose the correct surgery, the causes of the impairment on the locomotion system must be identified. Nowadays, different methods exist to help identify the disorders and their causes: physical examination, instrumental methods [Thoumie et al., 2002] and medical imaging. These methods allow to evaluate the impairments before and after a treatment is engaged, but do not allow to predict the result of the treatments beforehand. In this context, simulation of human walking can be not only of

great help to understand the causes of the disorder, but also help to estimate the effect of the surgery. Simulation of human walking could them be used to improve diagnosis and help surgical decision.

In this work, special focus is made to the gait disorders presented by Cerebral Palsy Children.

1.1 Context

This work is part of the project **SiM PC²** - **Si**mulation prédictive de la **M**arche et du bénéfice fonctionnel **P**ost **C**hirurgical dans la **P**aralysie **C**érébrale[1] - of the Ellen Poidatz Foundation, directed by Eric Desailly. This multidisciplinary project benefits from the financial support of the Bettencourt-Schueller and Ellen Poidatz Foundations, the Ile-de-France Region (PICRI2012) and the National Agency for the Research and Technology (CIFRE convention No. 2013/0316). Different partners are involved in this project: academic (Paris-Saclay University by University of Evry Val d'Essonne and Télécom Sud-Paris Institute, as well as Pierre and Marie Curie University by Institute for Intelligent Systems and Robotics - ISIR), clinical (Necker-Enfants Malades Hospital, Ellen Poidatz Foundation) and representatives of the civil society (Fondation Motrice, SESEP, Institut de Motricité Cérébrale).

The **SiM PC²** project arises from the need of a simulation tool enabling the testing of different surgical scenarios and their respective outcomes, on a specific patient, in order to personalize the surgical plan. The project is coupled around two PhD thesis:

- The first one is focused on the definition of machine learning algorithms that can be used to predict the result of a surgery, or set of surgeries, from a database of clinical cases [Galarraga C., 2017].

- The second one, of which the work is developed here, focus on the biomechanical representation of the locomotion system, its simulation and the analysis of the resulting patterns.

For the physician, such simulation tool presents a great interest, since it would make possible to test the effect of several surgical treatments and their association beforehand. For the patient, besides the contribution in improving the therapeutic treatment, it would

---

[1]Predictive Simulation of Gait and Surgical Functional Benefit in Cerebral Palsy

allow him to visualize its expected outcome. He would be able then to discuss more pertinently the objectives expected by the care team.

This PhD thesis is the result of a partnership between the Ellen Poidatz Foundation and the Institute for Intelligent Systems and Robotics of the Pierre and Marie Curie University, validated by the CIFRE convention No. 2013/0316.

1.1.1 Cerebral Palsy

In France, Cerebral Palsy affects 1 newborn over 450, that is, 1800 newborns each year[2]. According to the most recent collective international definition [Rosenbaum et al., 2007], Cerebral Palsy consists of "a group of permanent disorders of the development of movement and posture, causing activity limitation, that are attributed to non-progressive disturbances that occurred in the developing foetal or infant brain. The motor disorders of cerebral palsy are often accompanied by disturbances of sensation, perception, cognition, communication, and behaviour, by epilepsy, and by secondary musculoskeletal problems.".

Prematurely born children are the most affected by cerebral palsy, but the precise cause of brain damage is unknown in most cases. Even though the brain damage does not get any better or worse as time passes, clinical manifestations appear and/or change as the child grows, especially musculoskeletal disorders. These manifestations determine whether and how children with cerebral palsy will walk.

In the literature, there are different means of classifying cerebral palsy children. The principal one is the Gross Motor Function Classification System GMFCS described in [Palisano et al., 2008]. It relies on the deterioration of the motor function, and children are classified according to five levels. The current version of GMFCS, the Gross Motor Function Classification System Expanded and Revised (GMFCS - E&R) [3] gives a mean of classification according to the children's age: before 2nd birthday, between 2nd and 4th birthday, between 4th and 6th birthday, between 6th and 12th birthday, see figure 1.1, and between 12th and 18th birthday.

Another strategy is to classify children according to the areas of the body affected:
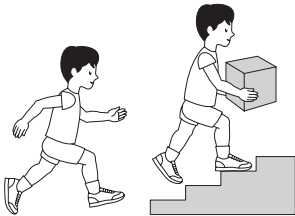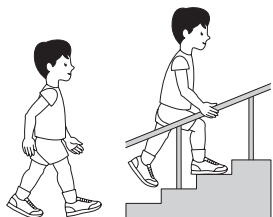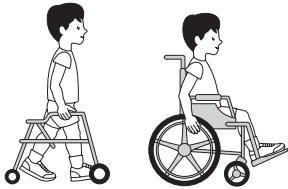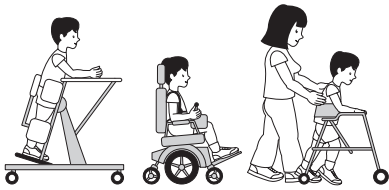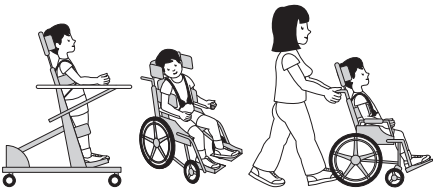
- Hemiplegia: where only one side of the body is affected, one arm and one leg on the same side.

---

[2]Data from the Fondation Motrice's website. [Last consulted on 22/08/2017.]
[3]`motorgrowth.canchild.ca/en/gmfcs/resources/gmfcs-er.pdf`

GMFCS E & R between 6th and 12th birthday: Descriptors and illustrations

GMFCS Level I

Children walk at home, school, outdoors and in the community. They can climb stairs without the use of a railing. Children perform gross motor skills such as running and jumping, but speed, balance and coordination are limited.

GMFCS Level II

Children walk in most settings and climb stairs holding onto a railing. They may experience difficulty walking long distances and balancing on uneven terrain, inclines, in crowded areas or confined spaces. Children may walk with physical assistance, a hand-held mobility device or used wheeled mobility over long distances. Children have only minimal ability to perform gross motor skills such as running and jumping.

GMFCS Level III

Children walk using a hand-held mobility device in most indoor settings. They may climb stairs holding onto a railing with supervision or assistance. Children use wheeled mobility when traveling long distances and may self-propel for shorter distances.

GMFCS Level IV

Children use methods of mobility that require physical assistance or powered mobility in most settings. They may walk for short distances at home with physical assistance or use powered mobility or a body support walker when positioned. At school, outdoors and in the community children are transported in a manual wheelchair or use powered mobility.

GMFCS Level V

Children are transported in a manual wheelchair in all settings. Children are limited in their ability to maintain antigravity head and trunk postures and control leg and arm movements.

GMFCS descriptors: Palisano et al. (1997) Dev Med Child Neurol 39:214-23
CanChild: www.canchild.ca

Illustrations Version 2 © Bill Reid, Kate Willoughby, Adrienne Harvey and Kerr Graham,
The Royal Children's Hospital Melbourne   ERC151050

Figure 1.1: Gross Motor Function Classification System Expanded and Revised between 6th and 12th birthday.

- Diplegia: where both legs are affected.

- Quadriplegia: where there is involvement of the four limbs.

Over the years, several attempts to classify cerebral palsy according to gait pattern have been made [Dobson et al., 2007]. However, the range of gait deviations in children with cerebral palsy is very large, and a consensual and complete classification system has not yet emerged [Rodda and Graham, 2001, Rodda et al., 2004]. Nevertheless, some gait abnormalities are common among Cerebral Palsy children [Wren et al., 2005][4], see table 1.1.

Table 1.1: Some examples of common gait abnormalities among children with Cerebral Palsy [Wren et al., 2005].

Gait Abnormality	Definition
Equinus	Ankle plantarflexion greater than one standard deviation (SD) below the mean for normal during stance phase, with or without hindfoot and/or forefoot varus or valgus - Toe walking, see figure 1.2.
Crouch gait	Increased knee flexion (one standard deviation above the healthy mean) in a significant portion of stance phase, see figure 1.3.
Stiff-knee gait	Decreased arc of knee motion from maximum knee extension in stance to peak knee flexion in swing, and/or delay in peak swing knee flexion to mid- or terminal swing, hindering foot clearance.
Vaulting	Going up on the toes on the stance limb to increase ground clearance for the swing limb.
Out and Intoeing	External, and internal, foot progression greater than the corresponding one normal standard deviation, respectively.

These gait abnormalities are usually the result of four kind of impairments: spasticity, muscle contracture, weakness and bone deformities.

Spasticity is a muscle control disorder "manifested by increased stretch reflex which is intensified with movement velocity" [Bar-On et al., 2015]. Muscles affected by spasticity are susceptible to develop contractures. This leads to a restriction in the range of movement of the joints, since the passive length of the muscle and its tendon are reduced. This condition is mostly developed during childhood. Even though it can be a consequence of spasticity, the origin of muscle contractures is not well known.

---

[4]If the names of the gait abnormalities are quiet consensual, their definition are heterogeneous among the authors.

Figure 1.2: Example of toe walking. Front (left) and side (right) views.
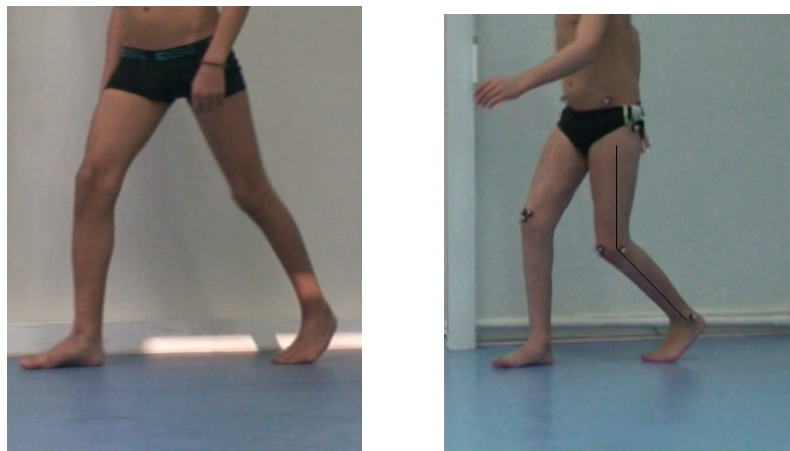
Figure 1.3: Normal (left) versus Crouch (right) Gaits.

Along with contractures, Cerebral Palsy children may present muscle weakness. This can arise either because of anatomy and physiology of the muscles or because of reduced neural activity to stimulate contraction. This condition tends to become more problematic with age, specially in late childhood and early adolescence, when weight increases rapidly.

Bone deformities are also common in Cerebral Palsy children, with excessive anteversion of the femur being the most frequent example. In this case, the femoral neck is pointing too far forward in relation to the knee joint axis.

Besides structural or neural causes, gait abnormalities may also be the result of compensatory mechanisms, in which even if some anatomical regions are not affected, they may present abnormalities during walking in order to avoid pain or instability, for instance.

As in the case of other gait disorders, different strategies are present when it comes to the clinical management of cerebral palsy children gait impairments. In the case of

spasticity, one of the strategies may be to realize botulinum toxin injections in the affected muscle. This chemical substance is a way of suppressing specific muscular activity in a period varying between 3 and 9 months. Less invasive treatments can be employed, but some times these are insufficient, and orthopaedic surgery may be necessary, specially when contractures and bone deformities are impossible to prevent.

1.1.2 Orthopaedic Surgery

The main goals of Orthopaedic Surgery are the management of impairment, pain control, optimization of independence, maximization of movement, balance and coordination and the preservation of functionality. It is performed in two structures: muscle/tendon complex and bones.

In muscles, different kinds of surgeries can be performed: recession, release and transfer. The most common example of recession surgery is the Achilles tendon lengthening, where the tendon linking the muscle to the Achilles tendon is cut. This surgery is called gastrocnemius recession. Partial releases of muscles, to allow more normal gait and posture, can also be performed and are nowadays preferred to recessions as they are easier to adjust and allow quicker recoveries. Transfer surgery is the archetype of the functional surgery that is proposed to cerebral palsy children. Its purpose is not only to lengthen or to weaken a muscle but also to modify its lever arm. For instance, if the rectus femoris is contractured, it can be better to transfer its insertion from the patella to the posterior aspect of the proximal tibia (i.e. the gracilis tendon), making it act as a knee flexor, instead of a knee extensor while maintaining its hip flexor component.

Concerning bones surgery, femoral anteversion, which is one of the most common bone deformities, can be corrected by an osteotomy. In this procedure, the bone is transversely cut, untwisted and then hold in its new position by a metal plate attached with screws. Deformities in the foot bones can also be corrected by several osteotomies.

In the past, if a patient needed several corrections, a surgery was made for each one of them. As intermediate results were not always satisfactory and physical recovery can be a long and painful process, following surgeries eventually could not be performed, as family and patient refused it.

Over the years, as the surgeon's experience increased, the several corrections started being treated in one single surgery. This process is known as Single Event Multi-Level Surgery (SEMLS).

To determine the appropriate surgical treatment to follow, surgeons rely not only on the different exams available but also on their personal experience.

1.2   Motivation

This work arises from the need of a simulation tool capable of testing different surgical scenarios and their respective outcomes, on a specific patient, in order to personalize the surgical plan.

In order to achieve that, one needs to:

- be able to numerical represent the patient whom walking is to be studied;

- be able to accurately simulate human walking, both healthy and pathological;

- be able to modify the system to be simulated according to the surgery intended and to analyse the resulting walking patterns.

The methodology presented in this work for the simulation of walking activities relies on a virtual manikin built from patient data. This patient data is obtained through motion capture procedures and then used to more accurately represent the patient anatomy.

Since the patient is virtually represented, changes in its anatomy can be easily done. Thus, walking motion can be simulated for the patients' current anatomy, but also for a modified virtual human which takes into account changes from surgical procedures. This enables to test beforehand the result of a surgery, without any procedure being engaged.

Here, the walking motion is simulated through a Linear Quadratic Programming controller, which allows to take into account the different anatomical constraints of each patient. The proposed methodology allows the simulation of walking motions presenting non pathological contacts, but also toe walking motions and gait patterns where the initial contact is made with the entire foot - flat feet walking.

The methodology presented here allows to recover not only kinematic but also dynamical data, like joint torques, power and ground reaction forces, to enable the analysis and the comparison of the different walking patterns generated.

1.3 Manuscript contents

In this work, a framework for the simulation of healthy and pathological human walking is proposed. The organization of this manuscript is detailed hereafter.

Chapter 2 reviews the main aspects characterizing human walking: spatio-temporal parameters, kinematics, dynamics and balance. The Clinical Gait Analysis exam, used to assess Cerebral Palsy children's locomotion is presented along with the most common surgeries performed within this population. A review on statistical means to predict surgical outcomes and tools for the simulation of human walking are also presented. The proposed approach of this work is introduced at the end of the chapter.

The simulation framework upon which this work relies on is presented in chapter 3. The method for the construction of the virtual manikin is described. The Linear Quadratic Programming Controller used for the simulation of human walking is detailed. The actuation and contact constraints considered are presented and the tasks used in the walking motion generation are introduced. The contacts management scheme is also detailed. A walking simulation example is presented and analysed at the end of the chapter.

Chapter 4 dedicates to the development of an articulated foot, in order to improve walking simulations. Different foot modelling approaches used are reviewed and the chosen one is detailed. The changes induced in the walking simulation procedure (contacts management and foot tasks) are presented. A gait initialization procedure is described in the end of the chapter.

The walking patterns possible to simulate with the developments of Chapter 4 are presented in Chapter 5. Three types of walking patterns are explored: non pathological contacts, toe walking and flat feet initial contact. The range of possible motions is explored and the gait patterns generated are analysed.

Finally, in Chapter 6 an application of the proposed framework in the simulation of abnormal walking patterns is presented. The gait abnormalities explored are introduced and walking simulations are done in the case of non pathological contacts and toe walking. The walking patterns generated are compared with the patterns found in Cerebral Palsy Children, when possible. Possibilities and limits of the walking motion generation framework proposed are discussed.

WALKING: DEFINITION, ANALYSIS, DISORDERS, TREATMENT AND SIMULATION

The main interest of this thesis is human walking, either healthy or pathological.

Therefore, it is important to understand how the human walking activity can be analysed. In fact, only by defining a standard for a healthy walking pattern, one is able to detect, evaluate and treat gait pathologies. This is the subject of this chapter.

The chapter is organized as follows:

- Section 2.1 presents the most usual parameters and quantities used to define the walking activity;

- Section 2.2 reviews detection and treatment of locomotion disorders by presenting the Clinical Gait Analysis and the most common surgeries performed on Cerebral Palsy Children;

- Section 2.3 presents the state of the art in the prediction of the outcome of some surgical procedures;

- Section 2.4 presents some tools for the simulation of human walking and its disabilities;

- Section 2.5 ends the chapter with the proposed approach for the synthesis of human walking.

2.1 The walking activity

Walking is the most natural mode of locomotion for the human being.

The walking routine is a set of consecutive gait cycles, which can be defined as the time interval between two successive occurrences of one of the repetitive walking events. These events can be divided as follow:

1. Initial Contact (IC) - the foot establishes contact with the ground, usually through the heel;

2. Opposite Toe Off (OTO) - the opposite toes break contact with the ground, and so the opposite foot is no longer in contact with the ground;

3. Heel Rise (HR) - the heel starts to rise breaking the contact with the ground;

4. Opposite Initial Contact (OIC) - the opposite foot establishes contact with the ground, usually through the heel;

5. Toe Off (TO) - the toes break contact with the ground, and so the foot is no longer in contact with the ground;

6. Opposite Heel Rise (OHR) - the opposite heel starts to rise breaking the contact with the ground;

7. Initial Contact (IC) - the foot establishes contact with the ground, usually through the heel, and the gait cycle re-starts.

Here, the opposite foot is considered to be the foot in contact with the ground at the beginning of step 1. This subdivision can be seen in figure 2.1 (top). Even if any event could be considered to define the gait cycle, it is usual to choose the instant at which one foot contacts with the ground (initial contact). For the sake of simplicity, throughout this document, this event is considered to be the initial contact of the left foot.

The most simple subdivision of the gait cycle is introduced by Ducroquet *et al.* in 1965 [Ducroquet et al., 1965], see figure 2.1 (bottom). According to this division, the events that divide the different phases are the different foot contact and foot leaving the ground. The gait cycle is then divided into four phases:

1. Double Support Phase: both feet are in contact with the ground, the posterior lower limb extends.

2. Single Support Phase: the posterior lower limb leaves the contact with the ground, oscillates around the hip et becomes the anterior lower limb.

3. Double Support Phase: the new anterior lower limb re-establishes the contact with the ground.

4. Single Support Phase: the anterior lower limb supports the body's weight while the other lower limb is on swing phase.
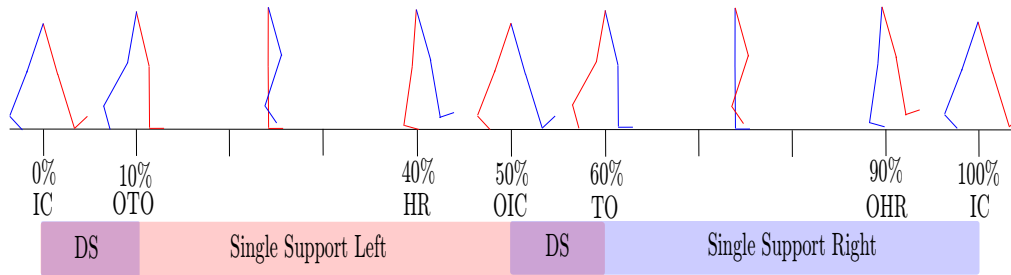
Figure 2.1: Gait cycle dvision: temporal division with gait events (top) and the division according to Ducroquet *et al.* [Ducroquet et al., 1965] (bottom). Red and blue colours correspond to left and right sides, respectively. Violet bands correspond to double support phases, blue and red bands correspond to right and left single support phases, respectively.

The double and single support phases succeed each other, alternating the swinging limb.

Besides its phases and important events, the walking routine can be analysed throughout some parameters divided as: spatio-temporal parameters, kinematics, dynamics and balance. In the following, these different types of parameters are presented.

2.1.1 Gait Spatio-Temporal Parameters

Spatio-temporal parameters, as its name indicates, can be divided into two categories: the step parameters, related to spatial configuration, and the time related parameters.

Spatial parameters   The spatial parameters are used to describe distances travelled by the feet during the gait cycle. These are:

- **stride length** - total distance covered by the left (or right) foot during a gait cycle. It includes two **step lengths**: left and right;

- **(left) step length** - distance measured from the anterior right foot to the posterior left foot in the displacement direction, see figure 2.2. The definition of the right step length follows the same logic;

- **(left) step height** - maximum height reached by the left foot during its displacement. The maximum toe height is considered. The definition for the right side is likewise;

- **step width** - sidewards distance between the two feet;

- **foot progression angle** - foot angle measured with respect to the displacement direction.

These parameters, with the exception of the step height, can be seen in figure 2.2.
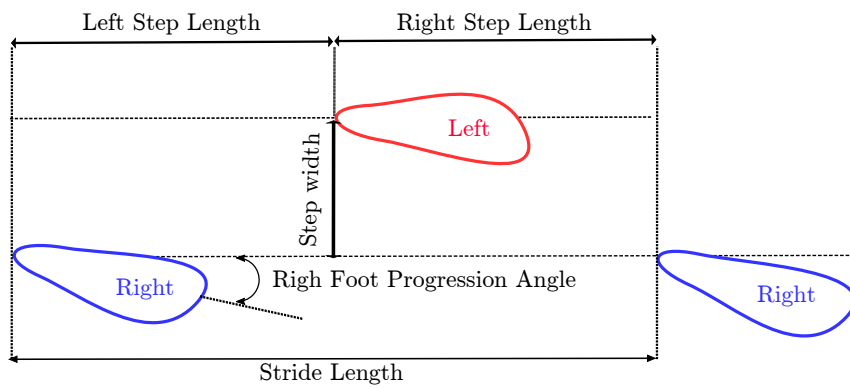
Figure 2.2: Terminology used to describe the foot placement on the ground.

Temporal parameters   The temporal parameters are used to determine and divide the temporal events of a gait cycle. These are:

- **cadence** - number of steps taken in a given time, usually minutes.

- **cycle time** - total duration of a gait cycle.

- **double support** - time period during which both feet are in contact with the ground.

- **single support** - time period during which only one foot is in contact with the ground.

The **gait speed** accounts for the time it takes to travel a certain distance. Here, the distance is set to be the stride length, and therefore, the time is the cycle time. So, gait speed is defined here as the quotient between stride length and cycle time. A different, but equivalent definition could be used by choosing a different reference distance.

2.1.2 Kinematical Parameters

Kinematics is the study of motion without considering the forces and moments that produce that motion. Kinematics measures the motion by means of linear and angular displacements, velocities and accelerations.

In the case of the walking activity, the system in study is the human body. This is a complex musculoskeletal system, composed of bodies, linked together by joints. Around this joints, ligaments and muscles can be found. However, for kinematic measures, the human body is reduced to its segmental parts.

Modelling the human body   It is usual to represent the human multibody system as a tree structure, where the different body parts are represented by different segments, linked together by joints. The number of segments used to represent the human body may vary. For instances, the foot, composed of several bones and joints, is represented with a three segment modelling in the Oxford Foot Model [Carson et al., 2001], but it is divided into nine different segments in the modelling presented in the work of MacWilliams *et al* [MacWilliams et al., 2003]. It is clear that the number of segments directly impacts the number of joints of the model. The number of segments used to describe the human body depends on the degree of precision to be achieved and the object of the study. In this work, the different body parts are represented by rigid segments.

Besides the number of segments, the modelling of the joints is also important. Usually, the joints present between one (hinge joint) and three (ball and socket joint) degrees of freedom in rotation. However, some human joints are much more complex than a simple gathering of concentric rotations. It is the case of the knee, for instance, that can have some sliding motion, when it is flexed, but not when extended [Kapandji, 1994]. For the sake of simplicity, the joints are from now on considered with only pure rotational movements.

Since different models can be made to represent the human joint motion, in the biomechanical field a standard for reporting kinematics has been developed by Wu *et al.* [Wu and Cavanagh, 1995, Wu et al., 2002, Wu et al., 2005]. The model used to describe the human body kinematics in this work is a close adaptation of the International Society of Biomechanics standard [Wu and Cavanagh, 1995, Wu et al., 2002, Wu et al., 2005] and can be found in figure 2.3[1].

---

[1]The detailed description of the model is in Chapter 3.
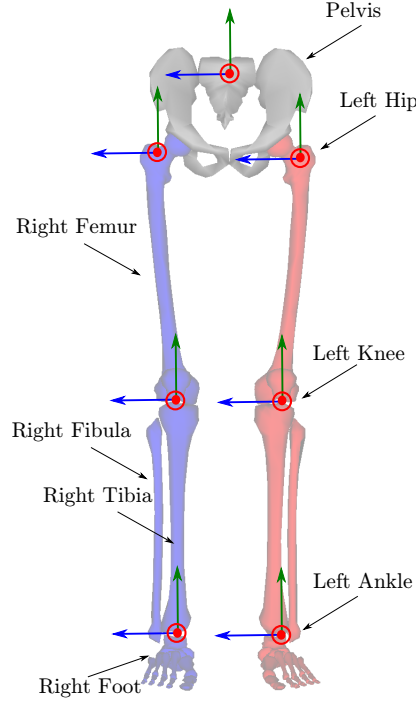
Figure 2.3: Rigid body model for reporting kinematics for the lower limb: segments and joints that describe the lower body from the pelvis to the feet. To each body part, a reference frame its attached at the joint level. z axis in blue goes right, x axis in red goes forward, and y axis in green goes up.

Even though only the lower body is shown, the upper body is also modelled and has an impact on the locomotion. To each body part (pelvis, thigh (left and right), shank (left and right), foot (left and right), trunk, head, arm (left and right), forearm (left and right), hand (left and right)) a reference frame is attached. This reference frame allows to describe the body motion, not only with respect to a given inertial frame $\mathcal{R}_0$, but also to describe the segments relative motion (angular joint displacements).

Coordinate systems for angular description   In order to describe the segments relative motion, to each body part, a position $\boldsymbol{p}_j \in \mathbb{R}^3$ and an orientation $R_j \in SO(3)$, with respect to a given inertial frame $\mathcal{R}_0$, are associated, where

$$SO(3) = \left\{ \boldsymbol{R} \in \mathbb{R}^{3\times3} \middle| \boldsymbol{R}^{-1} = \boldsymbol{R}^T, \quad \det(\boldsymbol{R}) = 1 \right\}$$

is the Special Orthogonal Group. With $\boldsymbol{p}_j$ and $\boldsymbol{R}_j$, the pose $\boldsymbol{H}_j \in SE(3)$ of $\mathcal{R}_j$, the frame attached to body part j, with respect to $\mathcal{R}_0$, can be defined, where

$$SE(3) = \left\{ \boldsymbol{H} = \begin{bmatrix} \boldsymbol{R} & \boldsymbol{p} \\ \boldsymbol{0} & 1 \end{bmatrix} \middle| \boldsymbol{R} \in SO(3), \quad \boldsymbol{p} \in \mathbb{R}^3 \right\}$$

is the special Euclidean group.

With this representation, during a walking activity it is possible to describe the full displacement of each segment with respect to the inertial frame $\mathcal{R}_0$, but also to describe the displacement $\boldsymbol{H}_{k,j}$ of segment j with respect to segment k with:

$$\boldsymbol{H}_{k,j} = \boldsymbol{H}_k^{-1} \boldsymbol{H}_j$$

where $\boldsymbol{H}_k^{-1}$ is the inverse of matrix $\boldsymbol{H}_k$.

$\boldsymbol{H}_{k,j}$ is also in $SE(3)$, and so, it is of the form

$$\boldsymbol{H}_{k,j} = \begin{bmatrix} \boldsymbol{R}_{k,j} & \boldsymbol{p}_{k,j} \\ \boldsymbol{0} & 1 \end{bmatrix}$$

where $\boldsymbol{R}_{k,j}$ represents the relative orientation between segments k and j and $\boldsymbol{p}_{k,j}$ represents the local coordinates of segment j in the reference frame of segment k.

When reporting kinematics for medical evaluation purposes, the measurements focus on the joints positions during walking, *i. e.*, the relative orientation between a segment with respect with another, except for the pelvis segment, which is usually reported with respect to a given inertial frame.

In order to report angular positions, one needs to compute these angles from matrices $\boldsymbol{R}_{k,j}$. Lets note $(\vec{Z}, \vec{X}, \vec{Y})$ the coordinate system attached to segment k, and $(\vec{z}, \vec{x}, \vec{y})$ the coordinate system attached to segment j. One of the most usual conventions to report kinematic angles, recommended by the Internationat Society of Biomechanics, is the Euler or Cardan angles convention [Robertson et al., 2013]. Any rotation can be described by three successive rotations of known axes. Lets note $\boldsymbol{R}_Z$, $\boldsymbol{R}_X$ and $\boldsymbol{R}_Y$ the rotation of angles α, β and θ of the reference frame j around axes Z, X and Y, see figure 2.4[2]

Matrices $\boldsymbol{R}_Z$, $\boldsymbol{R}_X$ and $\boldsymbol{R}_Y$ can be expressed as:

---

[2]This chosen convention order ZXY is in accordance with the International Society of Biomechanics standard.
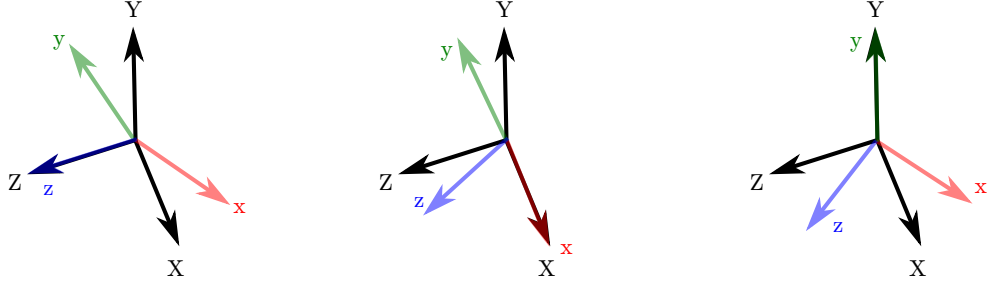
(a) Rotation about the Z-axis. (b) Rotation about the X-axis. (c) Rotation about the Y-axis.

Figure 2.4: Euler angles rotation.

$$\boldsymbol{R}_Z = \begin{bmatrix} 1 & 0 & 0 \\ 0 & \cos(\alpha) & \sin(\alpha) \\ 0 & -\sin(\alpha) & \cos(\alpha) \end{bmatrix} \quad \boldsymbol{R}_X = \begin{bmatrix} \cos(\beta) & 0 & -\sin(\beta) \\ 0 & 1 & 0 \\ \sin(\beta) & 0 & \cos(\beta) \end{bmatrix} \quad \boldsymbol{R}_Y = \begin{bmatrix} \cos(\theta) & \sin(\theta) & 0 \\ -\sin(\theta) & \cos(\theta) & 0 \\ 0 & 0 & 1 \end{bmatrix}$$

And so, matrix $\boldsymbol{R}_{k,j} = \boldsymbol{R}_Y \boldsymbol{R}_X \boldsymbol{R}_Z$ is

$$\begin{bmatrix} \cos(\beta)\cos(\theta) & \cos(\theta)\sin(\beta)\sin(\alpha) + \sin(\theta)\cos(\alpha) & \sin(\theta)\sin(\alpha) - \cos(\theta)\sin(\beta)\cos(\alpha) \\ -\sin(\theta)\cos(\beta) & \cos(\alpha)\cos(\theta) - \sin(\alpha)\sin(\beta)\sin(\theta) & \sin(\theta)\sin(\beta)\cos(\alpha) + \cos(\theta)\sin(\alpha) \\ \sin(\beta) & -\cos(\beta)\sin(\alpha) & \cos(\alpha)\cos(\beta) \end{bmatrix}$$

With matrix $\boldsymbol{R}_{k,j}$ expressed like this, and assuming $r^{11} = \cos(\beta)\cos(\theta) \neq 0$ and $r^{33} = \cos(\alpha)\cos(\beta) \neq 0$, then, α, β and θ can be computed as:

$$\alpha = \tan^{-1}\left(\frac{-r^{32}}{r^{33}}\right), \quad \beta = \tan^{-1}\left(\frac{-r^{31}}{\sqrt{(r^32)^2 + (r^33)^2}}\right), \quad \theta = \tan^{-1}\left(\frac{-r^{21}}{r^{11}}\right)$$

Therefore, providing that the means to compute these matrices exist, the relative motion of bodies can be expressed.

Anatomical Planes of Reference Even though we all walk in our own way, patterns of progression of lower limb's joints during a gait cycle arise, making it possible to define a standard non-pathological gait. This progression can be characterized according to the three anatomical planes of reference, see figure 2.5:

- Sagittal ($X - Y$ plane) - dividing the body into left and right parts;

- Frontal/Coronal ($Y - Z$ plane) - dividing the body into anterior (front) and posterior (back) parts;

- Transverse/Horizontal ($Z - X$ plane) - dividing the body into upper (superior) and lower (inferior) parts.
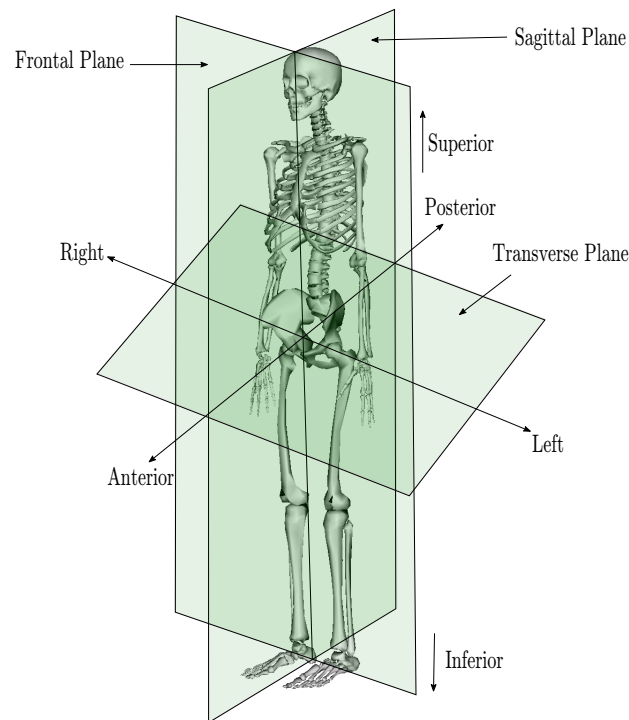
Figure 2.5: Anatomical planes of reference.

Moreover, the next terms can be used to describe relationships within a single part of the body:

- Medial - towards the midline of the body. E.g.: The big toe is on the medial side of the foot.

- Lateral - away from the midline of the body. E.g.: The little toe is on the lateral side of the foot.

- Proximal - towards the rest of the body. E.g.: For a limb, the proximal part is that nearest to the trunk.

19

- Distal - away from the rest of the body. E.g.: The toes are the distal part of the lower limb.

Angular displacements   When describing human walking kinematics, frequently, only the angular displacements of the lower limbs' joints are of interest. These are:

- Flexion/Extension: movements in the sagittal plane, where the distal segment increases/decreases the angle relatively to the proximal segment. In the foot, these movements are called dorsiflexion and plantar flexion, respectively.

- Abduction/Adduction: movements in the frontal plane, where the distal segment moves away/towards the midline of the body relative to the proximal segment.

- Internal/External rotations: movements in the transverse plane, also called medial/lateral rotations.

The movements of the pelvis are usually reported with respect to the given fixed frame $\mathcal{R}_0$, and are:

- Anteversion/Retroversion: movements in the sagittal plane.

- Internal/External bending: movements in the frontal plane.

- Internal/External rotations: movements in the transverse plane.

2.1.3   Dynamical Parameters

Another important aspect of human walking is dynamics. Dynamics is the study of motion by considering the forces and moments that produce it. In the case of the walking motion, the most reported dynamic measures are the Ground Reaction Force, the Joint Torque and the Joint Power.

Ground Reaction Force (GRF)   When walking, the body exerts a force on the ground, through the body parts in contact with it. This force generates an equal and opposite reaction force of the ground on the body. This force, called the Ground Reaction Force (GRF), can be represented by a single equivalent force acting on a single point of the ground [Robertson et al., 2013], see figure 2.6.
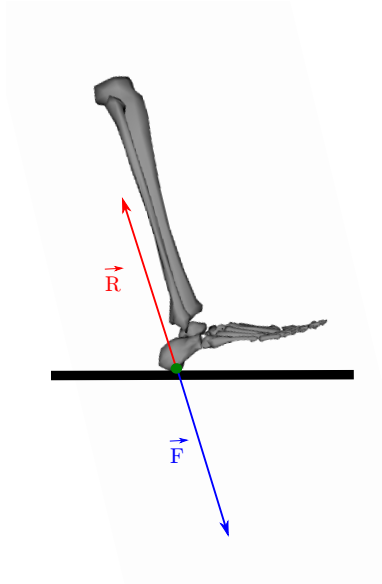
Figure 2.6: Ground Reaction Forces - $\vec{R}$.

The vertical component of the GRF is always positive, since the ground can only push the feet up, not down. However, the other two components can be either positive or negative. Since the GRF supports body against gravity, the magnitude of the vertical component of the GRF is considerably larger than the other two components [Baker, 2013].

Joint Torque While forces produce linear accelerations, moments produce rotational accelerations. Joint Torques emerge when some force is exerted at some distance of the joint in question.

The usual reported joint torques are the result of all the internal structures acting across the joint [Baker, 2013]. When the joint is moving within its range of motion, its torque is almost exclusively due to the muscles acting across the joint. Near the limits of the range of motion, stretching of ligaments and bone geometry may also have an impact on joint torque.

Joint torques can be computed from the equations of motion, that relate both joint kinematics, gravitational and centrifugal forces, external disturbances (ground reaction forces) and inertial forces[3]. In order to use the equations of motion, it is then necessary to attach an anthropometric model to the system. There are many anthropometric mod-

---

[3]See the next chapter for more details

els available in the literature, [Hanavan, 1964, De Leva, 1996, Ganley and Powers, 2004, Dumas et al., 2007], and the choice of the model depends on the accuracy needed in the calculations, and the data available.

The joint torque computed gives information about the combined action of the different muscles acting on a specific joint. However, the contribution of each muscle to the joint motion cannot be deducted from the internal joint torque, only the dominant muscle group (antagonist or agonist[4]).

The knowledge of muscle actioning is still a subject of active research and its out of the scope of this work.

Joint Power   Assuming that there is a unique actuator generating the motion at each joint, joint power is defined as the product of joint angular velocity and joint torque. It is possible to establish a normative data within healthy subjects and therefore identify locomotion disorders through joint power as well.

2.1.4   Balance Parameters

Aside from kinematics and dynamics, another important aspect of human locomotion is balance. In automatic control, balance stands for the case where a system does not evolve unless a change is made on the inputs. In the case of a standing still position or movement, this definition of balance is no longer adapted. For instance, the standing still position is possible thanks to a series of small movement adjustments [Bidaud et al., 2009].

In human motion, balance states can be divide in two main categories: static balance (like in the case of the standing still position) and dynamic balance (like in the case of a walking activity).

The most usual methods to analyse et evaluate these balance states usually rely on the analysis of some characteristic points. These are presented next.

Center of Mass (CoM)   The Center of Mass (CoM) of a body is considered to be the point of the body where the total mass of the body can be assumed to be concentrated [Whittle, 2007]. The position P_{CoM} of the center of mass of the human body is calculated

---

[4]Antagonist muscles are those who oppose to a specific movement and agonist muscles are those who help the motion to occur by contracting.

as the average weighted sum of the center of mass of all the segments composing body:

$$\boldsymbol{P}_{CoM} = \frac{\sum_{i=1}^{N} m_i \boldsymbol{P}_{CoM}^i}{\sum_{i=1}^{N} m_i}$$

where N is the number of segments composing the body, m_i the mass of body segment i, and $\boldsymbol{P}_{CoM}^i$ the position of the center of mass of segment i.

Lets define the support polygon as the convex envelope containing all the contact points between the feet and the ground. In the case of a standing position, if the projection of the CoM on the ground is outside this polygon, then there is automatically a loss of balance. This is only the case for static poses.

Center of Pressure (CoP)   The Center of Pressure (CoP) is the point on the ground where the net moment of all forces acting on the body is zero in the horizontal axes [Sardain and Bessonnet, 2004].

Lets consider a point C on the ground. If the ground reaction effects $\left(\boldsymbol{F}_{GRF}^C, \boldsymbol{M}_{GRF}^C \right)$ are known at point C, then the position $\boldsymbol{P}_{CoP}$ is defined as:

$$\boldsymbol{M}_{GRF}^{\boldsymbol{P}_{CoP}} = \boldsymbol{C}\boldsymbol{P}_{CoP} \times \boldsymbol{F}_{GRF}^C$$

By definition of the CoP: $\boldsymbol{M}_{GRF}^{CoP} \times \boldsymbol{n} = \boldsymbol{0}$, with $\boldsymbol{n}$ the normal vector to the ground.

If $\boldsymbol{P}_{CoP}$ is near the support polygon, then a fall is induced and balance is lost.

Zero Moment Point (ZMP)   When it exists, the Zero-Moment Point (ZMP), introduced in [Vukobratović and Juricic, 1969], is defined as the point on the ground where the net moment of all forces acting on the body is zero in the horizontal axes. Lets note $\left(\boldsymbol{F}_{GI}^{CoM}, \boldsymbol{M}_{GI}^{CoM} \right)$ the inertial and gravity effects. The inertial and gravity effects at any point A, may be computed as:

$$\boldsymbol{F}_{GI}^A = m\boldsymbol{g} - m\boldsymbol{a}_{CoM}$$
$$\boldsymbol{M}_{GI}^A = \boldsymbol{A}\boldsymbol{P}_{CoM} \times m\boldsymbol{g} - \boldsymbol{A}\boldsymbol{P}_{CoM} \times m\boldsymbol{a}_{CoM} - \dot{\boldsymbol{H}}_{CoM}$$

where $\boldsymbol{g}$, $\boldsymbol{a}_{CoM}$ and $\dot{\boldsymbol{H}}_{CoM}$ represent the gravity acceleration vector, the CoM acceleration, and the rate of angular momentum at the CoM, respectively.

By definition of the ZMP: $\boldsymbol{M}_{GI}^{ZMP} \times \boldsymbol{n} = \boldsymbol{0}$, with $\boldsymbol{n}$ the normal vector to the ground.

It is worth noting that when the ZMP exists it coincides with the Centre of Pressure

(CoP)[5]. The main difference between the ZMP and the CoP is the method of computation. In fact, the CoP is computed taking into account the ground reaction forces, while the ZMP is calculated thanks to inertial and gravity effects. A review on the differences between ZMP and CoP can be found in [Sardain and Bessonnet, 2004]. Like in the previous case of the CoP, if the $\boldsymbol{P}_{ZMP}$ is near the support polygon, then a fall is induced and balance is lost.

The parameters and measures just presented have a standard pattern when it comes to healthy subjects. Therefore, by analysing them in Cerebral Palsy Children and comparing them to Typically Developed Children, locomotion disorders can be detected. In the next section, means for the analysis and treatment of locomotion disorders are presented.

2.2 Analysis and treatment of CP locomotion disorders

Nowadays, in order to help therapeutic analysis and decision, two main type of exams are performed:

- a physical examination, which allows the establishment of an analytical evaluation of the orthopaedic state of the different anatomical regions considered;

- a Clinical Gait Analysis (CGA), which takes advantage of biomechanical parameters (kinematics, kinetics and electromyography (EMG)) to answer medical needs. Its purpose is to identify, quantify and understand the gait abnormalities found in a specific patient, in order to help choosing the most appropriate treatment. As it helps to identify the underlying causes of the gait disorders, the CGA helps improving the therapeutic recommendations [DeLuca et al., 1997, Kay et al., 2000a, Kay et al., 2000b]. In France, this exam is part of the medical acts recognized by the health insurance (act NKQP003), and increasingly more centres of CGA are in activity or in project.

In a standard CGA exam, reflective markers are placed on the patient according to a chosen representation model. A set of electrodes to capture muscle activity during gait is also placed. The patient is then asked to walk on a corridor, where force plates may

---

[5]It should be noted that only movement on horizontal ground is considered in this work.

be in place. The trajectory of the markers in space, which allows the computation of kinematics of section 2.1.2, activity of muscles and ground reaction forces and moments may be recorded, see figure 2.7. A video can also be captured at the same time. The recorded data is then processed, by the recording software or by a personal developed software, and a report is made. Gait abnormalities and potential causes can then be found by analysing the data.

Inverse kinematics of the lower limbs and 3D markers data.

EMG Data.

Ground Reaction Forces measured by Forceplates.

Video camera.
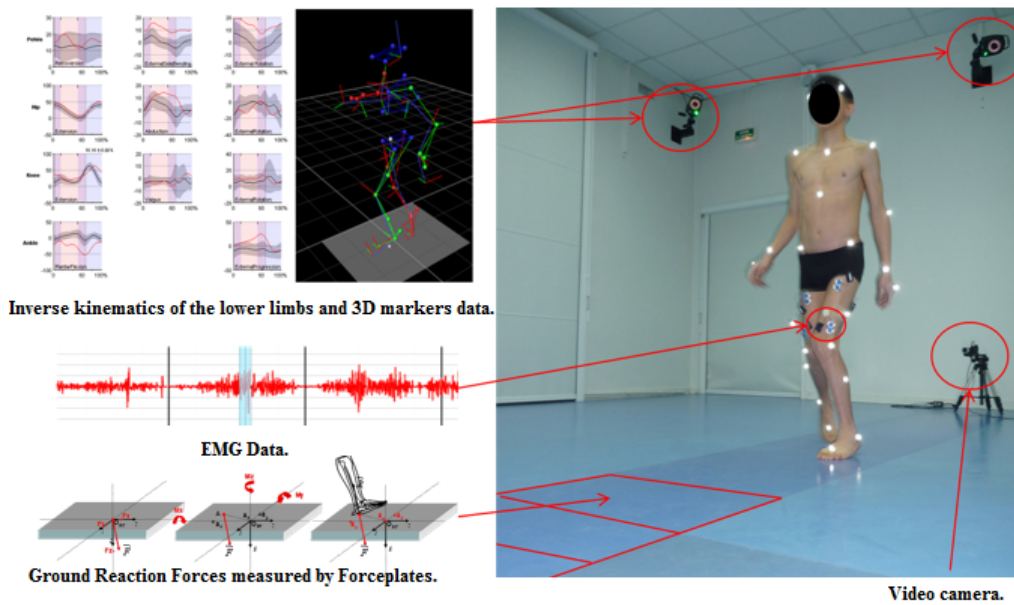
Figure 2.7: Clinical Gait Analysis set-up at Ellen Poidatz Foundation. (Courtesy of E. Desailly [Desailly, 2008].)

In figure 2.8, an example of a kinematics report issued from a CGA exam performed at Ellen Poidatz Foundation can be found. If a reference norm is provided [6], different gait abnormalities can be determined by analysing the data. For instance, at the knee level, in the sagittal plane, an excessive flexion at initial contact is present, and the knee flexion peak is delayed.

Even if the clinical interest of CGA is no longer to be proved [Simon, 2004], certain authors [Noonan et al., 2003, Skaggs et al., 2000] pointed out the variability of interpretation between experts leading sometimes to different therapeutic recommendations. This interpretation, which consists on relating the data issued from the CGA between them and

---

[6]It can be calculated from the mean walking patterns of healthy subjects, if these are available, for instance.
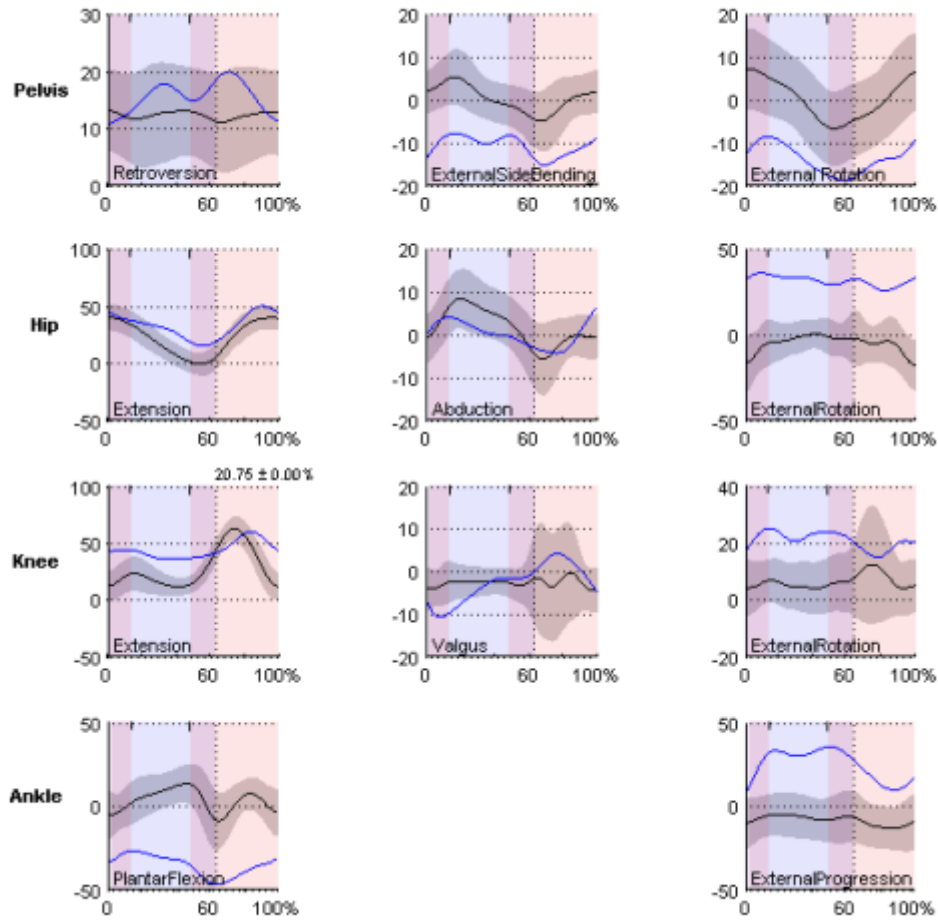
Figure 2.8: Kinematics for the right lower limb (blue curves). Angular amplitudes are in degrees and are represented as a function of the normalized time by percent of the gait cycle. The kinematics's mean data for healthy subjects is given in black with the confidence interval of two standard deviations given in gray. Dark pink, blue and light pink backgrounds represent double support, right single support and left single support phases, respectively. The columns represent, from left to right, the motion in sagittal, frontal and transversal planes, respectively.

the clinical data issued from the physical examination, is still a difficult task. The expert, usually a physician, interprets the data using the knowledge acquired during his training and his own experience to identify the underlying causes of the observed disorders, and, thereby, take a therapeutic decision.

2.2.1   Most common surgeries among CP

Even though the therapeutic decision is not straight forward and depends on the patient data, some surgeries are common among Cerebral Palsy children. They can be divide in two groups: muscle/tendon and bone surgery.

Examples of common surgeries performed on the muscle/tendon complex, are: Psoas lengthening, Hamstrings lengthening, Rectus Femoris Transfer, . . .

Examples of common surgeries performed on the bones are: Femoral Derotation Osteotomy, Femoral Extension Osteotomy, . . .

In what follows, a brief and schematic description of the therapeutic indications and expected outcomes for these procedures is made.

Psoas lengthening   Psoas is a muscle that relies the lumbar spine and the pelvis to the femur, passing in front of the hip.

The surgical procedure of psoas lengthening is recommended when there is:

- a deficit in the hip extension at physical examination;

- an excess of anteversion of the pelvis during walking (in certain cases);

- a deficit in the hip extension at the end of the single support phase.

This procedure is expected to improve hip extension.

Hamstrings lengthening   The hamstrings are bi-articular muscles inserted over the ischium, and terminating in the tibia and the fibula. They cross the hip and the knee from behind, so their maximum length may limit the combined movement of hip flexion and knee extension.

The surgical procedure is recommended when these muscles are contractured (too short), as they may limit the knee extension at initial contact.

This procedure is expected to improve knee extension at initial contact.

Rectus Femoris transfer   The rectus femoris is part of the quadriceps muscle group. It originates on the anterior inferior iliac spine and terminates on the top of the patella and on the tibial tuberosity. It crosses the hip joint and is a knee extensor.

The surgical procedure of rectus femoris transfer consists in the transfer of the rectus femoris insertion from the superior face of the patella onto the muscle tendon of the

gracilis, behind the knee flexion axis. Theoretically, the muscle becomes a knee flexor instead of a knee extensor.

This procedure is recommended when there is a decrease associated or not to a delay in the peak knee flexion at swing phase, and is expected to improve knee flexion at swing phase.

Femoral Derotation Osteotomy   The femoral derotation osteotomy consists in transversely sectioning the femur, in order to rotate the distal segment with respect to the proximal segment by a certain angle. An ostheosynthesis is then realized in the chosen rotation.

The surgical procedure is recommended when there is an internal hip rotation during walking associated to an excessive femoral anteversion.

This procedure is expected to shift the rotational mobility sector of the hip if there is a limit in the external rotation of the hip, and also to stabilize the hip in a more balanced range of motion, by improving the lever arm of the hip abductors muscles.

Femoral Extension Osteotomy   The femoral extension osteotomy consists in sectioning the femur across its front just above the knee. A wedge of bone is then cut out of the femur, the leg is straightened and a metal plate and screws are used to hold it.

The surgical procedure is recommended in the presence of a knee flessum[7].

This procedure is expected to:

- shift the extension mobility sector of the knee;

- improve the knee extension during the support phase, in particular, during the single support.

An extensive review on the identification and treatment of Cerebral Palsy children gait pathologies can be found in [Gage et al., 2009].

Even though the recommendations are quite consensual between physicians, the threshold for these recommendations do not agree between experts. Besides, the patients specificities and the association of surgeries make it difficult to predict the resulting outcome.

---

[7]Knee flessum means there is a limit in the extension of the knee.

2.3 Statistical prediction of surgical outcomes

Given the different thresholds for the recommendations and the difficulty to predict the result of surgeries association, researchers concentrate on how to improve these recommendations. A common approach found in the literature for this improvement is statistics. This is the approach used in the other part of the project in which this thesis take part, as explained in the introduction.

With the use of statistical tools, researchers are able to predict, within a certain range of accuracy and parameters, the expected outcome of a surgery. Two main categories of results can be established: qualitative and quantitative studies.

Qualitative studies In this first category of studies, the works of [Hicks et al., 2011, Reinbolt et al., 2009, Schwartz et al., 2013, Sebsadji et al., 2012] can be cited.

In the work of Hicks *et al.* [Hicks et al., 2011], the prediction study is narrowed down to one condition, the crouch gait. As the surgical outcomes for these patients may be variable, they develop a regression model able to predict if kinematics is improved or not with over 70% accuracy, given biomechanical variables and other subject measures taken during CGA and physical examination.

In this same category, studies concerning a unique surgical gesture can be found [Reinbolt et al., 2009, Schwartz et al., 2013, Sebsadji et al., 2012].

In [Reinbolt et al., 2009], only the rectus femoris transfer is considered. This surgery is a common treatment for stiff knee gait in children with cerebral palsy, but the improvement in knee motion afterwards is not always the same. Using a predictive model based on some preoperative CGA measurements, the authors reach a 88% accuracy in predicting if the outcome of rectus femoris transfer is good (improvement of knee motion), or bad, providing therefore a tool able to help indications for rectus femoris transfer.

Another surgery that interests Schwartz *et al.* [Schwartz et al., 2013] is psoas lengthening. Based upon preoperative data extracted from a database, the authors develop a criteria able to predict the outcome of a limb for this surgery. The authors estimate that the application of the criteria may increase the rate of good pelvis-hip outcome in psoas lengthening from 58% to 72% among children with diplegia who undergo SEMLS with a psoas lengthening.

In the study of Sebsadji *et al.* [Sebsadji et al., 2012], using Support Vector Machines [Burges, 1998] after PCA, the authors classified good or bad results of hamstring lengthening surgery in cerebral palsy.

Quantitative studies   On the second category, quantitative studies, the authors focus not in a good or bad classification, but in the prediction of gait parameters, like in the works of [Hersh et al., 1997, Sullivan et al., 1995], and more recently [Galarraga C. et al., 2016, Niiler et al., 2007].

As before, some researchers concentrate on a unique surgical gesture, Rectus Femoris Transfer, as in the case of [Hersh et al., 1997, Sullivan et al., 1995].

In the work of Hersh *et al.* [Hersh et al., 1997], using neural networks, the authors developed a method to predict the outcome of the rectus femoris transfer surgery in children with cerebral palsy. In order to do that, authors use a large database for pre and postoperative gait patterns for specific surgical procedures, and are able to predict the postoperative knee and hip angles, with great accuracy, for all the patients in the training set.

Using a regression analysis, Sullivan *et al.* [Sullivan et al., 1995] develop a method to visualize the expected gait patterns outcome of rectus femoris transfer. Even though the small size of the data set used (15 patients), the results of this approach are encouraging.

In more recent results [Galarraga C. et al., 2016, Niiler et al., 2007], authors predict kinematics given a combination of surgical gestures.

In the work of Niiler *et al.* [Niiler et al., 2007], the authors use a multivariate jack-knifed linear regression to predict the change in the knee range of motion due to concurrent surgeries on rectus femoris transfer. Four groups of surgery are considered and the only meaningful parameter found to influence postoperative knee range of motion is preoperative knee range of motion. It is considered a useful predictor of outcome for the rectus femoris transfer surgery.

Using statistical machine learning techniques, Galarraga *et al.* [Galarraga C. et al., 2016] simulate the effect of SEMLS on kinematics of cerebral palsy children. Postoperative kinematics of cerebral palsy children are predicted with an error always smaller than the best naive predictor error, given preoperative kinematics, physical examination and the surgical procedure combination. Moreover, the method allows the estimation of the impact of each surgical procedure in the postoperative outcome.

Even though statistical studies provide helpful information for the therapeutic choice, they only concentrate on a small group of variables, and only on kinematics. Moreover, they

may present a lack of realism, in the case of parameters prediction, since physical models are not considered.

2.4   Tools for the simulation of human walking

Parallel to statistical analysis, different software solutions for the simulation of normal and pathological gait have arisen. These software solutions decompose in publicly available [Damsgaard et al., 2006, Delp et al., 2007, Delp and Loan, 2000], custom made software [Ady et al., 2013, Krogt et al., 2010, Lengagne et al., 2011], and hybrid approaches [Galdeano et al., 2012, Park et al., 2016].

Publicly available software solutions   The public software solutions described hereafter have mostly been developed by the biomechanics community, where the needs to evaluate and understand the human locomotion are of great importance.

One of the first software to appear is the SIMM software [Delp and Loan, 2000]. Introduced in the early 1990s, it allows users to create, alter, and evaluate models of different musculoskeletal structures, simulate movements such as walking, cycling, running and stair climbing. However, the tools for analyzing the results of dynamic simulations are limited, and no assistance is provided for the computation of muscle excitation that produce movement. Besides, being a commercial software, full access to source code is not provided, which limits the extension of capabilities by the users.

In order to overcome SIMM's limits, an open-source software, OpenSim is developed [Delp et al., 2007]. This software allows to create subject-specific models and muscle-driven simulations. Given motion capture data, the movement of markers, and other information like ground reaction forces, can be tracked, allowing the computation of the muscle forces that come along. It is designed as a cooperative platform for researchers around the world, as users libraries can be exchanged and improved by other users. Some of the OpenSim software applications can be found in [Reinbolt et al., 2011, Seth et al., 2011].

Another software available for muscle-driven simulations is the Anybody Modeling System [Damsgaard et al., 2006]. As in OpenSim, the model can be scaled to fit a subject, and the motion is reconstructed by tracking marker's movements. Muscle recruitment can be simulated by inverse dynamics.

It should be noted that the Clinical Gait Analysis introduced early, that relies on motion capture systems, also constitutes a mean for simulate the human walking.

Custom made solutions   Along with the development of software solutions, some researchers develop their own tools to simulate pathological gait [Ady et al., 2013, Krogt et al., 2010, Lengagne et al., 2011]. This is done specially to treat a single problem, and not in a perspective of developing a more generalized tool.

In the work of Ady *et al.* [Ady et al., 2013], synthesis of pathological gait is used to evaluate the use of a walking aid device. In this work, the authors use nonlinear optimization to simulate pathological and cane assisted gaits, in order to analyse the beneficial impact of the use of an active cane in impaired gaits. The study is conducted only in the sagittal plane.

With a different purpose, van der Krogt and colleagues [Krogt et al., 2010] use a planar model to simulate different kinds of crouch gaits. This is done in order to see if a cause-relationship can be found between a crouched posture and the development of stiff-knee gait.

As for Lengagne *et al.* [Lengagne et al., 2011], leg impairments are simulated for the HRP-2 robot. The walking gait synthesized is then analyzed, and different energy consumption are found for different leg impairments.

Even though these works overcome the drawback of the need of motion capture data to simulate the movement, they all present a lack of realism. This lack of realism can come from oversimplified models [Ady et al., 2013, Krogt et al., 2010], or by the use of a robotic model not necessarily presenting human inertial properties [Lengagne et al., 2011].

Hybrid approaches   Hybrid approaches rely on a set of motion capture data to generate walking motions. The difference with these approaches is that the data serves of guidance and can be applied to different manikins without loss of generalization.

In the work of [Galdeano et al., 2012], the authors use data from the trajectory of the CoM of a human subject and its relative feet position to generate walking motion for a humanoid robot simulator. The generated motion is human resembling, and the pelvis trajectory follows that of the human data used, when a correction of the CoM's altitude is applied. The walking pattern generated is human-like, however, no contact forces are considered in this work, only kinematics. The results are nevertheless encouraging and the authors expect to improve them with the introduction of a dynamical model.

In the work of [Park et al., 2016], the authors are able to generate different motions given a set of discrete contacts. A three-phase optimisation algorithm is used to ensure that the generated motion between these discrete states is collision-free, smooth and satisfies dynamic balance constraints. The method presented is faster than similar approaches described in the literature and is adaptable to different motions like climbing or walking. However, the jerk minimisation used, which imposes zero velocities and accelerations conditions between the discrete states, may generate not so natural motions. Yet, the produced motions are dynamically stable and quickly obtained.

At the best of our knowledge, currently, the most advanced tool for the simulation of human walking may be Santos [Abdel-Malek and Arora, 2013], developed by the Virtual Soldier Research group at the University of Iowa since 2003 for US Army applications. It relies on an optimization-based approach to predict motion, by using human performance measures[8] as objectives of the functions to be optimized. Results with the Santos platform are quite impressive, yet it is not available to public use.

The means may be different, but the purpose of all these researchers is the same: understand the cause-effect relationship behind certain gait pathologies and/or impairments through simulation of human gait. At the best of our knowledge, a simulation tool capable of predicting surgery outcomes has not yet been made available to public use.

2.5 Proposed Approach

In this chapter, a review on the principal parameters and quantities that allow the definition and evaluation of the human walking activity is done, section 2.1.

The Clinical Gait Analysis for the evaluation of human walking is presented in section 2.2, together with the most common surgeries performed in Cerebral Palsy Children.

In sections 2.3 and 2.4, methods for the prediction of some surgeries outcomes and for the simulation of walking are presented.

Despite the different solutions available to treat the problem of simulating walking motions, none fully fulfils the requirements of this project. Indeed, this thesis aims at developing a simulation tool that:

---

[8]These performance measures include different kinematic and dynamical criteria such as time minimization, torque minimization, energy minimization, etc.

- is able to measure most of the parameters presented in sections 2.1.2 ,2.1.3 and 2.1.4;

- guarantees the physical consistency of all the measurements, specially the dynamical ones;

- ensures the realism of simulated walking motion, otherwise the results of the benefit assessment are not reliable;

- is able to automatically generate walking motions, otherwise the development of each simulation is excessively time consuming;

- is able to give a straightforward interpretation of the results, because the tool is intended to help the surgeon. The comparison between the results must, therefore, be easily done.

Statistical means may lack of realism, since no physical model is attached to the predictions. In the case of software solutions, on one hand publicly available software solutions, even though presenting high realism, demand great input data, making the development of the simulation time consuming. On the other hand, more robotic solutions are at this point not sufficiently close to the human representation. Nevertheless, some hybrid methods start to approach the resolution of the human walking motion generation problem.

Therefore, in this work, a mixed solution using robotic methods for walking pattern generation and real human data is used. The control of a walking motion is done thanks to a modified version of the Linear Quadratic Programming (LQP) controller developed by Salini *et al.* [Salini et al., 2010, Salini, 2012]. Indeed, this controller is primarily developed to control very slow motions for humanoid systems. This walking motion is simulated in the dynamic simulation framework XDE [Merlhiot et al., 2012].

The lack of human resemblance in terms of motion for the robotics approach is dealt with the implementation of a virtual mannequin with the anthropometric measures of that of a human. Further on this document, integration of human data for the walking motion control is also done.

In the next chapter, the original version of the LQP controller used is presented. A first virtual mannequin, intended to numerically represent a human being is developed. Some results on walking motions are presented.

FRAMEWORK FOR THE SIMULATION OF A WALKING MOTION FOR A VIRTUAL HUMAN

In this chapter, a simulation framework for the generation of walking motions for a virtual human is presented. Recall that this thesis aims at developing a tool which enables:

1. the simulation of human walking, both healthy and pathological;

2. an automatic straightforward assessment of the simulated motion, in order to compare the simulation with the real motion, and to easily study the impact of changes of the model and/or actuation on the walking motion.

Therefore, the developed tool must:

- be able to automatically generate different walking motions for a variety of subjects;

- be able to quantify the human-likeliness (which needs to be defined) of walking motion, and therefore, be able to take into account the different parameters that characterize human walking, as described in the previous chapter (section 2.1);

- ensure the physical consistency of all the measurements, otherwise any analysis of the simulation is meaningless;

Lets note that for the remaining of the chapter, human data is only used to define the virtual human and to compare simulation motion with real human motion. The issue of human resembling motion is addressed in chapter 4.

The chapter is organized as follows:

- Section 3.1 deals with the XDE Physics Engine, the simulation framework used;

- Section 3.2 presents the LQP-Controller used for the control of the walking motion;

- Section 3.3 presents the results obtained for the walking simulations obtained with the presented simulation tool;

- Section 3.4 summarizes the main ideas of the chapter.

3.1   XDE Physics Engine

To simulate a walking motion for a virtual human, the dynamic simulation framework XDE [Merlhiot et al., 2012] is used. Interactions with its surrounding environment, in this case contacts with the ground, must also be treated.

The virtual human is modelled as a tree structure composed of rigid bodies, linked together by joints. Its displacement is calculated from the displacement of a root body (here the pelvis), called the free-floating base. The displacement of the root is described by the position $p_r \in \mathbb{R}^3$ and orientation $R_r \in SO(3)$ of a reference frame $\mathcal{R}_r$ attached to this body, with respect to a given inertial frame $\mathcal{R}_0$, called the world frame, see figure 3.1. With p_r and R_r, the pose $q_r \in SE(3)$ of $\mathcal{R}_r$ with respect to $\mathcal{R}_0$ can be defined. The associated twist (see [Salini, 2012]) is noted ν_r, and is in $\mathbb{R}^6$.

The free-floating condition imposes that this body is linked to the world frame with a six degrees of freedom unactuated joint. Bodies are considered linked together by revolute joints. Virtual joints are then considered, in order to reproduce a triple rotation (like the hip joint, for instances). For a system composed of n_b bodies linked together by a total of n_j joints (the total number of degrees of freedom of the system, excluding the root), $q_j \in \mathbb{R}^{n_j}$ denotes the vector parametrizing the joint configuration in the joint space. It can then be defined $q = (q_r, q_j) \in SE(3) \times \mathbb{R}^{n_j}$, the generalized coordinates. Thus, the system generalized velocities is defined by $\nu = (\nu_r, \dot{q}_j) \in \mathbb{R}^{6+n_j}$.

The equations of motion for this kind of system can be derived form the Lagrange formalism [Murray et al., 1994] and written as:

$$M(q)\dot{\nu} + n(q,\nu) + g(q) = \begin{bmatrix} 0_6 \\ S\tau \end{bmatrix} + J_c^T W_c \qquad (3.1)$$

where

- M is the mass matrix of the system,
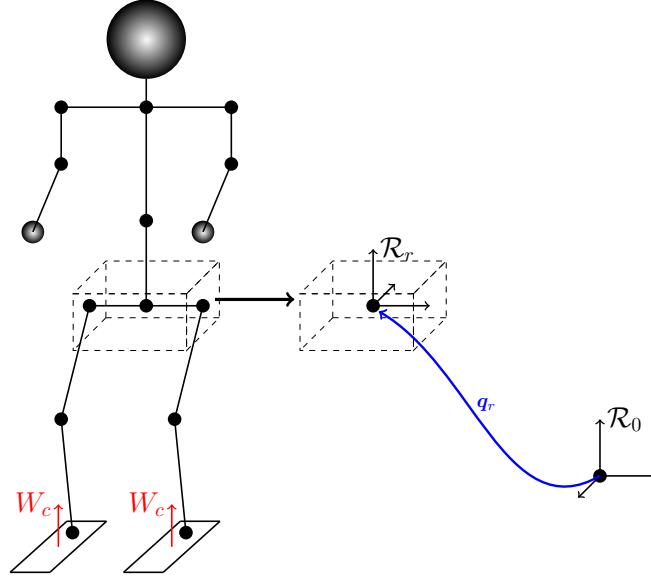
Figure 3.1: Kinematic representation of the virtual human. Its root body is free-floating in a reference inertial frame $\mathcal{R}_0$. W_c stands for the contact wrenches with respect to the ground.

- $\boldsymbol{n}$ is the vector of non-linear effects, regrouping Coriolis and centrifugal ones,

- $\boldsymbol{g}$ is the vector of gravity, in the generalized coordinates space,

- $\boldsymbol{S} \in \mathbb{R}^{n_j \times n_a}$, with $n_a \leq n_j$ being the number of actuated degrees of freedom, is a matrix representing the actuation characteristics,

- $\boldsymbol{\tau} \in \mathbb{R}^{n_a}$ is the actuation vector in the generalized coordinates space,

- $\boldsymbol{J}_c^T$ represents the Jacobian of contacts,

- $\boldsymbol{W}_c$ represents the contact wrenches.

Even though this modelling does not include muscles, equation (3.1) would still be valid if it was the case; the actuation vector $\boldsymbol{\tau}$ would then depend on muscle-related variables, like muscle activations, for instance.

It is worth noting that the modelling presented here assumes multiple simplifications on the virtual representation of a human:

- actuation - as previously seen, human joints can be actuated by multiple muscles, their conjugated action resulting in joint actuation. Considering all the possible

muscular actuations would greatly complefixy our model. Moreover, real data on muscle activation and action at joint level is not easily gathered, and remains an open question in the scientific community.

- joint axis of motion - mobile axis are not considered. This simplifies the motion and the description, and thus simplifies solving the walking motion generation problem.

- the soft tissue artefacts are not taken into account, nor the inertial effects thereby created. These movements are still a subject of research in the scientific community and will not be considered in this work, as bodies are assumed to be rigid.

For the Internal Model used in XDE Physics to be complete, contacts of the manikin with the ground must be handled. Here, they are treated using a simplified version of the Coulomb-Contensou Friction Law [Leine and Glocker, 2003].

In the next subsection, a description of the kinematic structure and the inertial parameters used to create the dynamical tree model in the XDE framework is done.

3.1.1   Kinematic structure and Inertial Parameters

In order to reproduce the human walking behaviour as accurately as possible, the number of degrees of freedom in the virtual manikin needs to be appropriately chosen. Moreover, segment lengths corresponding to those of the subject in study, and corresponding dynamical parameters, such as mass and inertia, are essential.

Body Segment Inertial Parameters model   To personalize the model representing the patient, body segment inertial parameters (BSIPs) and kinematic/geometric properties must be taken into account. These two are closely related, as BSIPs are given according to a specific kinematic model.

Several models are available in the literature to represent human BSIPs like [Hanavan, 1964, Jensen, 1986, Jensen, 1989, De Leva, 1996], and more recently [Ganley and Powers, 2004, Dumas et al., 2007], for example.   Methods to define BSIPs can be classified in three main categories: cadaveric studies [Dumas et al., 2007], scanning and imaging techniques [Jensen, 1986, Jensen, 1989, De Leva, 1996, Ganley and Powers, 2004], and measure methods [Hanavan, 1964].

In this work, the method of Dumas *et al.* [Dumas et al., 2007] is chosen. The studies conducted on children are either for planar analysis [Jensen, 1986, Jensen, 1989] or

recurring to scanning and imaging techniques [Ganley and Powers, 2004], which are not always available, and thus discarded. In the work of Dumas *et al.* [Dumas et al., 2007], differentiation between genders is considered. Even though it represents young adults, this model its still admissible since:

1. studies showed that different BSIPs in children [Ganley and Powers, 2004] and specifically in diplegic cerebral palsy children [Kiernan et al., 2014] do not have a major influence in the inverse dynamics calculation;

2. specific kinematic parameters are more important for the accuracy of the inverse dynamics calculation than BSIPs [Reinbolt et al., 2007].

The choice of the work by Dumas *et al.* [Dumas et al., 2007] relies on the fact that it reports BSIPs in the conventional segment coordinate system [Wu et al., 2002, Wu et al., 2005]. Since the experimental data recorded during CGA exams at the Fondation Ellen Poidatz allows for the calculation of most of this coordinate system, the work by Dumas *et al.* [Dumas et al., 2007] remains easier and reliable to use.

The calculations of the different reference frames mostly follows the ones presented in [Dumas et al., 2007]. For the torso, hand and pelvis reference frames, the alternatives presented in Table 2 of [Dumas et al., 2007] are used. Missing data required some adaptations. These are listed below from the upper to the lower body:

1. The Sellion (SEL) is estimated as the middle of the two head temples.

2. The Head Vertex (HV) is estimated equal to the sellion but with its vertical position 5 centimetres below the sellion.

3. The Lumbar Joint Center (LJC) is estimated by proportion using the data reported on Table 1 of [Dumas et al., 2007].

4. The origin of the torso reference frame is placed at the origin of the pelvis reference frame.

5. The Elbow Joint Center (EJC) is estimated as the middle of the Lateral (LHE) and Medial (MHE) Humeral Epicondyles, with the (MHE) being estimated as:

$$\text{(MHE)} = \begin{cases} \text{(RS)} + \boldsymbol{v}, & \text{if left side} \\ \text{(US)} + \boldsymbol{v}, & \text{if right side} \end{cases} \quad \text{where} \quad \boldsymbol{v} = \begin{cases} \text{(LHE)} - \text{(US)}, & \text{if left side} \\ \text{(LHE)} - \text{(RS)}, & \text{if right side} \end{cases}$$

with (US) the Ulnar Styloid and (RS) the Radial Styloid[1].

6. The middle point of the 2nd and 5th Metacarpal Heads (MH_2 and MH_5) is replaced by MH_3.

7. The Hip Joint Center (HJC) is estimated by proportion using the data reported on Table 1 of [Dumas et al., 2007].

8. The Fibula Head (FH) is replaced by the Lateral Malleolus (LM) in the calculation of the leg reference frame.

9. The Foot reference frame follows that described by [Dumas et al., 2007], except for the Y axis which is as the vertical axis normal to the ground. The inertial parameters are calculated using the inertial properties of a box.

The anatomical location of these points and those usually used in CGA exams at the Ellen Poidatz Foundation can be seen in appendix A. These points are used in the computation of a kinematic tree model composed of 15 rigid segments linked together by 14 joints. This model has a total of 38 internal degrees of freedom (3 for each hip, 3 for each knee, 3 for each ankle, 3 for the pelvis-torso joint, 3 for the torso-head joint, 3 for each shoulder, 1 for each elbow and 3 for each wrist), plus 6 degrees of freedom for the free flyer segment, the pelvis. The rigid model is actuated by revolute actuators located in each joint. In figure 3.2 a schematic representation of the model can be found. In table 3.1, the internal degrees of freedom of this tree model are listed.

Together with equation (3.1), this virtual manikin defines the Full Dynamical Model representing the system. By modelling the interaction with the environment - contacts with the ground in this case - the Internal Model of XDE Physics is completely described. In order to simulate a walking motion in XDE Physics Engine, one needs torques to actuate the model. Without actuation, the virtual manikin would simply fall. Thus, its inputs are the actuation of the system $\boldsymbol{\tau}$, and in return it gives the system state $(\boldsymbol{q}, \boldsymbol{\nu})$ as outputs, see figure 3.3.

The torques used to actuate the XDE Physics Model are given by the Linear Quadratic Programming (LQP) Controller presented in the next section. This LQP-Controller

---

[1]It is assumed that the human is in a static pose and that the elbow does not present any degree of supination. A solution working in all case scenarios has not yet been found. This solution is considered good enough for the purposes of this thesis.
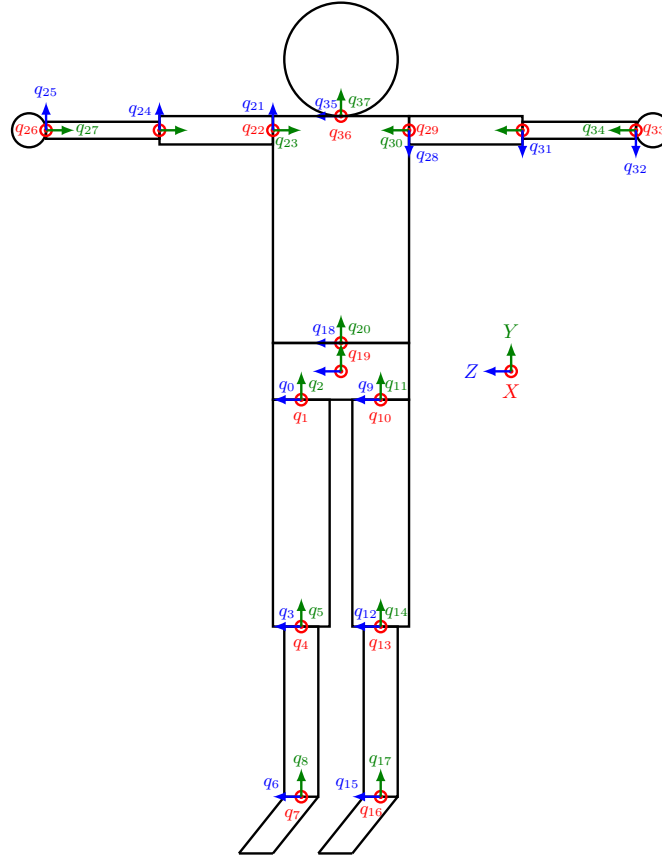
Figure 3.2: Kinematic model of the manikin, in the front view. The degrees of freedom are listed in table 3.1.
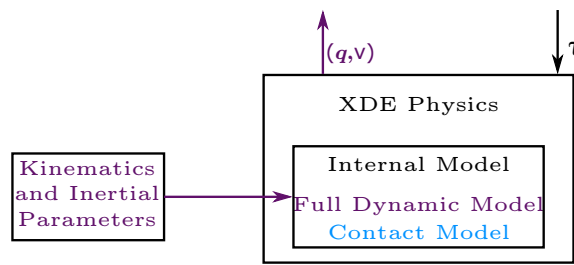
Figure 3.3: XDE Physics - framework for dynamical simulation. Giving kinematics and inertial properties, a dynamical model representing a virtual human can be designed. Given input torques $\boldsymbol{\tau}$ to actuate the system, XDE Physics gives its current state $(\boldsymbol{q}, \boldsymbol{\nu})$.

is used to control the walking motion for the virtual human just presented. The Full Dynamical Model described in this section is the same used in the LQP-Controller, only the

Table 3.1: Listing of the DoF's represented on figure 3.2.

	Parent Body	Child Body	Joint
q_0, q_1, q_2	Pelvis	Right Thigh	Right Hip
q_3, q_4, q_5	Right Thigh	Right Shank	Right Knee
q_6, q_7, q_8	Right Shank	Right Foot	Right Ankle
q_9, q_{10}, q_{11}	Pelvis	Left Thigh	Left Hip
q_{12}, q_{13}, q_{14}	Left Thigh	Left Shank	Left Knee
q_{15}, q_{16}, q_{17}	Left Shank	Left Foot	Left Ankle
q_{18}, q_{19}, q_{20}	Pelvis	Torso	Pelvis-Torso
q_{21}, q_{22}, q_{23}	Torso	Right Arm	Right Shoulder
q_{24}	Right Arm	Right Forearm	Right Elbow
q_{25}, q_{26}, q_{27}	Right Forearm	Right Hand	Right Wrist
q_{28}, q_{29}, q_{30}	Torso	Left Arm	Left Shoulder
q_{31}	Left Arm	Left Forearm	Left Elbow
q_{32}, q_{33}, q_{34}	Left Forearm	Left Hand	Left Wrist
q_{35}, q_{36}, q_{37}	Torso	Head	Torso-Head

contacts modelling changes.

3.2 Linear Quadratic Programming Controller

In this section, the LQP-Controller used to control the walking motion for a virtual human is presented.

The walking motion can be generated by the combination of several objectives to be achieved simultaneously: moving one foot, maintaining balance... Due to the redundancy present in the human body, these objectives can be achieved by different combinations of joints motions. However, conflicting situations can arise at some point, making it difficult for the motion to be performed. This incompatibility problem may be caused by interference of one objective with another, or by constraints violation issues. In the case of objectives interferences, priorities need to be established, in order to solve this incompatibility problem. To prioritize the objectives with respect to one another, two main strategies may be employed: a hierarchical or a weighting strategy.

In strict hierarchical strategies, higher priority objectives are guaranteed to be solved within the solution space defined by the constraints of the system, whereas the lower priority ones may be only partially fulfilled, since they cannot interfere

with the higher ones. The most common resolution technique is null-space projectors [Siciliano and Slotine, 1991, Khatib et al., 2008].

In weighting strategies, each elementary objective is given a weight, which sets the relative priority between them. Priorities not being strict, the solution becomes a compromise between all the objectives. The most common resolution technique in this case is quadratic programming optimization [Abe et al., 2007, Salini et al., 2010].

Hybrid methods, like the one described in [Kanoun et al., 2009], takes advantage of both strategies.

In this work, the weighting strategy developed by Salini *et al.* [Salini et al., 2010, Salini, 2012] is used to compute the virtual human's motion. The Full Dynamical Model of the system used in the controller is the same as in the XDE framework.

Given the set of all the objectives, the method consists in minimizing a cost function resulting from the weighted sum of all the squared tasks $\mathbb{T}_i$ associated with each objective in order to find $\mathbb{X}$, as follows:

$$
\min_{\mathbb{X}} \sum_{i=1}^{n_t} \omega_i \mathbb{T}_i^2(\mathbb{X})
$$
$$
\text{s.t.} \begin{cases} \text{equation (3.1)} \\ \boldsymbol{G}\mathbb{X} \preceq \boldsymbol{h} \end{cases}
\tag{3.2}
$$

where ω_i represents the weight associated to task $\mathbb{T}_i$, pair of matrix-vector $(\boldsymbol{G}, \boldsymbol{h})$ is used to define inequality constraints. The constraints delimit the set of possible solutions for variable $\mathbb{X} = (\boldsymbol{\tau}, \boldsymbol{W}_c, \dot{\boldsymbol{\nu}})^T$. It should be noted that $\dot{\boldsymbol{\nu}}$ can be expressed in function of variables $(\boldsymbol{\tau}, \boldsymbol{W}_c)$ thanks to equation (3.1).

The tasks represent the error between a desired acceleration and the system acceleration, and thus, each task $\mathbb{T}_i$ simply translates as:

$$
\mathbb{T}_i = \left\| \boldsymbol{a}_i - \boldsymbol{a}_i^{des} \right\|
\tag{3.3}
$$

where $\boldsymbol{a}_i, \boldsymbol{a}_i^{des}$ represent the system acceleration, and the desired one, respectively. These accelerations can be expressed on operational or joint space, depending on the objective one wants to achieve. In both cases, the acceleration $\boldsymbol{a}_i$ only depends on the generalized acceleration $\dot{\boldsymbol{\nu}}$, and so equation (3.3) can be rewritten as:

$$
\mathbb{T}_i = \left\| \boldsymbol{J}_i(\boldsymbol{q}) \dot{\boldsymbol{\nu}} + \dot{\boldsymbol{J}}_i(\boldsymbol{q}, \boldsymbol{\nu}) \boldsymbol{\nu} - \boldsymbol{a}_i^{des} \right\|
\tag{3.4}
$$

where $\boldsymbol{J}_i\left(\boldsymbol{q}\right), \dot{\boldsymbol{J}}_i\left(\boldsymbol{q}, \boldsymbol{\nu}\right)$ represent the Jacobian of the controlled parts i of the manikin and its derivative, respectively. Depending on the space considered, operational or joint, $\boldsymbol{a}_i$ may represent a subset of the twist derivative $\dot{\boldsymbol{T}}_i$ related to the frame $\boldsymbol{\Psi}_i$, or a subset of $\dot{\boldsymbol{\nu}}$, composed of the selected DoF to control, respectively. Matrices $\boldsymbol{J}_i$ and $\dot{\boldsymbol{J}}_i$ are defined accordingly.

The structure of the LQP-controller described in this section can be found in figure 3.4.
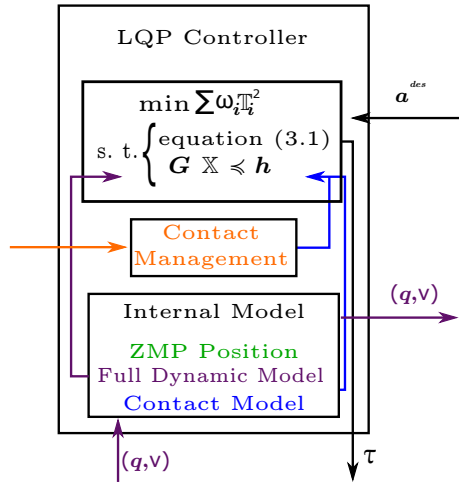
Figure 3.4: LQP-controller used for the control of the walking motion.

The optimization problem is not continuously solved in time, but in discrete time parametrized by a time step dt.

In the next subsections the inequality constraints (actuation and contacts), the tasks used in the optimisation process and the contact manager are presented.

3.2.1 Actuation Constraints

Human joints do not have unbounded capabilities, and, therefore, the actuation must be restricted to some limits.

3.2.1.1   Torque limits

Given $\boldsymbol{\tau}_{max}$, the maximum torque vector of the joint actuators, the torque limit is expressed as:

$$-\boldsymbol{\tau}_{max} \preceq \boldsymbol{\tau} \preceq \boldsymbol{\tau}_{max} \Leftrightarrow \begin{bmatrix} \boldsymbol{S} & \boldsymbol{0} \\ -\boldsymbol{S} & \boldsymbol{0} \end{bmatrix} \mathbb{X} \preceq \begin{bmatrix} \boldsymbol{\tau}_{max} \\ \boldsymbol{\tau}_{max} \end{bmatrix} \tag{3.5}$$

3.2.1.2   Acceleration limits

Torques being bounded, from equation (3.1) it results that generalized accelerations $\ddot{\boldsymbol{q}}_j$ must also be limited. Even though this should be sufficient to limit joint accelerations, one may want to set its own limits. By denoting $\ddot{\boldsymbol{q}}_j^{min}, \ddot{\boldsymbol{q}}_j^{max}$ the acceleration lower and upper boundaries, with $\ddot{\boldsymbol{q}}_j^{min} \preceq \boldsymbol{0}$ and $\ddot{\boldsymbol{q}}_j^{max} \succeq \boldsymbol{0}$, acceleration limits can then be stated as:

$$\ddot{\boldsymbol{q}}_j^{min} \preceq \ddot{\boldsymbol{q}}_j \preceq \ddot{\boldsymbol{q}}_j^{max} \Leftrightarrow \begin{bmatrix} \boldsymbol{0} & \mathbb{I} \\ \boldsymbol{0} & -\mathbb{I} \end{bmatrix} \mathbb{X} \preceq \begin{bmatrix} \ddot{\boldsymbol{q}}_j^{max} \\ -\ddot{\boldsymbol{q}}_j^{min} \end{bmatrix} \tag{3.6}$$

where $\mathbb{I} \in \mathbb{R}^{n_j \times n_j}$ is the identity matrix.

3.2.1.3   Velocity limits

As before, one could want to set its own limits to joints velocities. Lets denote $\dot{\boldsymbol{q}}_j^{min}, \dot{\boldsymbol{q}}_j^{max}$, the joint velocities lower and upper boundaries, respectively, with $\dot{\boldsymbol{q}}_j^{min} \preceq \boldsymbol{0}$ and $\dot{\boldsymbol{q}}_j^{max} \succeq \boldsymbol{0}$. Joint velocities $\dot{\boldsymbol{q}}_j$ do not depend directly on $\mathbb{X}$, as $\ddot{\boldsymbol{q}}_j$, and so, velocity bounds cannot be expressed like it is done in (3.6). Given that a linear relationship between $\dot{\boldsymbol{q}}_j$ and $\mathbb{X}$ is hard to compute, a uniformly accelerated motion of the joints is assumed in order to constrain the future velocities. Therefore, given the current acceleration and an anticipation horizon of h_1 s, the velocities constraints can be written as:

$$\dot{\boldsymbol{q}}_j^{min} \preceq \dot{\boldsymbol{q}}_j + h_1 \ddot{\boldsymbol{q}}_j \preceq \dot{\boldsymbol{q}}_j^{max} \Leftrightarrow \begin{bmatrix} \boldsymbol{0} & \mathbb{I} \\ \boldsymbol{0} & -\mathbb{I} \end{bmatrix} \mathbb{X} \preceq \frac{1}{h_1} \begin{bmatrix} \dot{\boldsymbol{q}}_j^{max} - \dot{\boldsymbol{q}}_j \\ -\left(\dot{\boldsymbol{q}}_j^{min} - \dot{\boldsymbol{q}}_j \right) \end{bmatrix} \tag{3.7}$$

Here, h_1 is equal to dt, the control time step.

3.2.1.4   Joint limits

As before, lets denote $\boldsymbol{q}_j^{min}, \boldsymbol{q}_j^{max}$, with $\boldsymbol{q}_j^{min} \preceq \boldsymbol{0}$, $\boldsymbol{q}_j^{max} \succeq \boldsymbol{0}$, the lower and upper bounds of joint limits, respectively. Once again, these cannot be directly expressed in terms of

the variable $\mathbb{X}$. Thus, using the same reasoning as in 3.7:

$$q_j^{min} \preceq q_j + h_2 \dot{q}_j + \frac{(h_2)^2}{2} \ddot{q}_j \preceq q_j^{max} \Leftrightarrow \begin{bmatrix} \mathbf{0} & \mathbb{I} \\ \mathbf{0} & -\mathbb{I} \end{bmatrix} \mathbb{X} \preceq \frac{2}{(h_2)^2} \begin{bmatrix} q_j^{max} - (q_j + h_2 \dot{q}_j) \\ -\left(q_j^{min} - (q_j + h_2 \dot{q}_j)\right) \end{bmatrix} \quad (3.8)$$

where h_2 is an anticipation horizon, in our case dt.

The anticipation horizons h_1, h_2 allow to discretize the joint positions and velocities, in order to express them in terms of the optimization variable $\ddot{q}$. These coefficients need to me chosen carefully not only to guarantee that all the constraints in $q, \dot{q}, \ddot{q}$ are compatible with one another, but also to ensure that the constraints are still respected in the next time step of simulation. Also, they must not greatly constraint the space of admissible solutions. For this kind of compatibility management of the constraints, see [Decré et al., 2013, Rubrecht et al., 2010].

Joint, Velocity and Acceleration Limits Expressed as One   Since constraints (3.6) - (3.8) must be respected at all times, by picking up the minimum and maximum of each one at all times, these constraints can be written in only one constraint like:

$$\begin{bmatrix} \mathbf{0} & \mathbb{I} \\ \mathbf{0} & -\mathbb{I} \end{bmatrix} \mathbb{X} \preceq \begin{bmatrix} \min\left(\ddot{q}_j^{max}, \frac{\dot{q}_j^{max} - \dot{q}_j}{h_1}, \frac{2\left(q_j^{max} - (q_j + h_2 \dot{q}_j)\right)}{(h_2)^2} \right) \\ -\max\left(\ddot{q}_j^{min}, \frac{\dot{q}_j^{min} - \dot{q}_j}{h_1}, \frac{2\left(q_j^{min} - (q_j + h_2 \dot{q}_j)\right)}{(h_2)^2} \right) \end{bmatrix} \quad (3.9)$$

3.2.2 Contact Constraints

The contacts are modelled using the Coulomb friction model. For each foot, 4 contact points are defined, at each corner of the foot sole, see figure 3.5.

The contacts are considered to be activated or not, depending on the gait stage. Thus, at contact points, two cases may occur:

1. the contact is persistent and no motion occurs between the contact point c_i and the ground. In this case:

   - $\boldsymbol{v}_{c_i} = \mathbf{0}$, with $\boldsymbol{v}_{c_i}$ the velocity at contact point c_i, and so,

   $$\boldsymbol{v}_{c_i} = \boldsymbol{J}_{c_i}(\boldsymbol{q})\boldsymbol{\nu} = 0 \Leftrightarrow \boldsymbol{J}_{c_i}(\boldsymbol{q})\dot{\boldsymbol{\nu}} + \dot{\boldsymbol{J}}_{c_i}(\boldsymbol{q},\boldsymbol{\nu})\boldsymbol{\nu} = \mathbf{0}$$

   where $\boldsymbol{J}_{c_i}$ represents the Jacobian at contact point c_i;
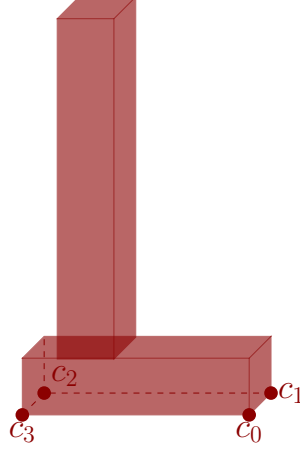
Figure 3.5: Contact points for the left foot: c_0, c_1, c_2 and c_3.

- $\boldsymbol{F}_{c_i}$, the force at contact point, lies inside the Coulomb friction cone. Here, this cone is linearised, see figure 3.6, and so $\boldsymbol{C}_{c_i}\boldsymbol{F}_{c_i} \preceq \boldsymbol{0}$, where $\boldsymbol{C}_{c_i}$ represents the linearised friction cone.

These two conditions can be expressed in terms of the variable of the system $\mathbb{X}$ as follows:

$$\begin{cases} \boldsymbol{J}_{c_i}(\boldsymbol{q})\dot{\boldsymbol{\nu}} + \dot{\boldsymbol{J}}_{c_i}(\boldsymbol{q},\boldsymbol{\nu})\boldsymbol{\nu} = \ \boldsymbol{0} \\ \boldsymbol{C}_{c_i}\boldsymbol{F}_{c_i} \preceq \ \boldsymbol{0} \end{cases} \Leftrightarrow \begin{cases} \begin{bmatrix} \boldsymbol{0} & \boldsymbol{J}_{c_i} \end{bmatrix}\mathbb{X} = \ -\dot{\boldsymbol{J}}_{c_i}(\boldsymbol{q},\boldsymbol{\nu})\boldsymbol{\nu} \\ \begin{bmatrix} \boldsymbol{C}_{c_i}\boldsymbol{S}_{\boldsymbol{F}_{c_i}} & \boldsymbol{0} \end{bmatrix}\mathbb{X} \preceq \ \boldsymbol{0} \end{cases} \tag{3.10}$$

where $\boldsymbol{S}_{\boldsymbol{F}_{c_i}}$ is a selection matrix such that $\boldsymbol{F}_{c_i} = \boldsymbol{S}_{\boldsymbol{F}_{c_i}}\begin{bmatrix} \boldsymbol{\tau} & \boldsymbol{W}_c \end{bmatrix}$.

2. there is no contact between the body and the ground. When no contact occurs between the body and the ground, *i.e.*, no interactions between them, the contact constraint at point c_i simply translates by:

$$\begin{bmatrix} \boldsymbol{S}_{\boldsymbol{F}_{c_i}} & \boldsymbol{0} \end{bmatrix}\mathbb{X} = \boldsymbol{0} \tag{3.11}$$

As seen in Figure 2.1, the walking cycle is divided in four stages: double support, right single support, double support, left single support. As we pass from double to single support, or vice-versa, the contact type changes from persistent to lifting to no contact at all, and from no contact to persistent. These contact transitions are not directly managed, instead, particular attention is devoted to feet displacement generation, as it is seen in the
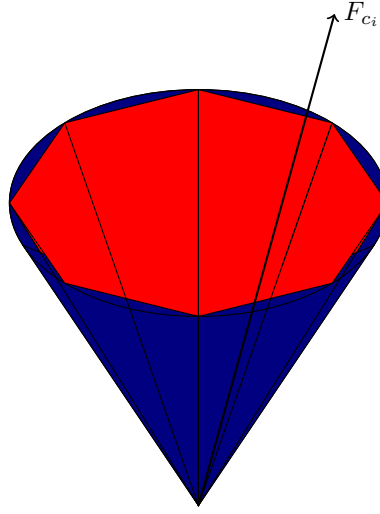
Figure 3.6: Linear approximation (red) of the Coulomb cone of friction (blue). If the force F_{c_i} stays inside the friction cone during the contact, no slide motion occurs.

next subsection. It should be noted that sliding contacts are not considered in our case.

3.2.3 Tasks for the Walking motion

As mentioned before, the tasks are divided into two categories: operational ($\mathbb{O}$) and joint ($\mathbb{J}$) space tasks. The tasks generated for the walking motion are:

1. Full Joint Task ($\mathbb{J}$), noted $\mathbb{T}_{\ddot{q}_j}$, controlling all the joint angles;

2. Left/Right Foot Task ($\mathbb{O}$), noted $\mathbb{T}_{lf}$ and $\mathbb{T}_{rf}$, respectively, controlling the left/right foot frames during foot displacements;

3. CoM Task ($\mathbb{O}$), noted $\mathbb{T}_{CoM}$ responsible for the control of the CoM acceleration;

4. Pelvis Height Task ($\mathbb{O}$), noted $\mathbb{T}_{pelvis_Z}$, controlling the pelvis frame altitude;

5. Pelvis Orientation Task ($\mathbb{O}$), noted $\mathbb{T}_{pelvis_R}$, controlling the pelvis frame orientation;

6. Pelvis-Torso Joint Task ($\mathbb{J}$), noted $\mathbb{T}_{PTJ}$, controlling the DoF's linking the torso to the pelvis;

7. Torso-Head Joint Task ($\mathbb{J}$), noted $\mathbb{T}_{THJ}$, controlling the DoF's linking the head to the torso.

3.2.3.1 Full Joint Task

Since the problem of synthesising walking resumes to solving problem (3.2), this task, with a very small weight, is essential, as it ensures that a unique solution is always found. Due to the weighting strategy, this task has a very small impact on the achievement of higher priority tasks.

From the general expression of the task (3.4), and since this task only depends on the joint accelerations $\ddot{q}_j$, it can be directly written as:

$$\mathbb{T}_{\ddot{q}_j} = \left\| \ddot{q}_j - a_{\ddot{q}_j}^{des} \right\| \tag{3.12}$$

For the task to be completely described, it remains to define $a_{\ddot{q}_j}^{des}$. By giving the system a general global constant configuration q_j^{goal2}, its velocity can be derived $\dot{q}_j^{goal} = 0$, as well as its acceleration $\ddot{q}_j^{goal} = 0$. $a_{\ddot{q}_j}^{des}$ could then be set equal to $\ddot{q}_j^{goal}$

$$a_{\ddot{q}_j}^{des} = \ddot{q}_j^{goal} = 0.$$

However, with this approach, the system would not have real time feedback of its configuration, and it could deviate from the goal, since only acceleration is controlled. To overcome that, $a_{\ddot{q}_j}^{des}$ is calculated using a proportional derivative (PD) controller, in order to enforce the tracking behaviour of the task. Thus, $a_{\ddot{q}_j}^{des}$ is expressed as:

$$a_{\ddot{q}_j}^{des} = \ddot{q}_j^{goal} + k_{p_{\ddot{q}_j}} \left(q_j^{goal} - q_j \right) + k_{d_{\ddot{q}_j}} \left(\dot{q}_j^{goal} - \dot{q}_j \right)$$

where $k_{p_{\ddot{q}_j}}, k_{d_{\ddot{q}_j}}$ are the proportional and derivative gains, respectively. For simplicity, in the remaining of the text, the dependency of the task on k_p, k_d is removed.

Since $\dot{q}_j^{goal} = \ddot{q}_j^{goal} = 0$, $a_{\ddot{q}_j}^{des}$ simplifies as:

$$a_{\ddot{q}_j}^{des} = k_{p_{\ddot{q}_j}} \left(q_j^{goal} - q_j \right) - k_{d_{\ddot{q}_j}} \dot{q}_j \tag{3.13}$$

Replacing $a_{\ddot{q}_j}^{des}$ of equation (3.12) by its value given by equation (3.13), equation (3.12) becomes:

$$\mathbb{T}_{\ddot{q}_j} = \left\| \ddot{q}_j - \left(k_p \left(q_j^{goal} - q_j \right) - k_d \dot{q}_j \right) \right\| \tag{3.14}$$

and the task is defined for the entire motion.

---

[2]The stand up initial configuration is used here.

3.2.3.2 Left/Right Foot Task

Walking consists in a displacement from a point S (start) to a point E (end) on the ground, figure 3.7 a), by alternating the two legs movement and by keeping always at least one foot in contact with the ground, at all times. If we consider the line relying these two points S and E, it defines the theoretical trajectory, projected on the ground, that the CoM would accomplish during the walking motion, figure 3.7 b).

The walking motion is a succession of cycles, and, as seen in chapter 2, these cycles are primarily characterized by spatio-temporal parameters.

Thus, given the theoretical trajectory of the CoM, the step lengths (left and right), the step width and the starting foot, footprints respecting these data can be defined along the CoM trajectory, figure 3.7 c). The feet are supposed to be equally distant in the lateral direction from the CoM trajectory.
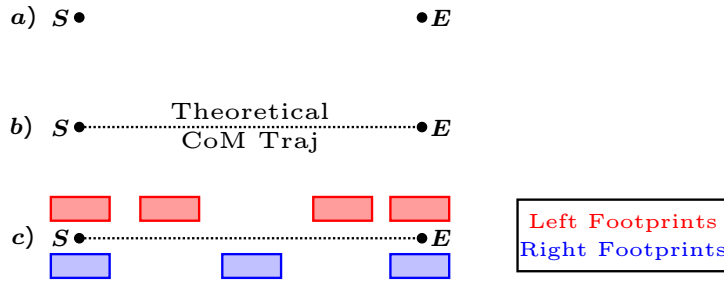
Figure 3.7: Walking motion design. a) Points S and E represent the start and ending points, respectively, of the walking motion. b) The line relying points S and E represents the theoretical CoM trajectory to achieve, projected on the ground. c) The footprints are placed around the theoretical CoM trajectory taking into account step limits.

In the spatio-temporal parameters, there is also the walking cycle duration and the double and single support periods. Here, the double and single support phases are defined through the time ratio between their relative duration. These informations, together with the footprints spatial distribution, allows us to know for how long and where each foot stays in contact with the ground. It follows that the time needed for one foot to go from one footprint to the next is also known.

To define the walking motion, the foot displacement from one footprint to the next one needs to be defined. In order to do that, the step height is also considered. So, for each foot displacement, a trajectory $\boldsymbol{traj}_f(t) = (\boldsymbol{x}_f(t), \boldsymbol{y}_f(t), \boldsymbol{z}_f(t))$ is defined, where $\boldsymbol{x}_f, \boldsymbol{y}_f, \boldsymbol{z}_f$ are in the anterior/posterior, meadial/lateral and vertical directions, respectively. As for

the rotation of the foot, it is considered constant, with the foot always parallel to the ground and aligned with the anterior/posterior direction. Recall that the foot consists of one rigid body, and so, to give the displacement of the foot, one only needs to define the position and rotation associated with a single point of the foot. Here,the most anterior medial point of the foot sole is chosen.

The trajectory $\boldsymbol{traj}_f(t)$ is defined for each foot as follows:

- $\boldsymbol{x}_f(t)$ such that:

$$\boldsymbol{x}_f(t_0) = x_0; \quad \dot{\boldsymbol{x}}_f(t_0) = 0; \quad \ddot{\boldsymbol{x}}_f(t_0) = 0$$
$$\boldsymbol{x}_f(t_f) = x_f; \quad \dot{\boldsymbol{x}}_f(t_f) = 0; \quad \ddot{\boldsymbol{x}}_f(t_f) = 0$$

  where t_0, t_f are the times of beginning and end, respectively, of the foot displacement, with respect to the entire motion, and x_0, x_f are the start and end position of the foot point we want to control. The trajectory is then a polynomial of degree 5, which is exactly the degree required for all the previously conditions to be satisfied.

- $\boldsymbol{y}_f(t)$ such that:

$$\boldsymbol{y}_f(t_0) = y_0; \quad \dot{\boldsymbol{y}}_f(t_0) = 0; \quad \ddot{\boldsymbol{y}}_f(t_0) = 0$$
$$\boldsymbol{y}_f(t_f) = y_f; \quad \dot{\boldsymbol{y}}_f(t_f) = 0; \quad \ddot{\boldsymbol{y}}_f(t_f) = 0$$

  where y_0, y_f are the start and end position of the foot point we want to control. From the assumptions on the orientation, we have that $y_0 = y_f$ and thus $\boldsymbol{y}_f(t) = y_0$.

- $\boldsymbol{z}_f(t)$ such that:

$$\boldsymbol{z}_f(t_0) = 0; \qquad \dot{\boldsymbol{z}}_f(t_0) = 0; \qquad \ddot{\boldsymbol{z}}_f(t_0) = 0$$
$$\boldsymbol{z}_f\left(\frac{t_0 + t_f}{2}\right) = \text{step height}; \quad \dot{\boldsymbol{z}}_f\left(\frac{t_0 + t_f}{2}\right) = 0; \quad \ddot{\boldsymbol{z}}_f\left(\frac{t_0 + t_f}{2}\right) = 0$$
$$\boldsymbol{z}_f(t_f) = 0; \qquad \dot{\boldsymbol{z}}_f(t_f) = 0; \qquad \ddot{\boldsymbol{z}}_f(t_f) = 0$$

  where t_0, t_f are time of beginning and end, respectively, of the foot displacement, with respect to the entire motion. The trajectory is then a polynomial of degree 8, which is exactly the degree required for all the previously conditions to be satisfied.

An example of the $\boldsymbol{traj}_f$ generated by this process can be found in figure 3.8. In this case, the step length is of 0.22 m and the step height of 0.02 m.
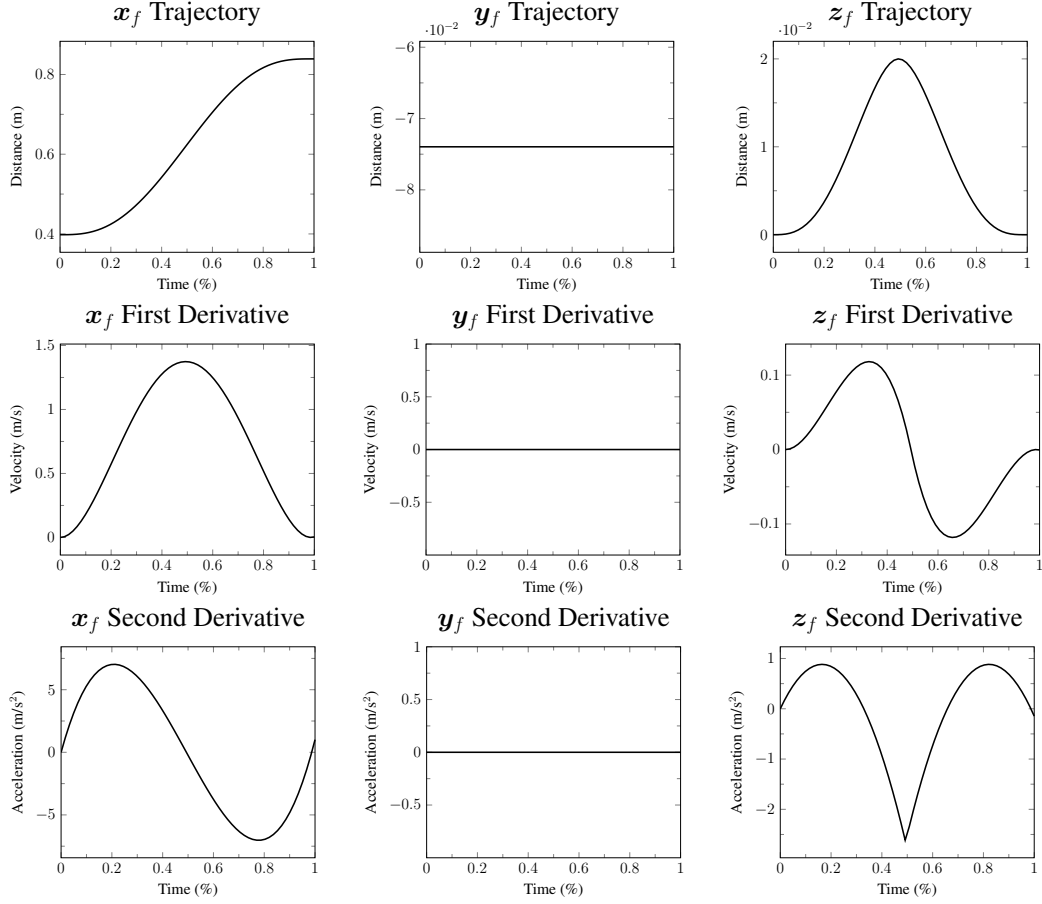
Figure 3.8: Foot trajectories generated for a step length of 0.22 m, a step height of 0.02 m. The first row corresponds to the x_f, y_f, z_f trajectories, the second row to their first derivatives and the last row to their second derivatives.

The zero conditions on the trajectory velocity and acceleration at the endpoints, allow us to minimize the discontinuities that may appear at contact transitions.

With the position and orientation displacement defined, the desired frame state associated with the foot during its displacement can be fully described. Lets denote H_f^{goal} the desired frame state, and T_f^{goal}, its associated twist. As before, a_f^{des} is calculated using a (PD) controller, and so:

$$a_f^{des} = \dot{T}_f^{goal} + k_p \mathbf{diff}\left(H_f^{goal} - H_f\right) + kd\left(T_f^{goal} - T_f\right) \tag{3.15}$$

The error between two positions in $\mathbb{R}^3$ is trivially computed as the euclidean difference in $\mathbb{R}^3$. To take in to account orientation, these are expressed as quaternions. The **diff** method

takes both position and orientation to calculate the error between two displacements.

Replacing $\boldsymbol{a}_i^{des}$ of equation (3.4) by its value given by equation (3.15), the foot task becomes:

$$\mathbb{T}_f = \left|\left| \boldsymbol{J}_f\left(\boldsymbol{q}\right)\dot{\boldsymbol{\nu}} + \dot{\boldsymbol{J}}_f\left(\boldsymbol{q},\boldsymbol{\nu}\right)\boldsymbol{\nu} - \left(\dot{\boldsymbol{T}}_f^{goal} + k_p\mathbf{diff}\left(\boldsymbol{H}_f^{goal} - \boldsymbol{H}_f\right) + k_d\left(\boldsymbol{T}_f^{goal} - \boldsymbol{T}_f\right)\right)\right|\right| \quad (3.16)$$

with $\boldsymbol{J}_f, \dot{\boldsymbol{J}}_f$ are the Jacobian associated with the foot frame and its derivative, respectively.

For each foot displacement, a trajectory is calculated, taking into account the starting and ending points. If the walking motion needs n_s steps to be accomplished, then n_s foot trajectories are calculated.

3.2.3.3 CoM Task

The displacement of the feet alone is not enough to define the displacement of the entire body. To generate the walking motion we make the hypothesis that the whole mass of the system is concentrated in one point, the Center of Mass (CoM), and that the altitude of this mass does not change during the walking motion, see figure 3.9. This walking motion is based on the Zero Moment Point (ZMP), introduced in [Vukobratović and Juricic, 1969] and on the Linear Inverted Pendulum Model (LIPM), by Kajita *et al* [Kajita et al., 2003].
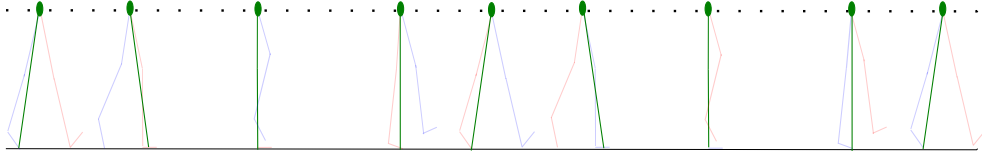

Figure 3.9: Illustration of the Linear Inverted Pendulum Model (LIPM), where the total mass of the human is assumed to be concentrated at one point (green) whose altitude does not change during the walking motion. The supporting foot of the walking motion is assumed as the support foot for the pendulum modelling.

In order for the ZMP criteria to be properly applied, the contact with the ground must be established with coplanar points and no interaction can be made through upper body parts, which is the case for the walking motion. It should be noted that friction is not taken into account, and must be handled separately.

The ZMP condition is sufficient, yet not necessary, to ensure the manikin's dynamical balance.

Given the footprints sequence previously created, a ZMP trajectory $\boldsymbol{P}_{\text{ZMP}}^{goal} = \left(x_{\text{ZMP}}^{goal}(t), y_{\text{ZMP}}^{goal}(t)\right)$ that will stay inside the "moving base of support" during the walk
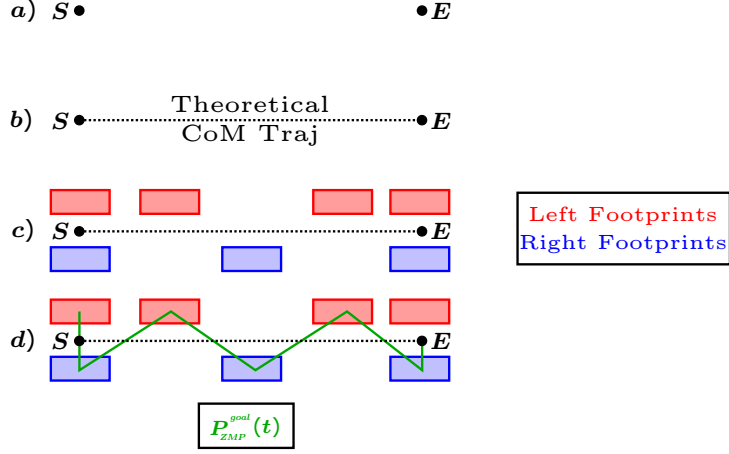
can be designed, figure 3.10 d).

Figure 3.10: Walking motion design. a) Points S and E represent the start and ending points, respectively, of the walking motion. b) The line relying points S and E represents the theoretical CoM trajectory to achieve, projected on the ground. c) The footprints are placed around the theoretical CoM trajectory taking into account step limits. d) Zero-Moment Point reference trajectory.

The ZMP and CoM are linked together as follows [Kajita et al., 2003]:

$$\boldsymbol{P}_{\text{ZMP}} = \boldsymbol{P}_{\text{CoM}} - \frac{z_{\text{CoM}}}{g} \ddot{\boldsymbol{P}}_{\text{CoM}} \tag{3.17}$$

where $\boldsymbol{P}_{\text{CoM}}, \boldsymbol{P}_{\text{ZMP}}$, are the CoM and ZMP horizontal positions, respectively, and z_{CoM} is the CoM height.

This system is very unstable, and its control must take into account the prediction of its future state. Following the method presented in [Wieber, 2006], lets consider a discretisation of the trajectories of the CoM and ZMP over time intervals of length T. For $t = kT$, we have that:

$$\boldsymbol{P}_{\text{CoM}}^{k} = \begin{bmatrix} \boldsymbol{P}_{\text{CoM}}(kT) \\ \dot{\boldsymbol{P}}_{\text{CoM}}(kT) \\ \ddot{\boldsymbol{P}}_{\text{CoM}}(kT) \end{bmatrix}, \quad \dddot{\boldsymbol{P}}_{\text{CoM}}^{k} = \dddot{\boldsymbol{P}}_{\text{CoM}}(kT), \quad \boldsymbol{P}_{\text{ZMP}}^{k} = \boldsymbol{P}_{\text{ZMP}}(kT) \tag{3.18}$$

Considering constant jerks $\dddot{\boldsymbol{P}}_{\text{CoM}}^{k}$ over each time interval and integrating, it follows that:

$$\boldsymbol{P}_{\text{CoM}}^{k+1} = \begin{bmatrix} 1 & T & \frac{T^2}{2} \\ 0 & 1 & T \\ 0 & 0 & 1 \end{bmatrix} \boldsymbol{P}_{\text{CoM}}^{k} + \begin{bmatrix} \frac{T^3}{6} \\ \frac{T^2}{2} \\ T \end{bmatrix} \dddot{\boldsymbol{P}}_{\text{CoM}}^{k} \tag{3.19}$$

Discretisation of equation (3.17) translates as:

$$\boldsymbol{P}_{\text{ZMP}}^{k} = \begin{bmatrix} 1 & 0 & \frac{z_{\text{CoM}}}{g} \end{bmatrix} \boldsymbol{P}_{\text{CoM}}^{k} \tag{3.20}$$

The ZMP Preview Control Scheme consists in minimizing the computed jerk and at the same time keeping the ZMP position near a reference. Here, this reference is $\boldsymbol{P}_{\text{ZMP}}^{goal}$ of figure 3.7 d).

Lets consider a time horizon of H time steps. Relation (3.19) can be iterated and combined with relation (3.20) to give:

$$\boldsymbol{P}_{\text{ZMP}}^{(k+1)^H} = \boldsymbol{P}_x \boldsymbol{P}_{\text{CoM}}^{k} + \boldsymbol{P}_u \dddot{\boldsymbol{P}}_{\text{CoM}}^{k^H} \tag{3.21}$$

where

- $\boldsymbol{P}_{\text{ZMP}}^{(k+1)^H} = \begin{bmatrix} \boldsymbol{P}_{\text{ZMP}}^{k+1}, \boldsymbol{P}_{\text{ZMP}}^{k+2}, \cdots, \boldsymbol{P}_{\text{ZMP}}^{H} \end{bmatrix}^T$

- $\dddot{\boldsymbol{P}}_{\text{CoM}}^{k^H} = \begin{bmatrix} \dddot{\boldsymbol{P}}_{\text{CoM}}^{k}, \dddot{\boldsymbol{P}}_{\text{CoM}}^{k+1}, \cdots, \dddot{\boldsymbol{P}}_{\text{CoM}}^{k+H-1} \end{bmatrix}^T$

- $\boldsymbol{P}_x = \begin{bmatrix} 1 & T & \frac{T^2}{2} - \frac{z_{\text{CoM}}}{g} \\ \vdots & \vdots & \vdots \\ 1 & HT & \frac{H^2 T^2}{2} - \frac{z_{\text{CoM}}}{g} \end{bmatrix}$

- $\boldsymbol{P}_u = \begin{bmatrix} \frac{T^3}{6} - T\frac{z_{\text{CoM}}}{g} & 0 & 0 \\ \vdots & \ddots & \vdots \\ (1 + 3H + 3H^2)\frac{T^3}{6} - T\frac{z_{\text{CoM}}}{g} & 0 & \frac{T^3}{6} - T\frac{z_{\text{CoM}}}{g} \end{bmatrix}$

Recall that the ZMP Preview Control Scheme consists in minimizing the computed jerk and at the same time keeping the ZMP position near $\boldsymbol{P}_{\text{ZMP}}^{goal}$. Thus, the design of the CoM trajectory, can be stated as a Quadratic Program (QP) and written as:

$$\min_{\dddot{\boldsymbol{P}}_{\text{CoM}}^{k^H}} \frac{1}{2} Q \left(\boldsymbol{P}_{\text{ZMP}}^{(k+1)^H} - \boldsymbol{P}_{\text{ZMP}}^{goal^{(k+1)^H}} \right)^2 + \frac{1}{2} R \left(\dddot{\boldsymbol{P}}_{\text{CoM}}^{k^H} \right)^2 \tag{3.22}$$

where the constants Q, R allow to balance the tracking of the ZMP trajectory and the minimization of the jerk, and $\boldsymbol{P}_{\mathrm{ZMP}}^{goal^{(k+1)^H}}$ is the part of $\boldsymbol{P}_{\mathrm{ZMP}}^{goal}$ involved at time step $k+1$ and horizon H.

This QP has an analytical solution which is:

$$\dddot{\boldsymbol{P}}_{\mathrm{CoM}}^{k^H} = -\left(\boldsymbol{P}_{\boldsymbol{u}}^T \boldsymbol{P}_{\boldsymbol{u}} + \frac{R}{Q}\mathbb{I}_{H\times H}\right)^{-1} \boldsymbol{P}_{\boldsymbol{u}}^T \left(\boldsymbol{P}_{\boldsymbol{x}}\boldsymbol{P}_{\mathrm{CoM}}^k - \boldsymbol{P}_{\mathrm{ZMP}}^{goal^{(k+1)^H}}\right) \tag{3.23}$$

where $\mathbb{I}_{H\times H}$ is an identity matrix.

Given $\boldsymbol{P}_{\mathrm{CoM}}^k$, and $\dddot{\boldsymbol{P}}_{\mathrm{CoM}}^k$, the first row of matrix in equation (3.23), $\boldsymbol{P}_{\mathrm{CoM}}^{k+1}$ can be calculated for each time step thanks to equation (3.19) and we have that:

$$\ddot{\boldsymbol{P}}_{\mathrm{CoM}}((k+1)T) = \ddot{\boldsymbol{P}}_{\mathrm{CoM}}((k)T) + T\boldsymbol{P}_{\mathrm{CoM}}^{k+1} \tag{3.24}$$

Recalling the general expression of a task of equation (3.4), the CoM task is then written as:

$$\mathbb{T}_{\mathrm{CoM}} = \left\| \boldsymbol{J}_{\mathrm{CoM}}\left(\boldsymbol{q}\right)\dot{\boldsymbol{\nu}} + \dot{\boldsymbol{J}}_{\mathrm{CoM}}\left(\boldsymbol{q},\boldsymbol{\nu}\right)\boldsymbol{\nu} - \boldsymbol{a}_{\mathrm{CoM}}^{des} \right\| \tag{3.25}$$

where $\boldsymbol{J}_{\mathrm{CoM}}, \dot{\boldsymbol{J}}_{\mathrm{CoM}}$ represent the CoM jacobian and it's derivative, respectively, and $\boldsymbol{a}_{\mathrm{CoM}}^{des}$ is given by equation (3.24). The position and velocity of the CoM are not controlled.

3.2.3.4 Pelvis Height & Pelvis Orientation Tasks

In the CoM Task previously presented, CoM height is not controlled, but assumed to be constant. Also, rotational motions around the CoM frame are also neglected. These two assumptions are part of the ZMP-Preview Control Scheme, and need to be addressed.

Thus, two Pelvis Tasks are introduced for the control of its height and orientation. The choice of the Pelvis segment could be replaced by the torso segment, but since this is an unactuaded segment, it is preferred here.

The height of the Pelvis z_p^{goal} is set constant, and its orientation $\boldsymbol{R}_p^{goal}$ is set to be parallel to ground, as in the case of the foot tasks.

Lets suppose the existence of $\boldsymbol{x}_p^{goal}, \boldsymbol{y}_p^{goal}$. As in the Foot Task case we can define $\boldsymbol{H}_p^{goal}$, and $\boldsymbol{T}_p^{goal}$, its associated twist.

By making the same reasoning as in equation (3.15), we have that:

$$\mathbb{T}_P = \left\| \boldsymbol{S}_P \left(\boldsymbol{J}_p\left(\boldsymbol{q}\right)\dot{\boldsymbol{\nu}} + \dot{\boldsymbol{J}}_p\left(\boldsymbol{q},\boldsymbol{\nu}\right)\boldsymbol{\nu} - \left(\dot{\boldsymbol{T}}_p^{goal} + k_p\mathbf{diff}\left(\boldsymbol{H}_p^{goal} - \boldsymbol{H}_p\right) + k_d\left(\boldsymbol{T}_p^{goal} - \boldsymbol{T}_p\right)\right)\right)\right\| \tag{3.26}$$

with

- $\boldsymbol{J}_p, \dot{\boldsymbol{J}}_p$ are the Jacobian associated with the pelvis frame and its derivative, respectively;

- subscript $P \in (\text{pelvis}_Z; \text{pelvis}_R)$, for the task considered;

- $\boldsymbol{S}_P$ is a selection matrix which allows to select the part of the error to consider, depending on the task: height or orientation;

- k_p, k_d the proportional and derivative gains associated with the task.

3.2.3.5 Pelvis-Torso Joint & Torso-Head Joint Tasks

The Pelvis Tasks alone may not be sufficient to control the orientation of the CoM frame. Two tasks are then added to control the Pelvis-Torso and the Torso-Head Joints.

These two tasks follow the same reasoning as the Full Joint Task, but only a partial part of the DoFs of the system is considered. The general expression for each one of these two tasks is written as:

$$\mathbb{T}_{\ddot{\boldsymbol{q}}_\lambda} = \left\| \ddot{\boldsymbol{q}}_\lambda - \boldsymbol{a}_{\ddot{\boldsymbol{q}}_\lambda}^{des} \right\| \tag{3.27}$$

where $\boldsymbol{q}_\lambda$ denotes the subset of joints to control: pelvis-torso or torso-head joints.

As in in the Full Joint Task case, the desired acceleration is computed as:

$$\boldsymbol{a}_{\ddot{\boldsymbol{q}}_\lambda}^{des} = \ddot{\boldsymbol{q}}_\lambda^{goal} + k_p \left(\boldsymbol{q}_\lambda^{goal} - \boldsymbol{q}_\lambda \right) + k_d \left(\dot{\boldsymbol{q}}_\lambda^{goal} - \dot{\boldsymbol{q}}_\lambda \right)$$

By setting $\boldsymbol{q}_\lambda^{goal}$ to be zero, it follows that $\dot{\boldsymbol{q}}_\lambda^{goal} = \ddot{\boldsymbol{q}}_\lambda^{goal} = \boldsymbol{0}$ and so, the desired acceleration simply becomes:

$$\boldsymbol{a}_{\ddot{\boldsymbol{q}}_\lambda}^{des} = -k_p \boldsymbol{q}_\lambda - k_d \dot{\boldsymbol{q}}_\lambda \tag{3.28}$$

The expression of the task for each one is then stated as:

$$\mathbb{T}_\lambda = \left\| \ddot{\boldsymbol{q}}_\lambda + k_p \boldsymbol{q}_\lambda + k_d \dot{\boldsymbol{q}}_\lambda \right\| \tag{3.29}$$

The tasks just presented are resumed in figure 3.11. All the tasks are active during the entire motion with the exception of the feet tasks. In fact, since we only define trajectories

for the feet displacement and not their static phases (since these are managed trough contacts), we need to select when and how the foot tasks are active. This is the object of the next section.
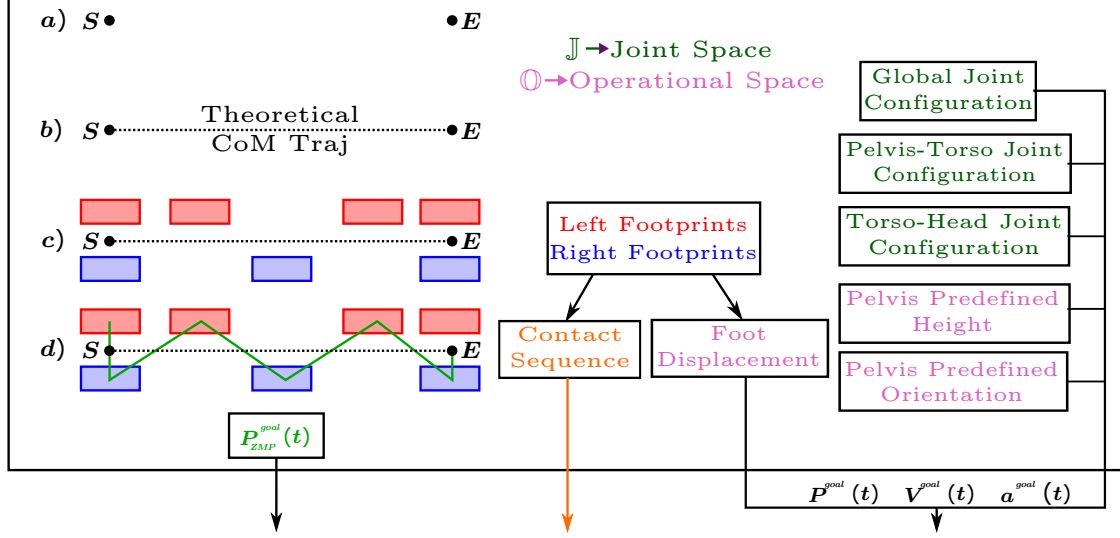

Figure 3.11: Tasks references needed for the tasks used in the control of the walking motion. $P^{\text{goal}}, V^{\text{goal}}, a^{\text{goal}}$ stand for position, velocity and acceleration goals respectively.

3.2.4 Contacts Manager

The Contacts Manager serves two purposes here:

1. the selection of the contact constraints that are active for the optimisation problem,

2. the activation of the feet tasks with the corresponding reference.

From the initial displacement from S to E points previously defined, see figure 3.7, and given the step lengths and the cycle duration $(2T)$ every contact event is well placed in time. The walking motion is considered symmetric here.

In figure 3.12, the contacts manager is illustrated.

As we can see, at $t = 0$, the beginning of the motion, the contact constraints of equation (3.10) are considered for all contact points, since both feet are on the ground. At $t = T$, the left foot starts its displacement to the next position, and thus, the contact constraints for the left foot points are those of equation (3.11). At the same time, the foot task for the left foot becomes active, and takes the first displacement as reference. The
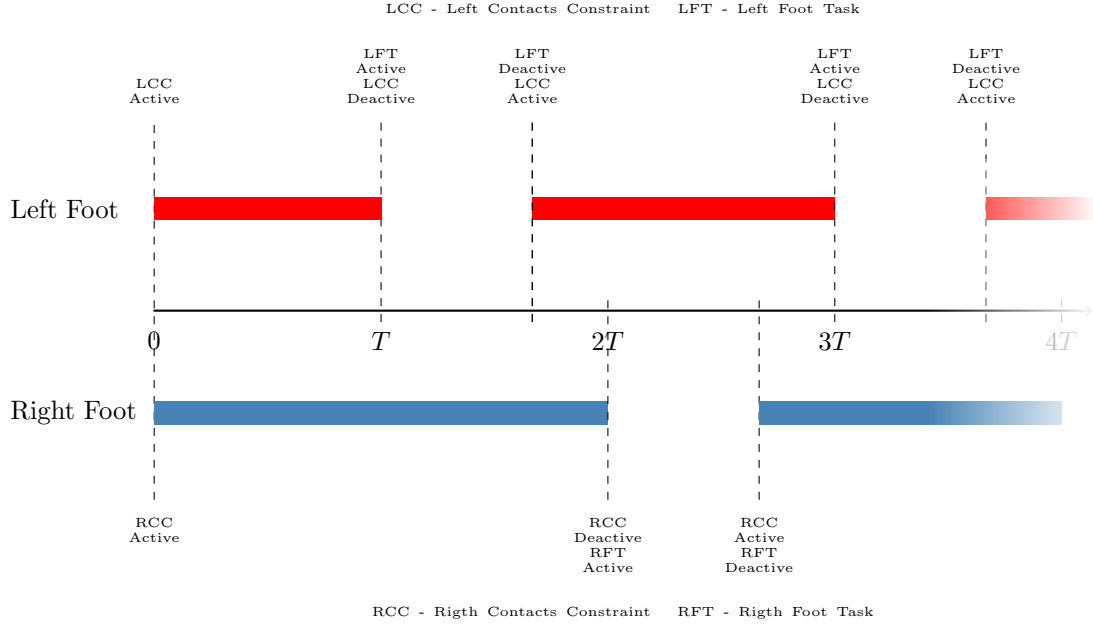
Figure 3.12: Contacts Manager schematics. T is the time duration between one foot taking off and the other one taking off.

ratio r defines the feet displacement duration with respect to the walking cycle duration. When this displacement is accomplished, the foot task finishes, and the constraints of equation (3.10) replace those of equation (3.11), for the left foot. At time $t = 2T$, the process begins for the right foot, and the sequence of transitions is handled the same way as for the left foot. This process goes on until the walking motion is finished, *i.e.*, until point E is reached.

This contacts manager allows us to have coherence between the planned motion and the executed one.

With this in place, walking motion can be generated for the virtual human of section 3.1.1. In figure 3.13, the simulation framework gathering XDE Physics and the LQP-Controller used for the generation of walking motions for a virtual human can be seen.

3.3   Simulation example

In this section, a simulation application of the motion generation method presented in this chapter is made.
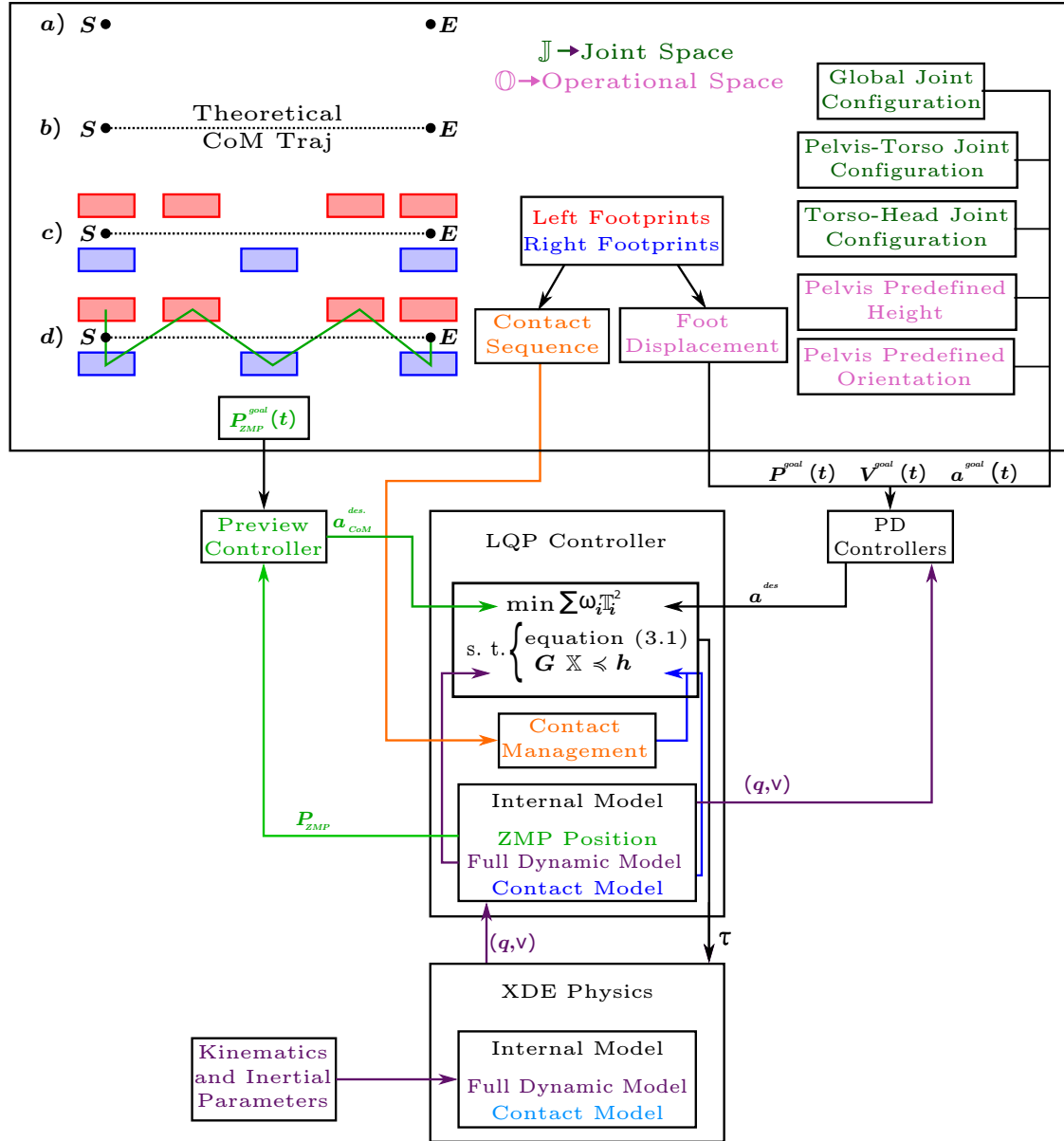
Figure 3.13: Complete simulation framework schematics.

For starters the methodology used to conduct the simulations is explained, followed by the presentation of the results obtained. A discussion on these results finishes the section.

3.3.1   Method

The numerical manikin needed for walking motion generation is created using data from a female subject with 1.630 m height and 51.5 kg, according to the procedure presented in section 3.1.1. The subject did not present any gait pathology or anatomic deformation.

The initial configuration of the manikin is calculated so that the legs are straighten up, both feet on the ground and the pelvis center located above the center of the feet. Since the torso is set straight, the projection of the subject's CoM on the ground is located in the base of support defined by the two feet.

The LQP-Controller presented in section 3.2 is used to generate walking motion. To evaluate the simulation space, the following parameters are tested:

- **step length**, made to vary between 0.2 m and 0.5 m with a 0.02 m increase step;

- **step height**, made to vary between 0.02 m and 0.06 m with a 0.02 m increase step;

- **walking cycle duration**, made to vary between 0.6m and 1.4 s with a 0.2 s increase step;

- **swing phase duration**, made to vary between 38% and 43% of total walking cycle duration, with a 1% increase step;

- **CoM reference altitude shift** (for the preview control calculations), made to vary between 0 m and 0.06 m, with a 0.02 m increase step. This parameter represents how much we lower the CoM's reference from its initial altitude, used for the LIP modelling. The Pelvis height reference is likewise adjusted.

Step length, **step height**, **walking cycle duration** and **swing phase duration** are considered step related parameters, and their values are chosen according to the minimum and maximum values calculated from the regression equations presented in [Wheelwright et al., 1993].

As for the **CoM reference altitude shift**, it is made to vary in order to test the influence of the LIP modelling on the walking motion.

Using a combination of these parameters, several walking simulations are tested. The simulation is considered to be successful when the manikin completes at least 4 gait cycles without falling.

3.3.2 Results & Discussion

By combining the parameters presented before, $5760\,(16 \times 3 \times 5 \times 6 \times 4)$ simulations are performed, with a total of 51 successful simulations.

An example of a walking cycle generated by this method can be found in figure 3.14.
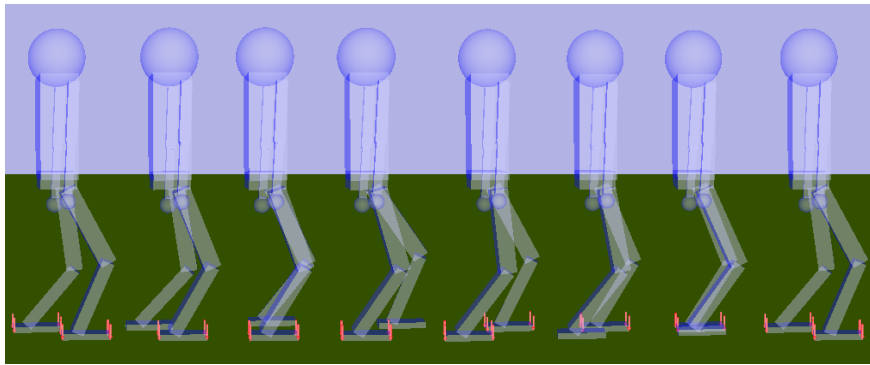

Figure 3.14: Walking cycle generated for a subject of 1.63 m of height and 51.5 kg of body mass. Simulation Parameters: step length - 0.22 m, step height - 0.02 m, walking cycle duration - 1.4 s, swing phase duration 43% of total walking cycle duration. CoM shift is set at 0.06 m.

3.3.2.1 Spatio-temporal Parameters

In figure 3.15, the total number the successful simulations for each step related parameter can be found. Using the step length and cycle duration parameters, walking speed values can be calculated. The ranges of speed attained for the successful simulations are presented in figure 3.15 d).

Regarding the step length, in figure 3.15 a), it can be seen that the more the step lengths increases, the less simulations are successful. Besides, step lengths of more than 0.24 m are not achievable. The range of step lengths usually presented by humans when walking, see [Wheelwright et al., 1993], cannot be attained.

As for the step height, figure 3.15 b), increasing it to does not seem to improve the rate of success of simulations, on the contrary.
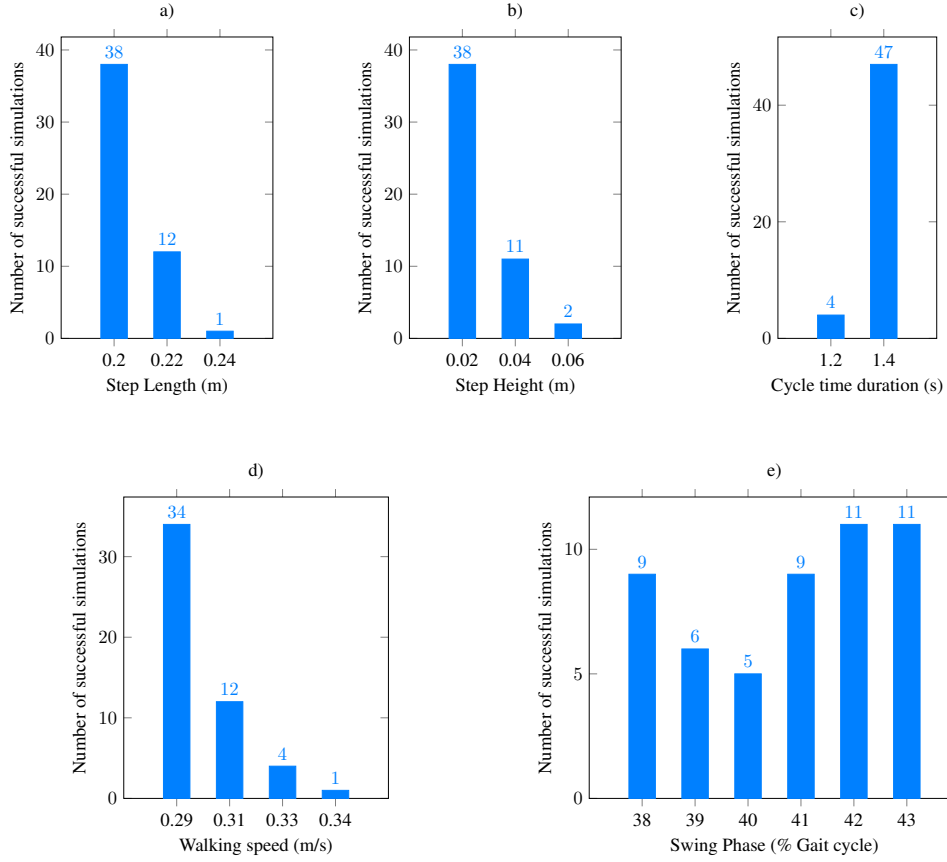
Figure 3.15: Number of successful simulations per: a) Step length; b) Step height; c) Walking cycle duration; d) Walking Speed; e) Swing phase duration.

Concerning the temporal parameters, the longer the cycle duration, the more walking motions are possible, figure 3.15 c). In this case, we are far away from the walking cycle durations usually observed in humans, as a closer look at the walking speed velocities, figure 3.15 d), shows that velocities are way below the usual standard for healthy subjects, which range from 0.65 m/s - 1.88 m/s according to [Wheelwright et al., 1993].

Finally, the duration of the swing phase, figure 3.15 e), shows some homogeneity, indicating that this parameter does not have much influence in the success of the simulations.

In figure 3.16, the number of successful simulations per CoM reference altitude shift length can be seen.

Since the manikin is initialized with the legs straighten up, variations are introduced
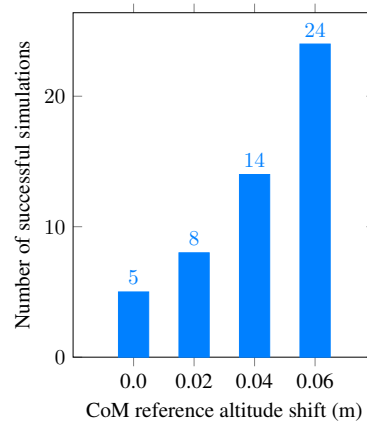
Figure 3.16: Number of successful simulations per CoM reference altitude shift. The distance in meters represents the shift in the vertical direction (to the bottom) in the CoM altitude reference.

on the CoM reference altitude to evaluate the impact of the LIP modelling on the walking simulation. As we can see, the more the CoM is lowered, the more walking motion is possible, so this parameter has a real impact on the walking motion generation.

3.3.2.2 Kinematical parameters

In order to do a first evaluation on human likeliness for the generated walking motions, a modified version of the Movement Analysis Profile (MAP) and the Gait Profile Score (GPS) [Baker et al., 2009] for all the successful simulations are computed. These quantities are computed thanks to the Gait Variable Scores (GVS), introduced in [Baker et al., 2009]. The GVS allow the comparison between two walking simulations with respect to the kinematics of a population mean reference, or of a specific subject. The kinematic variables involved in the computation of the GVS and MAP are:

- Pelvis angles: tilt, obliquity and rotation

- Hip angles: extension, abduction and rotation

- Knee flexion/extension

- Ankle plantar/dorsiflexion

- Foot progression angle

By normalizing the Gait cycle by its total duration, each angle trajectory can be expressed as 51 points, representing the angle value at every 2% of the gait cycle. Then, for each angle q, the GVS is calculated as:

$$\text{GVS}_q = \sqrt{\frac{1}{T} \sum_{t=1}^{T} \left(q_t - q_t^{ref} \right)^2} \tag{3.30}$$

where:

- t is a specific point in the gait cycle;

- T is the total number of points in the gait cycle, in this case 51;

- q_t is the value of the angle at time t of the gait cycle;

- q_t^{ref} is the value of the same angle for a reference population or subject.

If both left and right sides are considered, a total of 15 GVS indicators can be calculated for each walking simulation, since pelvis is no side specific. The bar plot of the GVS indicators is called the Movement Analysis Profile (MAP). While the GVS gives information about each joint separately, the Gait Profile Score (GPS), also introduced in [Baker et al., 2009], allows for a more global comparison. The GPS is computed as:

$$GPS = \sqrt{\frac{1}{N} \sum_{i=1}^{N} GVS_i^2} \tag{3.31}$$

where N is the total number of kinematic variables used. In fact, the GPS can be calculated separately for the right and left sides ($N = 9$) or gather the information of both limbs ($N = 15$).

Since the pelvis is fixed to be parallel to the ground, and the foot is set straight in the anterior/posterior direction, pelvis angles and foot progression angle are removed from the Movement Analysis Profile and the Gait Profile Score calculations. Therefore, here, $N = 10$.

In figure 3.17, the range of GVS and modified GPS values of the simulations are presented.

It can be seen that the simulations, for some values, like the hip abduction and hip rotation, present an important asymmetry. The other values are also asymmetric, but in a smaller amount. It should be noted that the reference subject also presents asymmetric
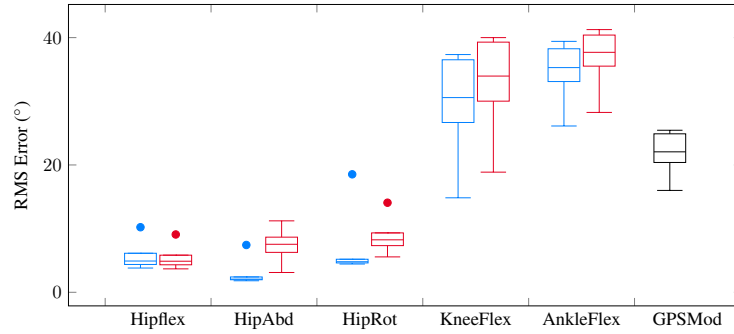
Figure 3.17: Box plot diagrams of the GVS considered and the overall modified GPS measures for the successful simulations. For each variable, blue and red box plots represent right and left sides respectively. Mid-line in the box plot represents the median value, upper and lower quartile represent values outside 75% and 25% respectively. Minimum and maximum values are also plotted as the bottom and top line or outlier, respectively.

values. Concerning the simulations, the asymmetric values could be explained by asymmetries in the lower limbs segments. In fact, the left thigh and the right shank are almost 1 cm greater than the corresponding segment on the other limb[3]. For the knee and ankle GVS, even the best value does not stay near the GVS of the reference subject.

Using the modified GPS criteria, the simulation presenting the best overall modified GPS (15,51°) can be chosen. In figure 3.18, the lower limbs' sagittal joint angles versus joint velocity are plotted.
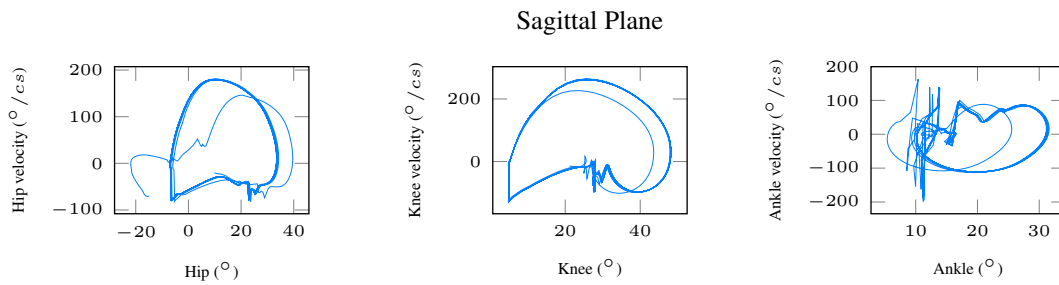

Figure 3.18: Lower limbs' sagittal joint angles trajectories versus joint velocity for the simulation presenting the best overall modified GPS (15,51°). Simulation Parameters: step length - 0.22 m, step height - 0.02 m, walking cycle duration - 1.4 s, swing phase duration 43% of total walking cycle duration. CoM shift is set at 0.06 m.

---

[3]This difference does not automatically makes the subject pathological.

The motion seems to converge to a limit cycle. Only the ankle kinematics appears a little messy.

The modified Movement Analysis Profile and Gait Profile Score for the simulation presenting the best overall modified GPS result (15,51°) is compared to the reference subject in figure 3.19.
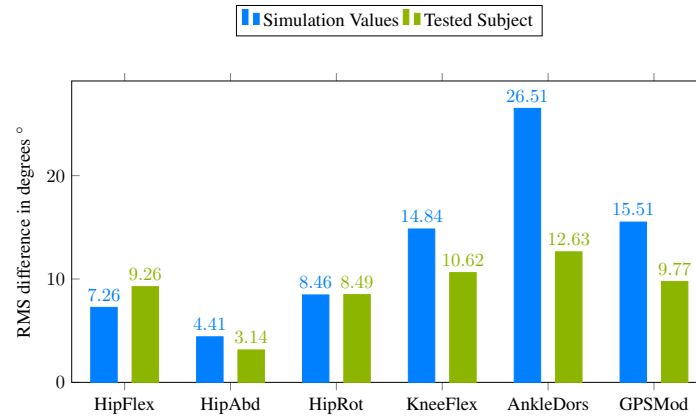

Figure 3.19: Modified Movement Analysis Profile and Gait Profile Score. Each pair of columns corresponds to one kinematic variable. Its height represents the (RMS) average difference across time between a specific gait cycle and the average gait cycle from people with no gait pathology. The values for the simulation presenting the minimal modified GPS value are in blue, the values for a specific gait cycle of the subject used for the construction of the virtual human are in green. The modified GPS for the overall gait pattern are displayed in the rightmost columns. For better reading, the results for the kinematic variables are shown only for the right side. The simulation parameters are: step length - 0.22 m, step height - 0.02 m, walking cycle duration - 1.4 s, swing phase duration 43% of total walking cycle duration. CoM shift is set at 0.06 m.

Even though simulation hip GVS present similar GVS values to that of the healthy human, the ankle and knee GVS are quite different and even duplicated with respect to the healthy human, in the ankle case.

Since GVS and GPS translate RMS errors, it is important to also analyse the angles shape, to determine where the error value comes from. This can be seen in 3.20, where some of the kinematics for a gait cycle of the lower right limb of the simulation presenting the best modified GPS value (15,51°) and of the reference subject used for the construction of the virtual human are compared.

As expected, the healthy human subject is most of the time within the range of mean healthy subjects. However, even for the best overall result, the simulation results are,
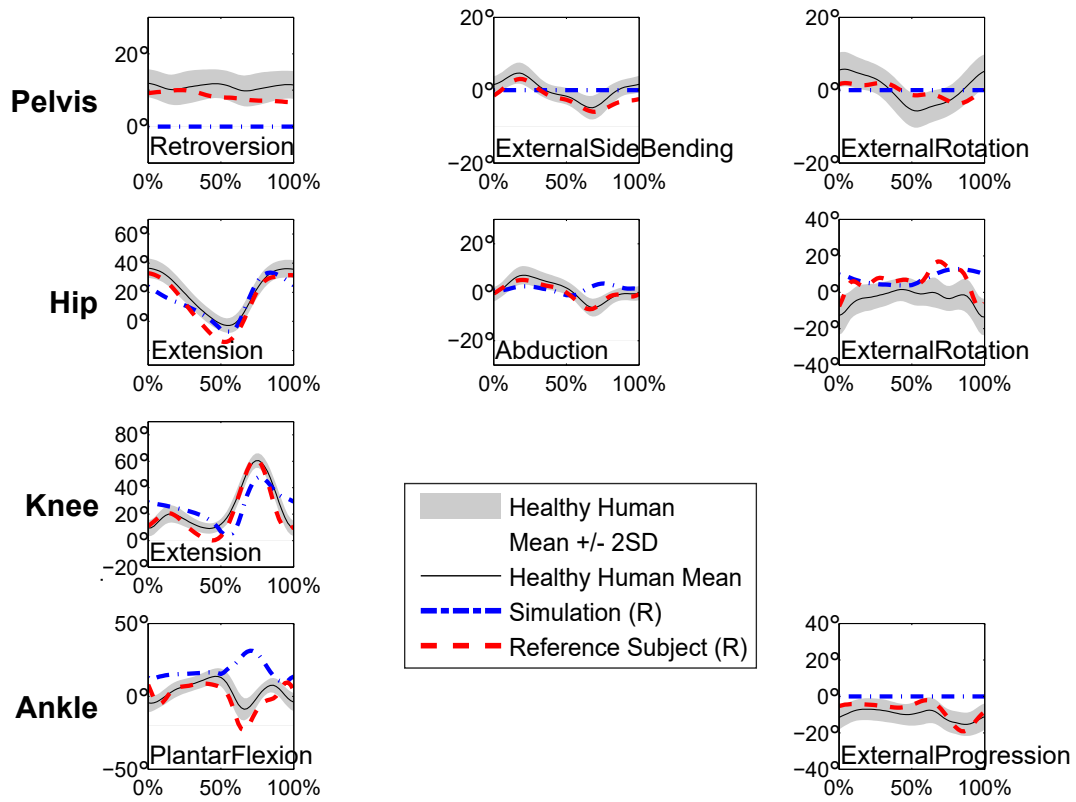
Figure 3.20: Comparison between simulated and reference subject kinematics. The real data was obtained at Fondation Ellen Poidatz with the Vicon Motion Capture System and the Plug In Gait Model for the markers placement. Kinematics is calculated using the model of section 3.1.1. Simulation kinematics is obtained for the following parameters: step length - 0.22 m, step height - 0.02 m, walking cycle duration - 1.4 s, swing phase duration 43% of total walking cycle duration. CoM shift is set at 0.06 m.

specially for the ankle dorsiflexion, not within the range of normal motion. In this angle, even a completely inverted motion is observed from 50% of the gait cycle. Since the pelvis and foot are set parallel to the ground during the entire motion, is normal to have a constant null value in those plots.

3.3.2.3 Dynamical parameters

In figure 3.21, a comparison between simulated and real human sagittal lower limbs joint torques is made.
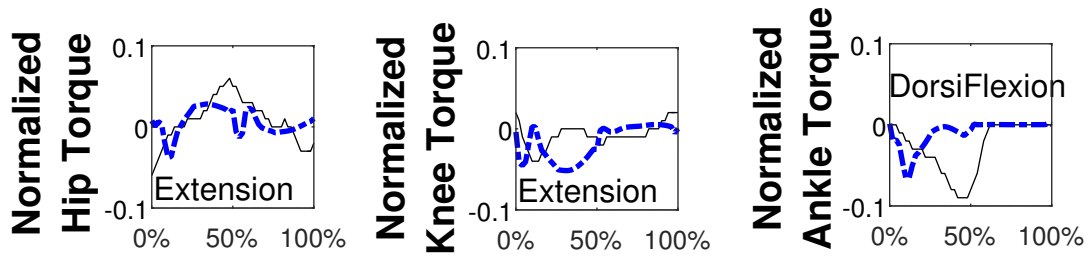

Figure 3.21: Comparison between simulated (dashed blue line) and recorded human (solid black line) [Stansfield et al., 2006] sagittal lower limbs joint torques. Torques are normalized by body weight and height. Simulation Parameters: step length - 0.22 m, step height - 0.02 m, walking cycle duration - 1.4 s, swing phase duration 43% of total walking cycle duration. CoM shift is set at 0.06 m.

It should be noted that the torques used for comparison are from children, and the numerical manikin used in simulation represents an adult. Since torques are normalised by body weight and height, these could still be compared.

During the walking movement, the peak moments magnitudes are generally smaller than those observed in natural speed human walking, but within the magnitudes observed in humans. However, knee and ankle torques present values completely opposite to human walking, in some intervals. For instance, the knee torque is negative before 50% of the gait cycle, figure 3.21 middle, while it is around 0 for healthy human walking. Similarly, the ankle torque, figure 3.21 right, is near 0 before 50% of the gait cycle, whereas in humans this value is negative.

In figure 3.22, the Ground Reaction Forces for the Left and Right Feet normalized by body mass during the first 1000 cs of simulation can be seen.

The vertical component of the GRF presents the greater value, which is consistent with the walking activity. Even though the values stay within the magnitude range of human walking (around 10 times body mass [Ady et al., 2013]), the usual "M" profile is not present. The GRF rapidly increases during the phase of double support when the foot establishes contact with the ground, and rapidly decreases during the double support phase when the foot is about to break contact with the ground. The GRF magnitude in
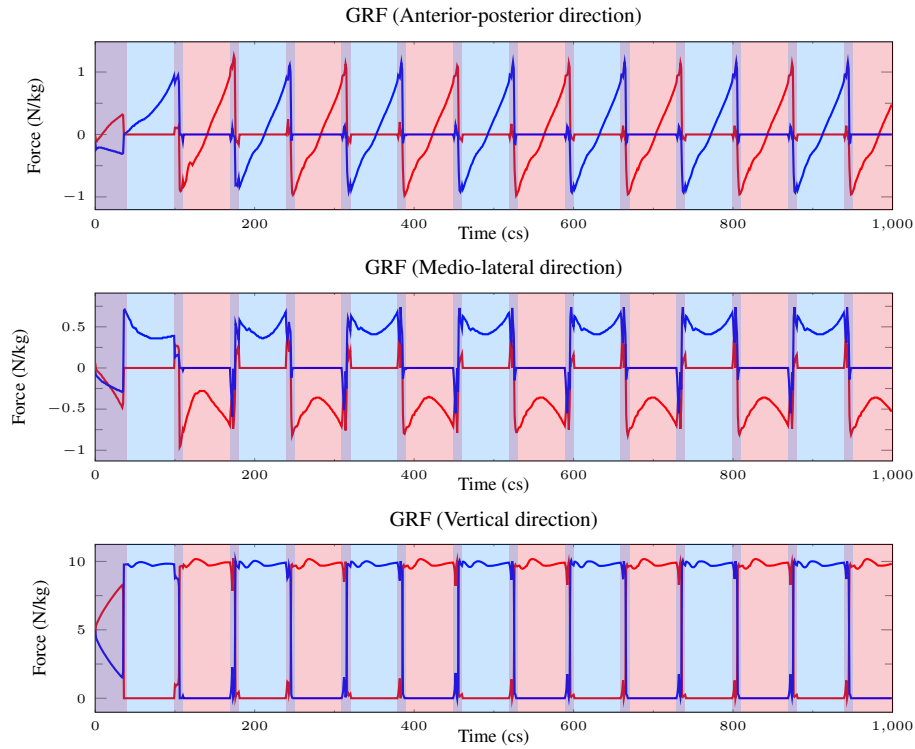
69

Figure 3.22: Ground Reaction Forces in the anterior-posterior (top), medio-lateral (middle) and vertical (bottom) directions. Forces are normalized by body mass (51,5 kg). Red and blue lines correspond to Left and Right sides respectively. Violet bands correspond to double support phases, blue and red bands correspond to right and left single support phases, respectively. Simulation Parameters: step length - 0.22 m, step height - 0.02 m, walking cycle duration - 1.4 s, swing phase duration 43% of total walking cycle duration. CoM shift is set at 0.06 m.

the anterior-posterior direction are about half those observed in human walking (around 2 times body mass [Ady et al., 2013]). When the foot establishes contact with the ground, a negative force is exerted in this direction, indicating an braking motion. The greater braking value is observed almost immediately after the contact is established. The braking force converts into an accelerating force during the single support to attain its peak when the other foot contacts the ground. Then during the double support, the force rapidly decreases to 0 as the foot is going to lift off the ground.

3.3.2.4 Balance parameters

In figure 3.23, the ZMP progression and its reference in the anterior-posterior (top) and medio-lateral (bottom) directions during the first 1000 cs of simulation can be seen.
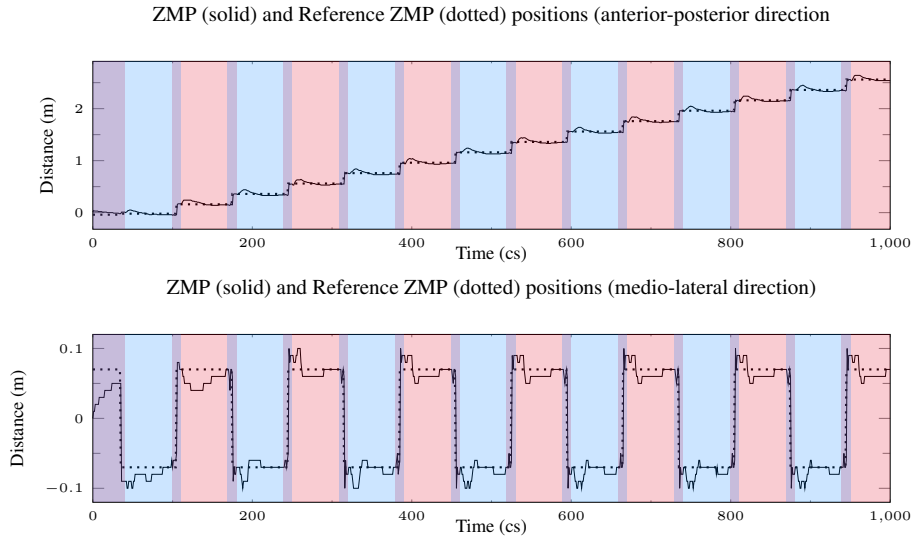

Figure 3.23: ZMP and CoM progression projected on the floor. Black solid line stands for the ZMP position, dashed black line for the CoM position on the ground. Violet bands correspond to double support phases, blue and red bands correspond to right and left single support phases, respectively. Simulation Parameters: step length - 0.22 m, step height - 0.02 m, walking cycle duration - 1.4 s, swing phase duration 43% of total walking cycle duration. CoM shift is set at 0.06 m.

In the anterior-posterior direction, figure 3.23 (top), the reference trajectory for the ZMP is followed by the real ZMP trajectory. As for the medio-lateral direction 3.23 (bottom), during single support some disturbances occur, but the reference trajectory is mostly ensured.

In figure 3.24, the ZMP and CoM progressions in the anterior-posterior (top) and medio-lateral (bottom) directions during the first 1000 cs of simulation can be seen.

In the anterior-posterior direction, figure 3.24 (top), the CoM progression is rather linear. In the medio-lateral direction, 3.24 (bottom), the progression the CoM is quite symmetric, around 0, the CoM reference.

71

ZMP (solid) and CoM(dashed) positions (anterior-posterior direction

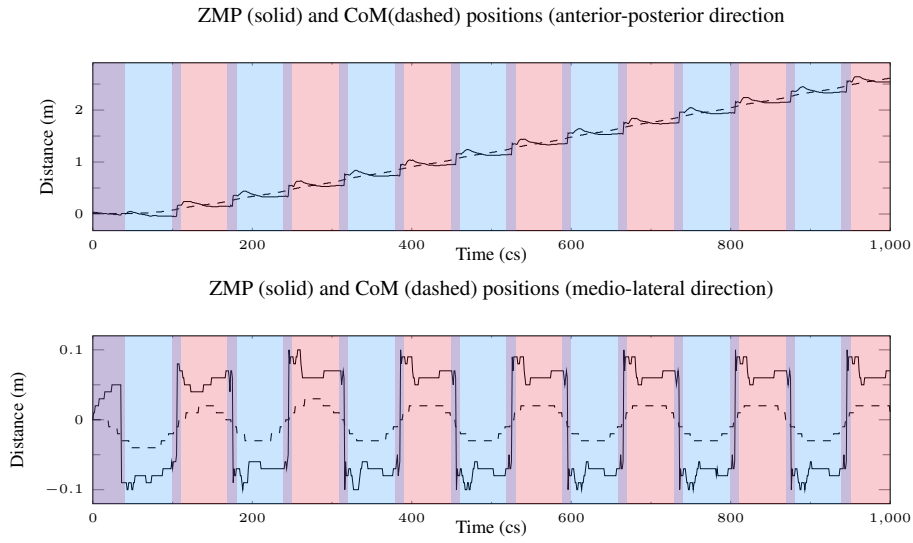ZMP (solid) and CoM (dashed) positions (medio-lateral direction)

Figure 3.24: ZMP (solid black line) and CoM (dashed black line) progression projected on the floor for the non pathological walking. Violet bands correspond to double support phases, blue and red bands correspond to right and left single support phases, respectively. Simulation Parameters: step length - 0.22 m, step height - 0.02 m, walking cycle duration - 1.4 s, swing phase duration 43% of total walking cycle duration. CoM shift is set at 0.06 m.

3.4 Conclusion

In this chapter, a framework for the control of a walking motion for a virtual human is presented.

In section 3.1, the simulation environment is presented, along with a method to generate a personalized virtual human from motion capture data, subsection 3.1.1.

The problem of controlling a walking motion for a numerical manikin is addressed in section 3.2, via a LQP-controller. This controller takes in to account actuation constraints, related to the system one wants to simulate walking for, and interactions with the ground. The walking motion is generated thanks to the definition of tasks, like maintaining balance, for instance, the manikin must accomplish during walking, subsection 3.2.3.

Simulations experiments of walking control for a virtual human using these methodology are presented in section 3.3. With this methodology and framework, given a virtual human, walking patterns with different combinations of step lengths, heights and cycle

duration are possible, figure 3.15. Different walking speeds are achievable 3.15 d).

Even though different walking patterns are possible, when compared to human data [Wheelwright et al., 1993], spatio-temporal parameters do not cover the range of human parameters. Indeed, step lengths are too limited, and walking cycle durations too long, which induce very slow motions. Also, without going into more particular details as dynamics, using the modified GPS index, it can be seen that the kinematics of the lower limb do not correspond to the usual human walking.

A possible and immediate explanation for this limitation in the range of possible motions is the foot modelling and the management of the contacts with the ground. Indeed, having a flat feet all the time and removing toe off and heel strike motions from the walking cycle greatly decreases the range of possible step lengths, and therefore, walking speeds as well.

Therefore, a first logical adaptation to increase the patterns generated concerns the feet and contacts modelling. In fact, the human foot is a very complex structure, composed of several segments and degrees of motion. However, here, only one segment is considered to model the foot. A division into two segments, to consider at least the toes complex separately is made in the next chapter. This subdivision allows to further explore feet rockers present in the human walking motion, as the toes support is then possible. Also, motions where the contact is made solely by the toes are then possible as well.

In the next chapter, another issue is also addressed, the walking initiation. Here, the virtual human goes from a standing still position to a walking state without any kind of acceleration, independently from the walking speed desired. In the next chapter, a period of acceleration is introduced in the beginning of the walking motion to evaluate the effect on the range of possible motions, specially on larger step motions.

DEVELOPING A MORE HUMAN-LIKE WALKING

In the previous chapter, a method to simulate a walking motion for a virtual human is presented. The method allows the generation of gait patterns with different ranges of step length, height and duration of cycle.

However, the spatio-temporal parameters for which the walking motion is possible do not achieve the range of parameters presented by humans when walking [Wheelwright et al., 1993]. Also, kinematics of the lower limb are quite different from the mean kinematics presented by healthy subjects.

To overcome these limits of simulation, two hypothesis are made:

- better foot modelling enlarges the range of stable gaits, improves the human resemblance, and also allows the simulation of pathological walking, like toe walking;

- including an initialization phase in the walking procedure increases the step lengths and velocities achieved.

In this chapter, a new foot model is presented, along with the changes in the simulation framework that allow different contact types between the feet and the ground. The inclusion of an initialization procedure is also described.

This chapter is organized as follows:

- section 4.1 reviews the foot modelling in the literature and introduces the proposed articulated foot;

- section 4.2 presents the principal changes in the contacts management in order to allow different contact types between the feet and the ground;

- section 4.3 establishes the changes needed in the previously defined tasks as a result of the developments of the two previews sections;

- section 4.4 explains the initialization procedure added to the gait generation;

- section 4.5 gives a general overview of the changes introduced in the walking simulation framework of chapter 3.

The resulting possible motions are left to the next chapter.

4.1   Foot Modelling

The human foot is a very complex structure, composed of several bones and joints [Hillstrom et al., 2013]. In the previous chapter, the foot segment is reduced to a single segment representation, having solely the ankle joint. Even though the ankle is the main joint involved in locomotion [Bähler, 1986], from previous chapter' results it can be seen that a flat foot with an ankle does not allow the generation of some walking patterns, like non pathological walking motion, or toe walking. Therefore, we make the hypothesis that a better foot modelling can increase the variety of patterns generated.

Recall from chapter 2 that the walking cycle for a human who does not present any locomotion disorder is made of the following sequential events:

1. Initial Contact (IC)

2. Opposite Toe Off (OTO)

3. Heel Rise (HR)

4. Opposite Initial Contact (OIC)

5. Toe Off (TO)

6. Opposite Heel Rise (OHR)

7. Initial Contact (IC) - step 1

Thus, the new foot modelling to be adopted must allow this sequence of events, in order to reproduce non pathological human walking. Since gait pathologies are of concern in this thesis, the new foot modelling must also allow a greater variety of walking patterns than the simple flat foot walking. The objective is set to simulate non pathological human walking, flat foot initial contact and toe walking.

4.1.1 Foot Models in the literature

The foot modelling concerns a variety of disciplines. In the particular case of walking, most of researches concentrate on the bioengineering/biomedical and robotics fields.

Foot Models in the bioengineering/biomedical fields   In the biomedical and bioengineering fields, the purposes of foot modelling are varied: kinematic or kinetic analysis, forward simulations, etc, but they have a common point, they mostly concern the understanding of human motion.

In Clinical Gait Analysis, the particular study of the foot is more recent, probably due to the complexity of this body part and the derived technical constraints for the analysis of its movement. The first works, like the one of Winter in 1984 [Winter, 1984], study only the ankle movement in the sagittal plane.

Latter on, another degree of freedom is introduced in the foot modelling to reproduce the movement of the subtalar joint, joining the talus and the calcaneus segments. Even though simple to study in healthy subjects, difficulties appear in pathological cases [van den Bogert et al., 1994].

In 1996, the International Society of Biomechanics proposed a 6 degree of freedom model of the rearfoot [Allard et al., 1996]. Since then, several models of the foot have been developed. One of the kinematical models of reference is the Oxford Foot Model [Carson et al., 2001]. It is a three segment foot model, composed by hindfoot (calcaneus and talus), forefoot (metatarsals) and hallux (toes) segments. Its repeatability is successfully tested in both healthy adult feet [Carson et al., 2001], and in children's feet [Stebbins et al., 2006], with a modified version.

A more complex model is introduced in 2003 by MacWilliams *et al* [MacWilliams et al., 2003]. Their foot model presents nine segments: hallux, medial toes, lateral toes, medial forefoot, lateral forefoot, calcaneus, cuboid, talus/navicular/cuneiform and tibia/fibula. These type of complex models allow the study of particular joints, like the subtalar joint [Jenkyn et al., 2010], for instance.

If muscles are joined to the foot modelling, musculoskeletal analysis like those proposed by the OpenSim team and network [Delp et al., 2007, Seth et al., 2011] can be performed. This type of modelling is out of the scope of this work.

Foot Models in the robotics field   In the robotics field, specially in humanoid robotics, the foot modelling appears as a necessity to gain in human resemblance. Indeed, most of

humanoid robots walk with flat feet, which inhibits them of walking human-likely. This flat feet walking is mostly used for safety reasons. Nevertheless, some researchers started to be interested in overcome this flat feet condition, in order to improve robots walking.

In [Li et al., 2010], using a one segment foot, the authors are capable of reproducing toe off and heel strike events. Still, they pointed out the decrease in walking stability with increasing step, limiting it to no more than 50% of full leg length. Therefore, this kind of approach is not suitable for this work, as step lengths would potentially be limited as well. Besides, toe walking motions would also be excluded from the variety of patterns that could be reproduced.

An interesting approach can be found in [Ogura et al., 2006]. In this work, the authors develop a humanoid robot with passive toe joints, see figure 4.1, in order for the simulated walking motion to be more human resembling. Stable walking up to 0.50 m step length and 0.96 s per step, is achieved.
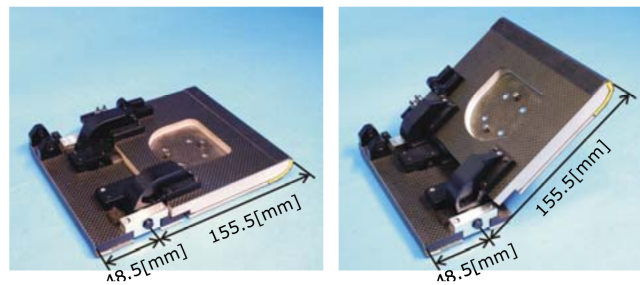

Figure 4.1: Foot mechanism from [Ogura et al., 2006], in rest (left) and bent (right) positions.

In the work of Ouezdou *et al* [Ouezdou et al., 2005], the feet are considered to be made of four segments: heel, central part of the foot and two toe parts (the toes are divided in two segments). The authors compare, in terms of energy consumption and vertical ground reaction force, four different types of feet for humanoids robots, see table 4.1. Using the rigid feet as a reference, they conclude that all the three types of foot decrease energy consumption, specially the active and flexible active foot. Furthermore, they found out that the flexible active foot greatly improves the vertical ground reaction force resemblance with that produced by humans (qualitatively speaking), even though an important peak still remained.

Other approaches try to improve the foot modelling by using rubber bushes and pads in the foot design in order to absorb shocks [Li et al., 2008], or to design a foot mechanism

Table 4.1: Foot types consider in [Ouezdou et al., 2005].

Foot type	Definition
Rigid Flat	No joints between the four parts.
Flexible	With a passive joint at the toes.
Active	With an active joint at the toes.
Flexible Active	With an active joint at the toes and two passive joints between the heel and the central part and between the two parts of the toes.

similar to that of a human composed of a toe, an ankle, a heel and springs to reproduce the foot muscles and tendons [Seo and Yi, 2009]. In both works, comparative results of the generated walking pattern with human walking are not presented.

Given the variety of possibilities to model the foot and the purposes intended in this work, a modelling approach with a rigid foot composed of two segments is chosen. This approach is detailed next.

4.1.2   Articulated Foot

In order to maintain the approach proposed in chapter 3 for the walking pattern generation, the foot segment as a whole is still considered as a box. This increases the surface of contact with the ground, and therefore increases the support polygon for the ZMP criteria to be satisfied.

To be able to consider heel strike and toe off, two important events of the walking cycle, the foot segment is divided into rear foot (comprising the rear foot and the mid foot) and forefoot, like in the work of [Ogura et al., 2006]. However, contrarily to [Ogura et al., 2006], the joint relying both segments is active. This joint is placed at the sole level and at the middle of the two segments.

For the rear foot, the reference frame follows that of the foot of chapter 3.

The forefoot reference frame is the same as the foot reference frame, except for its origin. The forefoot origin matches the joint origin. The new kinematic foot model can be found in figure 4.2. A list of the degrees of freedom of the new model is presented in table 4.2.

The inertial parameters are calculated using the inertial properties of a box. Foot mass is divided as 73% in the rear and 27% in the front [Luximon, 2013].

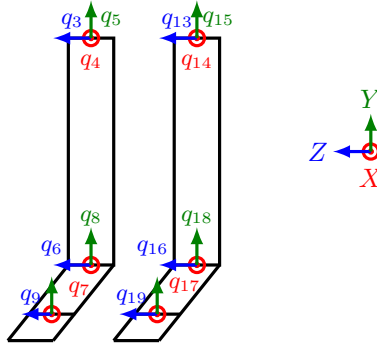This foot modelling allows for new modes of contact with the ground, besides the flat

79

Figure 4.2: Kinematic model of the new foot model, in the front view. The degrees of freedom of the whole body model are listed in table 4.2.

Table 4.2: Listing of the DoF's of the new kinematic model.

	Parent Body	Child Body	Joint
q_0, q_1, q_2	Pelvis	Right Thigh	Right Hip
q_3, q_4, q_5	Right Thigh	Right Shank	Right Knee
q_6, q_7, q_8	Right Shank	Right Rear Foot	Right Ankle
q_9	Right Rear Foot	Right Forefoot	Right Metatarsal
q_{10}, q_{11}, q_{12}	Pelvis	Left Thigh	Left Hip
q_{13}, q_{14}, q_{15}	Left Thigh	Left Shank	Left Knee
q_{16}, q_{17}, q_{18}	Left Shank	Left Rear Foot	Left Ankle
q_{19}	Left Rear Foot	Left Forefoot	Left Metatarsal
q_{20}, q_{21}, q_{22}	Pelvis	Torso	Pelvis-Torso
q_{23}, q_{24}, q_{25}	Torso	Right Arm	Right Shoulder
q_{26}	Right Arm	Right Forearm	Right Elbow
q_{27}, q_{28}, q_{29}	Right Forearm	Right Hand	Right Wrist
q_{30}, q_{31}, q_{32}	Torso	Left Arm	Left Shoulder
q_{33}	Left Arm	Left Forearm	Left Elbow
q_{34}, q_{35}, q_{36}	Left Forearm	Left Hand	Left Wrist
q_{37}, q_{38}, q_{39}	Torso	Head	Torso-Head

foot previously presented, that are detailed next.

4.2   Contacts Management

With the introduction of an articulated foot, new modes of contact with the ground are possible. In figure 4.3, the contact points defined for the articulated foot are shown.
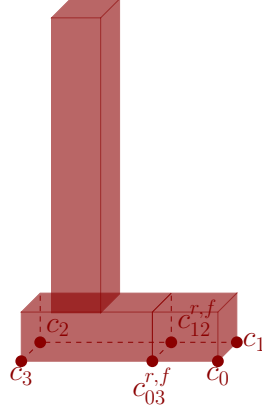
Figure 4.3: Contacts points for the new foot configuration. Here, two sets of contact points are defined, corresponding to the rear foot $\left(c_3, c_2, c_{03}^r, c_{02}^r\right)$ and the forefoot $\left(c_{03}^f, c_{02}^f, c_0, c_1\right)$.

As before, flat foot contact is possible, but also a contact through the forefoot only. Therefore, movements like heel strike and toe off are feasible, and new walking motions can be generated. Three types of contacts, generating three types of motion, are considered:

- contact through the forefeet only during the entire motion - toe walking;

- heel strike at initial contact and toe off motion, as presented in chapter 2 - non pathological walking;

- flat foot initial contact and toe off motion - new flat feet walking.

In the following, these three types of contact, and their respective motions, are detailed.

4.2.1 Toe Walking

This type of contact is simple to treat, as in fact it is very similar to the flat feet contact presented in the previous chapter. The walking generation method stays the same, with the difference that instead of the whole foot, only a part of it, the forefoot, contacts the ground. In order to make the method more realistic, changes are introduced, so that the gait generated can be asymmetric, both in space (step lengths) and in time (double and single support not equal for both sides). Instead of a predefined duration for the double

and single support phases, four durations are defined to determine the different phases of a walking cycle. Considering the temporal asymmetry now possible, the contacts management for the toe walking can be seen in figure 4.4.
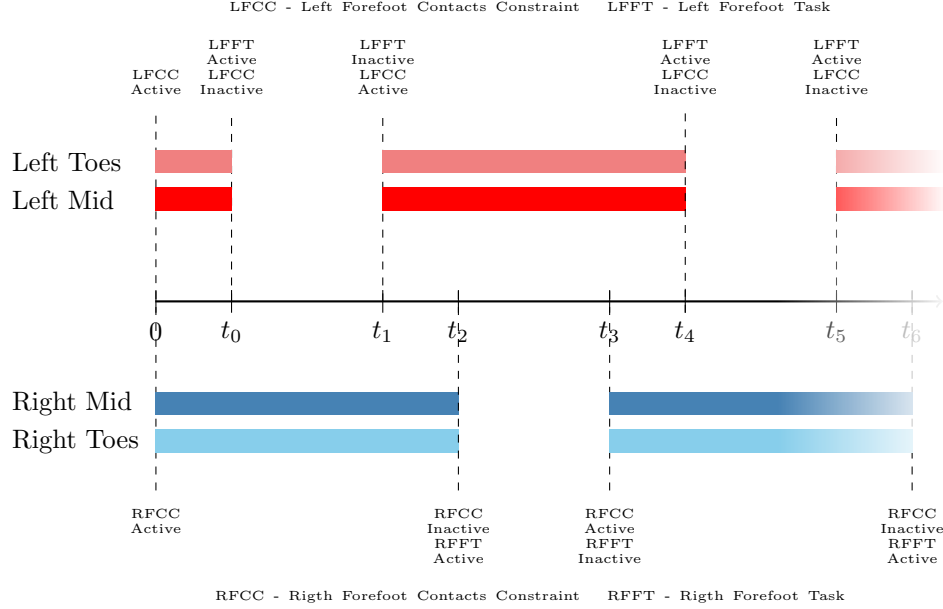

Figure 4.4: Contacts Manager schematics for the Toe Walking. The coloured rectangles indicate contact with the ground, and so, the absence of colour indicates no contact. The Left/Right Toes stand for contact points c_0, c_1 and Left/Right Mid stand for contact points c_{03}^f, c_{12}^f, see figure 4.3. The Forefoot contacts are composed of the Mid and Toes contact points.

As before, at the beginning of the walking motion, both forefeet are in contact with the ground and the contacts for these two segments are activated. Nothing is done with the rear foot, as it does not contact the ground at any time. At $t = t_0$, the left forefoot leaves the ground, and so the contact with the ground is deactivated. At the same time, the forefoot trajectory task for the left foot is activated (this trajectory is developed further). The left forefoot re-establishes contact with the ground at $t = t_1$, so the contact constraints for the left forefoot are reactivated, and the left forefoot trajectory task ends. There is a double support phase between t_1 and t_2, and at t_2, the right forefoot leaves the ground, so the contact constraints for the right forefoot are removed from the optimisation problem. The right forefoot trajectory task is initiated at the same time. The right forefoot re-establishes contact with the ground at $t = t_3$, and, so, the contacts for the right forefoot

are reactivated. The right forefoot task ends at this point. There is a new double support phase between t_3 and t_4, and the cycle re-starts at $t = t_4$.

Lets note T the total duration of the gait cycle. Since the cycle re-starts at t_4, see figure 4.4, we have that $T = t_4 - t_0$. Lets define:

$$p_0 = \frac{t_1 - t_0}{T}, \quad p_1 = \frac{t_2 - t_0}{T}, \quad p_2 = \frac{t_3 - t_0}{T}, \quad p_3 = \frac{t_4 - t_0}{T}. \tag{4.1}$$

To define a walking motion in time, only these time percentages p_i and the total duration T of the gait cycle are needed. They allow the generation of walking cycles until the end of the predefined steps. The number of walking cycles depends on the step length and the distance to achieve.

4.2.2 Non Pathological Walking

The existence of forefeet also allows the implementation of a walking sequence similar to that encountered in the walking of healthy subjects, see chapter 2, section 2.1. It can be seen that the foot contacts the ground sequentially by parts, and the same happens when breaking the contact. Therefore, the coordination between the different parts of each foot must be taken into account.

In figure 4.5, the sequence of activation and deactivation of the contacts for the non pathological contact can be seen. The walking motion starts with both feet on the ground. A description of the sequence of events illustrated in figure 4.5 can be found in table 4.3.

The events between t_2 and t_{14} give a complete gait cycle of total duration $T = t_{14} - t_2$. As before, lets define:
$$p_{i-3} = \frac{t_i - t_2}{T}, \quad i = 3, 4, ..., 14 \tag{4.2}$$

To define a walking motion in time, only these time percentages and the total duration T of the gait cycle are needed. They allow the generation of walking cycles until the end of the predefined steps. The number of walking cycles depends on the step length and the distance to achieve.

4.2.3 New Flat Feet Walking

As seen in the previous chapter, the flat feet condition for walking greatly constraints the motions achievable. Therefore, since the foot is now articulated in two segments, the flat feet motion seen earlier is adapted, so newer motions can be expected. The contact with
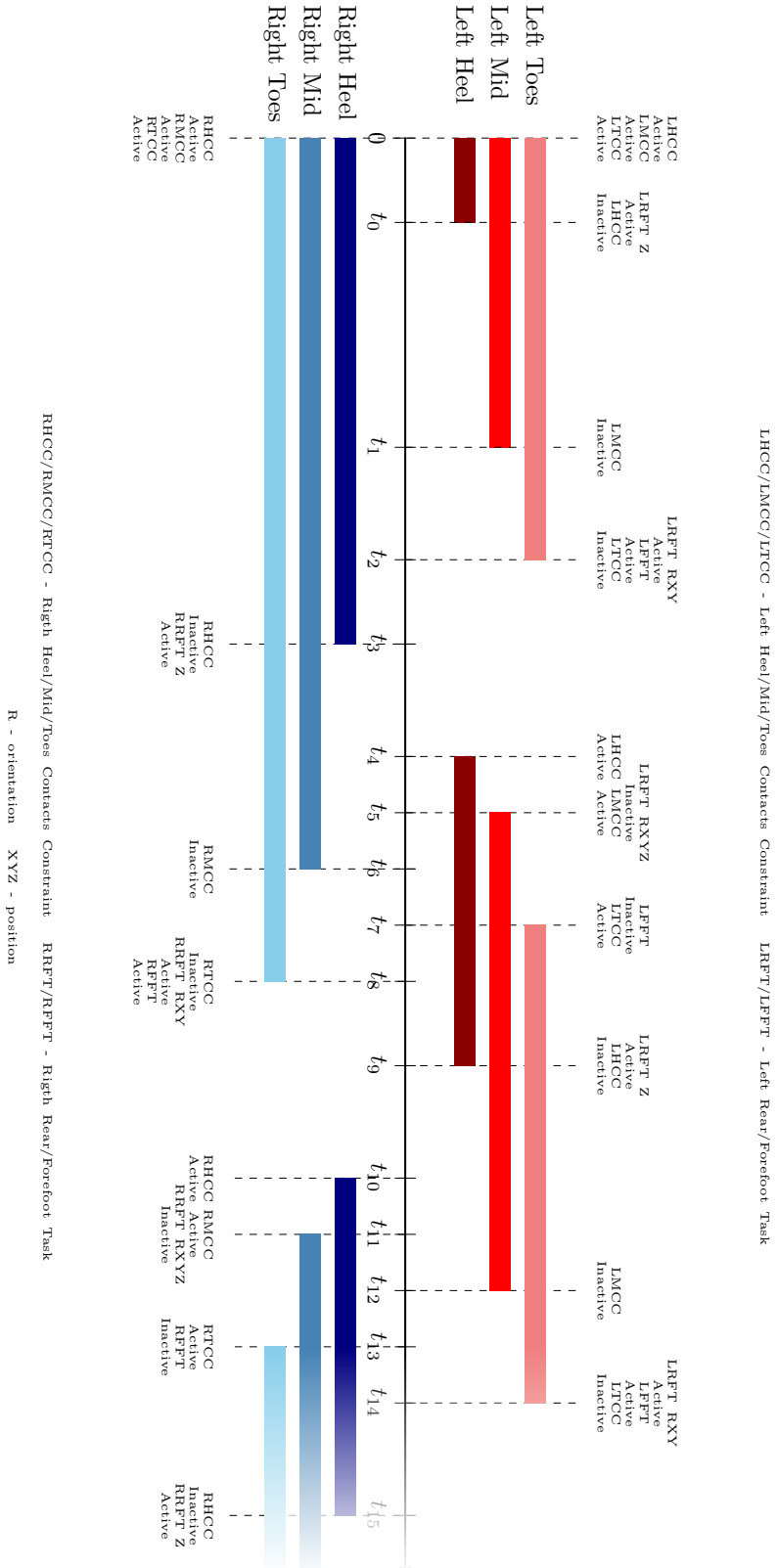
Figure 4.5: Contacts Manager schematics for the Non Pathological Walking. The coloured rectangles indicate contact with the ground, and so, the absence of colour indicates no contact. The Left/Right Toes stand for contact points c_0, c_1, Left/Right Mid stand for contact points c_{03}, c_{12} and Left/Right Heel stand for contact points c_3, c_2, see figure 4.3. Rear foot trajectory task is decomposed in different tasks related to orientation R and position XYZ. A description of the sequence of events can be found in table 4.3.

Table 4.3: Contacts Management of the non pathological walking illustrated in figure 4.5. LHCC/RHCC, LMCC/RMCC and LTCC/RTCC stand for left/right heel, mid and toe contacts, respectively. LRTF/RRTF and LFFT/RFFT stand for left/right rear foot and forefoot tasks, respectively.

Time	Left Foot Tasks	Left Foot Contacts	Right Foot Tasks	Right Foot Contacts
$t = 0$	-	LHCC active LMCC active LTCC active	-	RHCC active RMCC active RTCC active
$t = t_0$	LHCC inactive	LRFT Z active	-	-
$t = t_1$	LMCC inactive	-	-	-
$t = t_2$	LTCC inactive	LRFT RXY active LFTT active	-	-
$t = t_3$	-	-	RHCC inactive	RRFT Z active
$t = t_4$	LHCC active	-	-	-
$t = t_5$	LMCC active	LRFT RXYZ inactive	-	-
$t = t_6$	-	-	RMCC inactive	-
$t = t_7$	LTCC active	LFFT inactive	-	-
$t = t_8$	-	-	RTCC inactive	RRFT RXY active RFTT active
$t = t_9$	LHCC inactive	LRFT Z active	-	-
$t = t_{10}$	-	-	RHCC active	-
$t = t_{11}$	-	-	RMCC active	RRFT RXYZ inactive
$t = t_{12}$	LMCC inactive	-	-	-
$t = t_{13}$	-	-	RTCC active	RFFT inactive
$t = t_{14}$	LTCC inactive	LRFT RXY active LFTT active	-	-

the ground is established with the whole foot, as before, but when leaving the ground, the motion is sequential, as in the non pathological walking. As for the contact with the ground, $t_4 = t_5 = t_7$ and $t_{10} = t_{11} = t_{13}$, in the previous case to generate the flat feet motion. The new flat feet approach is illustrated in figure 4.6.

The events between t_2 and t_{10} give a complete gait cycle of total duration $T = t_{10} - t_2$. As before, lets define:

$$p_{i-3} = \frac{t_i - t_2}{T}, \quad i = 3, 4, ..., 10 \tag{4.3}$$

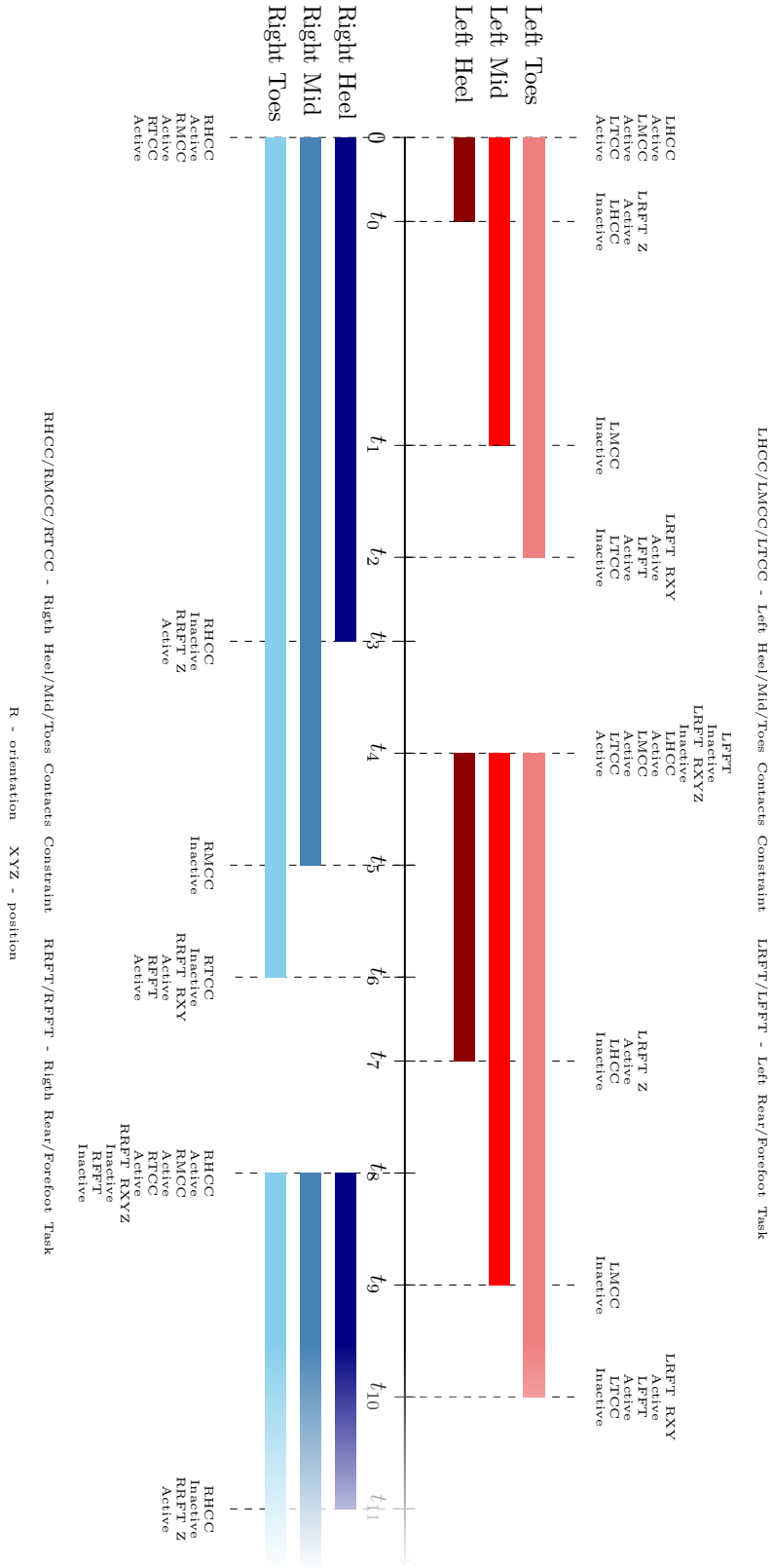The walking motion is defined likewise the non pathological walking.

Figure 4.6: Contacts Manager schematics for the New Flat Feet Walking. The coloured rectangles indicate contact with the ground, and so, the absence of colour indicates no contact. The Left/Right Toes stand for contact points c_0, c_1, Left/Right Mid stand for contact points c_{03}, c_{12} and Left/Right Heel stand for contact points c_3, c_2, see figure 4.3. Rear foot trajectory task is decomposed in different tasks related to orientation R and position XYZ.

4.3 References for the Foot Related Tasks

The changes in the contacts sequence induce changes in the tasks dependent of foot placements. These tasks are treated hereafter.

As mentioned before, the toe walking does not induce changes in the foot placement besides the segments in contact with the ground, which instead of the whole foot is simply the forefoot. The only changes introduced are in the step lengths and in the timings handling, which now can be asymmetric. These changes are easily integrated in the previous method. Therefore, with small adaptations, the built method of the references from the previous chapter can still be applied.

This is not the case for the non pathological walking and the flat feet case. Indeed, the moving base of support for the walking changes and the ZMP can not simply alternate between one foot and the other, as the base of support can be formed by parts of a single foot or a combination of different parts of both feet. Therefore, the ZMP reference used for the CoM task needs to be adapted accordingly. Also, since the foot is no longer a unique segment and consequently all the parts do not move together in these cases, the foot displacements from one footprint to the next must be rebuilt as well. These are treated next.

4.3.1 The CoM Task

As the base of support for the walking sequence changes with the non pathological and the new flat feet walking, the ZMP reference must be adapted. In fact, instead of alternating the ZMP reference between the middle of one segment and the other, a continuous ZMP reference is designed.

Non pathological walking   In order to design a ZMP trajectory for the non pathological walking, two conditions are taken into account:

- real center of pressure (CoP), equivalent to ZMP when ZMP exists, progression must be considered in the design of ZMP references;

- numerical consistency with segments in contact with the ground must be ensured.

Concerning the first part, in figures 4.7 and 4.8, CoP progression is compared to Foot Markers positioning for a healthy subject. The data was collected at Fondation Ellen

Poidatz for a healthy female subject with 1.63 m of height and 54.2 Kg of body mass. The data presented starts at gait initiation, both feet on the ground over a force platform, and ends when no more force platform data is available to perform the CoP calculation. The subject was asked to walk at her preferential speed in the anterior-posterior direction. Four force platforms were disposed in a row for the data collection. The Vicon system was used for the collection of the data.

In figure 4.7, the progression of the CoP in the anterior-posterior direction, with respect to foot markers position, can be seen.
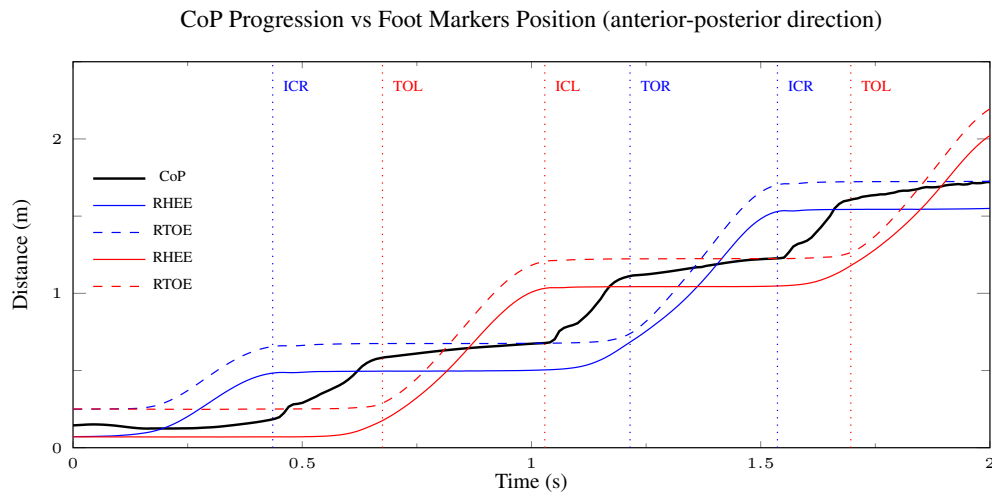
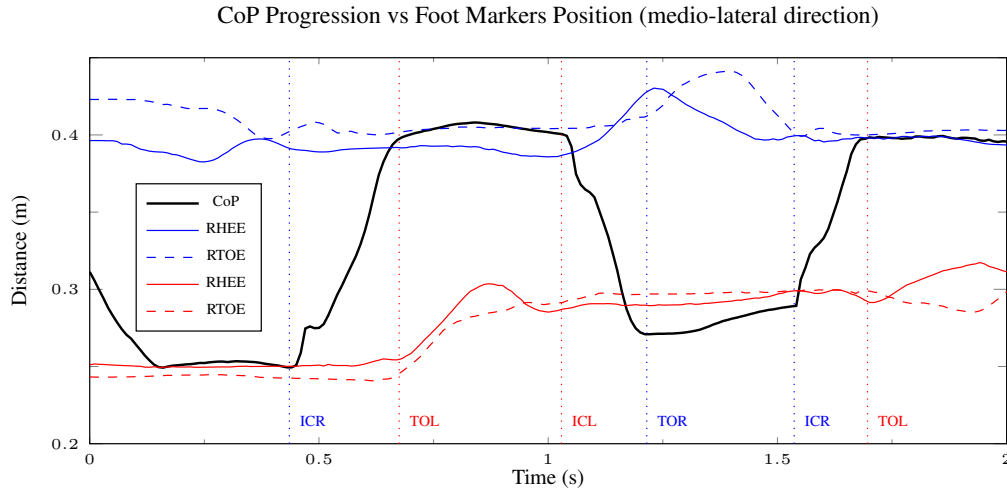Figure 4.7: CoP progression versus Foot Markers position, in the displacement direction. LHEE,RHEE stand for the heel marker at left and right heels, respectively, and LTOE, RTOE stand for the markers at left and right second metatarsal head. ICR/ICL and TOR/TOL stand for Initial Contact and Toe Off for the right/left foot, respectively.

The walking starts with the displacement of the right foot.

At $t = 0$, the foots are aligned in the anterior-posterior direction, and the CoP is located around the middle of HEE[1] and TOE[2] markers.

Until the initial contact of the right foot, the CoP varies around its initial position. Between the right initial contact and the left toe off, the CoP goes from its position to the middle of the right HEE and TOE markers.

After initiation, the CoP displacement follows the same routine:

---

[1]"Placed on the calcaneous at the same height above the plantar surface of the foot as the toe marker." [Robertson, 2009], see appendix A.

[2]"Placed over the second metatarsal head, on the mid-foot side of the equinus break between fore-foot and mid-foot." [Robertson, 2009], see appendix A.

1. from its position, at the middle of the support HEE and TOE markers, to the TOE of the support foot, from swing foot toe off until swing foot initial contact;

2. from TOE to the middle of the new support foot HEE and TOE markers, from initial contact of the new support foot until toe off of the new swing foot;

3. repeat the displacement from 1 until the end of the data.

It should be noted that in the anterior-posterior direction the CoP movement is almost piecewise linear.

In figure 4.8, the progression of the CoP in the medio-lateral direction, with respect to foot markers position, is plotted.

Figure 4.8: CoP progression versus Foot Markers position, in the medio-lateral direction. LHEE, RHEE stand for the heel marker at left and right heels, respectively, and LTOE, RTOE stand for the markers at left and right second metatarsal head. ICR/ICL and TOR/TOL stand for Initial Contact and Toe Off for the right/left foot, respectively.

At $t = 0$, the CoP is between the left and right foots, closer to the left rather than the right foot. CoP goes to the left foot, to become aligned with the HEE marker, in the medio-lateral direction.

It stays constant in the left foot until the right foot initial contact, where it starts its displacement to attain the right foot at left toe off.

Even though the medio-lateral movement of the feet is less "linear" than that in the anterior-posterior direction, after initiation, the CoP follows the same routine:

1. stays constant within the support foot, from swing foot toe off until the swing foot initial contact;

2. goes from one foot to the other, from swing foot initial contact until new swing foot toe off;

3. repeat the displacement from 1 until the end of the data.

By taking these anterior-posterior and medio-lateral displacement into account, a ZMP reference trajectory can be designed. This must take into account the position of the HEE and TOE markers in the modelled articulated foot. This positioning is showed in figure 4.9. The motion is assumed to be straightforward, therefore the foot position on the ground is considered constant in the medio-lateral direction during the entire motion.
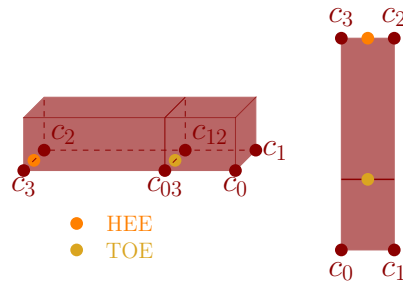
Figure 4.9: HEE and TOE markers position in the modelled foot in the lateral (left) and top (right) views.

The designed ZMP reference trajectory for non pathological contact and the respective changes in foot contacts are illustrated in figure 4.10. In figure 4.10 a), the ZMP location with respect to the feet locations on the ground is illustrated for key instants of the walking motion. These key instants are related to the changes in the foot contacts depicted in figure 4.10 b).

When the walking procedure starts at $t = 0$, the feet are aligned on the ground and the ZMP reference is located at the middle of the rear feet. Once the walking motion is cyclic started (from t_2 on, see figure 4.10), the ZMP progression follows the same pattern:

- it goes from the middle of the support rear foot until the middle of the support forefoot, from opposite toe off until heel off;

- stays constant in the support forefoot, from heel off until opposite initial contact;

(a) ZMP position with respect to feet position for non pathological walking.

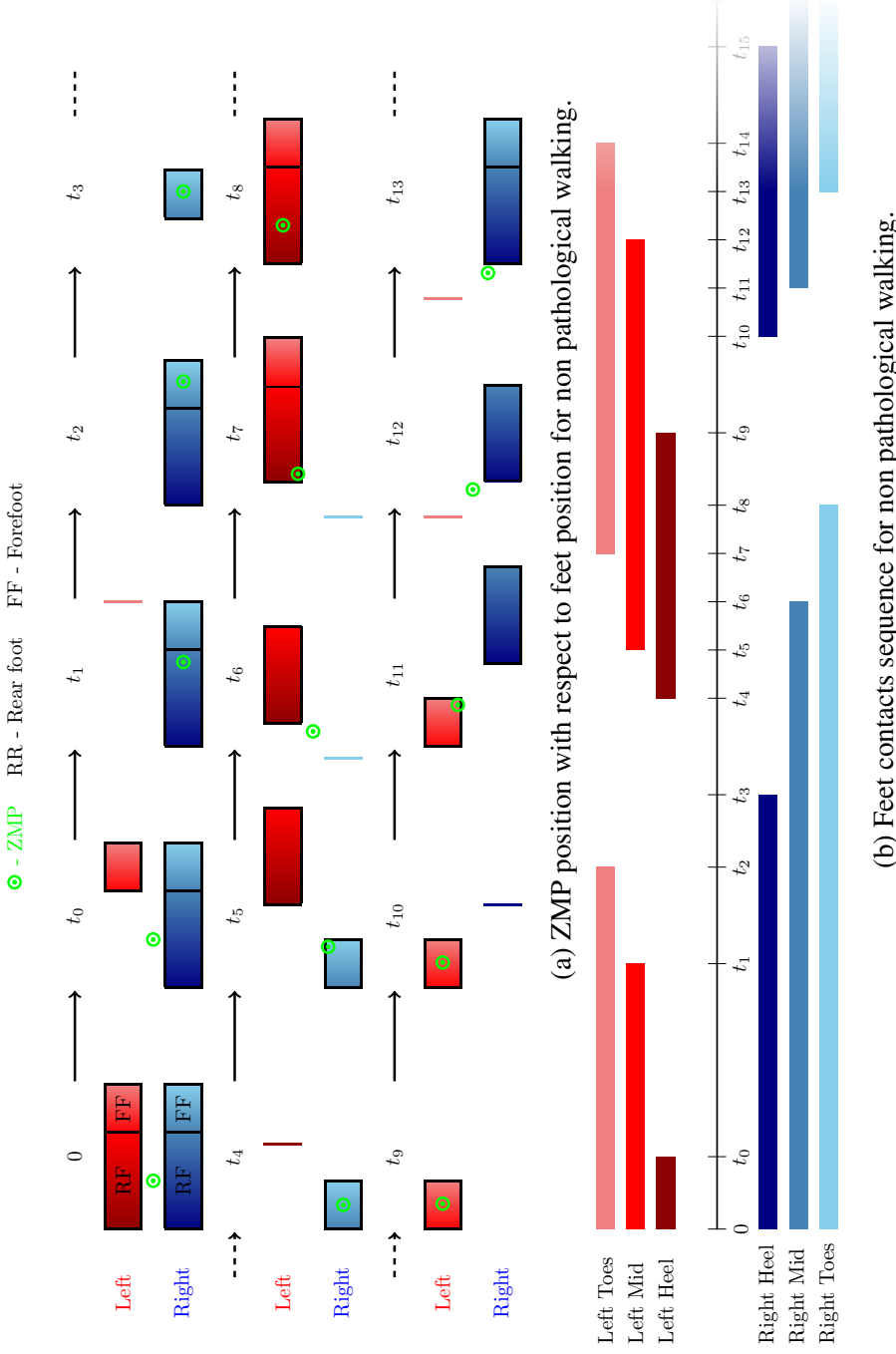
(b) Feet contacts sequence for non pathological walking.

Figure 4.10: ZMP position with respect to feet position and Feet contacts sequence for non pathological walking. When the walking procedure starts at $t = 0$, the feet are aligned on the ground and the ZMP reference is located at the middle of the rear feet. Until $t = t_0$, instant where the left heel starts to rise and so only the forefoot stays completely in contact with the ground, the ZMP reference stays constant in its initial position. From $t = t_0$ to $t = t_1$, in the medio-lateral direction, the ZMP reference linearly changes from its current position until the middle of the right foot. At $t = t_1$, when the left rear foot completely leaves the ground, in the medio-lateral direction, the ZMP changed from the middle of the feet to the middle of the right foot. From $t = t_0$ to $t = t_2$, in the anterior-posterior direction, the ZMP reference linearly changes from its current position until the middle of the right forefoot. The ZMP stays constant in the middle of the right forefoot until $t = t_4$, when the left heel strikes the ground. From $t = t_4$ to $t = t_8$, the ZMP position linearly changes from the middle of the right forefoot to the middle of the left rear foot. It continues its progression from the middle of the left rear foot, from $t = t_8$ until $t = t_9$. From $t = t_9$ to $t = t_{10}$, it stays constant in the middle of the left forefoot. At $t = t_{10}$, the ZMP starts its progression from the middle of the left forefoot to the middle of the right rear foot, attained at $t = t_{14}$.

91

- goes from the middle of the forefoot until the middle of the opposite rear foot, from opposite initial contact until toe off;

And the sequence repeats itself until the end of available steps.

Flat feet walking   As done for the contacts sequence, the ZMP trajectory is adapted from that just presented for the non pathological walking. The main difference concerns the initial contact of the foot. The ZMP trajectory designed for this case is illustrated in figure 4.12.

4.3.2   The Foot Tasks

For the non pathological walking and the flat feet walking, the foot does not leave the ground as a whole as before. Therefore, adaptations must be done to the feet displacement from one footprint to the next one, in order to make the walking motion possible.

Non pathological walking   In the same way that ZMP references are designed taking into account real data, foot displacement from one footprint to the next one is also based in healthy subjects data.

In order to get a mean reference for feet displacement, motion capture data already available from 4 healthy subjects (3 female and 1 male) is used. The subjects characteristics in terms of height and body mass distribution are given in table 4.4.

Table 4.4: Subjects characteristics: mean and standard deviation of height and body mass.

Number	Height (m)	Body mass (kg)
4	1.628 ± 0.086	52.6 ± 8.7

From those subjects, a total of 12 foot displacements are treated. Mean reference is calculated as follow:

- **anterior-posterior direction:** foot displacement is normalized by stride length, and time is normalized by foot displacement duration[3]. Mean normalized anterior-posterior displacement is calculated from the normalized data, see figure 4.13;

- **medio-lateral direction:** no reference is calculated as the walking is assumed to be straightforward;

---

[3]Duration of foot displacement is defined from heel off to complete flat foot on the ground.
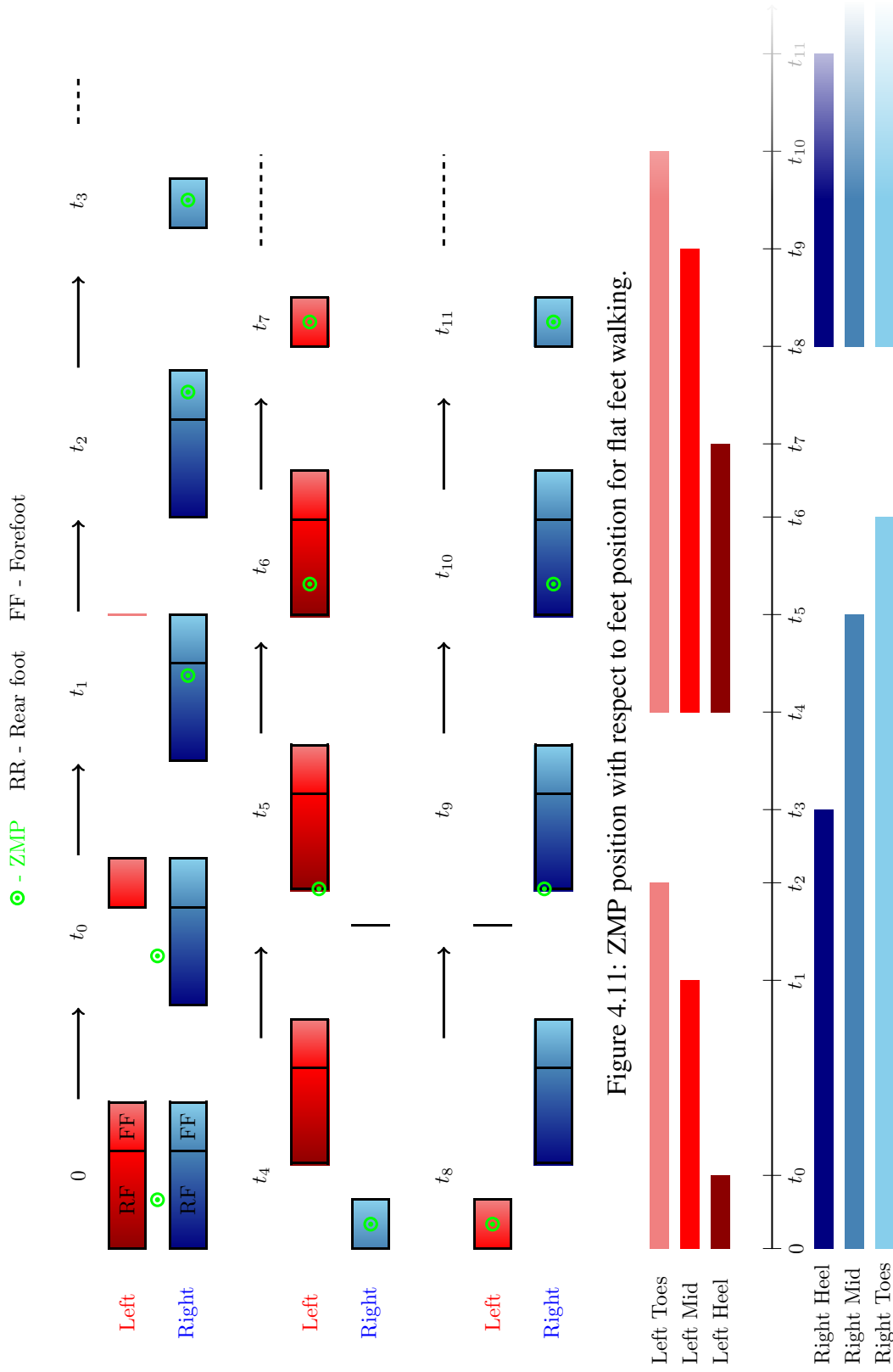
Figure 4.11: ZMP position with respect to feet position for flat feet walking.

(a) Feet contacts sequence for flat feet walking.

Figure 4.12: ZMP position with respect to feet position and Feet contacts sequence for flat feet contact walking.

- **vertical direction:** foot displacement is normalized by maximum heel height, and time is normalized by foot displacement duration. Mean normalized vertical displacement is calculated from normalized data and then corrected to have a maximum of 1, see figure 4.14;

- **orientation:** since no medio-lateral movements are considered (foot progression angle is assumed to be 0), the angle between the foot and the ground is calculated using the angle between the vector relying the HEE and TOE markers[4] with the ground. Angular displacement is normalized by maximum angular amplitude, and time is normalized by foot displacement duration. Mean normalized angular displacement is calculated from normalized data and then corrected to have a maximum of 1, see figure 4.15.
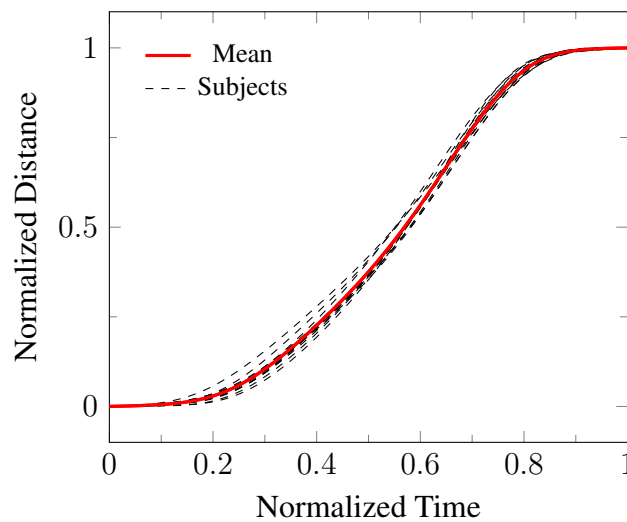
Figure 4.13: Foot anterior-posterior displacement: trajectories from healthy subjects (dashed black lines) and their mean (red line). Time is normalized by duration of the foot displacement, and distance is normalized by stride length.

The foot displacement characteristics in terms of stride length, maximum heel height, and maximum angular amplitude distribution are given in table 4.5.

When generating gait patterns, by fixing step lengths and heel maximum heights, reference trajectories for the feet anterior-posterior and vertical displacements can be easily calculated. In fact, multiplying the normalized trajectory for each displacement by stride

---

[4]In standing position, the HEE and TOE markers form a vector parallel to the ground.
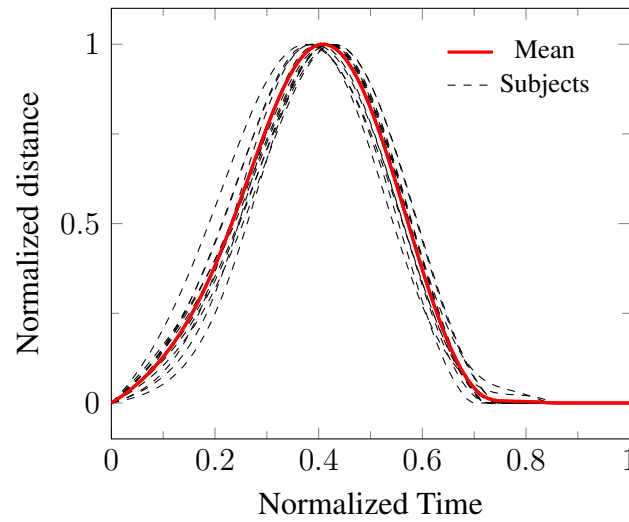
Figure 4.14: Foot vertical displacement: trajectories from healthy subjects (dashed black lines) and their corrected mean (red line). Time is normalized by duration of the foot displacement, and distance is normalized by maximum heel height. Mean displacement is calculated from normalized data and then corrected to have a maximum of 1.
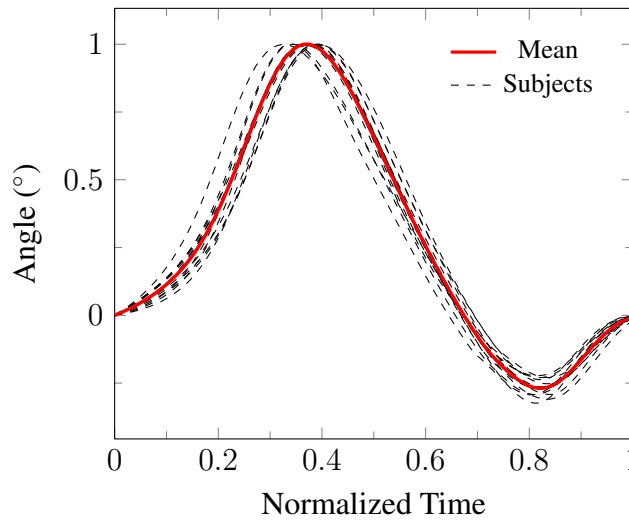

Figure 4.15: Foot angular displacement: trajectories from healthy subjects (dashed black lines) and their corrected mean (red line). Time is normalized by duration of the foot displacement, and angle is normalized by maximum angular amplitude. Mean displacement is calculated from normalized data and then corrected to have a maximum of 1.

length (calculated from step lengths) and maximum height, respectively, gives the corresponding adapted trajectory, in normalized time.

Table 4.5: Anterior-Posterior, Vertical and Angular Foot Displacement characteristics: mean and standard deviation of stride length, heel maximum height, and foot maximum angular amplitude.

Number	Stride Length (m)	Heel Maximum Height (m)	Maximum angular amplitude (°)
12	1.25 ± 0.138	0.187 ± 0.0088	71.41 ± 9.49

The angular displacement case is not that straightforward, as the maximum amplitude for the angular displacement is not fixed by the simulation parameters. So, this maximum, which is denoted by α_{max} must be calculated in order to ensure at least the non collision of the foot with the ground.

Lets note L, the rear foot length, measured from HEE to TOE. By definition, the foot measures approximately $1.5L$. α_{max} occurs when the foot is no longer in contact with the ground, since a change of angular variation is then engaged. Therefore, by knowing the heel (foot) height $h_{\alpha_{max}}$ at time of maximum angle, with simple geometry relationships, α_{max} can be defined with:

$$\sin\left(\alpha_{max}\right) = \frac{h_{\alpha_{max}}}{1.5L}$$

By analysing the data of the 12 foot trajectories used to calculate the normalized references, a relationship between $h_{\alpha_{max}}$ and h_{max} can be found:

$$\text{mean}\left(\frac{h_{\alpha_{max}}}{h_{max}}\right) = 0.9647, \quad sd = 0.0124$$

And so, α_{max} can be computed as:

$$\alpha_{max} = \sin^{-1}\left(\frac{0.9647 h_{max}}{1.5L}\right)$$

Recall from section 3.2.3.2, in the previous chapter, that accelerations are needed to define the Feet Tasks. The method previously presented with polynomial approximation is ill-adapted for the approximation of these trajectories, as the curves are defined by hundred points, and normalized in time.

Another strategy is then employed: B-splines approximation. Using B-splines to approximate the foot displacement trajectories allows not only the curve to be approximated, but also analytical first and second derivatives to be computed, avoiding therefore numerical derivation issues.

In this work, B-splines curves[5] of 6th order with 9 control points are chosen to approximate the curves. These values allow an approximation of the original curve with a cumulated root mean square error inferior to 1 mm.

The references resulting from B-spline approximation can be found in figure 4.16, for a step length of 0.42 m (corresponding stride length of 0.84 m) and a heel maximum height of 0.22 m.
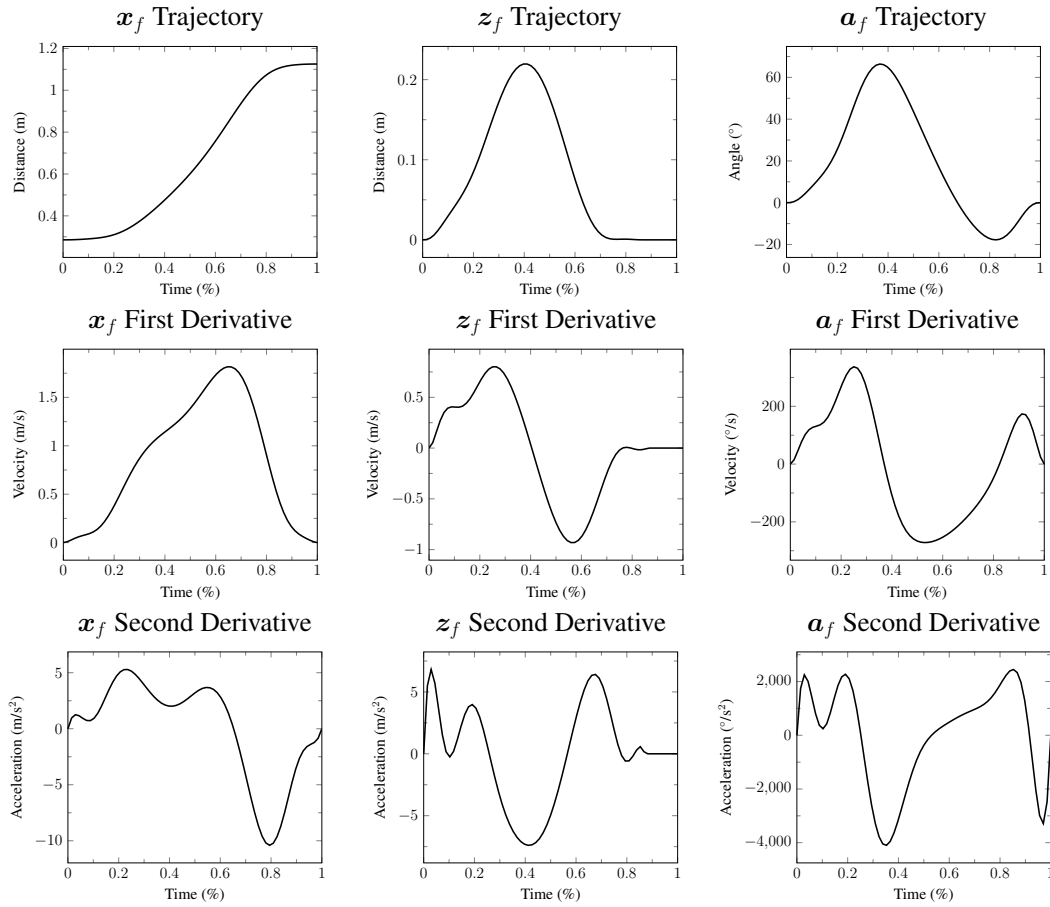

Figure 4.16: Rear foot trajectories generated for a step length of 0.42 m and a heel height of 0.22 m. The first row corresponds to the x_f, z_f, a_f trajectories, the middle row to their first derivatives and the last row to their second derivatives.

---

[5]The B-spline approximation implemented uses the B-spline approximation code provided by John T. Foster, `https://github.com/johntfoster/bspline`. [Last consulted on 24/08/2017.] The control points used for the B-Spline approximation are computed according to the online course CS3621: Computing with Geometry from Professor Ching-Kuang Shene of the Departement of Computer Science of the Michigan Technological University, `http://www.cs.mtu.edu/~shene/COURSES/cs3621/NOTES/`. [Last consulted on 24/08/2017.]

Since the foot is divided in two parts, the forefoot must also be treated. Here, only an orientation task is defined as follows:

- the forefoot is set to be parallel to the ground at toe off, to avoid toe slipping on the ground;

- once the angular displacement of the rear foot changes sign, to prepare the heel strike, the forefoot is set to have the same orientation as the rear foot.

With this tasks, the movement of the whole foot is defined for the displacement from one footprint to the next one.

Flat feet walking As done before, the foot displacement for the flat feet walking is inspired from the foot trajectories presented for the non pathological walking.

The difference between non pathological initial contact and the flat feet contact is that in the latter the foot contacts the ground as a whole. So, in the foot angular displacement, figure 4.15, there is not an inversion of foot angle to contact the ground with the heel. Therefore, for the flat feet contact, the angular displacement is set to remain $0°$ - parallel to the ground - when around 70% of foot displacement duration has passed. This adjustment can be seen in figure 4.17.

The foot trajectories are treated exactly as in the non pathological walking, with B-splines approximation.

With the contacts and tasks properly adapted for the three types of contact, the first hypothesis made in the beginning of the chapter can be tested. But before testing the first hypothesis, the changes needed to test the second one are presented in the nex section.

4.4   Gait Initialization

For now, no period of initialization of the gait is considered. In fact, the virtual human starts to walk with the spatio-temporal parameters imposed for the walking cycle. Yet, this is not the case for humans, where an initialization period occurs before entering stable cycles.

4.4.1   Gait Initialization in the literature

In 1990, Nissan and Whittle [Nissan and Whittle, 1990] studied the initiation of gait in 15 normal subjects (8 females and 7 males). Walking data was recorded using a reflective
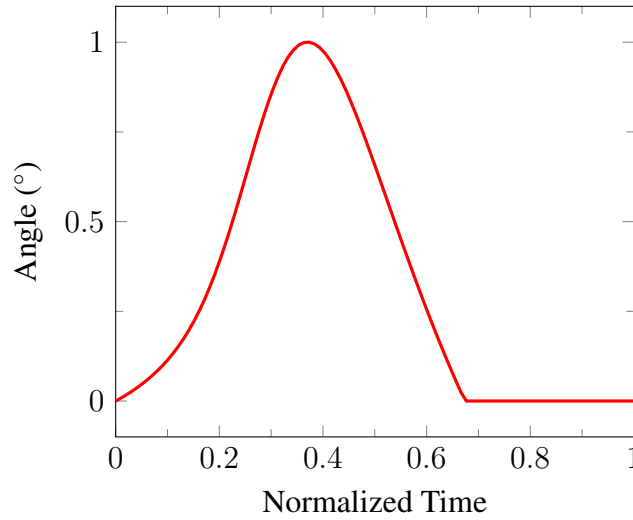
Figure 4.17: Foot vertical displacement for the flat feet walking. The angular displacement is adapted from mean displacement for non pathological walking, figure 4.15, by transforming the angular displacement to $0°$ - parallel to the ground - when around 70% of foot displacement duration has passed.

marker recording system. The subjects were asked to start walking with a sound signal, at their selected speed and in their own flat shoes. The authors found out that the initial acceleration for walking continues at least until the second step. No data was possible to record after the second step.

Latter on, using a mechanical energy analysis, Miller and Verstraete [Miller and Verstraete, 1996] determined the step duration of gait initiation. Seven young male subjects were used in this study. Using a Vicon Motion Analysis System and two AMTI force plates, markers displacement, ground reaction forces and moments were recorded. Steady state was found out to be attained when three full steps were completed.

More recently, Najafi and colleagues [Najafi et al., 2010] were interested in the impact of footwear in gait initiation. The number of steps required to achieve steady state gait, with and without foot orthoses (barefoot and with usual footwear), for fifteen healthy subjects (6 female, 9 male) were studied. The number of steps needed to reach steady state gait varied from a mean of 3.5 ($\pm$ 2.0 standard deviation) steps for usual foot and orthoses to 5.20 ($\pm$ 3.0 standard deviation) steps for the barefoot condition.

There are also studies concerning specific populations, see for instance [Roemmich et al., 2012] for Parkinson's Disease in the elderly. All the studies agree in one point, there is a period of gait initiation. Therefore, this period is included in our

simulations, as explained next.

4.4.2   Gait Initialization in the Walking Procedure

Since literature does not agree in the exact number of steps to be taken to achieve the steady state gait, and since the purpose here is to see if an initialization period affects the range of stable gaits, the initialization procedure is done as follows:

- if the step length is less or equal than 0.20 m, no initialization procedure is done;

- if the step length is longer than 0.20 m then:

    - the first step length L_1 is fixed at $L_1 = c \times L$, where L is the wanted step length and constant c is such that $L_1 = 0.2$ m;

    - the next step lengths are calculated like the first one $L_i = c \times L$, with c increased of $\frac{1}{10}$ at each step taken until $c = 1$.

With this implementation, and taking into account the step lengths considered, the virtual human does at least one initialization step before achieving steady state gait when the desired step length is greater than 0.2 m.

4.5   Summary

In this chapter, two hypothesis to improve the walking simulations are made. The developments needed to test this hypothesis are explained. In figure 4.18, the complete simulation framework schematics is presented with the modified components enlightened.

With these changes in place, the two hypothesis can be tested. This is the subject of the next chapter.
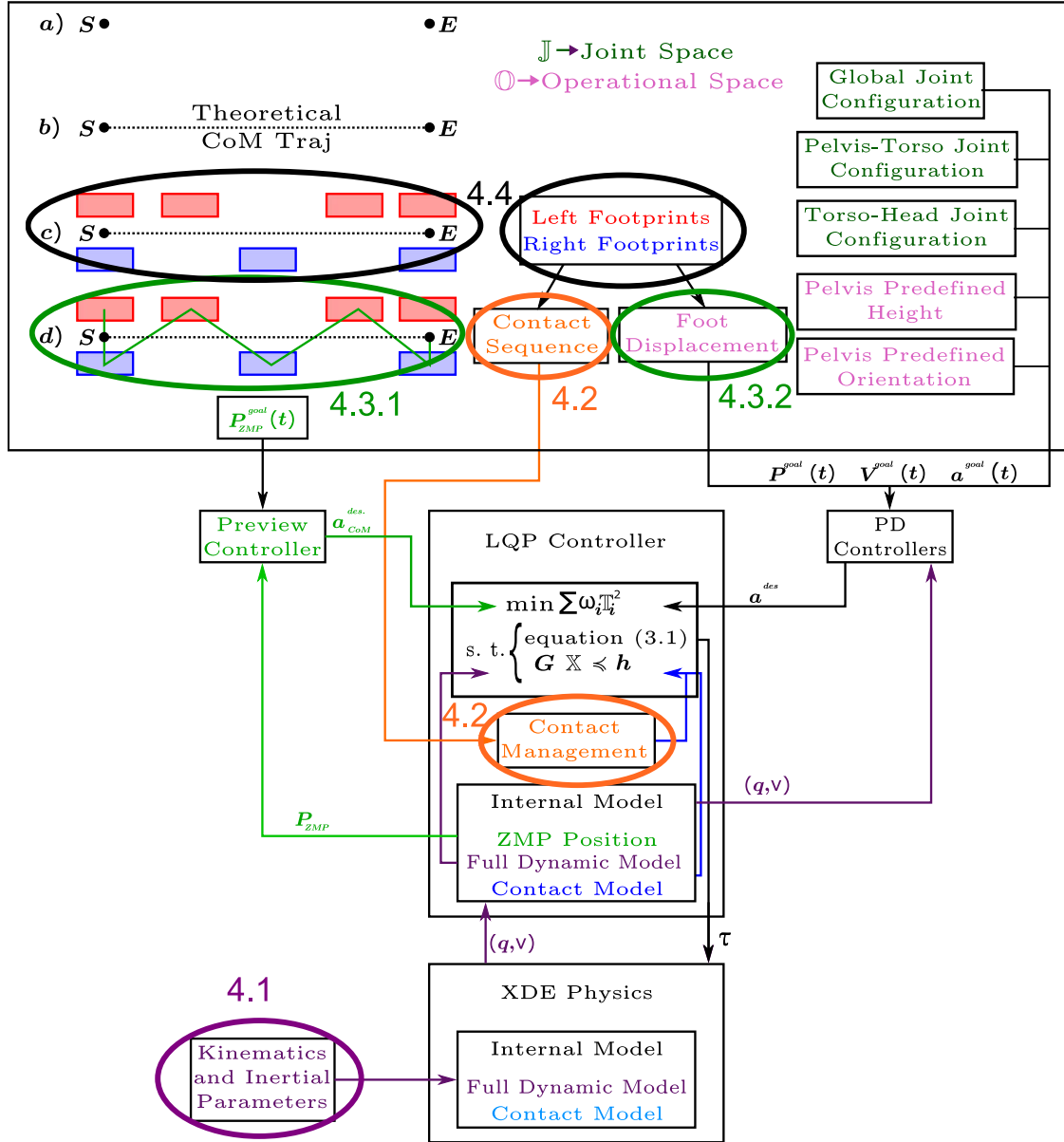
Figure 4.18: Complete simulation framework schematics. The components changed in this chapter are enlightened accordingly.

SIMULATION EXPERIMENTS

In this chapter, simulation examples of the motions possible to achieve with the developments of the previous chapter are shown.

The numerical manikin needed for the walking motion generation is created using data from a female subject with 1.630 m height and 51.5 kg of body mass, according to the procedure presented in sections 3.1.1 and 4.1.2 for the foot. The subject did not present any gait pathology or anatomic deformation. However, the subject did present an asymmetry in the lower limbs length, the left thigh and the right shank being almost 1 cm greater than the corresponding segment on the other limb. Still, the two lower limbs present very similar total length.

The LQP-Controller presented in section 3.2, with the adaptations described in the previous chapter, is used to generate walking motion. Simulations with and without initialization procedure are done and compared.

For starters the methodology used to conduct the simulations is explained, followed by the presentation of the results obtained for the three modes of contact: non pathological, toe and flat feet. A simulation is considered successful when the virtual human completes 4 gait cycles in the steady state gait.

5.1 Non Pathological Walking

5.1.1 Method

The initial configuration of the manikin is calculated so that the legs are straighten up, both feet on the ground and the pelvis center located above the center of the feet.

To evaluate the range of possible motions, the following parameters are tested:

- **step length**, made to vary between: 0.2 m and 0.6 m with a 0.02 m increase step;

- **maximum heel height**, made to vary between: 0.14 m and 0.22 m with a 0.02 m increase step;

- **CoM reference altitude shift** (for the preview control calculations), made to vary between: 0 m and 0.12 m with a 0.02 m increase step[1];

Walking cycle duration is fixed to be 1.10 s for all the simulations, which corresponds to the mean cycle time of the healthy subjects used in the computation of foot trajectories. All the simulations are set with $p_0 = 0.28$, $p_1 = 0.39$, $p_2 = 0.41$, $p_3 = 0.44$, $p_4 = 0.47$, $p_5 = 0.5$, $p_6 = 0.78$, $p_7 = 0.89$, $p_8 = 0.91$, $p_9 = 0.94$, $p_{10} = 0.97$, and $p_{11} = 1$, see equation (4.2)[2].

Using a combination of these parameters, several walking simulations are performed. The simulation is considered to be successful when the manikin completes at least 4 gait cycles in the steady state gait.

5.1.2 Results & Discussion

By combining the parameters previously presented, 735 ($21 \times 5 \times 7$) simulations are performed. Without initialization, a total of 203 successful simulations are accomplished, whereas with an initialization procedure this number rises to 229, which represents an increase of 12% of the number of successful simulations.

An example of a non pathological walking cycle generated by this method can be found in figure 5.1.

5.1.2.1 Spatio-temporal Parameters

In figure 5.2, a comparison between the total number of successful simulations without and with initialization procedure for the step length a) and maximum heel height b) can be found. As expected, when considering a step length of 0.2 m, both walking, with and without initialization, have the same number of successful simulations. Recall that the initialization procedure does not change the general process for step lengths less or equal to 0.2 m.

Using the step length and cycle duration parameters, walking speed values can be calculated. The ranges of speed attained for the successful simulations, without and with

---

[1]The initial CoM altitude is lowered down of 0.12 m (at most) to test the impact in LIP calculations.
[2]These values are taken from the motion capture data used in the construction of feet displacement of last chapter.
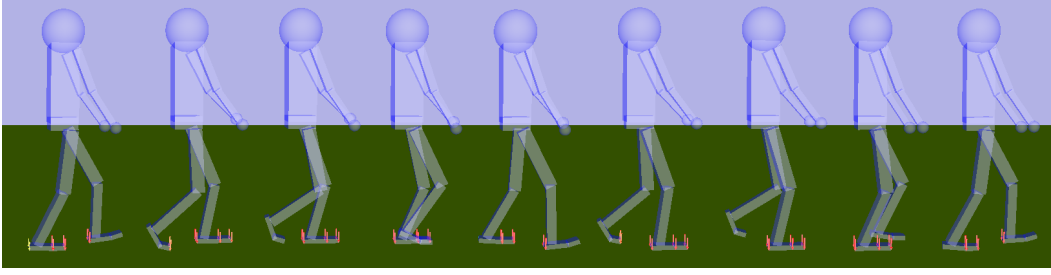
Figure 5.1: Non pathological walking cycle generated for a subject of 1.63 m of height and 51.5 kg of body mass. Simulation Parameters: step length - 0.42 m, heel maximum height - 0.22 m. CoM shift is set at 0.02 m.
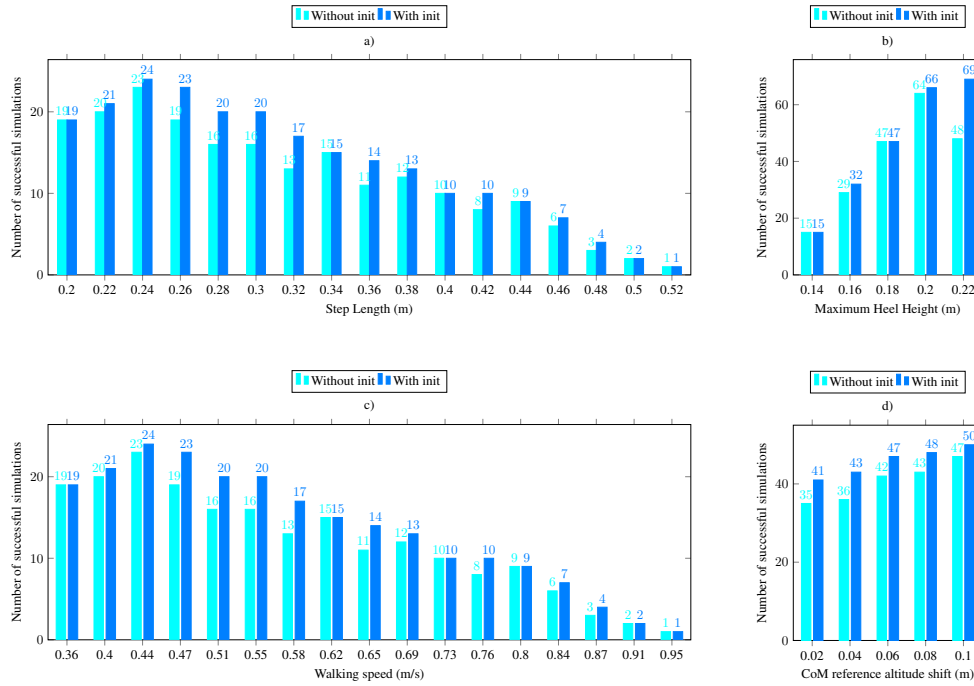

Figure 5.2: Number of successful simulations for the non pathological walking without (light blue) and with (dark blue) initialization procedure per: a) Step length; b) Maximum heel height; c) Walking speed; d) CoM reference altitude shift.

initialization procedure, are presented in figure 5.2 c). With this non pathological walking, a larger range of speeds than that presented in chapter 3 is reached. Walking speed ranges of human walking, which go from 0.65-1.88 m/s according to [Wheelwright et al., 1993], are approached. Compared to the results of [Ogura et al., 2006], the motions achieved

here are faster.

In figure 5.2 d), a comparison between the total number the successful simulations without and with initialization procedure per CoM reference altitude shift can be seen. The LIP modelling seems to impact the simulation success, since decreasing the CoM's altitude reference increases the number of successful simulations. However, shifts of 0.12 m do not produce successful walking simulations.

Overall, with the initialization procedure, more simulations are successful. Even though the step lengths and walking speeds reached stay the same with or without initialization, the range of possible motions still is increased with initialization, where more combinations of parameters are possible.

5.1.2.2 Kinematical parameters

In figure 5.3, whiskers box plots of the GVS considered and the overall modified GPS are shown, in order for variability of the simulations to be appreciated.
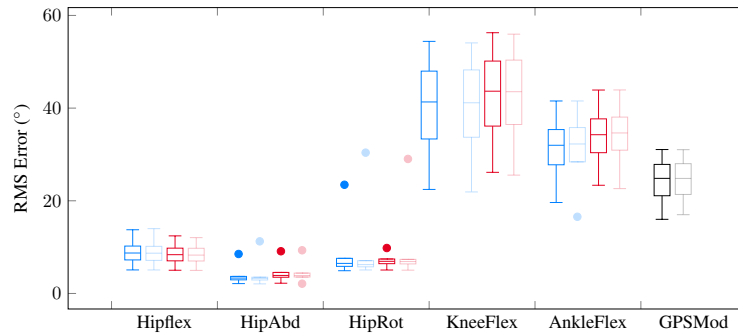
Figure 5.3: Box plot diagrams of the GVS considered and the overall GPS measures for the successful simulations of non pathological walking. For each variable, blue and light blue, and, red and light red box plots represent right and left sides, respectively. Light colors represent the results without initialization. Mid-line in the box plot represents the median value, upper and lower quartile represent values outside 75% and 25% respectively. Minimum and maximum values are also plotted as the bottom and top line or outlier, respectively.

When compared, the GVS and modified GPS values variation within simulations do not substantially change with the initialization procedure. The ranges of GVS and modified GPS values show that the simulations present some homogeneity in the hip movements, but a larger variation in the knee and ankle sagittal movements. Values for the

right and left sides present some asymmetries which can be the result of the asymmetries in the numerical manikin.

Using the GPS criteria, the simulation kinematically closer to human walking is selected among the ones without initialization procedure. In figure 5.4, the lower limbs' sagittal joint angles versus their velocity for this simulation and the corresponding[3] one with initialization procedure, can be seen. Aside some small differences in the beginning of walking, the two motions converge to the same one, so the initialization procedure only impacts the beginning of the walking motion.

Sagittal Plane
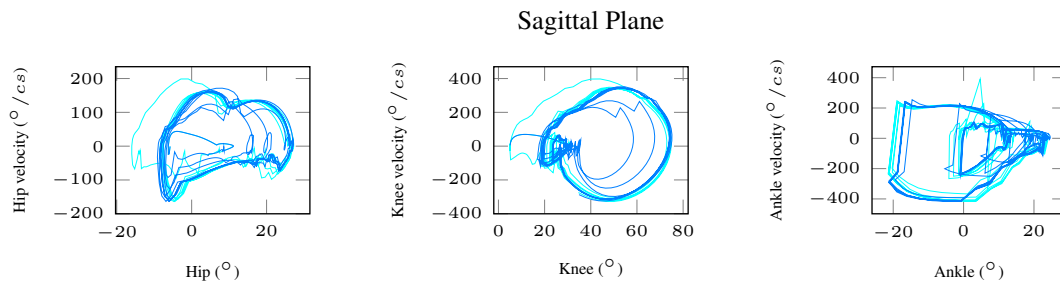
Figure 5.4: Lower limbs' sagittal joint angles trajectories versus velocity for the non pathological walking. Light and dark blue correspond to simulations without and with initialization procedure respectively. Simulation Parameters: step length - 0.42 m, maximum heel height - 0.22 m. CoM shift is set at 0.02 m.

The modified MAP for the simulations without and with initialization procedure presenting the minimal modified GPS are shown in figure 5.5. The GVS and GPS values are similar within the two simulations, nevertheless, smaller values are observed in the simulation with initialization procedure, except for the hip flexion-extension angle.

Since GVS and GPS values only translate a RMS error, it is important to compare kinematic curves, in order to be able to appreciate that error. In figure 5.6, kinematics of the right lower limb for the simulation presenting the best overall modified GPS $(16, 07°$ - simulation with initialization procedure) are compared to the kinematics of the right lower limb of the human subject used to create the numerical manikin.

As already showed in the GVS values of figure 5.5, hip flexion-extension movements are close of those observed in healthy subjects. Even if knee and ankle movements in the sagittal plane present GVS values around $20°$, by analysing the normalized kinematics

---

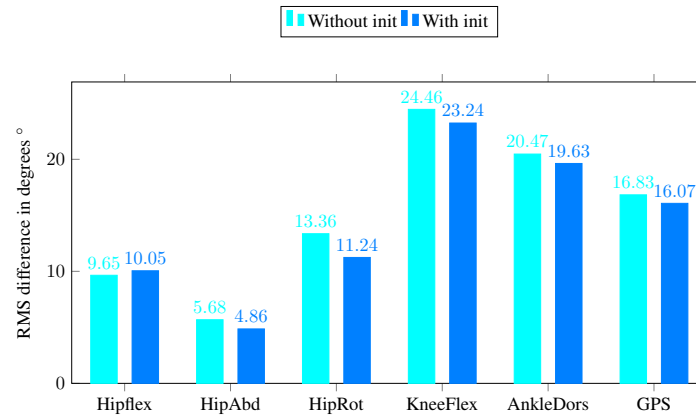[3]Corresponding means generated with the same spatio-temporal parameters.

Figure 5.5: Modified Movement Analysis Profile and Gait Profile Score. Each pair of columns corresponds to one kinematic variable. Its height represents the (RMS) average difference across time between a specific gait cycle and the average gait cycle from people with no gait pathology. The values for the simulations of non pathological walking presenting the minimal modified GPS value without and with initialization are in light and dark blue, respectively. The GPS for the overall gait pattern are displayed in the rightmost columns. For better reading, the results for the kinematic variables are shown only for the right side. The simulation parameters are: step length - 0.42 m (without) and 0.44 m (with), step height - 0.22 m. CoM shift is set at 0.02 m.

curves it can be seem that the shape of the variation is quite similar to that presented by healthy subjects. However, in the knee case, flexion is exaggerated during the walking cycle, therefore increasing the GVS value for the knee. As for the ankle, dorsiflexion is exaggerated before initial contact of the opposite side, approximately at 50% of the gait cycle. In the swing phase, ankle variations are within the range of mean values for healthy subjects. Hip abduction and hip rotation angles do not resemble the evolution presented by healthy humans. Pelvis and foot progression angles are fixed, and therefore their analysis is meaningless.

5.1.2.3 Dynamical parameters

In figure 5.7, a comparison between simulated and real human sagittal lower limbs joint torques is made.

It should be noted that the torques used for comparison are from children, and the numerical manikin used in simulation represents an adult. Since torques are normalised by body weight and height, these could still be compared. The ranges of magnitude of
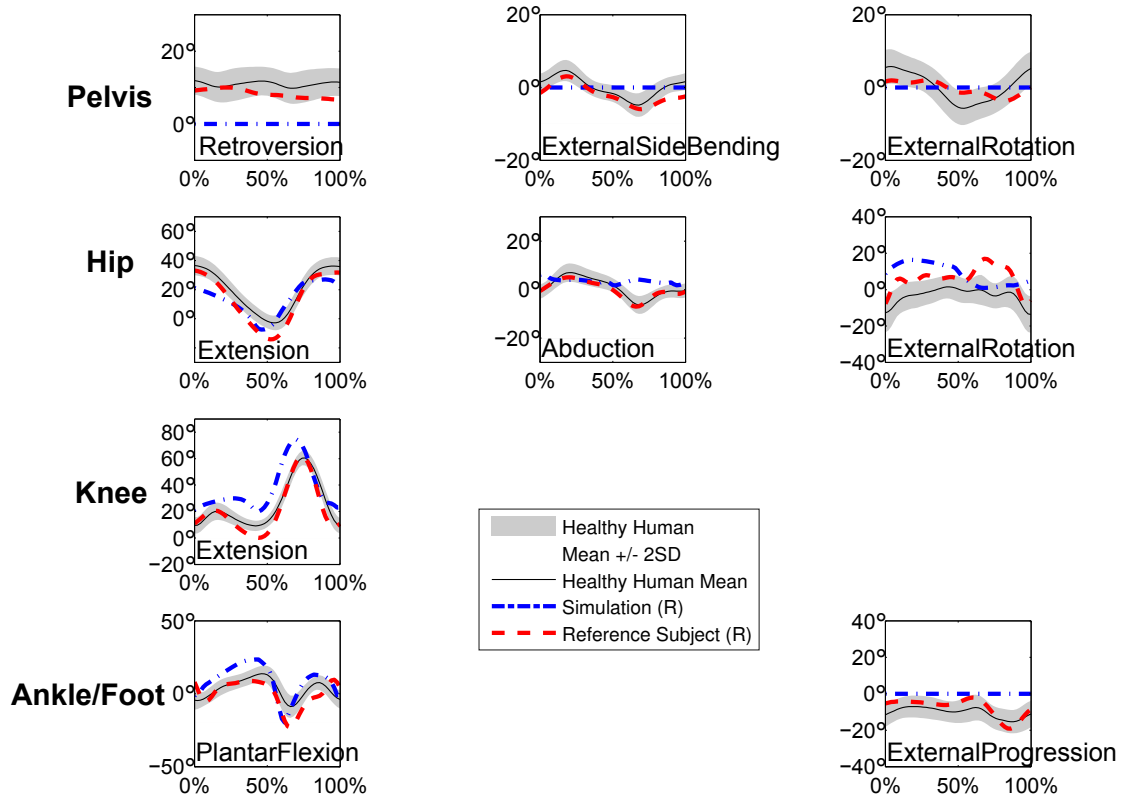
Figure 5.6: Comparison between simulated non pathological walking and mean healthy human kinematics. Kinematics is calculated for the model of sections 3.1.1 and 4.1.2 for the foot. Simulation kinematics is obtained for the following parameters: step length - 0.44 m, maximum heel height - 0.22 m. CoM shift is set at 0.02 m.

torques are similar, and as for the ankle torque, this is quite closer of real human torque, contrarily to the simulations in chapter 3.

In figure 5.8, the Ground Reaction Forces for the Left and Right Feet normalized by body mass during the first 700 cs of simulation can be seen.

Considering the GRF variations without the spikes, the values presented by the simulation are within the magnitudes presented by humans while walking. However, GRF values are very noisy, specially in the transition of contacts. For instance, in the medio-lateral direction, a great disturbance appears just before initial contact of the opposite foot, and in the vertical direction, a disturbance appears during support phase when the rear part of the foot breaks the contact with the ground, and the contact is made solely through the forefoot.
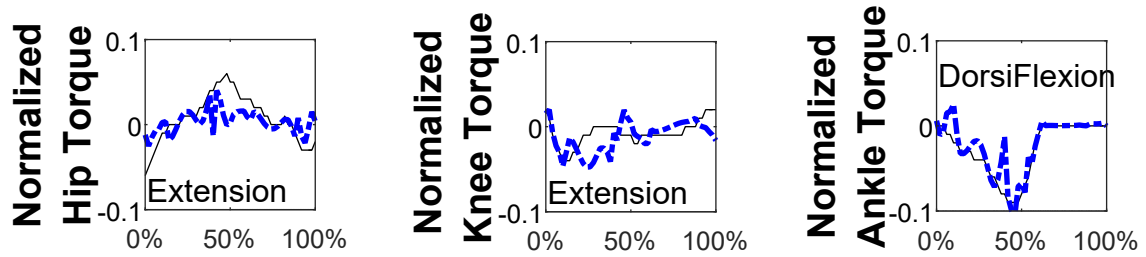
Figure 5.7: Comparison between simulated non pathological walking (dashed blue line) and recorded human (solid black line) [Stansfield et al., 2006] sagittal lower limbs joint torques. Torques are normalized by body weight and height. Simulation Parameters: step length - 0.44 m, maximum heel height - 0.22 m. CoM shift is set at 0.02 m.

5.1.2.4 Balance parameters

In figure 5.9, the ZMP progression and its reference in the anterior-posterior (top) and medio-lateral (bottom) directions during the first 700 cs of simulation can be seen.

The ZMP follows the pre-calculated reference, although some spikes are present. The ZMP trajectories are less smoother than in the previous case. In the anterior-posterior direction, spikes appear in transitioning from one foot to the next one. In the medio-lateral direction, ZMP progression is very noisy.

In figure 5.10, the ZMP and CoM progressions in the anterior-posterior (top) and medio-lateral (bottom) directions during the first 700 cs of simulation can be seen.

CoM progression trajectories are quite similar to those seen previously, *i.e.*, linear in the anterior-posterior direction and slightly oscillating around 0, its reference, in the medio-lateral direction.

5.2 Toe Walking

5.2.1 Method

The initial configuration of the manikin is calculated so that the legs are straighten up, only the forefeet on the ground and the pelvis center located above the center of the forefeet.

To evaluate the range of possible motion, the following parameters are tested:

- **step length**, made to vary between: 0.2 m and 0.5 m with a 0.02 m increase step;
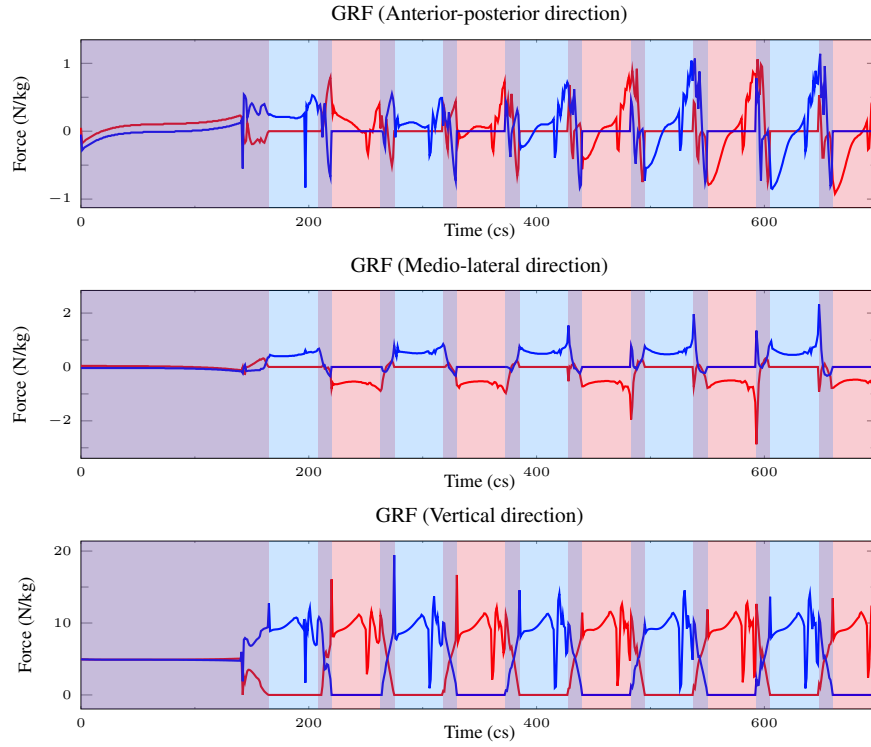
Figure 5.8: Ground Reaction Forces in the anterior-posterior (top), medio-lateral (middle) and vertical (bottom) directions for the non pathological walking. Red and blue lines correspond to Left and Right sides respectively. Dashed, dotted and solid lines correspond to the ground reaction forces of the rear feet, forefeet and feet as a whole, respectively. Violet bands correspond to double support phases, blue and red bands correspond to right and left single support phases, respectively. Simulation Parameters: step length - 0.44 m, maximum heel height - 0.22 m. CoM shift is set at 0.02 m.

- **maximum toes height**, made to vary between: 0.02 m and 0.10 m with a 0.02 m increase step;

- **CoM reference altitude shift** (for the preview control calculations), made to vary between: -0.06 m and 0.06 m with a 0.02 m increase step[4];

Walking cycle duration is fixed to be 1.40 s for all the simulations. All the simulations are set with $p_0 = 0.1$, $p_1 = 0.5$, $p_2 = 0.6$, and $p_3 = 1$, see equation (4.1).

Using a combination of these parameters, several walking simulations are performed. The simulation is considered to be successful when the manikin completes at least 4 gait

---

[4]A negative value for the CoM reference altitude shift indicates an increase of the reference value.

ZMP (solid) and Reference ZMP (dotted) positions (anterior-posterior direction)

ZMP (solid) and Reference ZMP (dotted) positions (medio-lateral direction)
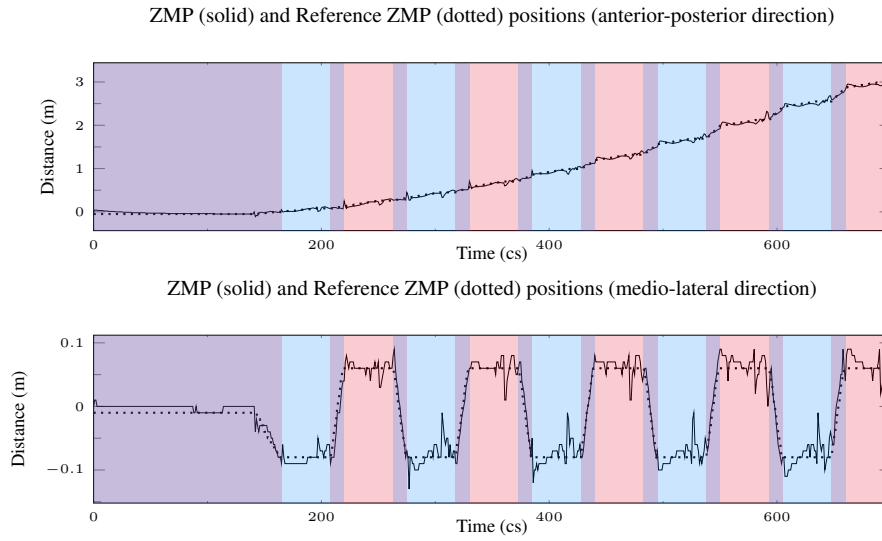

Figure 5.9: ZMP (solid black line) and ZMP reference (dotted black line) positions for the non pathological walking. Violet bands correspond to double support phases, blue and red bands correspond to right and left single support phases, respectively. Simulation Parameters: step length - 0.44 m, maximum heel height - 0.22 m. CoM shift is set at 0.02 m.

cycles in the steady state gait.

5.2.2   Results & Discussion

By combining the parameters previously presented, 560 ($16 \times 5 \times 7$) simulations are performed. Without initialization, a total of 83 successful simulations are accomplished, whereas with an initialization procedure this number rises to 101, which represents an increase of 21% of the number of successful simulations.

An example of a toe walking cycle generated by this method can be found in figure 5.11.

5.2.2.1   Spatio-temporal Parameters

In figure 5.12, a comparison between the total number the successful simulations without and with initialization procedure for the step length a) and maximum toes height b) can be found. Once again, as expected, when considering a step length of 0.2 m, both walking, with and without initialization have the same number of successful simulations.

ZMP (solid) and CoM (dashed) positions (anterior-posterior direction)

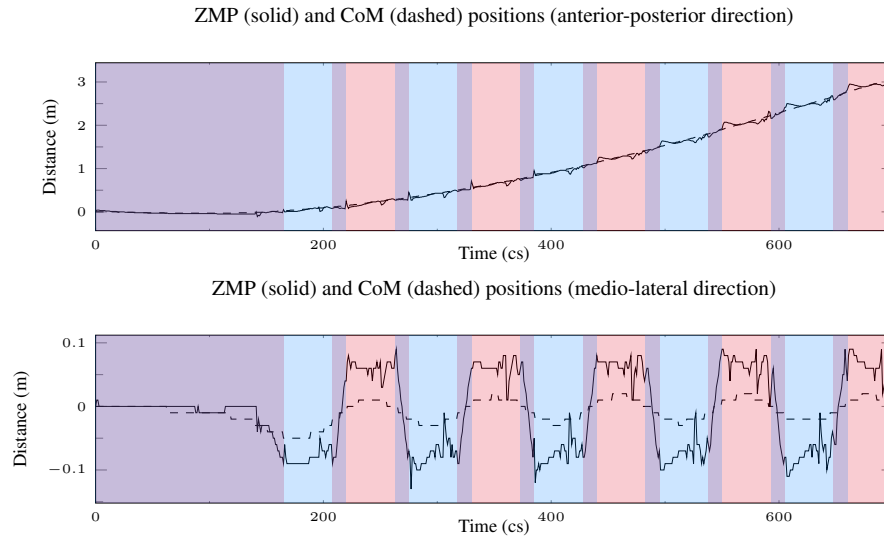ZMP (solid) and CoM (dashed) positions (medio-lateral direction)

Figure 5.10: ZMP (solid black line) and CoM (dashed black line) progression projected on the floor for the non pathological walking. Violet bands correspond to double support phases, blue and red bands correspond to right and left single support phases, respectively. Simulation Parameters: step length - 0.44 m, maximum heel height - 0.22 m. CoM shift is set at 0.02 m.
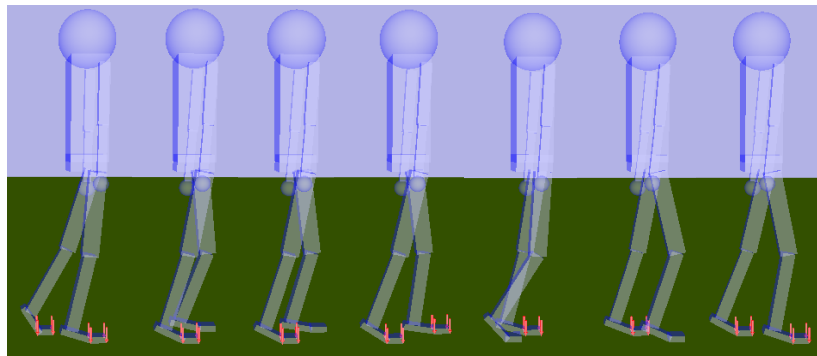
Figure 5.11: Toe walking cycle generated for a subject of 1.63 m of height and 51.5 kg of body mass. Simulation Parameters: step length - 0.26 m, maximum toes height - 0.02 m. CoM shift is set at 0.02 m up.

Using the step length and cycle duration parameters, walking speed values can be calculated. The ranges of speed attained for the successful simulations, without and with initialization procedure, are presented in figure 5.12 c). The attained speeds are lower than those reached with non pathological walking. Still, they are greater than in the flat
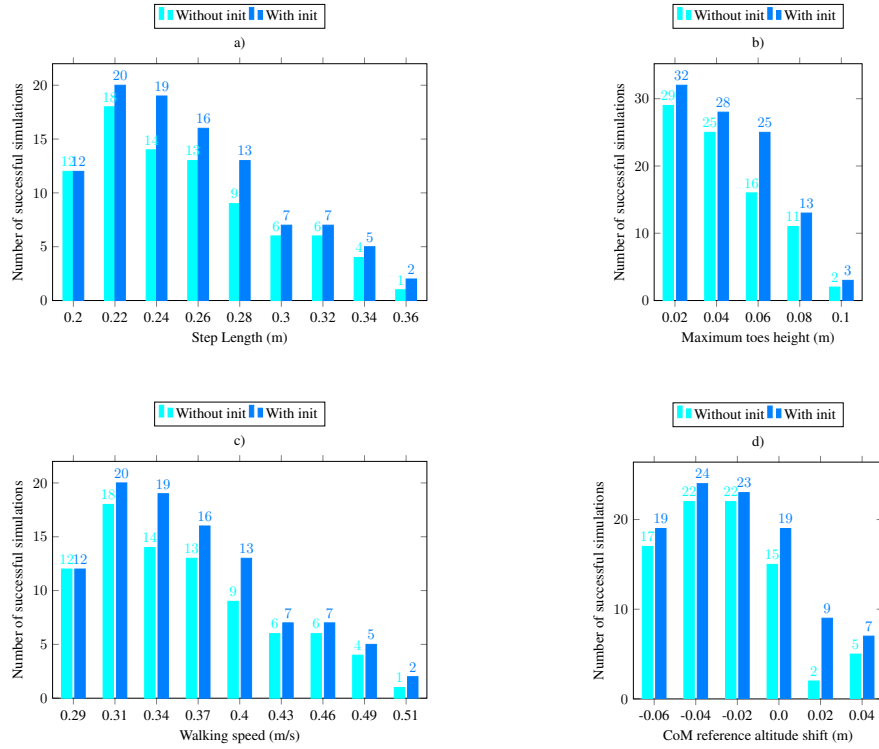
113

Figure 5.12: Number of successful simulations for the toe walking without (light blue) and with (dark blue) initialization procedure per: a) Step length; b) Maximum toes height; c) Walking Speed; d) CoM reference altitude shift.

feet case of chapter 3.

In figure 5.12 d), a comparison between the total number the successful simulations without and with initialization procedure per CoM reference altitude shift can be seen. In both cases, the LIP-modelling impacts the simulation, and the number of successful simulations is greater when the CoM is higher (which corresponds to the negative shift).

As in the previous case, with the initialization procedure more simulations are possible.

5.2.2.2 Kinematical Parameters

In figure 5.13, whiskers box plots of the GVS considered and the overall modified GPS are shown, in order for variability of the simulations to be appreciated.

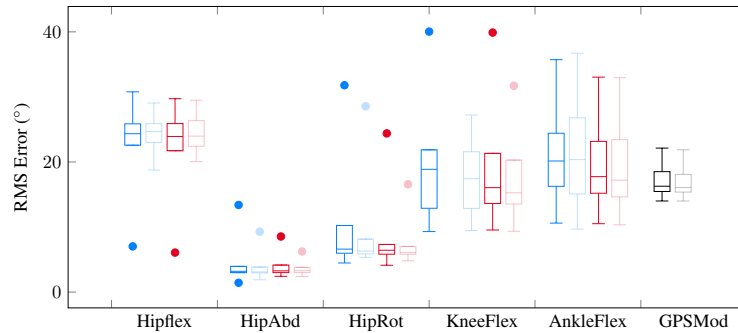When compared, the GVS and modified GPS values variation within simulations does

Figure 5.13: Box plot diagrams of the GVS considered and the overall GPS measures for the successful simulations of toe walking. For each variable, blue and light blue, and, red and light red box plots represent right and left sides respectively. Mid-line in the box plot represents the median value, upper and lower quartile represent values outside 75% and 25%, respectively. Minimum and maximum values are also plotted as the bottom and top line or outlier, respectively.

not substantially change with the initialization procedure, except the right hip rotation, which presents a greater variation. The ranges of GVS and modified GPS values show that the simulations present some homogeneity in the hip movements, but a larger variation in the knee and ankle sagittal movements. Once again, values for the right and left sides present some asymmetries which can be the result of the asymmetries in the numerical manikin.

Using the GPS criteria, the simulation kinematically closer to human walking is selected among the ones without initialization procedure. In figure 5.14, the lower limbs' sagittal joint angles versus their velocity for this simulation and the corresponding one with initialization procedure, can be seen. Aside some small differences in the beginning of walking, the two motions converge to the same one, so the initialization procedure only impacts the beginning of the walking motion. It should be noted that the phase plots are smoother than in the non pathological walking case.

The modified MAP for the simulations without and with initialization procedure presenting the minimal modified GPS are shown in figure 5.15. The GVS and GPS values are quite similar (differences less than $1°$) within the two simulations, since they are generated with the same parameters, and, therefore, converge to the same motion.

Toe walking obviously generate an abnormal gait pattern. In figure 5.16, kinematics of the lower limbs for the simulation presenting the best overall modified GPS ($14, 15°$ - simulation with initialization procedure) is shown together with the mean values for
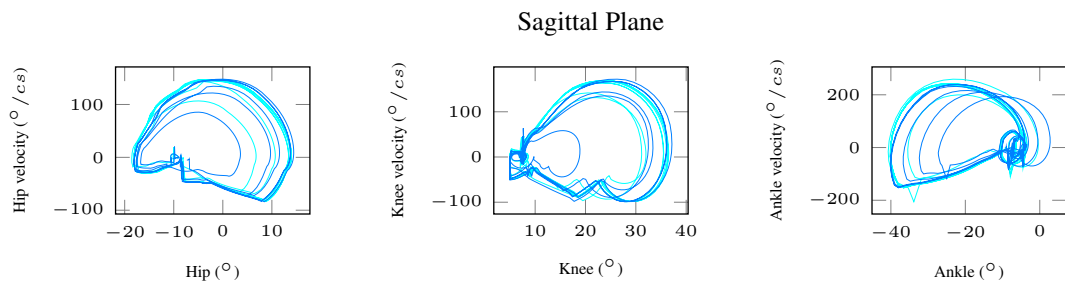
Sagittal Plane

Figure 5.14: Lower limbs' sagittal joint angles trajectories versus velocity for the toe walking. Light and dark blue correspond to simulations without and with initialization procedure respectively. Simulation Parameters: step length - 0.26 m, maximum toes height - 0.02 m. CoM shift is set at 0.02 m up.
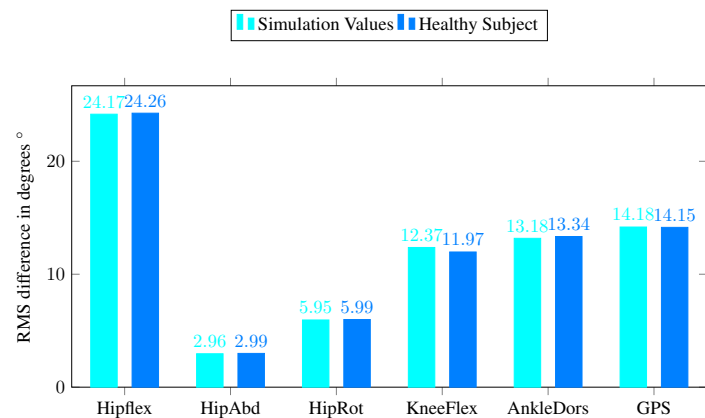

Figure 5.15: Modified Movement Analysis Profile and Gait Profile Score. Each pair of columns corresponds to one kinematic variable. Its height represents the (RMS) average difference across time between a specific gait cycle and the average gait cycle from people with no gait pathology. The values for the simulations of toe walking presenting the minimal modified GPS value without and with initialization are in light and dark blue, respectively. The GPS for the overall gait pattern are displayed in the rightmost columns. For better reading, the results for the kinematic variables are shown only for the right side. The simulation parameters are: step length - 0.26 m, maximum toes height - 0.02 m. CoM shift is set at 0.02 m up.

healthy human.

As already shown by the GVS values, the joint angle presenting the greater error when compared to human mean kinematics is the hip flexion-extension, which is way below
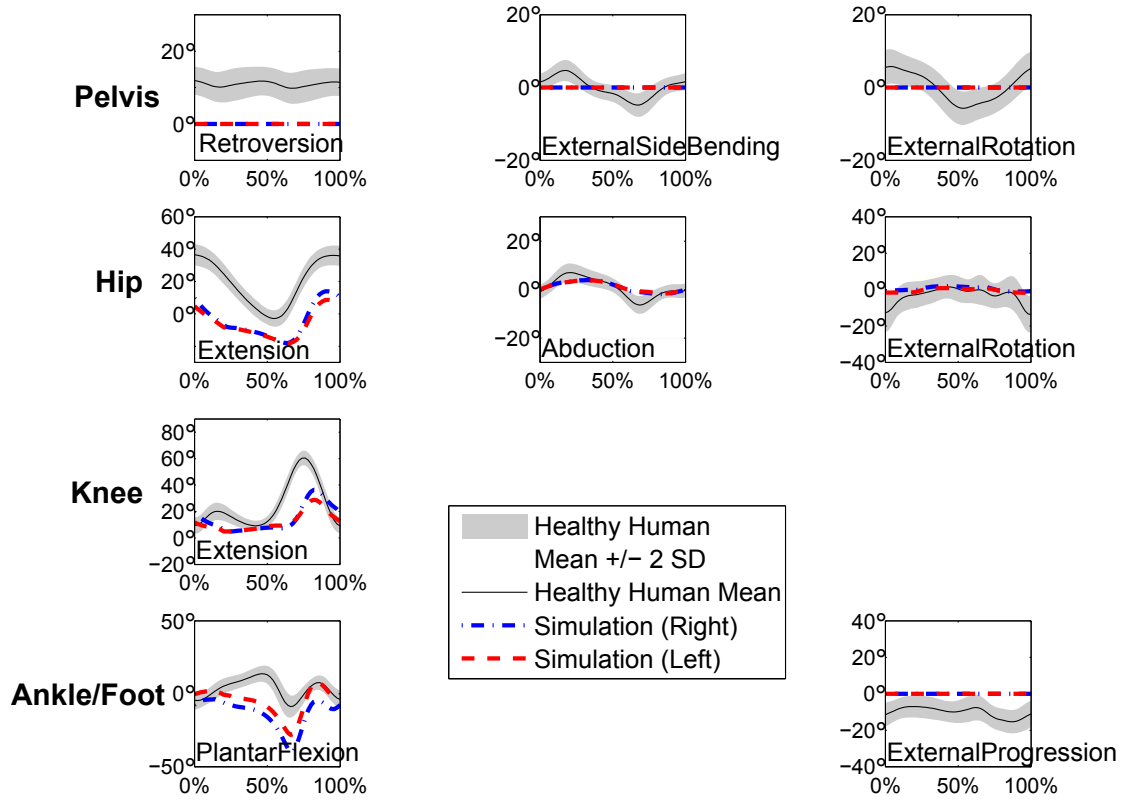
Figure 5.16: Comparison between simulated toe walking and mean healthy human kinematics. Kinematics is calculated for the model of sections 3.1.1 and 4.1.2 for the foot. Simulation kinematics is obtained for the following parameters: step length - 0.26 m, maximum toes height - 0.02 m. CoM shift is set at 0.02 m up.

the healthy human mean variation. Knee flexion presents a smaller range of motion, but similar behaviour, and ankle plantarflexion is exaggerated through approximately the entire gait cycle. Hip abduction and rotation angles stay almost constant.

5.2.2.3 Dynamical Parameters

In figure 5.17, a comparison between simulated and real human sagittal lower limbs joint torques is made.

Since toe walking is by nature a pathological walking, it is normal that disparities exist between simulated torques and reference torques. Nevertheless, it should be noted that these torques stay within the magnitudes of human walking.

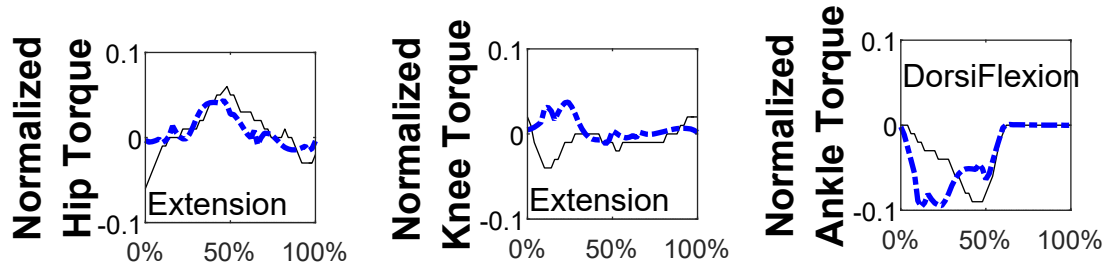In figure 5.18, the Ground Reaction Forces for the Left and Right Feet normalized by

Figure 5.17: Comparison between simulated toe walking (dashed blue line) and recorded human (solid black line) [Stansfield et al., 2006] sagittal lower limbs joint torques. Torques are normalized by body weight and height. Simulation Parameters: step length - 0.26 m, maximum toes height - 0.02 m. CoM shift is set at 0.02 m up.

body mass during the first 700 cs of simulation can be seen.

The GRF values presented by the simulation are within the magnitudes presented by humans while walking. In terms of contact, toe walking resembles the flat feet walking of chapter 3, and, therefore, the GRF values are similar to those presented in that chapter.

5.2.2.4 Balance parameters

In figure 5.19, the ZMP progression and its reference in the anterior-posterior (top) and medio-lateral (bottom) directions during the first 700 cs of simulation can be seen.

The ZMP follows the pre-calculated reference smoother than in the non pathological walking. Some noise is present in the medio-lateral direction, but the pre-defined trajectory is globally satisfied.

In figure 5.20, the ZMP and CoM progressions in the anterior-posterior (top) and medio-lateral (bottom) directions during the first 700 cs of simulation can be seen.

CoM progression trajectories are quite similar to those seen previously, *i.e.*, linear in the anterior-posterior direction and slightly oscillating around 0, its reference, in the medio-lateral direction.
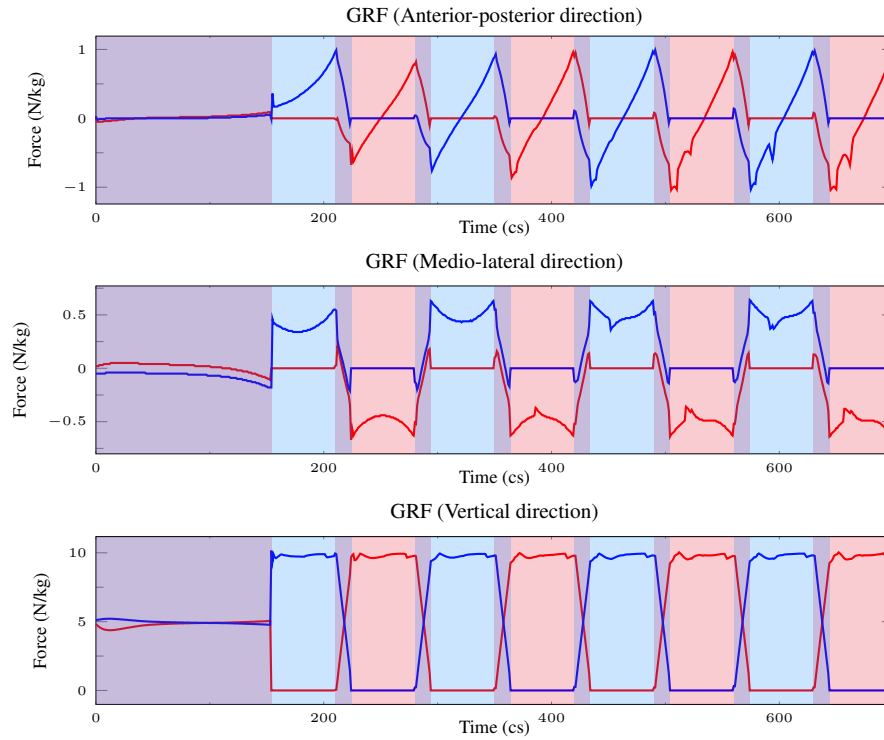
Figure 5.18:   Ground Reaction Forces in the anterior-posterior (top), medio-lateral (middle) and vertical (bottom) directions for the toe walking. Red and blue lines correspond to Left and Right sides respectively. Dashed, dotted and solid lines correspond to the ground reaction forces of the rear feet, forefeet and feet as a whole, respectively. Violet bands correspond to double support phases, blue and red bands correspond to right and left single support phases, respectively. Simulation Parameters: step length - 0.26 m, maximum toes height - 0.02 m. CoM shift is set at 0.02 m up.

5.3   Flat Feet Walking

5.3.1   Method

The initial configuration of the manikin is calculated so that the legs are straighten up, both feet on the ground and the pelvis center located above the center of the feet.

To evaluate the range of possible motions, the following parameters are tested:

- **step length**, made to vary between: 0.2 m and 0.5 m with a 0.02 m increase step;

- **maximum heel height**, made to vary between: 0.14 m and 0.22 m with a 0.02 m increase step;

119

ZMP (solid) and Reference ZMP (dotted) positions (anterior-posterior direction

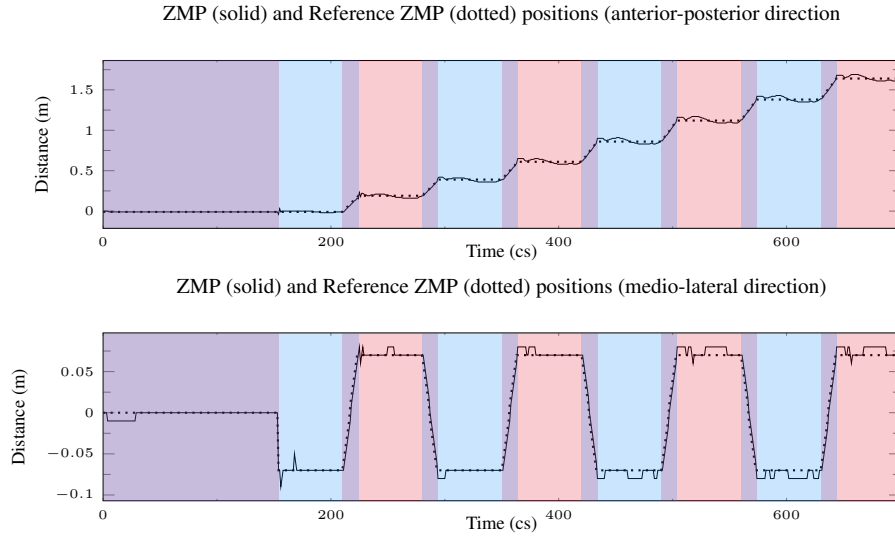ZMP (solid) and Reference ZMP (dotted) positions (medio-lateral direction)

Figure 5.19: ZMP (solid black line) and ZMP reference (dotted black line) positions for the toe walking. Violet bands correspond to double support phases, blue and red bands correspond to right and left single support phases, respectively. Simulation Parameters: step length - 0.26 m, maximum toes height - 0.02 m. CoM shift is set at 0.02 m up.

- **CoM reference altitude shift** (for the preview control calculations), made to vary between: 0 m and 0.12 m with a 0.02 m increase step;

Walking cycle duration is fixed to be 1.40 s for all the simulations. All the simulations are set with $p_0 = 0.28$, $p_1 = 0.42$, $p_2 = 0.46$, $p_3 = 0.5$, $p_4 = 0.78$, $p_5 = 0.92$, $p_6 = 0.96$, and $p_7 = 1.0$, see equation (4.3).

Using a combination of these parameters, several walking simulations are performed. The simulation is considered to be successful when the manikin completes 4 gait cycles in the steady state gait.

5.3.2   Results & Discussion

By combining the parameters previously presented, 560 ($16 \times 5 \times 7$) simulations are performed. Without initialization, a total of 170 successful simulations are accomplished, whereas with an initialization procedure this number rises to 235, which represents an increase of 38% of the number of successful simulations.

An example of a flat feet walking cycle generated by this method can be found in figure 5.21.

ZMP (solid) and CoM(dashed) positions (anterior-posterior direction

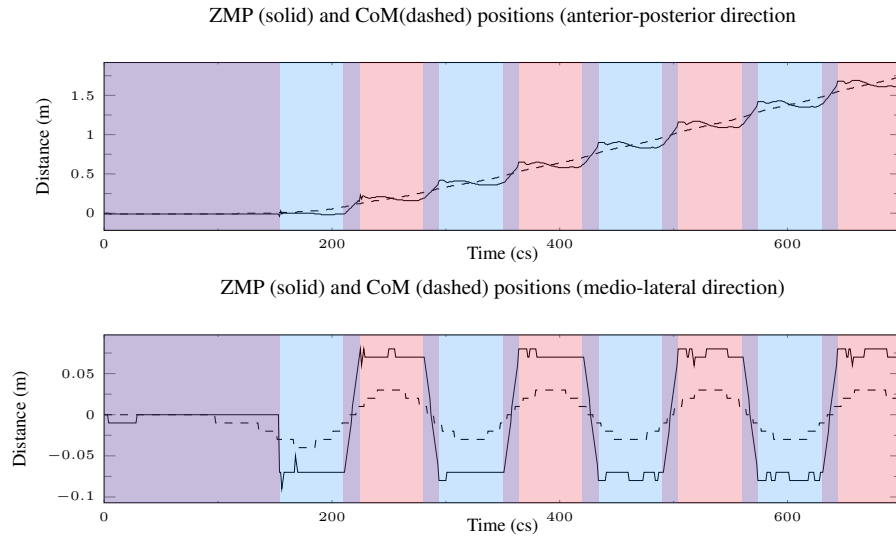ZMP (solid) and CoM (dashed) positions (medio-lateral direction)

Figure 5.20: ZMP (solid black line) and CoM (dashed black line) progression projected on the floor for the toe walking. Violet bands correspond to double support phases, blue and red bands correspond to right and left single support phases, respectively. Simulation Parameters: step length - 0.26 m, maximum toes height - 0.02 m. CoM shift is set at 0.02 m up.
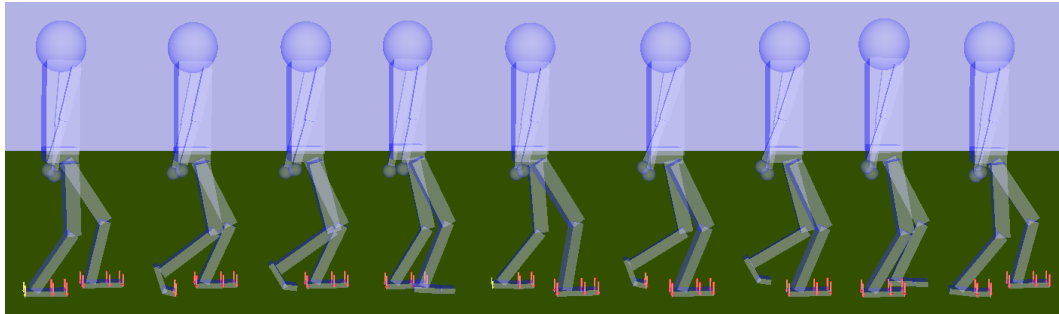
Figure 5.21: Flat feet walking cycle generated for a subject of 1.63 m of height and 51.5 kg of body mass. Simulation Parameters: step length - 0.36 m, maximum heel height - 0.18 m. CoM shift is set at 0.02 m.

5.3.2.1 Spatio-temporal Parameters

In figure 5.22, a comparison between the total number of successful simulations without and with initialization procedure for the step length a) and maximum heel height b) can be found. Once more, when considering a step length of 0.2 m, both walking, with and without initialization have the same number of successful simulations.
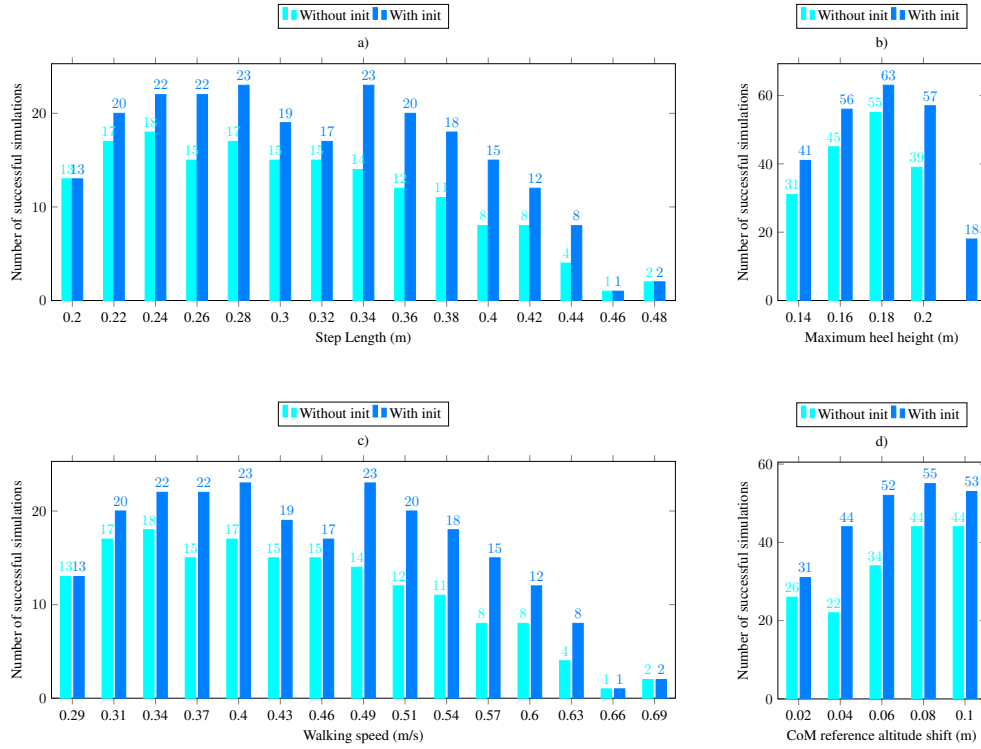
Figure 5.22: Number of successful simulations for the flat feet walking without (light blue) and with (dark blue) initialization procedure per: a) Step length; b) Maximum heel height; c) Walking speed; d) CoM reference altitude shift.

Using the step length and cycle duration parameters, walking speed values can be calculated. The ranges of speed attained for the successful simulations, without and with initialization procedure, are presented in figure 5.22 c). The speed values reached here are the double of those attained with the previous flat feet walking presented in chapter 3.

In figure 5.22 d), a comparison between the total number of successful simulations without and with initialization procedure per CoM reference altitude shift can be seen. As it happens for non pathological walking, decreasing the CoM's height reference increases the number of simulations. However, decreasing more than 0.1 m is not possible.

5.3.2.2   Kinematical Parameters

In figure 5.23, whiskers box plots of the GVS considered and the overall modified GPS are shown, in order for variability of the simulations to be appreciated.
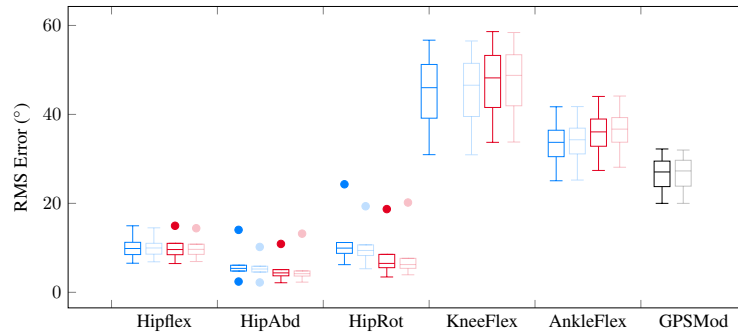
Figure 5.23: Box plot diagrams of the GVS considered and the overall GPS measures for the successful simulations of flat feet walking. For each variable, blue and red box plots represent right and left sides, respectively. Light colors represent the results without initialization. Mid-line in the box plot represents the median value, upper and lower quartile represent values outside 75% and 25% respectively. Minimum and maximum values are also plotted as the bottom and top line or outlier, respectively.

When compared, the GVS and modified GPS values variation within simulations do not substantially change with the initialization procedure. The ranges of GVS and modified GPS values show that the simulations present some homogeneity in the hip movements, but a larger variation in the knee and ankle sagittal movements. Once more, values for the right and left sides present some asymmetries which can be the result of the asymmetries in the numerical manikin.

Using the GPS criteria, the simulation kinematically closer to human walking is selected among the ones without initialization procedure. In figure 5.24, the lower limbs' sagittal angles versus their velocity for this simulation and the corresponding one with initialization procedure, can be seen. Aside some small differences in the beginning of walking, the two motions converge to the same motion, so the initialization procedure only impacts the beginning of the walking motion. It should be noted that the motions generated by this new flat feet walking are a lot a less smoother than the previous flat feet walking.

The modified MAP for the simulations without and with initialization procedure presenting the minimal modified GPS are shown in figure 5.25. The GVS and GPS values are quite similar (differences less than $1°$, except for the hip abduction error, almost $2°$ greater for the case with initialization) within the two simulations, since they are generated with the same parameters, and, therefore, converge to the same motion.

Flat feet walking generate an abnormal gait pattern. In figure 5.26, kinematics of the
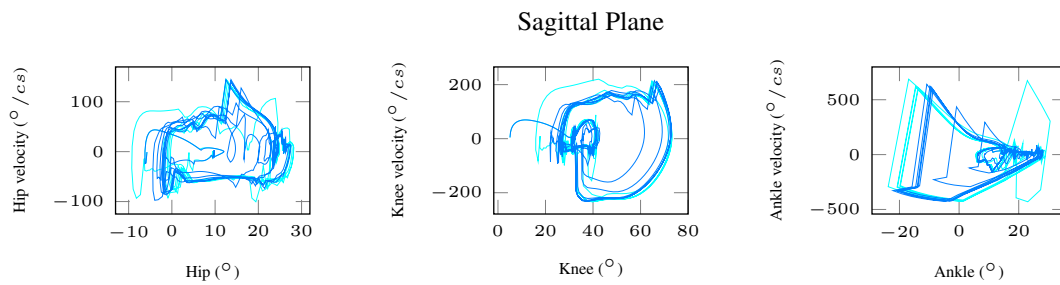
123

Sagittal Plane

Figure 5.24: Lower limbs' sagittal joint angles trajectories versus velocity for the flat feet walking. Light and dark blue correspond to simulations without and with initialization procedure, respectively. Simulation Parameters: step length - 0.36 m, maximum heel height - 0.18 m. CoM shift is set at 0.02 m.
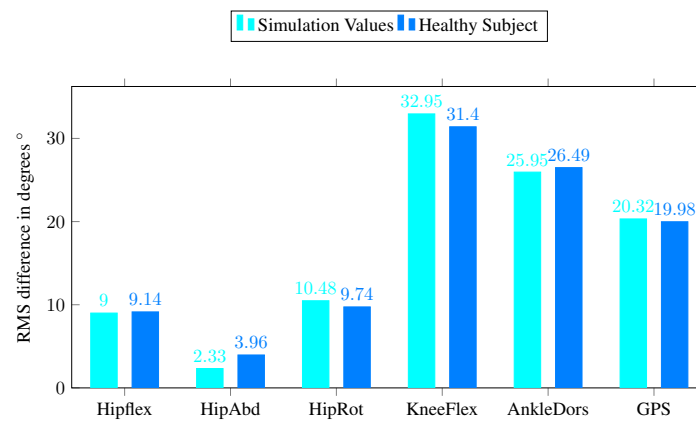

Figure 5.25: Modified Movement Analysis Profile and Gait Profile Score. Each pair of columns corresponds to one kinematic variable. Its height represents the (RMS) average difference across time between a specific gait cycle and the average gait cycle from people with no gait pathology. The values for the simulations of flat feet walking presenting the minimal modified GPS value without and with initialization are in light and dark blue, respectively. The GPS for the overall gait pattern are displayed in the rightmost columns. For better reading, the results for the kinematic variables are shown only for the right side. The simulation parameters are: step length - 0.36 m, maximum heel height - 0.18 m. CoM shift is set at 0.02 m.

lower limbs for the simulation presenting the best overall modified GPS (19.98° - simulation with initialization procedure) is shown together with the mean values for healthy human.
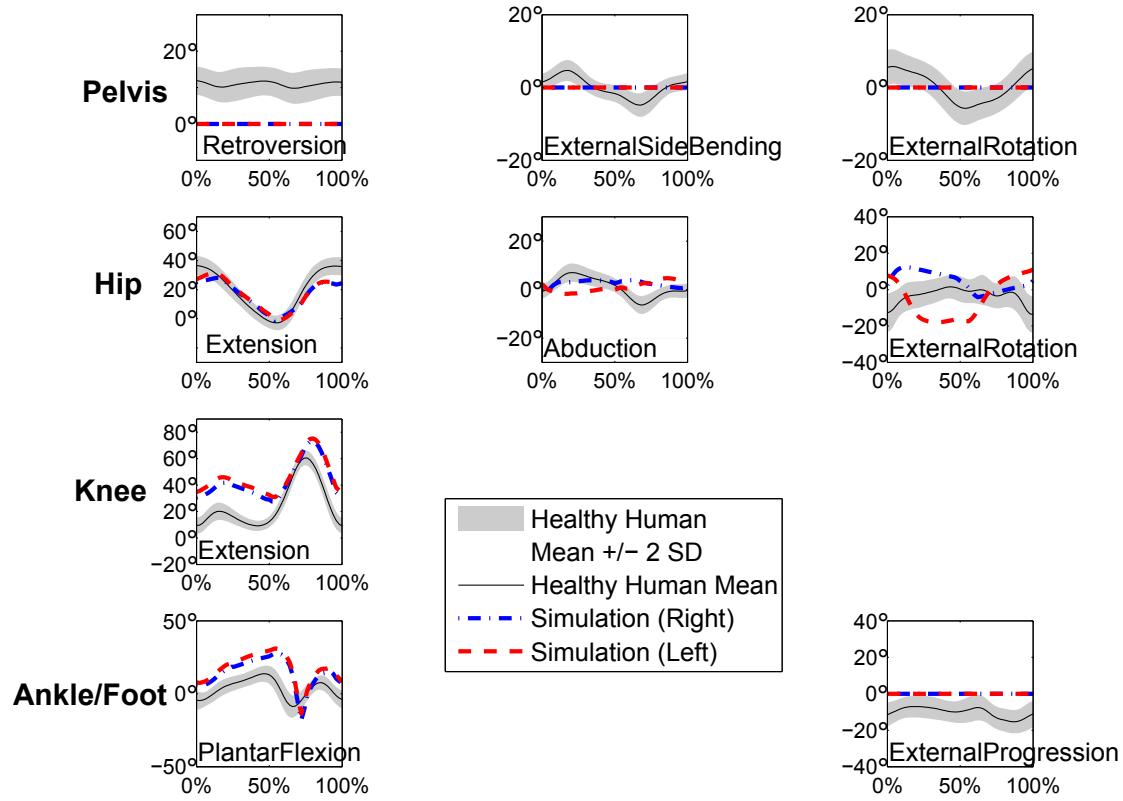
Figure 5.26: Comparison between simulated flat feet walking and mean healthy human kinematics. Kinematics is calculated for the model of sections 3.1.1 and 4.1.2 for the foot. Simulation kinematics is obtained for the following parameters: step length - 0.36 m, maximum heel height - 0.18 m. CoM shift is set at 0.02 m.

As already shown by the GVS values, the joint angle presenting the greater error when compared to human mean kinematics is the knee flexion-extension, in which flexion is more pronounced than in the healthy human mean variation. Ankle dorsiflexionflexion is a little exaggerated almost through the entire gait cycle. Hip flexion-extension stays close to healthy human mean values, and hip abduction presents a small variation.

5.3.2.3 Dynamical Parameters

In figure 5.27, a comparison between simulated and real human sagittal lower limbs joint torques is made. Joint torques present great spikes, making the motion not smooth. Due to these great variations, the comparison is made, but not commented.

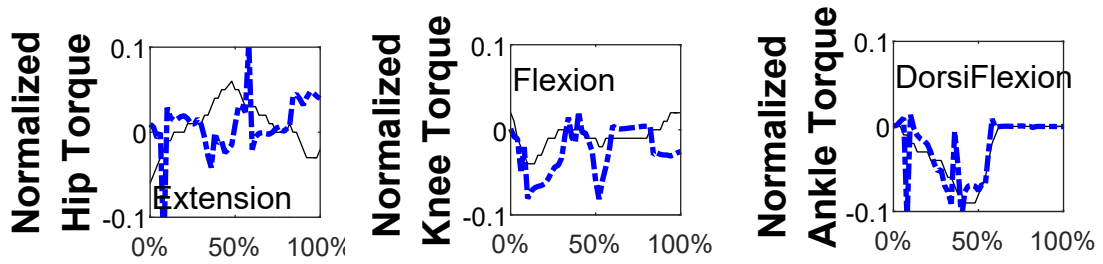In figure 5.28, the Ground Reaction Forces for the Left and Right Feet normalized by

125

Figure 5.27: Comparison between simulated flat feet walking (dashed blue line) and re-corded human (solid black line) [Stansfield et al., 2006] sagittal lower limbs joint torques. Torques are normalized by body weight and height. Simulation Parameters: step length - 0.36 m, maximum heel height - 0.18 m. CoM shift is set at 0.02 m.

body mass during the first 700 cs of simulation can be seen.

The GRF values presented by the simulation are within the magnitudes presented by humans while walking. In terms of contact, flat feet walking resembles the non patholo-gical walking introduced at the beginning of this chapter, and, therefore, their GRF values are similar. The large variations correspond to times of establishment and breaking of contacts with the ground.

5.3.2.4   Balance Parameters

In figure 5.29, the ZMP progression and its reference in the anterior-posterior (top) and medio-lateral (bottom) directions during the first 700 cs of simulation can be seen.

The ZMP follows the pre-calculated reference, but the trajectory is less smoother than in the non pathological walking. Some important noise is present in the medio-lateral direction, but the pre-defined trajectory is globally satisfied.

In figure 5.30, the ZMP and CoM progressions in the anterior-posterior (top) and medio-lateral (bottom) directions during the first 700 cs of simulation can be seen.

CoM progression trajectories are quite similar to those seen previously, *i.e.*, linear in the anterior-posterior direction and slightly oscillating around 0, its reference, in the medio-lateral direction.
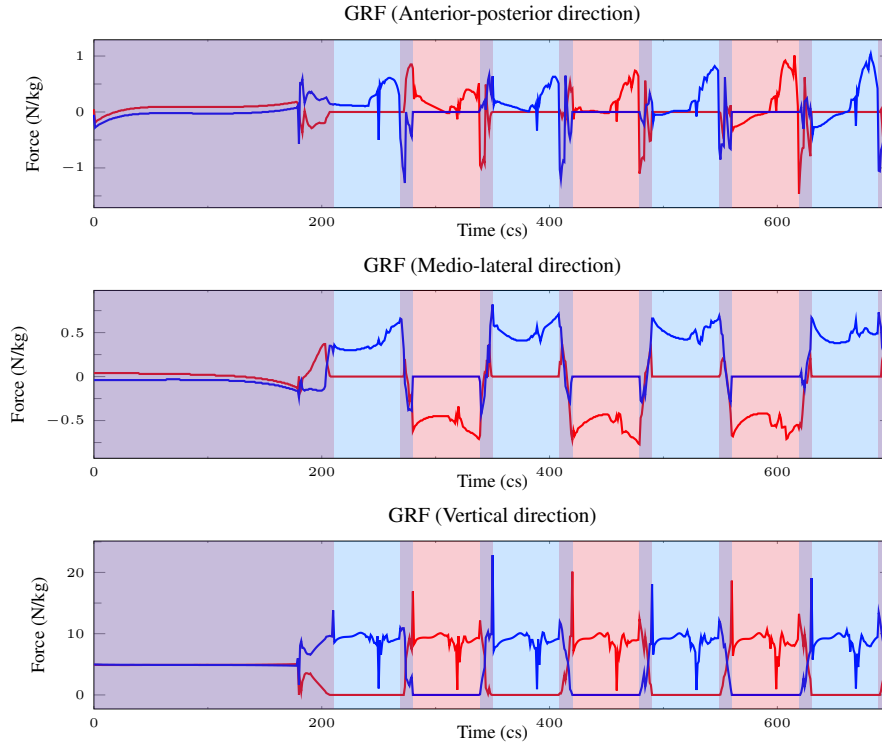
Figure 5.28: Ground Reaction Forces in the anterior-posterior (top), medio-lateral (middle) and vertical (bottom) directions for the flat feet walking. Red and blue lines correspond to Left and Right sides respectively. Dashed, dotted and solid lines correspond to the ground reaction forces of the rear feet, forefeet and feet as a whole, respectively. Violet bands correspond to double support phases, blue and red bands correspond to right and left single support phases, respectively. Simulation Parameters: step length - 0.36 m, maximum heel height - 0.18 m. CoM shift is set at 0.02 m.

5.4 Conclusion

In this chapter, the results of the walking patterns obtained with the method described in the previous chapter are presented.

No significant changes are found in the generated patterns, both in kinematics and dynamics, between the patterns generated with and without initialization procedure, when considering the same parameters to generate walking.

Nevertheless, the number of successful simulations increases for all the three modes of contact, allowing new combinations of parameters. Therefore, the initialization procedure increases the range of possible walking within certain spatio-temporal parameters.

ZMP (solid) and Reference ZMP (dotted) positions (anterior-posterior direction

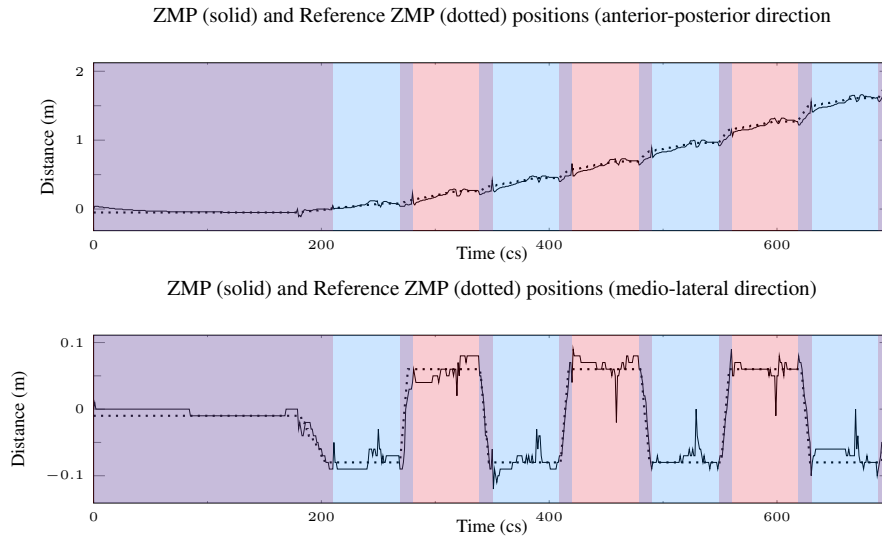ZMP (solid) and Reference ZMP (dotted) positions (medio-lateral direction)

Figure 5.29: ZMP (solid black line) and ZMP reference (dotted black line) positions for the flat feet walking. Violet bands correspond to double support phases, blue and red bands correspond to right and left single support phases, respectively. Simulation Parameters: step length - 0.36 m, maximum heel height - 0.18 m. CoM shift is set at 0.02 m.

With the improvements presented in the previous chapter, different gait patterns as toe walking, flat feet walking with toe off motion and non pathological walking are possible. Human kinematics and dynamics are approached, still, important differences subsist. These differences can be the result of many factors like:

- the LIP modelling, which has been seen to significantly affect the results, and imposes a constraint in the pelvic movement;

- the contacts modelling, here modelled between two rigid bodies contact. In fact, human feet present some compliance in contacts with the ground;

- the virtual human approximation, which can still be no sufficiently precise or accurate;

- the tasks used for the control of the virtual human walking, which are imposed, regardless of what the quantities humans optimize while walking are. It should be noted that this is still a subject of research.

ZMP (solid) and CoM(dashed) positions (anterior-posterior direction

ZMP (solid) and CoM (dashed) positions (medio-lateral direction)
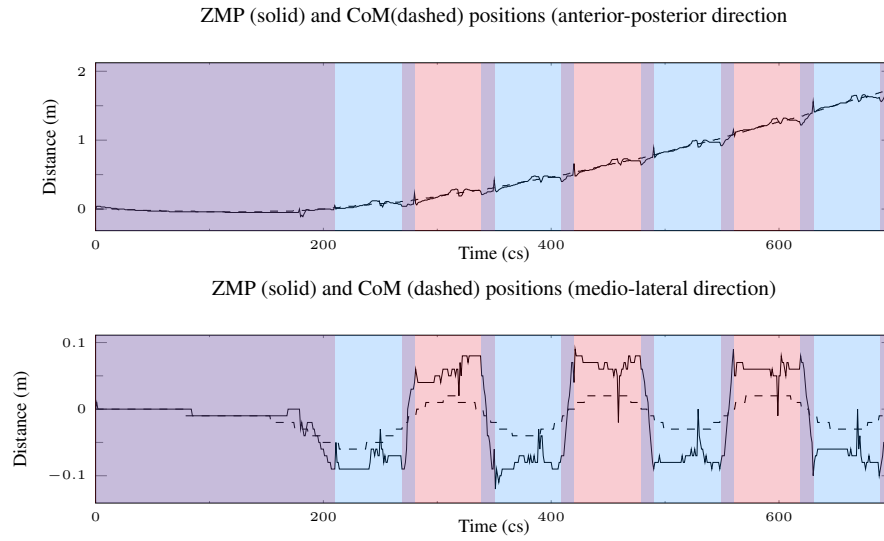

Figure 5.30: ZMP (solid black line) and CoM (dashed black line) progression projected on the floor for the flat feet walking. Violet bands correspond to double support phases, blue and red bands correspond to right and left single support phases, respectively. Simulation Parameters: step length - 0.36 m, maximum heel height - 0.18 m. CoM shift is set at 0.02 m.

Despite the disparities found between the presented simulations and observed human walking, the sagittal lower limbs' kinematics approach those observed in humans, for the non pathological walking, and joint moments and ground reaction forces present magnitudes of variation coherent with human walking. Faster motions, when compared to the literature, with spatio-temporal parameters resembling those of humans are possible.

Regarding the pathological gaits nothing is said in this chapter about their resemblance with real patients. The problem of reproducing abnormal gait patterns is the subject of the next chapter.

SIMULATION AND ANALYSIS OF PATHOLOGICAL WALKING PATTERNS

In the previous chapter, simulations of non pathological, toe and flat contact are presented. Different patterns of walking are synthesized, for a variety of spatio-temporal parameters.

In comparison with the simulations of chapter 3, the patterns generated with the non pathological contact allow a more human-like walking, presenting an increased similarity with mean healthy human gait specially in sagittal kinematics, sagittal moments (with an emphasis for the ankle dorsiflexion moment) and in contacts with the ground. Also, new abnormal contacts with the ground are possible, like toe walking.

The focus of this chapter is on the simulation of pathological walking patterns. In the previous chapter, comparisons with the healthy human walking is performed, but concerning the abnormal contact patterns, nothing is said about their resemblance to patterns presented by cerebral palsy children.

Recall that this work has a long term objective of allowing the simulation of surgical effects on gait patterns. Therefore, in this chapter, pathological walking patterns are simulated through modifications of the joints constraints. These new constraints are related to those found among children with cerebral palsy in specific gait patterns.

The adaptability of the developed simulator to changes in the joint constraints are then assessed, and the generated patterns are compared to those presented by Cerebral Palsy Children.

The pathological walking patterns explored in this chapter are detailed next.

6.1 Pathological Walking Patterns among Cerebral Palsy Children

In chapter 1, some examples of the different walking patterns that can be found among children with cerebral palsy are presented, see Table 1.1.

For the purposes of this chapter, two joint constraints limitations are explored: knee extension limitation, and ankle dorsiflexion limitation. The first one, when severe, is related to crouch gait, a common gait deviation among children with cerebral palsy. The second one usually translates in toe walking.

Given that these two abnormalities are frequent among Cerebral Palsy Children, they are relevant with respect to the purpose of this chapter. Furthermore, they are easily implemented with the methodology proposed in the previous chapter for the generation of walking patterns.

These gait deviations are detailed next.

6.1.1 Knee extension limitation

Crouch gait, see figure 6.1, is a common gait abnormality in children with cerebral palsy [Wren et al., 2005]. As already stated in Table 1.1, it is defined as an increased knee flexion (one standard deviation above the healthy mean) in a significant portion of the stance phase.
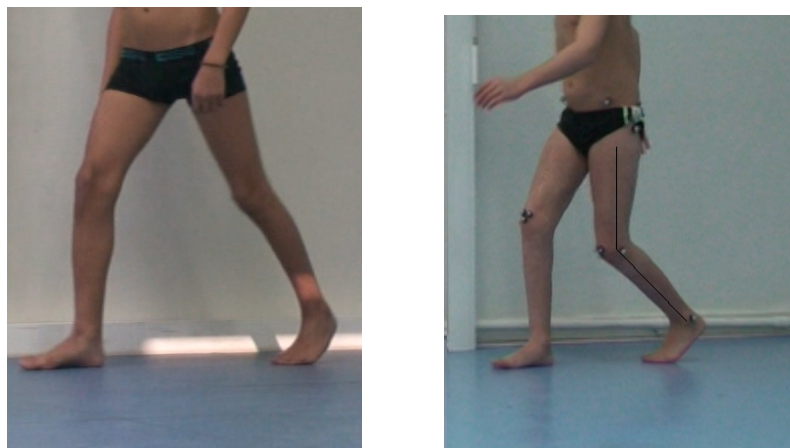

Figure 6.1: Normal (left) versus Crouch (right) Gaits.

Without treatment, crouch gait frequently aggravates over time [Bell et al., 2002]. In

order to decide the best treatment, the causes of the crouch gait must be identified. Different causes have been evoked to explain this gait abnormality such as muscular problems (contractures, weakness and spasticity) [Hoffinger et al., 1993, McNee et al., 2004, Arnold et al., 2005], skeletal deformities [Paley, 2002] and motor control disorders [Gage and Schwartz, 2004].

Since the causes can be multiple, researchers carried out different studies in order to gain insight in this pathology. Some studies use healthy subjects to induce the pathology and then compare the induced abnormality with real patients data [Matjacic and Olensek, 2007, Balzer et al., 2013]. By doing that, tertiary consequences of the crouch gait can be enlighten. Other studies use simulation to determine the muscles role in the crouch gait postures [Hoang and Reinbolt, 2012, Steele et al., 2012b], for instances. There are also retrospective studies who use data from patients to determine the conditions upon which some treatments will be more or less effective on treating crouch gait [Hicks et al., 2011, Steele et al., 2012a]. And there are also simulation studies who seek possible consequences of crouch walking [Krogt et al., 2010, Pimenta dos Santos et al., 2016].

6.1.2 Ankle dorsiflexion limitation

Another common gait abnormality among children with cerebral palsy is equinus walking [Wren et al., 2005], see figure 6.2. As introduced in Table 1.1, it is related to an excessive (greater than one standard deviation below the mean for normal healthy human walking reference during the stance phase) ankle plantarflexion. It may be accompanied by a hindfoot and/or forefoot varus or valgus, and it translates in a toe walking posture.

This toe walking, see figure 6.2, is the most noticeable deviation among cerebral palsy children, and has been, because of that, described as the gait abnormality that receives the most attention from physicians [Wren et al., 2005]. Equinus gait presents a higher than normal levels of energy expenditure [van den Hecke et al., 2007] and walking stability may decrease because of the smaller area of support [Cobeljic et al., 2009]. Cerebral Palsy children presenting an equinus gait often shown poor foot clearance, which increases the risk of tripping and falling [Cobeljic et al., 2009].

There are two types of equinus: dynamic and fixed. In the first one, there is no muscle contracture, whereas in the second one contractures of the calf musculature[1] im-

---

[1]The calf musculature is located on the back of the lower leg and is composed by *gastrocnemius* and *soleus* muscles.

Figure 6.2: Example of toe walking. Front (left) and side (right) views.

pairs the ankle [Zwick et al., 2004, Cobeljic et al., 2009]. Compensatory mechanisms for equinus walking include hip flexion, knee flexion, lumbar lordosis[2] or genu recurvatum[3] [Cobeljic et al., 2009, Houx et al., 2013].

The purpose of this thesis is in part the simulation of healthy and pathological human walking. The gait patterns resulting from the presented gait abnormalities can be implemented in the methodology proposed in the previous chapters, by introducing changes in the joint constraints. The gait deviations are simulated for the non pathological contact and toe contact in the case of the knee extension limitation, and solely for the toe contact in the ankle dorsiflexion limitation. Results from simulations are compared with real patients cases in order to evaluate the proposed walking generating process.

The flat feet contact is not used, as dynamical results of the previous chapter are very noisy, and could, therefore, generate numerical instabilities when the joint constraints used early are changed.

6.2   Simulation of gait abnormalities

As stated before, in this chapter we focus on the simulation of pathological patterns. These simulations present two goals:

- assess the capability of the simulator to adapt to a change in joint mobility constraints, in this case sagittal knee and ankle angles;

---

[2]Lumbar lordosis refers to the inward curvature of the lumbar spine.
[3]Genu recurvatum refers to an excessive extension of the knee joint - the knee bends backwards.

- determine whether or not the generated patterns present features found among children with cerebral palsy presenting the same gait problems.

The method for the simulation of the different walking scenarios is detailed next.

6.2.1 Method

Three different walking scenarios are simulated:

1. knee extension limitations on the non pathological contact walking;

2. knee extension limitations on the toe contact walking;

3. ankle dorsiflexion limitations on the toe contact walking.

The knee extension limitations occur in both patients walking with a non pathological contact and those presenting a toe walking. Therefore, it is simulated for the two cases. Concerning the ankle dorsiflexion limitation, it naturally induces a toe walking, and, thus, is only tested in this case.

In all the three cases, the numerical manikin needed for the walking motion generation is created using data from a female subject with 1.63 m height and 51.5 kg, according to the procedure presented in sections 3.1.1 and 4.1.2 for the foot. The manikin is the same that is used previously, who did not present any musculoskeletal abnormality. This choice is made to avoid abnormalities in the gait patterns other than those induced by the changes in the constraints.

The LQP-Controller, and its adaptations, presented in the previous chapters, is used to generate walking motion.

The initial configuration of the manikin is calculated so that the legs are as straighten up as possible, both feet, or only forefeet, on the ground, and the pelvis center located above the center of the feet or forefeet, depending on the type of contact consider, non pathological or toe contact, respectively.

The spatio-temporal parameters used in the simulations can be found in table 6.1.

For the non pathological contact, the cycle duration is fixed to be 1.10 s, and $p_0 = 0.28$, $p_1 = 0.39$, $p_2 = 0.41$, $p_3 = 0.44$, $p_4 = 0.47$, $p_5 = 0.5$, $p_6 = 0.78$, $p_7 = 0.89$, $p_8 = 0.91$, $p_9 = 0.94$, $p_{10} = 0.97$, and $p_{11} = 1$, see equation (4.2). For the toe contact, the cycle duration is fixed to be 1.40 s, and $p_0 = 0.11$, $p_1 = 0.5$, $p_2 = 0.61$, and $p_3 = 1$, see equation (4.1).

Table 6.1: Spatio-temporal parameters used in the simulations

Type of contact	Step length	Maximum heel/toe height	CoM shift
Non pathological	0.42 m	0.22 m	0.02 m
Toe	0.24 m	0.04 m	0 m

In order to assess the capability of the system to adapt to changes, for each walking scenario the following constraints are applied:

1. knee minimal flexion is made to vary from $5°$ up to $45°$, with a $1°$ step;

2. knee minimal flexion is made to vary from $5°$ up to $35°$, with a $1°$ step and a maximal ankle dorsiflexion angle of $25°$[4];

3. ankle maximal sagittal angle is made to vary from $25°$ dorsiflexion down to $25°$ plantarflexion, with a $1°$ step.

For each walking simulation, sagittal kinematics, joint torques and power of the lower limb are analysed, along with ground reaction forces. Recall that by definition of the walking procedure, the pelvis and the feet are set to be parallel to the ground, and therefore, pelvic movements or movements outside the sagittal plane are not very informative. These are not explored here. Sagittal kinematics is compared with real patients data in each case.

Since walking is a natural coordinated movement and kinematics only account for the variations within only one joint, cyclograms are used to assess the coordination between joints. Cyclograms are defined as the graphical plot of (α, β) during a gait cycle, where α, β are two joint angles. An example of the use of cyclograms for the study of human slope walking can be found in [Goswami et al., 1998].

A simulation is considered successful and is analysed if the virtual human completes 4 gait cycles in the steady state gait.

The results of simulations for the different walking scenarios are presented next. All the results are presented for a left cycle.

---

[4]Results from the previous chapter showed a dorsiflexion less then $25°$ when no restrictions are imposed on the toe walking. Therefore, the ankle dorsiflexion is limited to this value, in order to avoid ankle dorsiflexion mechanisms to compensate for the knee restriction.

6.2.2 Results & Discussion

6.2.2.1 Knee extension restriction effect on the non pathological contact

The knee minimal flexion angle is made to vary from 5° up to 45°, with a 1° step, which gives a total of 41 simulations performed. All the simulations are successful.

In figure 6.3, examples of walking cycles in three different conditions - no restriction (5° minimal flexion), mild restriction (20° minimal flexion), and severe restriction (40° minimal flexion) - are illustrated, figures (a) - (c), along with a walking pattern from a patient who walks in a flexed posture, figure (d).

It can be seen that with the increase of the restriction on knee extension the walking is done in a more flexed posture throughout the entire cycle, figures 6.3 (a) - (c). The patterns resemble that of the patient, although the patient presents a flat feet initial contact with the ground on the left side, which is compared[5].

The most direct effect of restraining the knee extension is on the knee flexion angle itself. Sagittal kinematics of the knee and knee range of motion[6] variation with respect to the different values of minimal knee flexion angle can be seen in figures 6.4 (a) and (b), respectively. In figure (a), the knee sagittal kinematics of the patient presented before is also shown.

In figure 6.4 (a), it can be seen that as the knee minimal flexion angle increases (orange color), the knee flexion angle kinematics is altered. In fact, the whole cycle presents an excessive flexion angle. This excessive flexion angle is also present in the patient, whose knee flexion stays above 40° almost through the entire gait cycle. It should be noted that a delay in the maximum peak knee flexion is present between simulation and patient data.

Besides the increased flexed posture, the knee range of motion decreases, figure 6.4 (b). In fact, the more crouched the position, *i.e.*, the more elevated the knee flexion minimal angle, the less range of motion the knee presents, even though the peak flexion angle is increased. From the less to the more flexed posture, more than 10° are lost in the knee range of motion. These results are consistent with the results from previous studies relating the crouch gait to the stiff-knee gait[7] [Krogt et al., 2010,

---

[5]Due to the numerical instabilities present in the flat feet contact simulations, the non pathological contact was preferred.

[6]Range of motion is defined as the difference between the maximum and minimal values of the angle during a gait cycle.

[7]Decreased arc of knee motion from maximum knee extension in stance to peak knee flexion in swing, and/or delay in peak swing knee flexion to mid- or terminal swing, hindering foot clearance [Wren et al., 2005].
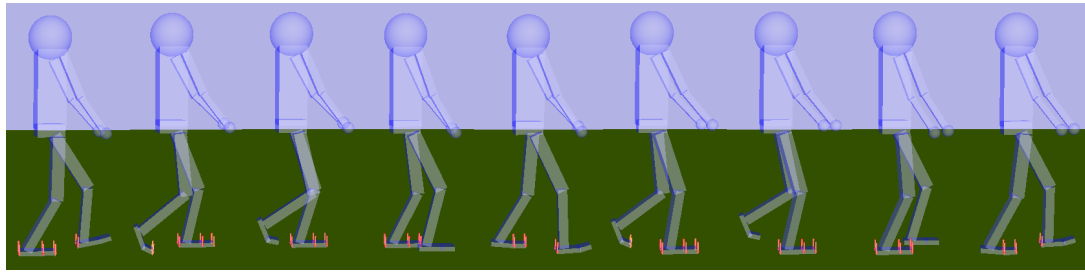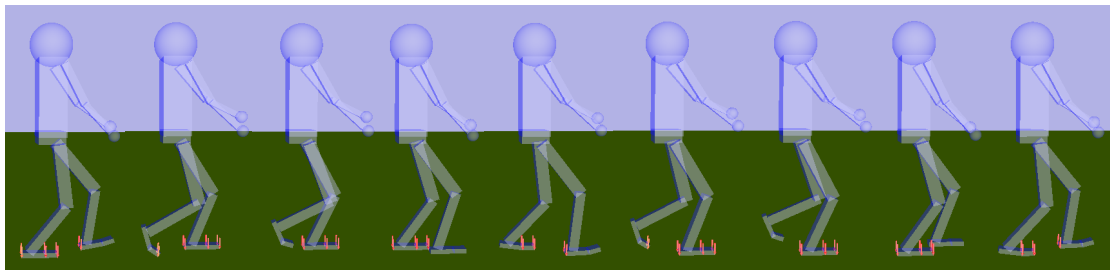
(a) Example of walking without knee extension restriction.
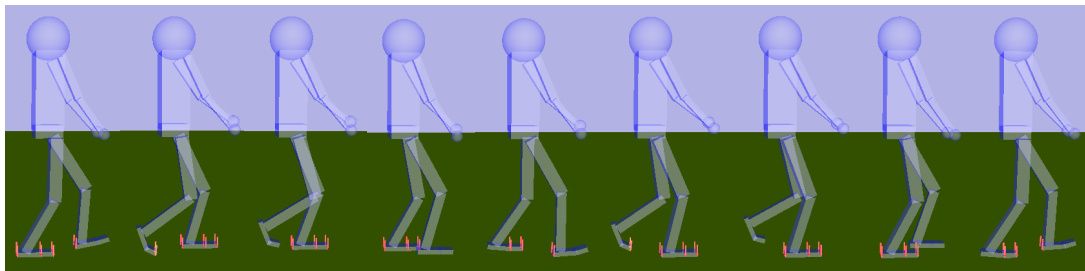
(b) Example of walking with mild knee extension restriction (minimal knee flexion $20°$).

(c) Example of walking with severe knee extension restriction (minimal knee flexion $40°$).


(d) Example of a patient walking in a flexed posture.

Figure 6.3: Walking cycles generated for non pathological contact (a) - (c), and walking cycle of a patient walking in a flexed posture (d).

Pimenta dos Santos et al., 2016].

The effect of the restriction of the knee extension is not limited to the knee joint. In figures 6.5 (a) and (b), the sagittal kinematics of the hip and ankle angles, respectively,
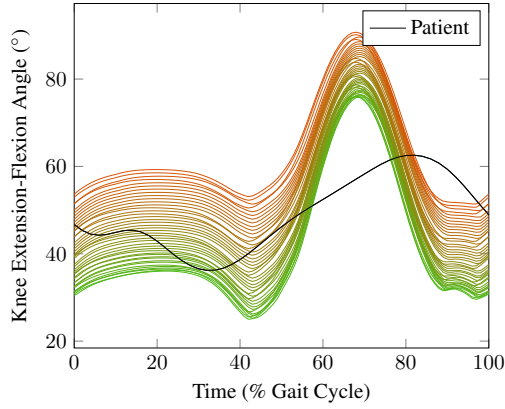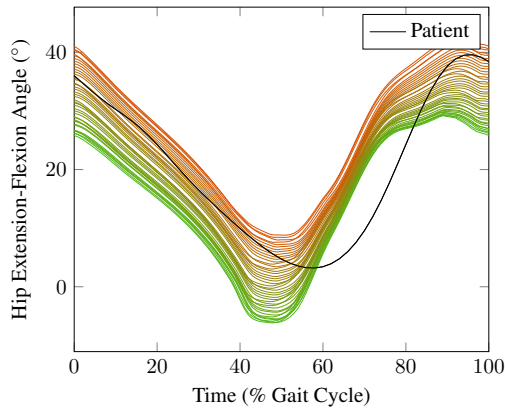
(a) Knee sagittal kinematics during a gait cycle for different values of minimal knee flexion angle (5° - green up to 45° - orange).
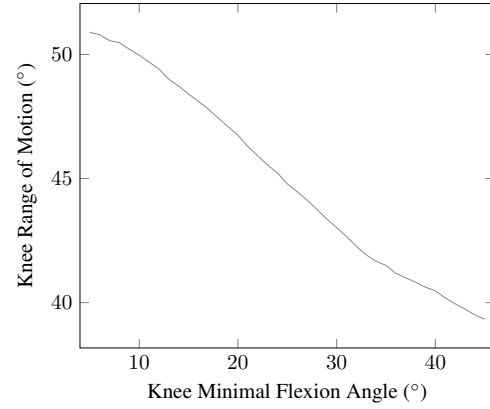
(b) Knee sagittal range of motion for different values of minimal knee flexion angle during a gait cycle.

Figure 6.4: Knee sagittal kinematics and range of motion during a gait cycle, for different values of minimal knee flexion angle.

are plotted for a gait cycle, with respect to the different values of minimal knee flexion angle. The equivalent patient results are shown in black.

(a) Sagittal hip kinematics.
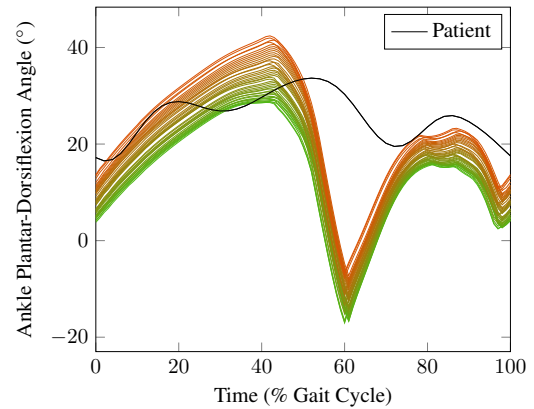
(b) Sagittal ankle kinematics.

Figure 6.5: Sagittal hip and ankle kinematics during a gait cycle for different values of minimal knee flexion angle (5° - green up to 45° - orange).

The restriction on the knee extension induces a greater hip flexion 6.5 (a) and a greater ankle dorsiflexion 6.5 (b). These results are also in accordance with previously reported

results [Hicks et al., 2008]. In the case of the hip, figure 6.5 (a), aside the delay in the minimal hip flexion, the simulations are also in accordance to the patients kinematics. As for the ankle, the variations are similar between simulations and patient, however, the peak ankle plantarflexion present in the simulations does not occur in the patient.

In figures 6.6 (a) and (b), the hip-knee and the knee-ankle sagittal cyclograms, with respect to the different values of minimal knee flexion angle, can be seen.
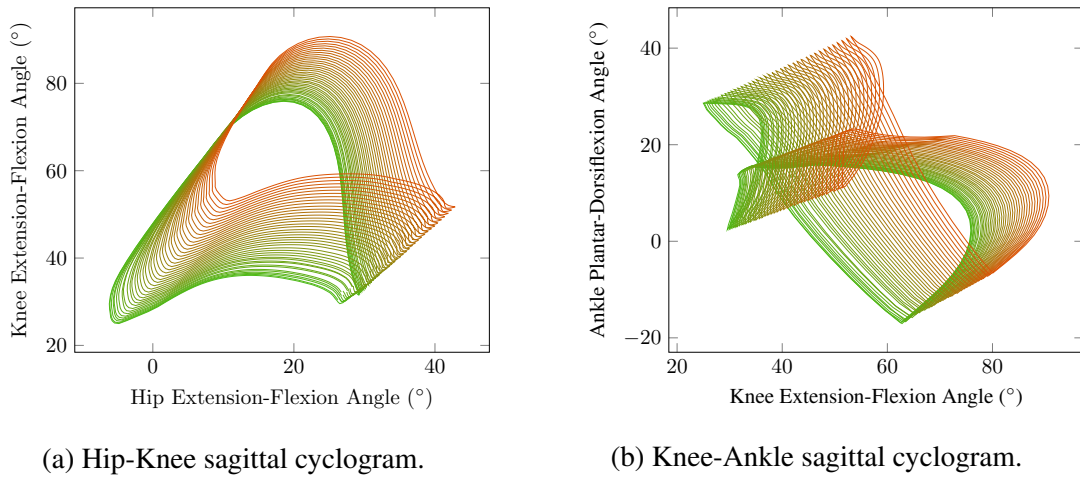

(a) Hip-Knee sagittal cyclogram.

(b) Knee-Ankle sagittal cyclogram.

Figure 6.6: Hip-Knee and Knee Ankle sagittal cyclograms for different values of minimal knee flexion angle ($5°$ - green up to $45°$ - orange).

Concerning the coordination between joints, figures 6.6, it does not greatly changes with the knee extension restriction. In fact, the shape of the curve seems to proportionally shrunk with knee restriction.

In figures 6.7 (a) - (f), the sagittal lower limbs joint torque and power are plotted for a gait cycle, for different values of minimal knee flexion angle ($5°$ - green up to $45°$ - orange).

Aside some differences just before the release of the left heel, around 40% of the gait cycle, the hip torque and power do not greatly change with the knee restriction, figures 6.7 (c) and (d) respectively.

The knee joint torque and power present the larger variation. Concerning knee torque, its absolute value increases with the increase of the knee extension restriction, figure 6.7 (a), almost until the initial contact of the right foot. Regarding knee power, figure 6.7 (b), between the period from left heel rise - around 40% of the gait cycle - to right heel initial contact - around 60% of the gait cycle - the more the knee extension restriction, the more
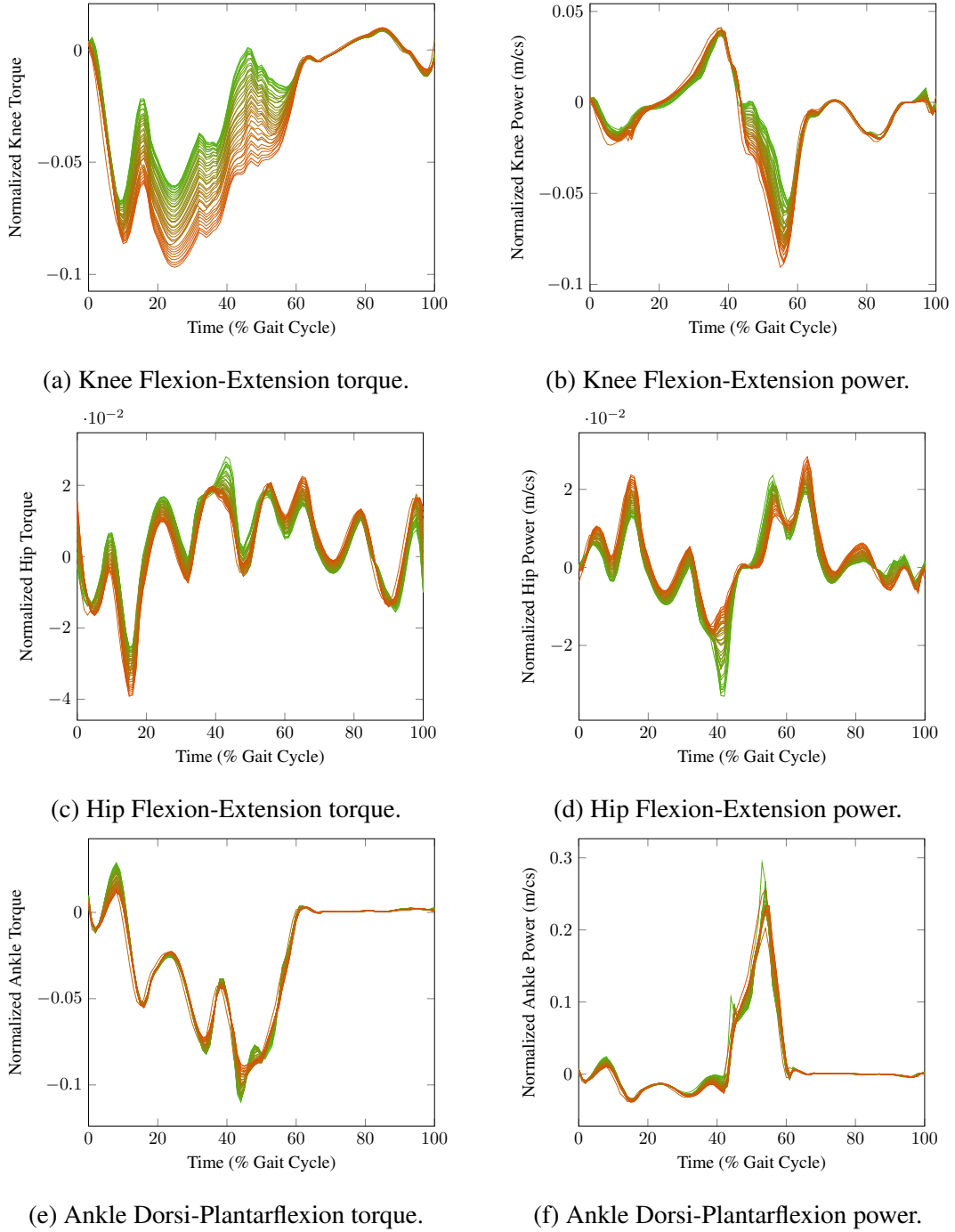
(a) Knee Flexion-Extension torque.

(b) Knee Flexion-Extension power.

(c) Hip Flexion-Extension torque.

(d) Hip Flexion-Extension power.

(e) Ankle Dorsi-Plantarflexion torque.

(f) Ankle Dorsi-Plantarflexion power.

Figure 6.7: Sagittal lower limbs joints torque and power during a gait cycle for different values of minimal knee flexion angle (5° - green up to 45° - orange). Torque and Power are normalized by body weight and height.

the absolute value of knee power.

Finally, for the ankle torque, figure 6.7 (e), no significant differences are found with the exception of a small perturbation in ankle torque when the left heel rises, around 40% of the gait cycle. For the ankle power, figure 6.7 (f), the curves are similar for all the values of knee extension. Still, it is worth noticing the important value of the ankle power just before the right heel contacts the ground and the transition of contact forces is done to the right foot, when compared to the remaining of the walking cycle.

In figure 6.8 (a), (b) and (c), the anterior-posterior, medio-lateral and vertical ground reaction forces for the left foot during a gait cycle for different values of minimal knee flexion angle (5° - green up to 45° - orange) can be seen.

As in the previous chapter results, the ground reaction forces are a bit noisy for this type of contact. No significant differences are found between the different knee extension restrictions, but some peaks like the Medio-Lateral GRF, figure 6.8 (b), before the initial contact of the right foot and the Vertical GRF, figure6.8 (c), between left heel rise and right heel initial contact are minimized as the knee is more flexed (orange curves).

It is worth noticing that the peaks on the ground reaction forces graphics are related to changes in the contact segments. Special attention should be paid to the Anterior-Posterior GRF, figure 6.8 (a), where there is an impulse forward around 40% of the gait cycle, when the left heel rises and the contact is solely concentrated on the left forefoot.

6.2.2.2 Knee extension restriction effect on toe walking

The knee minimal flexion angle is made to vary from 5° up to 35°, with a 1° step, which gives a total of 31 simulations performed. Only 16 simulations are successful - 5°, 6°, 7° and from 22° up to 35°, with the exception of 33°.

The simulations that crashed have done so mainly for one reason, breaking of the contacts between the feet and the ground. Toe walking is naturally hard to achieve, as the surface of contact between feet and ground is very reduced. Thus, in some cases, when the contact is established, it is not achieved properly and the feet penetrate the ground, violating the contact constraints and consequently leading to the manikin's fall. This could be the result of not only bad tuning of the tasks related both to contacts and feet trajectory, but also a simulator framework issue.

In figure 6.9, examples of walking cycles for two different conditions - 5° (a) and 30° (b) - are illustrated. Once again, a more flexed posture is adopted by the manikin with the increase of the minimal knee flexion angle. A walking cycle from a patient walking in his
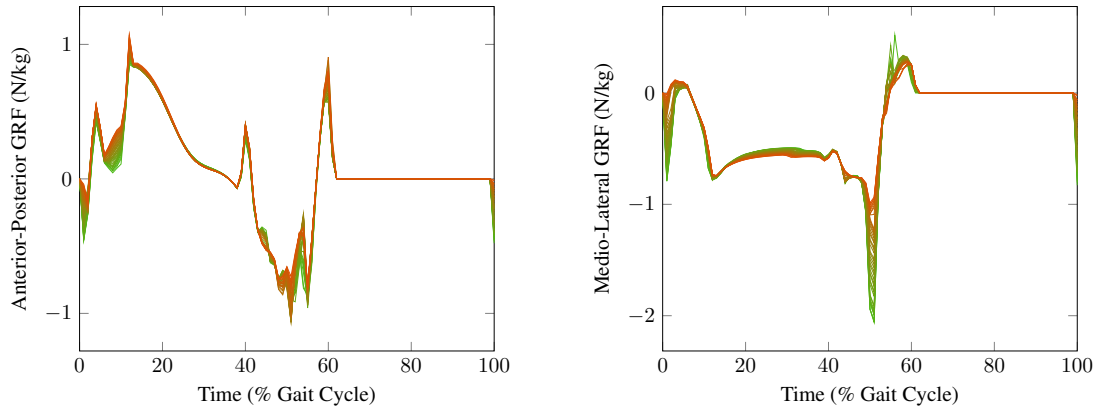
142

(a) Left Anterior-Posterior Ground Reaction Force.

(b) Left Medio-Lateral Ground Reaction Force.
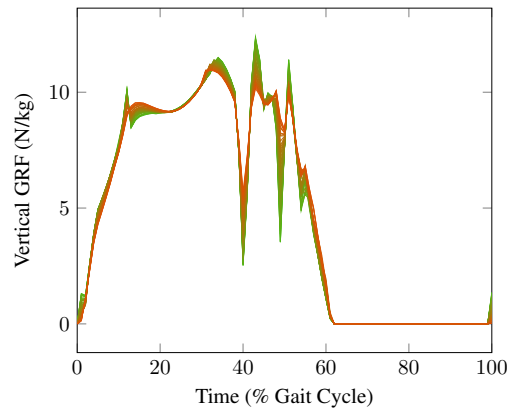
(c) Left Vertical Ground Reaction Force.

Figure 6.8: Ground Reaction Forces for the left foot during a gait cycle for different values of minimal knee flexion angle (5° - green up to 45° - orange). Forces are normalized by body weight.

toes with a flexed posture is shown in (c).

The simulations are able to reproduce the toe contact and the simulation with a 30° approaches the walking cycle of the patient, although this one presents more knee flexion than the simulations are able to achieve.

Sagittal kinematics of the knee for the different values of minimal knee flexion angle can be seen in figure 6.10. The patient knee kinematics is shown in black.

Despite the fact that not all the simulations are successful, it can be seen in figure 6.4 that with the increase of the knee minimal flexion, the peak of knee flexion is anticipated.

143
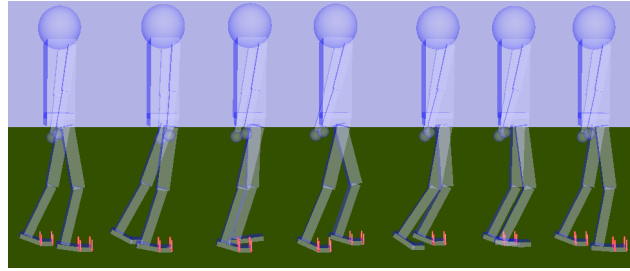
(a) Example of walking without knee extension restriction.
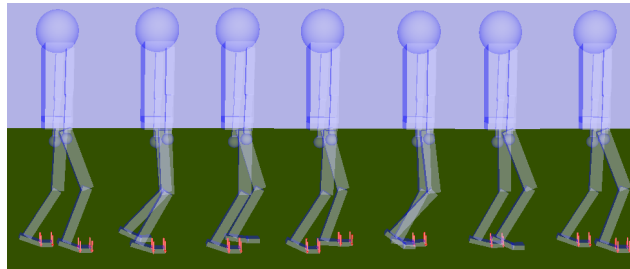
(b) Example of walking with a 30° minimal knee flexion.

(c) Example of a patient walking in his toes with an important knee flexion.

Figure 6.9: Walking cycles generated for toe contact (a) - (b), and walking cycle of a patient walking in his toes with a flexed posture (c).

Indeed, for small values of knee minimal flexion angle, green curves in figure 6.10, the knee flexion peak occurs immediately after the initial contact of the gait cycle, whereas for greater values of knee minimal flexion angles, orange curves, this same peak occurs at the middle of swig phase, around 80% of the gait cycle. It is worth noticing that for very small values of restriction, greener curves, the kinematics of the knee is completely different from the other cases, as the knee extends almost until its limit during swing phase. As already seen in figure 6.12, the patient presents a greater knee flexion than the simulations. Nevertheless, the pattern of progression of the knee flexion is similar to the one obtained for simulations with a greater knee flexion.

In figures 6.11 (a) and (b), the sagittal kinematics of the hip and ankle angles, respect-
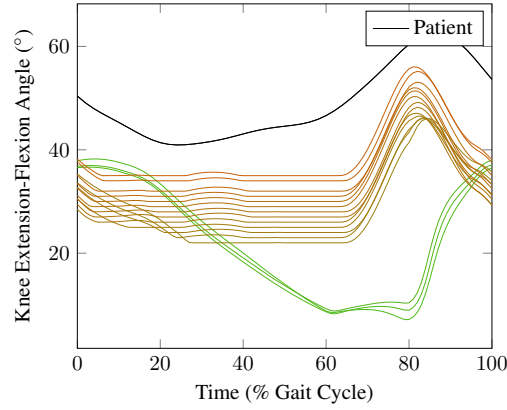
Figure 6.10: Knee sagittal kinematics during a gait cycle for different values of minimal knee flexion angle (5° - green up to 35° - orange)[*].
[*]Some shading colors between green and orange are not represented as they corresponded to non successful simulations values.

ively, are plotted for a gait cycle, with respect to the different values of minimal knee flexion angle. Patient data is represented in black.
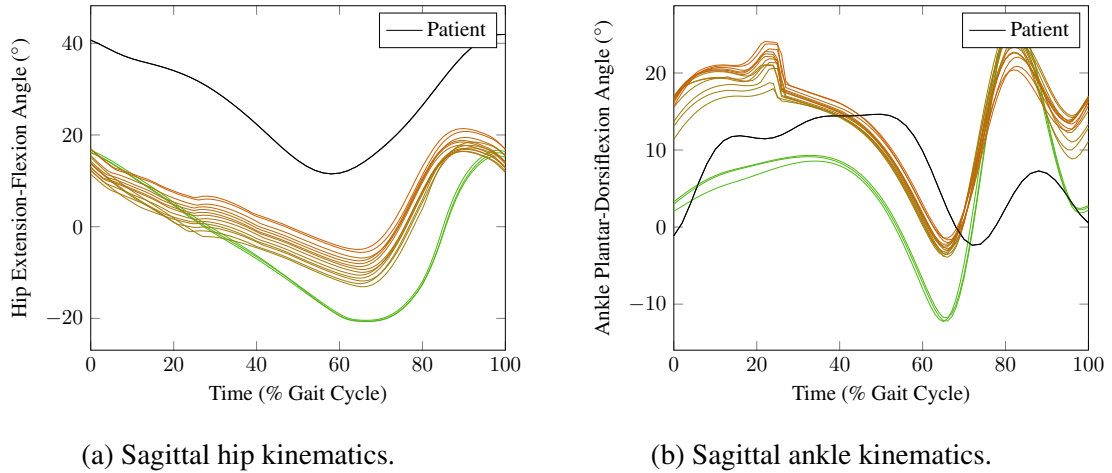

(a) Sagittal hip kinematics.

(b) Sagittal ankle kinematics.

Figure 6.11: Sagittal hip and ankle kinematics during a gait cycle for different values of minimal knee flexion angle (5° - green up to 35° - orange).

Once again, the changes on the knee minimal flexion angle also impact the hip and ankle sagittal angles, see figures 6.11 (a) and (b), respectively. As in the previous case, the hip, figure 6.11 (a), becomes more flexed, and the ankle presents greater dorsiflexion, figure 6.11 (b). In the hip case, simulations present less hip flexion than the patient, but the pattern of variation is similar. As for the ankle, the minimal and maximal peaks

of the patient ankle kinematics are also present in the simulations with a delay, and the maximum dorsiflexion is much more exaggerated in the simulations. It is worth noticing that in simulations a dorsiflexion peak occurs around 20% of the gait cycle.

In figures 6.12 (a) and (b), the hip-knee and the knee-ankle sagittal cyclograms, with respect to the different values of minimal knee flexion angle, can be seen.

(a) Hip-Knee sagittal cyclogram.
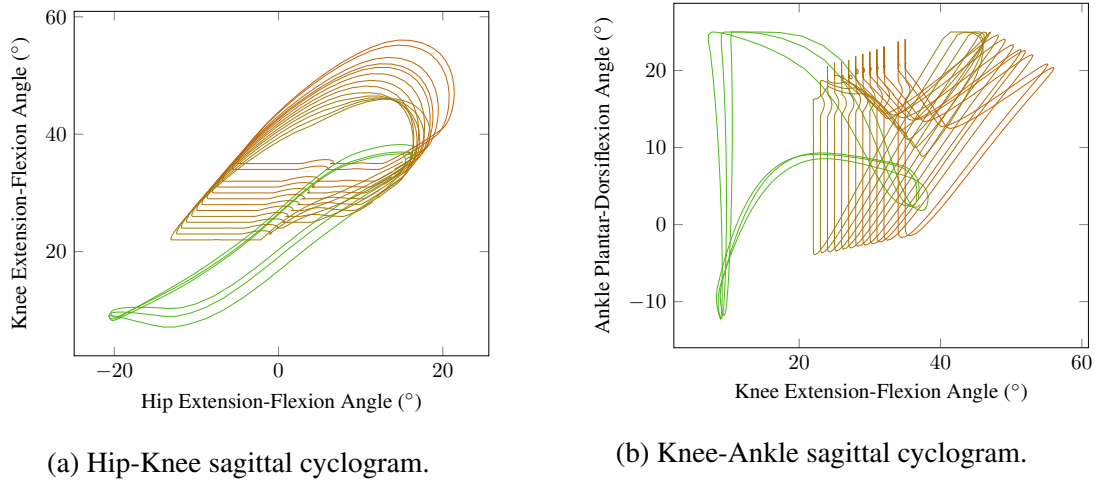
(b) Knee-Ankle sagittal cyclogram.

Figure 6.12: Hip-Knee and Knee-Ankle sagittal cyclograms for different values of minimal knee flexion angle (5° - green up to 35° - orange).

Since the knee sagittal angle profile changes with the increase of knee minimal flexion angle, the coordination between hip and knee joints, figure 6.18 (a), and knee and ankle joints, figure 6.18 (b), are also affected. A clear distinction of coordination between small, green, and great minimal knee flexion angle, orange, can be seen.
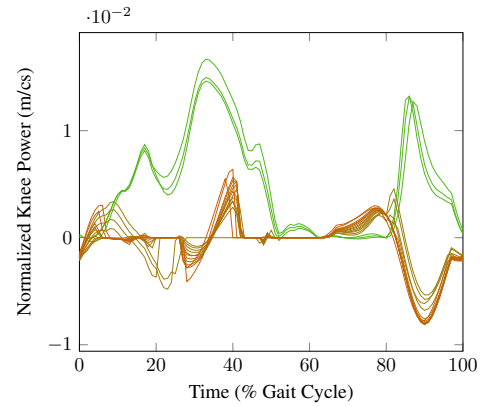
In figures 6.13 (a) - (f), the sagittal lower limbs joint torque and power are plotted for a gait cycle, for different values of minimal knee flexion angle (5° - green up to 35° - orange).

The knee torque and power change with the knee extension restriction. Regarding knee torque, figure 6.13 (a), the green curves, corresponding to small values of knee extension restriction present the same shape, whereas a larger variability is found among greater restrictions, orange curves. As for the knee power, figure 6.13 (b), there is also a clear distinction between green curves and more orange ones. This difference is mainly due to velocity values, coming from the knee angle variation, 6.10.

The hip torque and power, figures 6.13 (c) and (d), respectively, present a smaller variation than their equivalent for the knee joint. Nevertheless, for small values of knee
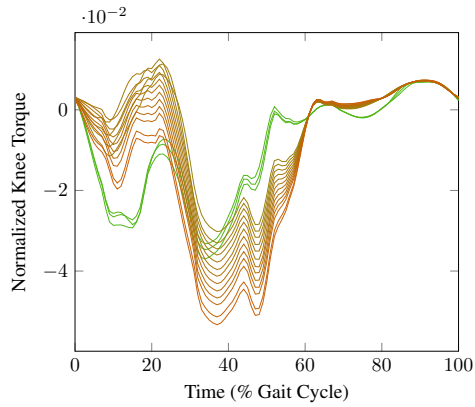
(a) Sagittal knee torque.

(b) Sagittal knee power.
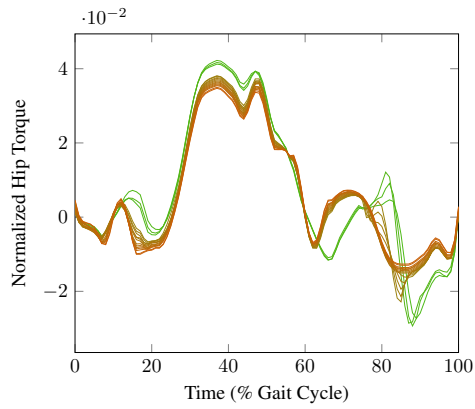
(c) Sagittal hip torque.

(d) Sagittal hip power.

(e) Sagittal ankle torque.

(f) Sagittal ankle power.

Figure 6.13: Sagittal lower limbs joints torque and power during a gait cycle for different values of minimal knee flexion angle ($5°$ - green up to $35°$ - orange). Torque and power are normalized by body weight and height.

extension restriction, green curves, the hip power presents a greater absolute value than those for the orange curves. In this case, both torque and velocity seem to impact the hip torque.

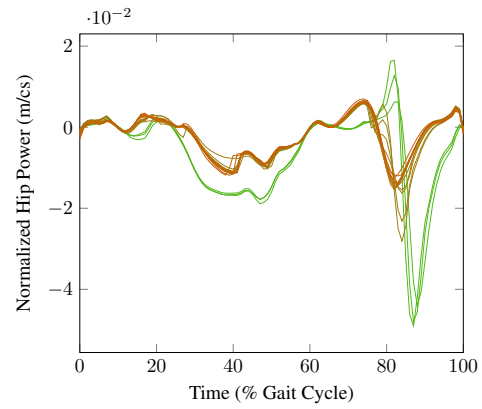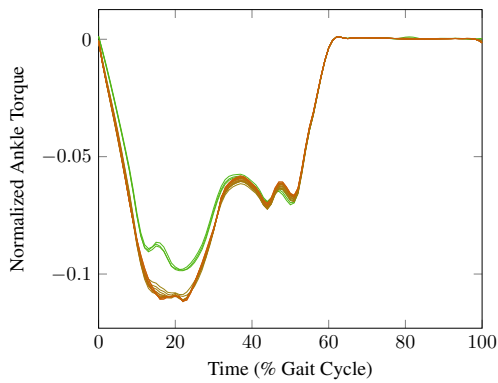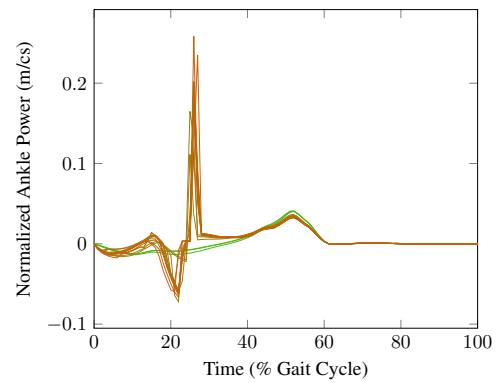Finally, the ankle torque, figure 6.13 (e), stays relatively constant for all values of knee restriction, except for a small decrease for green curves around 20% of the gait cycle. Shortly after 20% of the gait cycle, the ankle power, figure 6.13 (f), presents an important peak for orange curves, which could be the result of the ankle kinematics, as at this instant the ankle joint reaches its limit for the curves corresponding to the greater knee restriction.

In figure 6.14 (a), (b) and (c), the left anterior-posterior, medio-lateral and vertical ground reaction forces during a gait cycle for different values of minimal knee flexion angle ($5°$ - green up to $45°$ - orange) are presented.

The first noticeable thing in the ground reaction forces is the vertical component. Besides the fact that this component is much more regular for the toe walking than for the non pathological contact, which is already the case in the previous chapter, it stays relatively the same for all the simulations. This is not the case for the other two components, where disturbances occur near 30% of the gait cycle. This time is in the single support phase. The disturbances could be the result of a momentarily problem in the maintaining of the contacts, at least in these directions, since the vertical component is not affected. As previously said, the contacts for the toe walking are difficult to achieve and maintain due to the reduced area of support.

6.2.2.3 Ankle dorsiflexion restriction effect on toe walking

The ankle maximal sagittal angle is made to vary from $25°$ dorsiflexion down to $25°$ plantarflexion, with a $1°$ step, which gives a total of 51 simulations performed. Only 15 simulations are successful - $2°$ through $5°$, $13°$, and from $16°$ up to $25°$, all dorsiflexion values. Simulations in complete plantarflexion during the entire walking are not possible. Once again, the difficulty in establishing and maintaining the contacts for the toe walking is the main responsible for the number of unsuccessful simulations.

In figure 6.15, examples of walking cycles for two different conditions - $25°$ (a) and $5°$ dorsiflexion (b) - are illustrated. A walking cycle of a patient walking in her toes is presented in figure (c).

It can be seen that with the increase of the ankle dorsiflexion restriction, the ankle is more plantarflexed during the entire cycle, figures 6.15 (a) and (b). In the patient, the toe
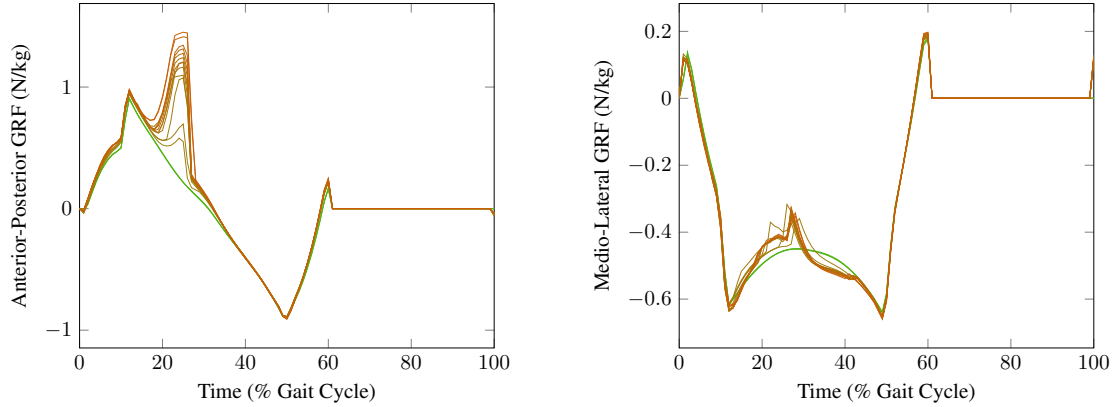
148

(a) Left Anterior-Posterior Ground Reaction Force.

(b) Left Medio-Lateral Ground Reaction Force.
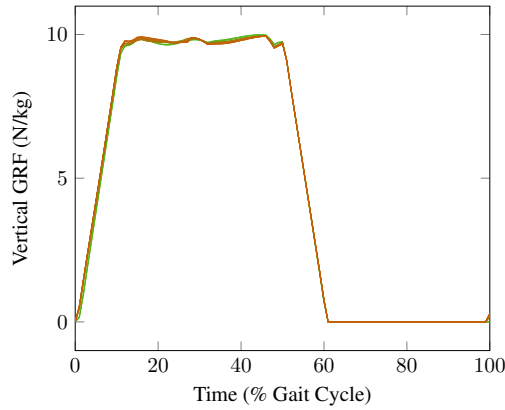
(c) Left Vertical Ground Reaction Force.

Figure 6.14: Ground Reaction Forces for the left foot during a gait cycle for different values of minimal knee flexion angle (5° - green up to 35° - orange). Forces are normalized by body weight.

contact is accompanied of an important flexion posture, contrarily to the simulations.

In figure 6.16, the sagittal kinematics of the ankle for the different values of maximal sagittal ankle angle are plotted. The patient data is in black.

Even though not all the simulations are successful, the orange curves (more dorsiflexion restriction), present more plantarflexion than the green ones, throughout the entire cycle. It should be noted, that contrarily to the two previous experiments, here the motions do not achieve limit cycles, as ankle angle at the beginning and end of the gait cycle are different. Concerning patient sagittal ankle kinematics, it resembles more the previous
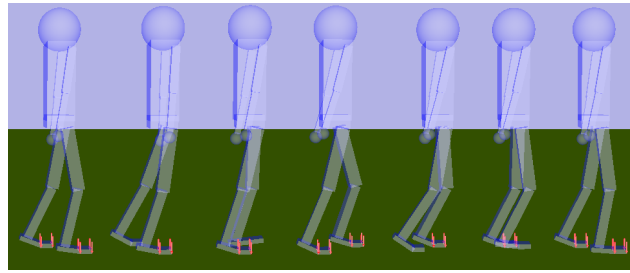
(a) Example of walking with a maximal 25° dorsiflexion.
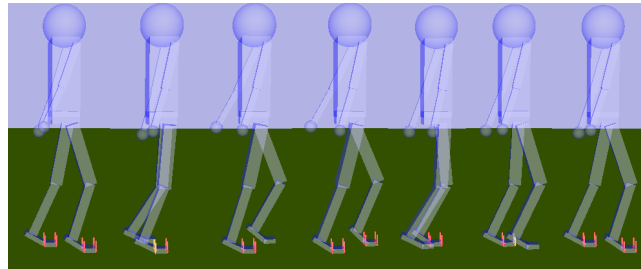
(b) Example of walking with a maximal 5° dorsiflexion.

(c) Example of a patient walking in her toes.

Figure 6.15: Walking cycles for toe contact(a) - (b), and walking cycle of a patient walking in her toes.

case than this one. This could be explained, by the important knee flexion present during the entire gait cycle.

In figures 6.17 (a) and (b), the sagittal kinematics of the hip and ankle angles, respectively, are plotted for a gait cycle, with respect to the different values of maximal sagittal ankle angle.

Kinematics of the hip and knee, figures 6.17 (a) and (b), respectively, confirm that the successful simulations in this case do no achieve limit cycles. These phenomena is worsened by the ankle dorsiflexion restriction, as orange curves present the greater disparity between angle values at the beginning and end of the gait cycle. Once again, patient hip and knee sagittal patterns resemble the previous case, as an important knee

Figure 6.16: Sagittal ankle kinematics during a gait cycle for different values of maximal sagittal ankle angle ($25°$ dorsiflexion - green down to $2°$ dorsiflexion - orange)[*].

[*]Since no walking in complete plantarflexion is possible, the gradient colors are done between the two most extreme values $2°$ and $25°$ dorsiflexion. Since not all the values between these extremes generate successful simulations, some shading colors are not represented.

(a) Sagittal hip kinematics.

(b) Sagittal knee kinematics.
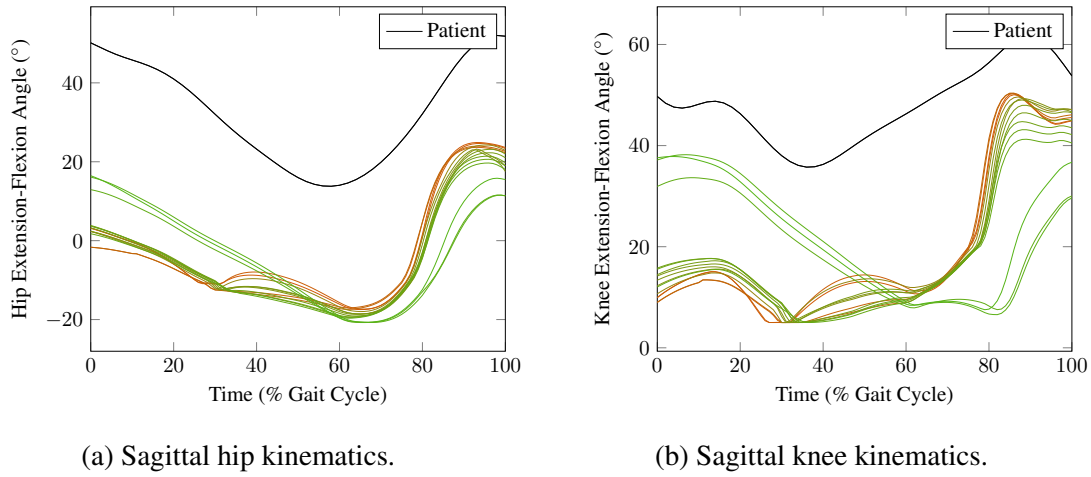
Figure 6.17: Sagittal hip and knee kinematics during a gait cycle for different values of maximal sagittal ankle angle ($25°$ dorsiflexion - green down to $2°$ dorsiflexion - orange).

flexion is present.

The hip-knee and the knee-ankle sagittal cyclograms, with respect to the different values of maximal sagittal ankle angle, are plotted in figures 6.18 (a) and (b), respectively.

Since the motions are not cyclic, the sagittal cyclograms are worthless to analyse.

In figures 6.19 (a) - (f), the sagittal lower limbs joints torque and power are plotted for a gait cycle, for different values of maximal sagittal ankle angle.

Aside some more visible differences in knee joint torque and power, figures 6.19 (e)

151

(a) Hip-Knee sagittal cyclogram.

(b) Knee-Ankle sagittal cyclogram.

Figure 6.18: Hip-Knee and Knee-Ankle cyclograms for different values of maximal sagittal ankle angle ($25°$ dorsiflexion - green down to $2°$ dorsiflexion - orange).

and (f), the other joints torques and powers seem similar throughout the simulations. However, the peaks found in the previous experiment on the ankle and hip powers, remain in this case also. Thus, since the restriction here concerns another joint, one could expected this behaviour to be a consequence of toe contact rather than the restriction imposed. Furthermore, new great peak variations appear in the hip torque around 80% of the gait cycle, figure 6.19 (c) and on the knee torque and knee power around 30% of the gait cycle, figure 6.19 (e) and (f), respectively. These peaks occur when the knee is at its maximum extension values.

In figure 6.20 (a), (b) and (c), the anterior-posterior, medio-lateral and vertical ground reaction forces during a gait cycle for different values of maximal sagittal ankle angle can be seen.

The vertical ground reaction force is less smoother than in the previous experiment, as a disturbance occurs around 30% of the gait cycle. Also, the peak disturbances of the previous case are exacerbated here.

6.3   Concluding remarks

In this chapter, the adaptability of the simulator to changes in the constraints of the model is assessed for two types of walking.

In the case of non pathological contact, great changes in the knee angle constraint are
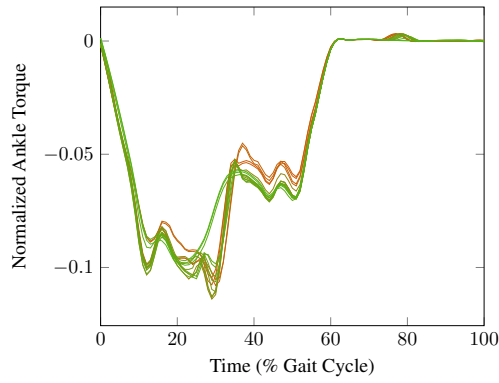
(a) Sagittal ankle torque.
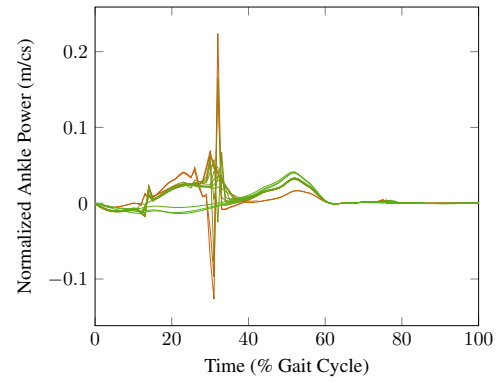
(b) Sagittal ankle power.
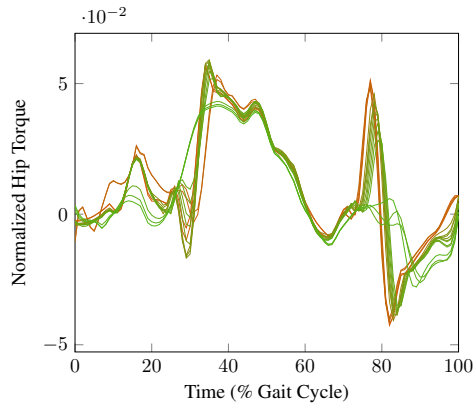
(c) Sagittal hip torque.
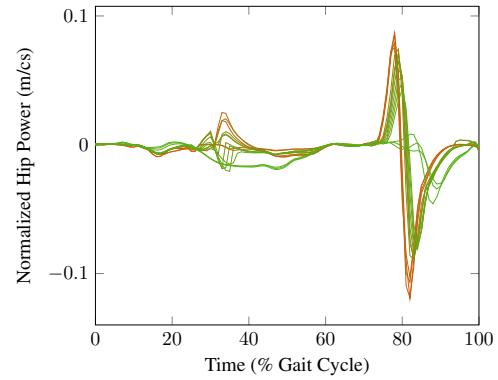
(d) Sagittal hip power.
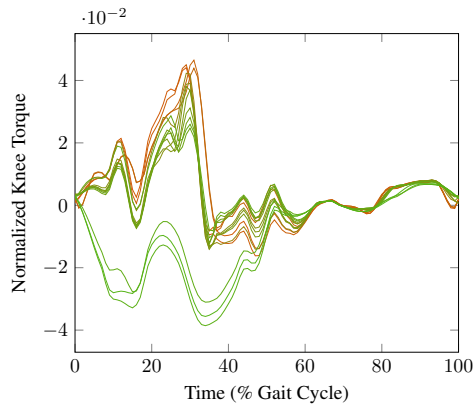
(e) Sagittal knee torque.
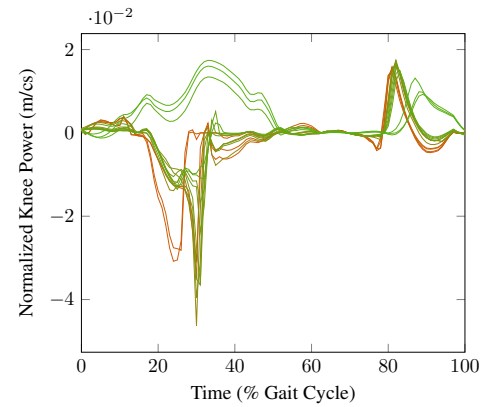
(f) Sagittal knee power.

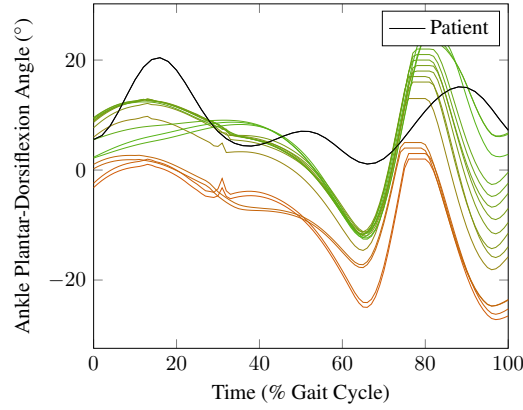Figure 6.19: Sagittal lower limbs joints torque and power during a gait cycle for different values of maximal sagittal ankle angle ($25°$ dorsiflexion - green down to $2°$ dorsiflexion - orange). Torques and power are normalized by body weight and height.
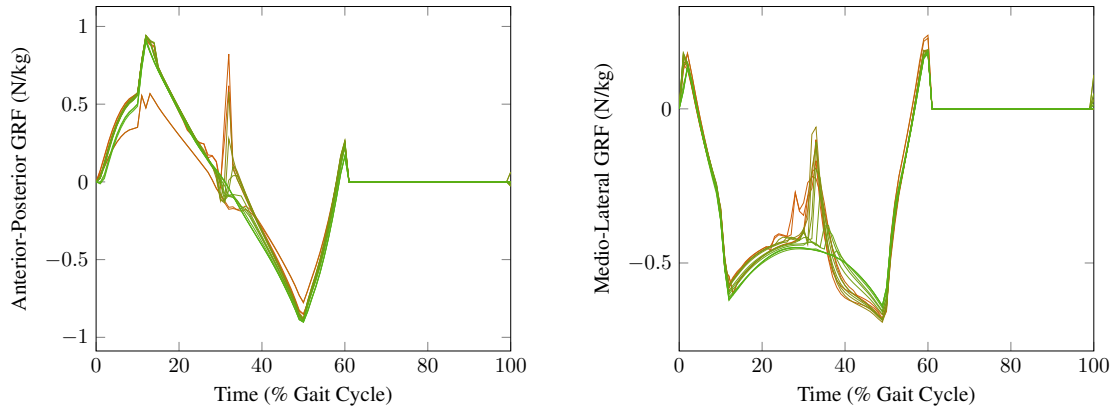
(a) Left Anterior-Posterior Ground Reaction Force.

(b) Left Medio-Lateral Ground Reaction Force.
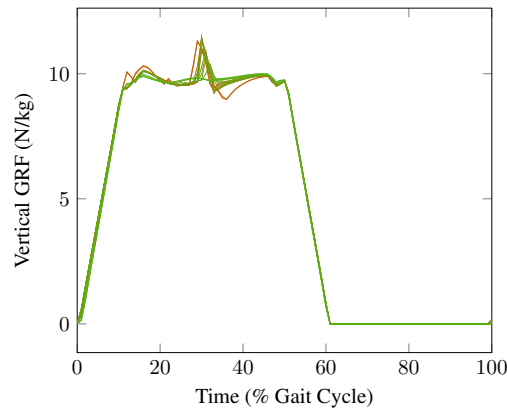
(c) Left Vertical Ground Reaction Force.

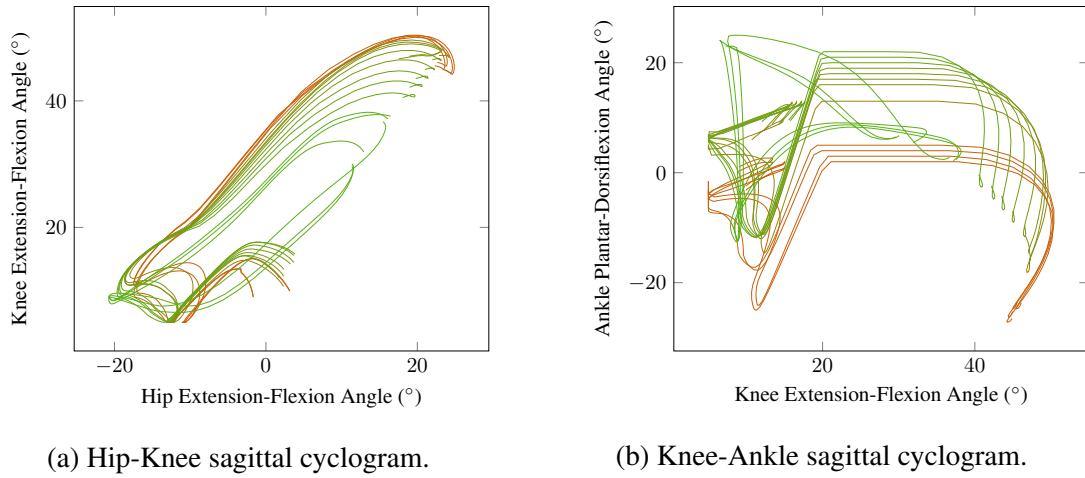Figure 6.20: Left Ground Reaction Forces during a gait cycle for different values of maximal sagittal ankle angle (25° dorsiflexion - green down to 2° dorsiflexion - orange).

possible, and results are in accordance with those reported in the literature, and patient data. In the case of toe walking, the range of proposed values cannot be entirely tested, as simulations do not successfully terminate. The flat feet contact is not used, as dynamical results of the previous chapter are very noisy, and could, therefore, generate numerical instabilities when the joint constraints used early are changed.

With the three experiments on pathological walking treated in this chapter, it can be seen that the simulator is able to adapt to restrictions in knee and ankle mobility in both non pathological and toe contact cases. Despite the fact that for some values simulations are not possible, the simulator still generates walking patterns. In the cases of knee re-

striction, patients presenting the same pathology are found and compared to simulation results. Similar behaviours are established between simulations and patients. The patients presented here all have arms and trunk movements during walking, which is not the case for simulations. It has been shown [Park, 2008], that the arms movement contribute to diminish the vertical reaction moment on the foot, and therefore, the motions produced with arm swing may differ from those without. In the future, arms motion should be studied and included in the proposed methodology. It should be noted that the simulations done in this chapter do not concern a specific patient, but rather a type of pathology.

Concerning not successful simulations, these were due mainly to feet contact problems. These problems may have several causes:

1. the rigid contact modelling;

2. lack of support area;

3. the tasks used in the walking generation.

Concerning the first cause, as seen in chapter 4, the contacts are treated as contacts between two rigid surfaces. No damping is considered, and every impact with the ground is propagated through the model. Moreover, contacts transitions are not treated directly. Instead, the contacts with the ground are planned such that the velocity of contacts points is zero at time of impact, in order to reduce discontinuities at contact transitions.

The second problem mostly affects the toe walking. The reduced area of support is a known factor of instability. This issue is also observed in the non pathological contact when the area of support is reduced to the forefoot part. In fact, at this moment, around 40% and near the end of the gait cycle in figure 6.8 (c), the vertical ground reaction force rapidly decreases, almost attaining 0, which is a potential source of numerical instability.

The third cause is related to the tasks, and respective regulation parameters, used in the optimization procedure. Indeed, both weights and proportional derivative parameters for each task were manually set to allow the simulation of the three types of walking, but no study about their influence on the walking pattern generation was done. As mentioned above, in some cases of toe walking simulations, the feet tasks and contact constraints were not sufficient to ensure the maintaining of the contact.

Aside these issues, other may impact the success or realism of the walking patterns generated. For instance, the LIP-modelling does not allow any adaptation of the posture during walking. Thus, as the manikin initial posture is defined with the knees as straight

as possible, if this posture is not the better to satisfy the constraints during the walking motion, this is is not corrected. The manikin will have the tendency to walk the knees extended at their maximum as step length increases. A first solution to overcome this problem was the CoM reference altitude shift introduced in the previous chapter. This indeed allows more motions to be accomplished, but still restrains the manikins CoM position.

Finally, the tasks chosen to be used in the walking generation procedure may also not be the best ones to reproduce human walking. With the ones used in this work, the non pathological contact is acceptable, but the toe walking and the flat feet contact are very constrained at walking speed and step length values. Only very slow motions are possible.

In order to improve the range of possible motions, as well as the stability of those generated, changes in the contacts modelling should also be done. Furthermore, a study to identify the tasks better suited for walking simulation should be undertaken.

CONCLUSION

The main contributions of this work are presented hereafter. Perspectives of this work on improvements and applications are also detailed.

7.1 Contributions

Nowadays, the results of Single Event Multi-Level Surgery on Cerebral Palsy Children are still difficult to predict. This thesis develops a physical based motion simulator that can produce different walking patterns, as function of geometrical and dynamical parameters of a numerical manikin, supposed to model with a relative accuracy healthy or pathological cases.

In Chapter 2, we present the different parameters used in the quantification and evaluation of the human walking, along with methods available to evaluate human walking. Even though very useful and relatively accurate, these methods can only be employed before and after the surgery, and not to predict its results. One way to overcome this issue is the use of statistics to estimate the result of the intervention, but the lack of an associated dynamical model impacts the physical realism of the prediction. Some software solutions exist to generate patterns, and help reproduce human walking, but these are still insufficient to predict the result of a surgery. This inadequacy is related to lack of human specifications on the model used, specific cases treatment, or the need of large motion capture data. Also, the resulting walking motions lack of human resemblance.

In this work, we present an hybrid approach to generate human walking. **We develop a virtual manikin with anthropomorphic characteristics** and present the framework upon which this work is based in chapter 3. A task-oriented LQP controller is used to dynamically simulate walking through constrained optimization. The optimization cost function is defined with a weighting sum of tasks that are related to feet motion, pelvis, torso and head orientation and to the CoM trajectory projected on the ground. A Linear Inverted Pendulum Model and the ZMP are used to determine the CoM trajectory.

The modelled system respects the equations of motion, used as constraints, together with joint angles and torques limits, and contacts constraints. The motion is simulated in the multibody dynamics XDE framework. We do a first evaluation of the generated patterns. Even though the patterns show non smooth motion, contrarily to humans, the presented framework allows to recover the parameters usually adopted to evaluate human walking. Also, we are able to generate walking patterns with different spatio-temporal parameters.

Since the focus of this work is both healthy and pathological walking, in chapter 4, we improve the foot modelling, which we assume to be responsible for some of the limits of the simulated patterns of chapter 3, by making it flexible, increasing by this way the walking velocity range. **We develop a two segments foot model, making it possible for new types of contact with the ground to be established. Also, an initiation period in the walking motion is included, to increase the range of spatio-temporal parameters achieved.**

We present the results of walking simulations with these changes in chapter 5. **With the non pathological contact we are able to reproduce some features of human walking: spatio-temporal parameters of healthy human walking are approached, sagittal kinematics is closed to human mean kinematics and joint torques are improved.** Even though more limited in terms of spatio-temporal parameters, **we can generate toe walking and flat feet walking with heel off motion.**

Finally, we present an application of the proposed methodology in the generation and analysis of pathological walking in chapter 6. We apply a knee extension restriction to the non pathological contact. **With the presented methodology, we are able to deal with the changes introduced by the new joint constraints and still generate walking patterns. These gait patterns present similar features to those observed in humans presenting the same conditions.** Joint restrictions are also applied to the toe walking, namely the aforementioned knee restriction and an ankle dorsiflexion restriction. **Even though the system does not deal with all the changes introduced, specially in the ankle dorsiflexion restriction, different walking patterns are possible and some features of human walking in the same conditions are found.**

7.2   Perspectives

In this work, some advances are made to achieve the goal of predicting the result of a surgery. We can simulate healthy and pathological human walking, and the proposed

methodology allows the introduction of some changes in the constraints of the model to achieve pathological cases. These changes are related to the surgery or pathology one wants to reproduce. Thus, some characteristics of specific locomotion disorders are possible to observe. With some improvements, the goal of predicting surgery results could be achieved. These are detailed next.

7.2.1 Improvements

A first set of improvements of this work regard the numerical representation of the human body. Indeed, at least two segments can be more complex: the torso and the foot. The human torso is composed of several vertebrae, which enables some liberty in the torso movement. In the model used in this work, the torso is composed of one single segment, which severely restrains its mobility. A first step towards the improvement of the human modelling can therefore be a new modelling of the torso. This would allow some movement which could benefit the fluidity of the generated walking patterns. Another segment that could be enhanced is the foot. A first upgrade is already done by the division in two segments, but a more complex model could also bring benefits to the generation of walking patterns.

Regarding the human modelling, a mid/long term improvement is the inclusion of muscles. As said near the end of section 3.1, the developments made here are suitable for a musculoskeletal representation. This way, joint and torques constraints can be defined with dependency on muscular lengths, but also on the joint positioning. Even without adding muscles, this dependency could be implemented, in order to take into account patients specificities like short length muscles that reduce the mobility of joints.

Other improvements concern mostly the generation of human walking process. First, as cited through this manuscript, the contacts modelling and handling need improvement. Even though different and human resemblance walking motions are possible, contacts are still a potential source of instability in the generated patterns. Together with an upgrade of the foot model, contacts that take into account shock absorbing properties of the human foot could be used to minimize disturbances in the contacts and ground reaction forces at times of contacts transitions.

Additionally, in order to increase the range of pathological movements, a controller taking different types of contacts for each foot (toe contact on the right side and flat foot on the left side, for instance), can be implemented from the current methodology.

A second aspect of the human walking generation process concerns the LIP modelling.

Even though very helpful and easy to use, the LIP modelling restrains the motion of the CoM of the numerical manikin and does not take into account angular momentum. These can be of importance, specially in balancing. One way to overcome this issue could be the use of a strategy as the one presented in [Englsberger and Ott, 2012], where vertical CoM motion and angular momentum are considered in the control of bipedal walking. Other methods based on non-linear optimisation or machine learning are quite promising for solving such complex problems with high degrees of freedom. However, the given results would be strongly dependent on the choice of the optimised criteria (walking cost).

Another improvement concerns the optimisation parameters used in the simulation, such as the k_p and k_d of the different proportional derivative controllers used. In fact, these values were chosen in order to have stable simulations, but not necessarily the closest to the human patterns. By choosing a set of different patients, these parameters could be optimised, by performing simulations with different values, and comparing the resulting walking patterns with those from patients.

7.2.2   Applications

A first application of the framework presented in this work is the study of human locomotion, in particular, what do human subjects minimize while walking [Mombaur et al., 2010]. In fact, by changing the tasks we use to define the optimisation problem, and by comparing the results of simulations to observed human walking, we can study the tasks behind human walking. Since the framework is developed for both healthy and pathological human walking, the two cases can be explored simultaneously. This would allow us to determine specific control changes between healthy and pathological walking. We could use global sensitivity analysis to examine the walking patterns, like it is done in [Maurice, 2015]. Even though the work developed there refers to ergonomic design of collaborative robots, the methods developed are easily transferred to the analysis of human walking, provided that the appropriated indicators to quantify human walking are defined.

Another application regards the joining of the two parts of the project in which this work takes part. Recall from the introduction of this work, that it takes part in a bigger project, where a statistical tool for surgery prediction has been developed [Galarraga C., 2017]. This statistical tool predicts kinematic results for each patient, based in the pre-operative state and the operative plan. Since our methodology relies on the computation of errors, associated with tasks in the optimisation process, to generate

human walking, the results from the statistical prediction could be fed to our generation process, in order to guide the solution of the dynamical model to the most probable one. On the one hand, this integration would give realism to the statistical prediction, which does not take into account any physical model. On the other hand, the solutions found with our methodology could be guided, and therefore improved. The resulting patterns would be closer to the specific patient in study.

The problem of predicting or even simulating human walking motions, both healthy and pathological, still represents a great challenge in the scientific community. Hopefully, this work will help to advance in the understanding and prediction of human walking, and therefore help in medical decision in such important matters.
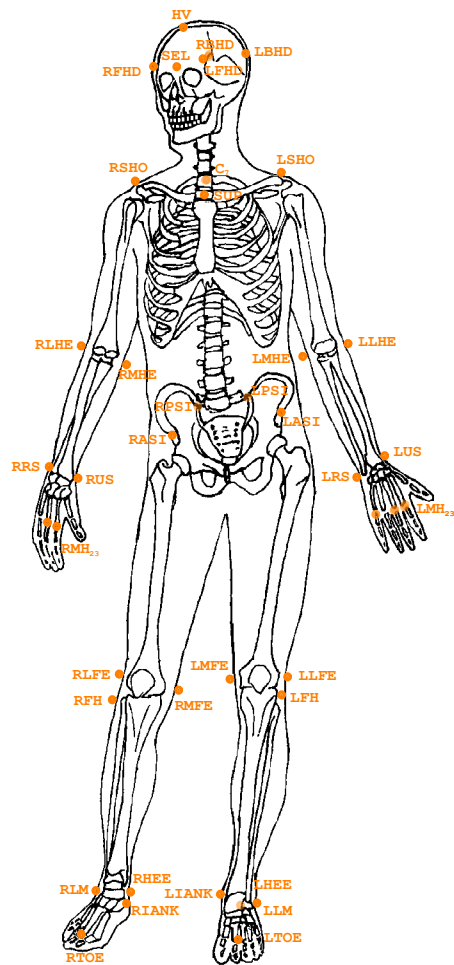
MARKERS USED IN CGA EXAMS

Figure A.1: Location of the markers used in the computation of the kinematic tree model presented in chapter 3. A description of these markers is done in table A.1.

Body Part	Left Marker	Right Marker	Location
Head	SEL		*Sellion* - Greatest indentation of the nasal root depression in the mid-sagittal plane.
	HV		*Head Vertex* - Top of the head in the mid-sagittal plane.
	LFHD	RFHD	*Front Head* - Approximately over the temple.
	LBHD	RBHD	*Back Head* - On the back of the head, roughly in a horizontal plane of the front head markers.
Torso	C_7		*7th Cervicale* - Superior tip of the spine of the 7th cervical vertebra.
	SUP		*Suprasternale* - Lowest point in the notch in the upper edge of the breastbone.
Arm	LSHO	RSHO	*Shoulder Marker* - On the Acromio-clavicular joint.
Forearm	LLHE	RLHE	*Lateral Humeral Epicondyle* - Most lateral point on the lateral epicondyle of the humerus.
	LMHE	RMHE	*Medial Humeral Epicondyle* - Most medial point on the medial epicondyle of the humerus.
Hand	LRS	RRS	*Radial Styloid* - Most distal point of the radius.
	LUS	RUS	*Ulnar Styloid* - Most distal point of the ulna.
	LMH$_{2,3,5}$	RMH$_{2,3,5}$	*Metacarpal Head* - Medial/Lateral prominent point on the medial/lateral surface of the second and third, and fifth metacarpal, respectively.
Pelvis	LASI	RASI	*Antero-Superior Iliac Spine* - Most prominent point on the anterior superior spine of ilium.
	LPSI	RPSI	*Postero-Superior Iliac Spine* - Most prominent point on the posterior superior spine of ilium.
Thigh	LLFE	RLFE	*Lateral Femoral Epicondyle* - Most lateral point on the lateral epicondyle of the femur.
	LMFE	RMFE	*Medial Femoral Epicondyle* - Most medial point on the medial epicondyle of the femur.
Shank	LFH	RFH	*Fibula Head* - Superior point of tibia.
	LLM	RLM	*Lateral Malleolus* - Lateral bony protrusion of ankle.
	LIANK	RIANK	*Medial Malleolus* - Medial bony protrusion of ankle.
Foot	LHEE	RHEE	*HEEL* - Posterior point of heel placed at the same height above the plantar surface of the foot as the toe marker.
	LTOE	RTOE	*TOE* - Over the second metatarsal head, on the midfoot side of the equinus break between the forefoot and midfoot.

Table A.1: Description of the markers presented in figure A.1. When no Right Marker is presented, the marker is no side specific, and by convention is written on the Left Marker column.

BIBLIOGRAPHY

[Abdel-Malek and Arora, 2013] Abdel-Malek, K. and Arora, J. S. (2013). *Human Motion Simulation Predictive Dynamics*. Academic Press, 1st edition edition.

[Abe et al., 2007] Abe, Y., da Silva, M., and Popović, J. (2007). Multiobjective control with frictional contacts. In *Proceedings of the 2007 ACM SIGGRAPH/Eurographics symposium on Computer animation*, pages 249–258. Eurographics Association.

[Ady et al., 2013] Ady, R., Bachta, W., and Bidaud, P. (2013). Analysis of cane-assisted walking through nonlinear optimization. In *2013 IEEE International Conference on Robotics and Automation (ICRA)*, pages 3866–3872.

[Allard et al., 1996] Allard, P., Kirlui, C., Rosenbaum, D., Siegler, S., and Whittle, M. (1996). Joint coordinate system for the ankle joint complex. *Society of Biomechanics Newsletter*, page 59.

[Arnold et al., 2005] Arnold, A. S., Anderson, F. C., Pandy, M. G., and Delp, S. L. (2005). Muscular contributions to hip and knee extension during the single limb stance phase of normal gait: a framework for investigating the causes of crouch gait. *Journal of Biomechanics*, 38(11):2181–2189.

[Baker et al., 2009] Baker, R., McGinley, J. L., Schwartz, M. H., Beynon, S., Rozumalski, A., Graham, H. K., and Tirosh, O. (2009). The Gait Profile Score and Movement Analysis Profile. *Gait & Posture*, 30(3):265–269.

[Baker, 2013] Baker, R. W. (2013). *Measuring Walking: A Handbook of Clinical Gait Analysis*. MacKeith Press, London, 1 edition.

[Balzer et al., 2013] Balzer, J., Schelldorfer, S., Bauer, C., and van der Linden, M. L. (2013). Effects of simulated crouch gait on foot kinematics and kinetics in healthy children. *Gait & Posture*, 38(4):619–624.

[Bar-On et al., 2015] Bar-On, L., Molenaers, G., Aertbeliën, E., Van Campenhout, A., Feys, H., Nuttin, B., and Desloovere, K. (2015). Spasticity and Its Contribution to Hypertonia in Cerebral Palsy. *BioMed Research International*, 2015:1–10.

[Bell et al., 2002] Bell, K. J., ?unpuu, S., DeLuca, P. A., and Romness, M. J. (2002). Natural Progression of Gait in Children With Cerebral Palsy:. *Journal of Pediatric Orthopaedics*, 22(5):677–682.

[Bähler, 1986] Bähler, A. (1986). The biomechanics of the foot. *Clinical Prosthetics and Orthotics*, 10(1):8–14.

[Bidaud et al., 2009] Bidaud, P., Barthélémy, S., and Micaelli, A. (2009). Contrôle de l'équilibre des humains virtuels. In *Le traité de la réalité virtuelle, volume 5: Les humains virtuels*, pages 41–64. Presses de l'Ecole des Mines de Paris.

[Burges, 1998] Burges, C. J. (1998). A tutorial on support vector machines for pattern recognition. *Data mining and knowledge discovery*, 2(2):121–167.

[Carson et al., 2001] Carson, M. C., Harrington, M. E., Thompson, N., O'Connor, J. J., and Theologis, T. N. (2001). Kinematic analysis of a multi-segment foot model for research and clinical applications: a repeatability analysis. *Journal of Biomechanics*, 34(10):1299–1307.

[Cobeljic et al., 2009] Cobeljic, G., Bumbasirevic, M., Lesic, A., and Bajin, Z. (2009). The management of spastic equinus in cerebral palsy. *Orthopaedics and Trauma*, 23(3):201–209.

[Damsgaard et al., 2006] Damsgaard, M., Rasmussen, J., Christensen, S. T., Surma, E., and de Zee, M. (2006). Analysis of musculoskeletal systems in the AnyBody Modeling System. *Simulation Modelling Practice and Theory*, 14(8):1100–1111.

[De Leva, 1996] De Leva, P. (1996). Adjustments to Zatsiorsky-Seluyanov's segment inertia parameters. *Journal of biomechanics*, 29(9):1223–1230.

[Decré et al., 2013] Decré, W., Bruyninckx, H., and De Schutter, J. (2013). Extending the iTaSC constraint-based robot task specification framework to time-independent trajectories and user-configurable task horizons. In *Robotics and Automation (ICRA), 2013 IEEE International Conference on*, pages 1941–1948. IEEE.

[Delp et al., 2007] Delp, S. L., Anderson, F. C., Arnold, A. S., Loan, P., Habib, A., John, C. T., Guendelman, E., and Thelen, D. G. (2007). OpenSim: Open-Source Software to Create and Analyze Dynamic Simulations of Movement. *IEEE Transactions on Biomedical Engineering*, 54(11):1940–1950.

[Delp and Loan, 2000] Delp, S. L. and Loan, J. P. (2000). A computational framework for simulating and analyzing human and animal movement. *Computing in Science & Engineering*, 2(5):46–55.

[DeLuca et al., 1997] DeLuca, P., Davis, R. r., Õunpuu, S., Rose, S., and Sirkin, R. (1997). Alterations in surgical decision making in patients with cerebral palsy based on three-dimensional gait analysis. *Journal of Pediatric Orthopaedics*, 17(5).

[Desailly, 2008] Desailly, E. (2008). *Analyse biomécanique 3D de la marche de l'enfant déficient moteur*. PhD thesis, Université de Poitiers.

[Dobson et al., 2007] Dobson, F., Morris, M. E., Baker, R., and Graham, H. K. (2007). Gait classification in children with cerebral palsy: A systematic review. *Gait & Posture*, 25(1):140–152.

[Ducroquet et al., 1965] Ducroquet, R., Ducroquet, J., and Ducroquet, P. (1965). *La marche et les boiteries: étude des marches normales et pathologiques*. Masson.

[Dumas et al., 2007] Dumas, R., Chèze, L., and Verriest, J.-P. (2007). Adjustments to McConville et al. and Young et al. body segment inertial parameters. *Journal of Biomechanics*, 40(3):543–553.

[Englsberger and Ott, 2012] Englsberger, J. and Ott, C. (2012). Integration of vertical COM motion and angular momentum in an extended Capture Point tracking controller for bipedal walking. In *Humanoid Robots (Humanoids), 2012 12th IEEE-RAS International Conference on*, pages 183–189. IEEE.

[Gage and Schwartz, 2004] Gage, J. R. and Schwartz, M. H. (2004). Pathological gait and lever-arm dysfunction. In *The Treatment of Gait Problems in Cerebral Palsy*, pages 180–204. MacKeith Press, London.

[Gage et al., 2009] Gage, J. R., Schwartz, M. H., Koop, S. E., and Novacheck, T. F. (2009). *The Identification and Treatment of Gait Problems in Cerebral Palsy*. MacKeith Press, London, 2nd edition edition.

[Galarraga C., 2017] Galarraga C., O. A. (2017). *Simulation de l'effet de la chirurgie sur la marche par apprentissage statistique chez des enfants atteints de paralysie cérébrale*. PhD thesis, University of Evry Val d'Essonne.

[Galarraga C. et al., 2016] Galarraga C., O. A., Khouri, N., Vincent Vigneron, Dorizzi, B., and Desailly, E. (2016). Predicting kinematic outcome of multi-level surgery in cerebral palsy. *Gait & Posture*, 49:1.

[Galdeano et al., 2012] Galdeano, D., Bonnet, V., Bennehar, M., Fraisse, P., and Chemori, A. (2012). Partial human data in design of human-like walking control in humanoid robotics. *IFAC Proceedings Volumes*, 45(22):485–490.

[Ganley and Powers, 2004] Ganley, K. J. and Powers, C. M. (2004). Anthropometric parameters in children: a comparison of values obtained from dual energy x-ray absorptiometry and cadaver-based estimates. *Gait & posture*, 19(2):133–140.

[Goswami et al., 1998] Goswami, A., Thuilot, B., and Espiau, B. (1998). A study of the passive gait of a compass-like biped robot: symmetry and chaos. *International Journal of Robotics Research*, 17(12).

[Hanavan, 1964] Hanavan, E. P. (1964). A mathematical model of the human body. AMRL-TR-64-102. *AMRL TR*, pages 1–149.

[Hersh et al., 1997] Hersh, L. A., Sun, J. Q., Richards, J. G., and Miller, F. (1997). The prediction of post-operative gait patterns using neural networks. *Gait & Posture*, 5(2):151.

[Hicks et al., 2011] Hicks, J. L., Delp, S. L., and Schwartz, M. H. (2011). Can biomechanical variables predict improvement in crouch gait? *Gait & Posture*, 34(2):197–201.

[Hicks et al., 2008] Hicks, J. L., Schwartz, M. H., Arnold, A. S., and Delp, S. L. (2008). Crouched postures reduce the capacity of muscles to extend the hip and knee during the single limb stance phase of gait. *Journal of biomechanics*, 41(5):960.

[Hillstrom et al., 2013] Hillstrom, H. J., Song, J., Kraszewski, A. P., Hafer, J. F., Mootanah, R., Dufour, A. B., Chow, B. S., and Deland III, J. T. (2013). Foot type biomechanics part 1: Structure and function of the asymptomatic foot. *Gait & Posture*, 37(3):445–451.

[Hoang and Reinbolt, 2012] Hoang, H. X. and Reinbolt, J. A. (2012). Crouched posture maximizes ground reaction forces generated by muscles. *Gait & Posture*, 36(3):405–408.

[Hoffinger et al., 1993] Hoffinger, S. A., Rab, G. T., and Abou-Ghaida, H. (1993). Hamstrings in cerebral palsy crouch gait. *Journal of Pediatric Orthopedics*, 13(6):722–726.

[Houx et al., 2013] Houx, L., Lempereur, M., Rémy-Néris, O., and Brochard, S. (2013). Threshold of equinus which alters biomechanical gait parameters in children. *Gait & Posture*, 38(4):582–589.

[Jenkyn et al., 2010] Jenkyn, T., Shultz, R., Giffin, J., and Birmingham, T. (2010). A comparison of subtalar joint motion during anticipated medial cutting turns and level walking using a multi-segment foot model. *Gait & Posture*, 31(2):153–158.

[Jensen, 1986] Jensen, R. K. (1986). Body segment mass, radius and radius of gyration proportions of children. *Journal of Biomechanics*, 19(5).

[Jensen, 1989] Jensen, R. K. (1989). Changes in segment inertia proportions between 4 and 20 years. *Journal of biomechanics*, 22(6-7):529–536.

[Kajita et al., 2003] Kajita, S., Kanehiro, F., Kaneko, K., Fujiwara, K., Harada, K., Yokoi, K., and Hirukawa, H. (2003). Biped walking pattern generation by using preview control of zero-moment point. In *Robotics and Automation, 2003. Proceedings. ICRA'03. IEEE International Conference on*, volume 2, pages 1620–1626. IEEE.

[Kanoun et al., 2009] Kanoun, O., Lamiraux, F., Wieber, P.-B., Kanehiro, F., Yoshida, E., and Laumond, J.-P. (2009). Prioritizing linear equality and inequality systems: application to local motion planning for redundant robots. In *Robotics and Automation, 2009. ICRA'09. IEEE International Conference on*, pages 2939–2944. IEEE.

[Kapandji, 1994] Kapandji, I. (1994). *Physiologie articulaire. 2. Membre inférieur*. Number ptie. 2 in Physiologie articulaire : schémas commentés de mécanique humaine. Maloine, 5 edition.

[Kay et al., 2000a] Kay, R., Dennis, S., Rethlefsen, S., Reynolds, R., Skaggs, D., and Tolo, V. (2000a). The effect of preoperative gait analysis on orthopaedic decision making. *Clinical Orthopaedics and Related Research*, 372.

[Kay et al., 2000b] Kay, R. M., Dennis, S., Rethlefsen, S., Skaggs, D. L., and Tolo, V. T. (2000b). Impact of postoperative gait analysis on orthopaedic care. *Clinical orthopaedics and related research*, 374:259–264.

[Khatib et al., 2008] Khatib, O., Sentis, L., and Park, J.-H. (2008). A unified framework for whole-body humanoid robot control with multiple constraints and contacts. In *European Robotics Symposium 2008*, pages 303–312. Springer.

[Kiernan et al., 2014] Kiernan, D., Walsh, M., O'Sullivan, R., O'Brien, T., and Simms, C. (2014). The influence of estimated body segment parameters on predicted joint kinetics during diplegic cerebral palsy gait. *Journal of Biomechanics*, 47(1):284–288.

[Krogt et al., 2010] Krogt, M. M., Bregman, D. J. J., Wisse, M., Doorenbosch, C. A. M., Harlaar, J., and Collins, S. H. (2010). How Crouch Gait Can Dynamically Induce Stiff-Knee Gait. *Annals of Biomedical Engineering*, 38(4):1593–1606.

[Leine and Glocker, 2003] Leine, R. and Glocker, C. (2003). A set-valued force law for spatial Coulomb–Contensou friction. *European Journal of Mechanics - A/Solids*, 22(2):193–216.

[Lengagne et al., 2011] Lengagne, S., Kheddar, A., Druon, S., and Yoshida, E. (2011). Emulating human leg impairments and disabilities on humanoid robots walking. In *Robotics and Biomimetics (ROBIO), 2011 IEEE International Conference on*, pages 2372–2377. IEEE.

[Levine et al., 2012] Levine, D., Richards, J., and Whittle, M. W. (2012). *Whittle's Gait Analysis*. Churchill Livingstone, Elsevier, 5th edition edition.

[Li et al., 2008] Li, J., Huang, Q., Zhang, W., Yu, Z., and Li, K. (2008). Flexible foot design for a humanoid robot. In *2008 IEEE International Conference on Automation and Logistics*, pages 1414–1419.

[Li et al., 2010] Li, Z., Vanderborght, B., Tsagarakis, N. G., and Caldwell, D. G. (2010). Human-like walking with straightened knees, toe-off and heel-strike for the humanoid robot iCub. In *Control 2010, UKACC International Conference on*, pages 1–6. IET.

[Luximon, 2013] Luximon, A. (2013). *Handbook of Footwear Design and Manufacture*. Woodhead Publishing Series in Textiles. Elsevier Science.

[MacWilliams et al., 2003] MacWilliams, B. A., Cowley, M., and Nicholson, D. E. (2003). Foot kinematics and kinetics during adolescent gait. *Gait & Posture*, 17(3):214–224.

[Matjacic and Olensek, 2007] Matjacic, Z. and Olensek, A. (2007). Biomechanical characterization and clinical implications of artificially induced crouch walking: Differences between pure iliopsoas, pure hamstrings and combination of iliopsoas and hamstrings contractures. *J. Biomech.*, 40(3):491–501.

[Maurice, 2015] Maurice, P. (2015). *Virtual ergonomics for the design of collaborative robots*. Theses, Université Pierre et Marie Curie - Paris VI.

[McNee et al., 2004] McNee, A., Shortland, A., Eve, L., Robinson, R., and Gough, M. (2004). Lower limb extensor moments in children with spastic diplegic cerebral palsy. *Gait & Posture*, 20(2):171–176.

[Merlhiot et al., 2012] Merlhiot, X., Le Garrec, J., Saupin, G., and Andriot, C. (2012). The xde mechanical kernel: Efficient and robust simulation of multibody dynamics with intermittent nonsmooth contacts.

[Miller and Verstraete, 1996] Miller, C. A. and Verstraete, M. C. (1996). Determination of the step duration of gait initiation using a mechanical energy analysis. *Journal of Biomechanics*, 29(9):1195–1199.

[Mombaur et al., 2010] Mombaur, K., Truong, A., and Laumond, J.-P. (2010). From human to humanoid locomotion—an inverse optimal control approach. *Autonomous Robots*, 28(3):369–383.

[Murray et al., 1994] Murray, R. M., Sastry, S. S., and Zexiang, L. (1994). *A Mathematical Introduction to Robotic Manipulation*. CRC Press, Inc., Boca Raton, FL, USA, 1st edition.

[Najafi et al., 2010] Najafi, B., Miller, D., Jarrett, B. D., and Wrobel, J. S. (2010). Does footwear type impact the number of steps required to reach gait steady state?: An innovative look at the impact of foot orthoses on gait initiation. *Gait & Posture*, 32(1):29–33.

[Niiler et al., 2007] Niiler, T. A., Richards, J. G., and Miller, F. (2007). Concurrent surgeries are a factor in predicting success of rectus transfer outcomes. *Gait & Posture*, 26(1):76–81.

[Nissan and Whittle, 1990] Nissan, M. and Whittle, M. W. (1990). Initiation of gait in normal subjects: a preliminary study. *Journal of Biomedical Engineering*, 12(2):165–171.

[Noonan et al., 2003] Noonan, K., Halliday, S., Browne, R., O'Brien, S., Kayes, K., and Feinberg, J. (2003). Interobserver variability of gait analysis in patients with cerebral palsy. *Journal of Pediatric Orthopaedics*, 23(3).

[Ogura et al., 2006] Ogura, Y., Shimomura, K., Kondo, H., Morishima, A., Okubo, T., Momoki, S., Lim, H.-o., and Takanishi, A. (2006). Human-like walking with knee stretched, heel-contact and toe-off motion by a humanoid robot. In *2006 IEEE/RSJ International Conference on Intelligent Robots and Systems*, pages 3976–3981. IEEE.

[Ouezdou et al., 2005] Ouezdou, F. B., Alfayad, S., and Almasri, B. (2005). Comparison of several kinds of feet for humanoid robot. In *5th IEEE-RAS International Conference on Humanoid Robots, 2005.*, pages 123–128.

[Paley, 2002] Paley, D. (2002). Dynamic Deformities and Lever Arm Considerations. In Paley, D., editor, *Principles of Deformity Correction*, pages 761–775. Springer Berlin Heidelberg, Berlin, Heidelberg. DOI: 10.1007/978-3-642-59373-4_22.

[Palisano et al., 2008] Palisano, R. J., Rosenbaum, P., Bartlett, D., and Livingston, M. H. (2008). Content validity of the expanded and revised Gross Motor Function Classification System. *Developmental Medicine & Child Neurology*, 50(10):744–750.

[Park et al., 2016] Park, C., Park, J. S., Tonneau, S., Mansard, N., Multon, F., Pettré, J., and Manocha, D. (2016). Dynamically balanced and plausible trajectory planning for human-like characters. pages 39–48. ACM Press.

[Park, 2008] Park, J. (2008). Synthesis of natural arm swing motion in human bipedal walking. *Journal of Biomechanics*, 41(7):1417–1426.

[Pimenta dos Santos et al., 2016] Pimenta dos Santos, A., Ben Amar, F., Bidaud, P., and Desailly, r. (2016). Influence of knee flexion angle at initial contact and hip internal rotation on 'stiff-knee' gait: A dynamical 3d approach. *Movement & Sport Sciences - Science & Motricité*, (93):71–76.

[Reinbolt et al., 2007] Reinbolt, J., Haftka, R., Chmielewski, T., and Fregly, B. (2007). Are Patient-Specific Joint and Inertial Parameters Necessary for Accurate Inverse Dynamics Analyses of Gait? *IEEE Transactions on Biomedical Engineering*, 54(5):782–793.

[Reinbolt et al., 2009] Reinbolt, J. A., Fox, M. D., Schwartz, M. H., and Delp, S. L. (2009). Predicting outcomes of rectus femoris transfer surgery. *Gait & Posture*, 30(1):100–105.

[Reinbolt et al., 2011] Reinbolt, J. A., Seth, A., and Delp, S. L. (2011). Simulation of human movement: applications using OpenSim. *Procedia IUTAM*, 2:186–198.

[Robertson, 2009] Robertson, D. G. E. (2009). *Vicon Workstation Quick Reference Guide*. FCSB School of Human Kinetics University of Ottawa.

[Robertson et al., 2013] Robertson, D. G. E., Caldwell, G. E., Hamill, J., Kamen, G., and Whittlesey, S. N. (2013). *Research Methods in Biomechanics*. Human Kinetics Publishers, Champaign, Illinois, 2nd revised edition edition.

[Rodda and Graham, 2001] Rodda, J. and Graham, H. K. (2001). Classification of gait patterns in spastic hemiplegia and spastic diplegia: a basis for a management algorithm. *European journal of neurology*, 8(s5):98–108.

[Rodda et al., 2004] Rodda, J. M., Graham, H. K., Carson, L., Galea, M. P., and Wolfe, R. (2004). Sagittal gait patterns in spastic diplegia. *Journal of Bone & Joint Surgery, British Volume*, 86(2):251–258.

[Roemmich et al., 2012] Roemmich, R. T., Nocera, J. R., Vallabhajosula, S., Amano, S., Naugle, K. M., Stegemöller, E. L., and Hass, C. J. (2012). Spatiotemporal variability during gait initiation in Parkinson's disease. *Gait & Posture*, 36(3):340–343.

[Rosenbaum et al., 2007] Rosenbaum, P., Paneth, N., Levinton, A., Goldstein, M., and Bax, M. (2007). A report: the definition and classification of cerebral palsy April 2006. *Developmental Medicine & Child Neurology*, 49:8–14.

[Rubrecht et al., 2010] Rubrecht, S., Padois, V., Bidaud, P., and De Broissia, M. (2010). Constraints Compliant Control: constraints compatibility and the displaced configuration approach. In *Intelligent Robots and Systems (IROS), 2010 IEEE/RSJ International Conference on*, pages 677–684. IEEE.

173

[Salini, 2012] Salini, J. (2012). *Dynamic control for the task/posture coordination of humanoids: towards synthesis of complex activities*. PhD thesis, Université Pierre et Marie Curie.

[Salini et al., 2010] Salini, J., Barthélemy, S., and Bidaud, P. (2010). LQP-Based Controller Design for Humanoid Whole-Body Motion. In *Advances in Robot Kinematics: Motion in Man and Machine*, pages 177–184. Springer.

[Sardain and Bessonnet, 2004] Sardain, P. and Bessonnet, G. (2004). Forces Acting on a Biped Robot. Center of Pressure-Zero Moment Point. *IEEE Transactions on Systems, Man, and Cybernetics - Part A: Systems and Humans*, 34(5):630–637.

[Schwartz et al., 2013] Schwartz, M. H., Rozumalski, A., Truong, W., and Novacheck, T. F. (2013). Predicting the outcome of intramuscular psoas lengthening in children with cerebral palsy using preoperative gait data and the random forest algorithm. *Gait & Posture*, 37(4):473–479.

[Sebsadji et al., 2012] Sebsadji, A., Khouri, N., Djemal, K., Yepremian, D., Hareb, F., Hoppenot, P., and Desailly, E. (2012). Description and classification of the effect of hamstrings lengthening in cerebral palsy children multi-site surgery. *Computer Methods in Biomechanics and Biomedical Engineering*, 15(sup1):177–179.

[Seo and Yi, 2009] Seo, J.-T. and Yi, B.-J. (2009). Modeling and analysis of a biomimetic foot mechanism. In *2009 IEEE/RSJ International Conference on Intelligent Robots and Systems*, pages 1472–1477. IEEE.

[Seth et al., 2011] Seth, A., Sherman, M., Reinbolt, J. A., and Delp, S. L. (2011). OpenSim: a musculoskeletal modeling and simulation framework for in silico investigations and exchange. *Procedia IUTAM*, 2:212–232.

[Siciliano and Slotine, 1991] Siciliano, B. and Slotine, J. J. E. (1991). *A general framework for managing multiple tasks in highly redundant robotic systems*.

[Simon, 2004] Simon, S. R. (2004). Quantification of human motion: gait analysis—benefits and limitations to its application to clinical problems. *Journal of Biomechanics*, 37(12):1869–1880.

[Skaggs et al., 2000] Skaggs, D., Rethlefsen, S., Kay, R., Dennis, S., Reynolds, R., and Tolo, V. (2000). Variability in gait analysis interpretation. *Journal of Pediatric Orthopaedics*, 20(6).

[Stansfield et al., 2006] Stansfield, B., Hillman, S., Hazlewood, M., and Robb, J. (2006). Regression analysis of gait parameters with speed in normal children walking at self-selected speeds. *Gait & Posture*, 23(3):288–294.

[Stebbins et al., 2006] Stebbins, J., Harrington, M., Thompson, N., Zavatsky, A., and Theologis, T. (2006). Repeatability of a model for measuring multi-segment foot kinematics in children. *Gait & Posture*, 23(4):401–410.

[Steele et al., 2012a] Steele, K., Damiano, D., Eek, M., Unger, M., and Delp, S. (2012a). Characteristics associated with improved knee extension after strength training for individuals with cerebral palsy and crouch gait. *Journal of pediatric rehabilitation medicine*, 5(2):99–106.

[Steele et al., 2012b] Steele, K. M., van der Krogt, M. M., Schwartz, M. H., and Delp, S. L. (2012b). How much muscle strength is required to walk in a crouch gait? *Journal of Biomechanics*, 45(15):2564–2569.

[Sullivan et al., 1995] Sullivan, K., Richards, J., Miller, F., Castagno, P., and Lennon, N. (1995). Predicting the outcome of surgery for children with cerebral palsy using pre-operative gait analysis. *Gait & Posture*, 3(2):92.

[Thoumie et al., 2002] Thoumie, P., Regnaux, J. P., Combeaud, M., Daniel, O., and Bussel, B. (2002). Évaluation instrumentale de la marche chez le sujet hémiplégique. *La Lettre du neurologue*, 6(5):169–171.

[van den Bogert et al., 1994] van den Bogert, A. J., Smith, G. D., and Nigg, B. M. (1994). In vivo determination of the anatomical axes of the ankle joint complex: an optimization approach. *Journal of biomechanics*, 27(12):1477–1488.

[van den Hecke et al., 2007] van den Hecke, A., Malghem, C., Renders, A., Detrembleur, C., Palumbo, S., and Lejeune, T. M. (2007). Mechanical work, energetic cost, and gait efficiency in children with cerebral palsy. *Journal of Pediatric Orthopedics*, 27(6):643–647.

[Vukobratović and Juricic, 1969] Vukobratović, M. and Juricic, D. (1969). Contribution to the Synthesis of Biped Gait. *IEEE Transactions on Biomedical Engineering*, 16(1).

[Wheelwright et al., 1993] Wheelwright, E. F., Minns, R. A., Law, H. T., and Elton, R. A. (1993). Temporal and Spatial Parameters of Gait in Children I: Normal Control Data. *Developmental Medicine & Child Neurology*, 35(2):102–113.

[Whittle, 2007] Whittle, M. (2007). *Gait analysis: an introduction*. Butterworth-Heinemann, Edinburgh; New York. OCLC: 123434520.

[Wieber, 2006] Wieber, P.-B. (2006). Trajectory free linear model predictive control for stable walking in the presence of strong perturbations. In *Humanoid Robots, 2006 6th IEEE-RAS International Conference on*, pages 137–142. IEEE.

[Winter, 1984] Winter, D. A. (1984). Kinematic and kinetic patterns in human gait: Variability and compensating effects. *Human Movement Science*, 3(1-2):51–76.

[Wren et al., 2005] Wren, T. A., Rethlefsen, S., and Kay, R. M. (2005). Prevalence of specific gait abnormalities in children with cerebral palsy: influence of cerebral palsy subtype, age, and previous surgery. *Journal of Pediatric Orthopaedics*, 25(1):79–83.

[Wu and Cavanagh, 1995] Wu, G. and Cavanagh, P. R. (1995). ISB recommendations for standardization in the reporting of kinematic data. *Journal of Biomechanics*, 28(10):1257–1261.

[Wu et al., 2002] Wu, G., Siegler, S., Allard, P., Kirtley, C., Leardini, A., Rosenbaum, D., Whittle, M., D'Lima, D. D., Cristofolini, L., Witte, H., Schmid, O., and Stokes, I. (2002). ISB recommendation on definitions of joint coordinate system of various joints for the reporting of human joint motion—part I: ankle, hip, and spine. *Journal of Biomechanics*, 35(4):543–548.

[Wu et al., 2005] Wu, G., van der Helm, F. C., (DirkJan) Veeger, H., Makhsous, M., Van Roy, P., Anglin, C., Nagels, J., Karduna, A. R., McQuade, K., Wang, X., Werner, F. W., and Buchholz, B. (2005). ISB recommendation on definitions of joint coordinate systems of various joints for the reporting of human joint motion—Part II: shoulder, elbow, wrist and hand. *Journal of Biomechanics*, 38(5):981–992.

[Zwick et al., 2004] Zwick, E. B., Leistritz, L., Milleit, B., Saraph, V., Zwick, G., Galicki, M., Witte, H., and Steinwender, G. (2004). Classification of equinus in ambulatory children with cerebral palsy - discrimination between dynamic tightness and fixed contracture. *Gait & Posture*, 20(3):273–279.